

OTHER TITLES IN THIS SERIES

- 1. Controlled Atmosphere Storage of Grains**
by J. Shejbal (Editor)
1980 viii + 608 pp.
- 2. Land and Stream Salinity**
by J.W. Holmes and T. Talsma (Editors)
1981 iv + 392 pp.

Developments in Agricultural Engineering, 3

Vehicle Traction Mechanics

RAYMOND N. YONG, EZZAT A. FATTAH and NICOLAS SKIADAS

Geotechnical Research Centre, McGill University, Montreal, Canada



ELSEVIER
Amsterdam — Oxford — New York — Tokyo 1984

ELSEVIER SCIENCE PUBLISHERS B.V.
Molenwerf 1,
P.O. Box 211, 1000 AE Amsterdam, The Netherlands

Distributors for the United States and Canada:

ELSEVIER SCIENCE PUBLISHING COMPANY INC.
52, Vanderbilt Avenue
New York, NY 10017, U.S.A.

ISBN 0-444-42378-8 (Vol. 3)
ISBN 0-444-41940-3 (Series)

© Elsevier Science Publishers B.V., 1984

All rights reserved. No part of this publication may be reproduced, stored in a retrieval system or transmitted in any form or by any means, electronic, mechanical, photocopying, recording or otherwise, without the prior written permission of the publisher, Elsevier Science Publishers B.V./Science & Technology Division, P.O. Box 330, 1000 AH Amsterdam, The Netherlands.

Special regulations for readers in the USA – This publication has been registered with the Copyright Clearance Center Inc. (CCC), Salem, Massachusetts. Information can be obtained from the CCC about conditions under which photocopies of parts of this publication may be made in the USA. All other copyright questions, including photocopying outside of the USA, should be referred to the publisher.

Printed in The Netherlands

PREFACE

The problem of determination and prediction of the capability of a particular piece of machinery to successfully traverse over a specific piece of terrain has only recently received the kind of attention richly deserving of a very complex problem. With the advent of more sophisticated machine computational techniques and also with the advances made in instrumentation and measurement capabilities, it has now been possible to set forward a structured format which permits us to rationally deal with the problem of vehicle mobility. The fundamental essence of the study of vehicle mobility is the development of traction between the vehicle and the supporting terrain. The subject material identified therein is generally defined as Vehicle Traction Mechanics.

Terrain material and terrain cover include a very broad spectrum of materials - e.g. soft soil, sand, snow, muskeg, etc. Since the types of vehicles and their running gears vary considerably depending on mission requirements and other priorities, the problem of describing specific traction capability between a particular running gear and the terrain over which it traverses has (a) traditionally been "solved" via field testing techniques designed to lead to extrapolations, and (b) more recently been studied in terms of vehicle-terrain interaction and more specifically, traction mechanics.

The basic material for this book has been gathered over many years of study in the laboratory and in the field. When the problem was first presented to the senior author, it was posed in terms of the need to explain why the drawbar-pull-slip curve decreased after it reached an optimum point, and why the curve took different forms. Approaching the problem in terms of an interaction phenomenon - between a forcing function defined by the running gear system and a response material defined by the terrain cover and substrate - the study used the basic principles of INTERFACE TRANSFER MECHANICS to define the mechanics of interaction between the contacting running gear element and the supporting ground material. The outcome of many years of study has been the significant development of ENERGY TRANSFER MECHANICS. The many postgraduate students and associates of the senior author had all contributed to the further development and application of the "principles of energy transfer" over all the past few years.

The first two chapters of the book introduce the subject material and the type of terrain surfaces and substrates encountered in vehicle traverse over "unprepared ground". Chapter 3 begins to examine the problem in terms of the various types of mobility elements and the requirements for traction production. The analytical methods in common use are presented in Chapter 4, whilst the mechanics of energy transfer are developed in Chapter 5. Finite element modelling as applied to vehicle mobility analysis is given in Chapter 6 and specific

application to analysis and prediction of mobility can be found in Chapter 7. Chapter 8 deals with soil compaction and methods for prediction of compactive efforts required to stabilize a piece of ground. Finally, Chapter 9 addresses the problem of "TRAFFICABILITY" as distinct from "mobility".

The subject of VEHICLE TRACTION MECHANICS should by no means be considered to be thoroughly and completely developed in this book, - partly because of the extent of the subject that needs to be treated, but mainly because of the fact that a considerable amount of fundamental research work still remains to be done to fully delineate the problems and the methods for solution of the problems. Rather than wait for continuing developments to materialize, the authors thought that there is considerable benefit in presenting the material in its present level of achievement since (a) the subject of "Vehicle Traction Mechanics" per se is indeed new, and (b) the subject in its present level of development forms a coherent and sufficient knowledge platform from which informed analyses of pertinent problems can be mounted.

Many individuals have contributed to the development of the subject material covered in this book. In particular, the authors wish to record the encouragement and assistance given by the various project officers from the Defence Research Establishments (DND), T.A. Harwood, I.S. Lindsay and J. Williams. The authors have benefited considerably from discussions with many of their colleagues at various research centres and universities. The concepts grow gradually in discussions and through studies of several research workers. The many postgraduate students working under the senior author have, through their studies, contributed directly via experiments, analyses, and discussions. To these individuals, and to the many others in the overall field of "Vehicle Mobility", who have directly and indirectly contributed to the learning process of the authors, we wish to record our appreciation and gratitude. We also wish to acknowledge the very conscientious efforts in the production of the drawings attended to by Mrs. P. Lytle.

The very careful and expert typing and preparation of the camera-ready manuscript provided by Mrs. M.L. Powell must be properly and fully acknowledged. Without her patient management of the manuscript, the outcome would have been somewhat ragged.

R.N. Yong
E.A. Fattah
N. Skiadas

February, 1984

Chapter 1

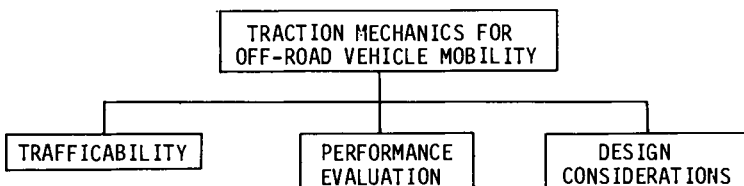
INTRODUCTION

1.1 GENERAL

Vehicle traction mechanics is concerned with the interaction between the running gear of a vehicle and the terrain over which the vehicle operates. In essence, the mechanics of vehicle motion or land locomotion deals with the complex problems of interaction between the vehicle's running gears (wheels, track, air cushion, legs, etc.) and various types and conditions of terrain surfaces. To that end, this book addresses the mechanics of off-road vehicle locomotion since the problems of response of natural terrain surfaces to tractive forces constitute a significant area of study. The need for basic studies on the ground properties which affect vehicle performance is evident from experience of land locomotion in the areas of military and civilian mobility, agricultural mechanization, timber harvesting and transportation, earth moving, soil compaction and construction, trenching and soil cutting.

The recent past has seen an increase in research efforts in the field of vehicle-terrain and machine tool-terrain interaction to obtain a better understanding of the action of soil-vehicle soil-tool systems. These studies are generally directed toward the problems most frequently encountered in the field of soil compaction, tillage, and land vehicles operating over natural ground surfaces that fall in the categories of loose or soft soil, and muskeg or snow. The basic problems in these soil or snow types and muskeg are (a) excessive wheel or track sinkage i.e. lack of flotation due to ground pressure imposed and physical characteristics of both the soil (snow or muskeg) and the vehicle, (b) excessive wheel or track slippage caused by insufficient traction because of interface shear failure. Whilst the primary attention in this book will be problems associated with vehicle traction mechanics, the general subject of traction due to cutting mechanisms (e.g. grousers and blades) applicable to soil cutting, and also soil compaction, will be addressed.

In general, the off-road vehicle traction mechanics can be divided into three interdependent areas as shown:



1.2 OFFROAD TRACTION MECHANICS

1.2.1 Trafficability

Trafficability is concerned with the determination of the surface and sub-surface characteristics which can be used to evaluate the performance of any running gear with respect to the terrain over which the vehicle operates. Different field measurement tools such as loaded plates, sliding plates, annular rings, Bevameter, cones, vane-cone systems, etc., can be used to determine terrain properties for 'translation' into mobility parameters and utilization in appropriate formats in the production of trafficability maps.

1.2.2 Performance evaluation

This is generally concerned with the determination of the traction performance of specific running gear systems (track or wheel) to specified terrain conditions. The traction performance can be expressed in terms of required input power, generated drawbar-pull, ride quality, travel speed, etc.

1.2.3 Design considerations

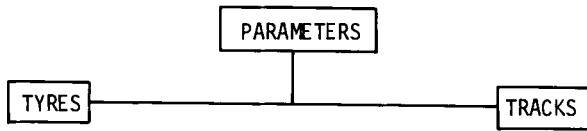
The design considerations in vehicle traction mechanics are generally concerned with the determination of the running gear geometrical dimensions and configurations, material mechanical properties, supporting and driving systems required to produce certain performance characteristics with respect to specific terrain conditions.

The three off-road divisions of mobility shown previously are inter-related and cannot be studied or investigated separately. This book deals with the aspects which control, define and determine the relations between the off-road vehicle running gear and the terrain over which the running gear performs.

1.3 OBJECTIVES

The object of a study of running gear (track or wheel) traction mechanics in natural terrain situations (soft or loose soil, snow, etc.) is to predict the performance of a vehicle tractive element under the given conditions imposed by the terrain. Assuming that all the necessary characteristics and properties of the tractive element (track or wheel) and the terrain (soil, snow, etc.) are known, the problem is to determine the relations between the load on the vehicle tractive element, the applied torque, the pull that the tractive element can develop (slip and sinkage), and the terrain conditions.

The developed slip is an important issue, especially in regard to efficiency of performance because, for a given tractive element speed, the vehicle reduces the distance over which the pull does work. Sinkage should be controlled, for it must remain smaller than the clearance of the vehicle. The tractive-soil parameters which control the vehicle performance are shown in Figs. 1.1 and 1.2.



- | | |
|---|--|
| (a) Geometrical configurations and dimensions: | (1) Geometrical dimensions, length and width |
| - cross-sectional shape | (2) Angle of attack and departure |
| - width, diameter and section height | (3) Sprocket position |
| (b) Structural parameters: | (4) Material type of mounted grousers |
| - number and direction of plies | (5) Mounted grousers |
| - mechanical properties of tyre material composite | - geometry (cross-section) |
| (c) Thermal properties of tyre material composite | - arrangement |
| (d) Tread geometrical configurations, thickness, width, shape | - spacing |
| (e) Inflation pressure | (6) Track type |
| (f) Contact area on rigid surface | (7) Road wheels |
| (g) Load deformation/distortion characteristics | - characteristics |
| | - dimensions |
| | - spacing |
| | (8) Track tension |

SOIL GROUND SURFACE

Flotation: Plate, cone and vane-cone penetration test; triaxial test.

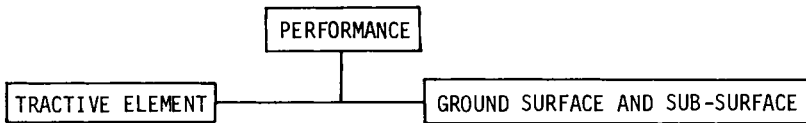
Traction: Triaxial, vane-cone rotation, shear plate (rectangular-annular)

Surface cover: Vegetation, snow, ice, barren, wetness, soil, etc.

Fig. 1.1. Tractive element-soil parameters.

1.4 REQUIREMENTS

The requirements for performance characteristics of any off-road vehicle vary according to operating field conditions and mission objectives. For example, a requirement for earth-moving equipment could be one which demands very high drawbar-pull at low ground contact pressures. On the other hand, in the case of off-road transport vehicles, high speed capability and good manoeuvrability plus ability for obstacle avoidance are desirable characteristics. In general, the requirements should satisfy the following:



Applied load and input torque	Surficial disturbance and disruption
Drawbar-pull and rolling resistance	Compaction and rut depth
Translational and angular velocity	Surface layer shear
Ride quality (characteristics)	Vegetation damage
Manoeuvrability	Infiltration
Obstacle clearance and gradability	Water flow
Operational efficiency	Compaction
Dynamic sinkage	Loss in soil strength

Fig. 1.2. Tractive element-soil performance

- (a) mission objectives, e.g. payload, work requirement, etc.,
- (b) economic constraints and energy efficiency,
- (c) safety,
- (d) comfortable operating conditions,
- (e) reliability.

Most off-road vehicles have more than one operating function for economic and practical purposes, e.g. landfill compactors are used for spreading, chopping, compacting of refuse and cover material.

Off-road field operations can be classified into four distinguishable categories.

(1) Field construction. Construction of earth dams, waterways and highways, airfields, etc., which requires movement of large quantities of earth and rock. In this type of operation the general requirements are (a) optimum speed, to permit quick and efficient movement of a mass of material, (b) length of haul, to permit movement over various distances and surface layers, and (c) size of load and equipment.

(2) Industrial operations. Operations in support of logging, mining and petroleum industries. Typical units include mobile cranes, self-contained pumps, and power plants. Nowadays, off-road operations require increased efficiency thus placing demands on running gears with flotation, traction characteristics and load-carrying capacities which once would have been considered impractical.

(3) Military operations. Various types of equipment which are being developed to operate over a great variety of surfaces in cross-country mobility, require agility, reliability and manoeuvrability.

(4) General off-road transportation.

1.5 BASIC PROBLEMS AND CONCERNS IN VEHICLE TRACTION MECHANICS

The basic issues and concerns in the study of vehicle traction mechanics revolve around the need to -

(a) establish a better knowledge and insight into the mechanics of interaction between elements of a vehicle running gear system and the surface layer over which it acts,

(b) develop a rational means for evaluation of performance characteristics of running gear systems over specific terrain conditions,

(c) provide the tools for prediction of performance of the running gear, thus leading to implementation of optimization procedures.

(d) establish the basic means for determination of the capability of a vehicle to move from one location to another.

The ability for a vehicle to travel from a specific location identified as point A to another location, point B (where the separation distance is characterized by natural unprepared terrain) is dependent on several key factors and considerations.

The three principal elements which control vehicle mobility - i.e. the ability of a specific vehicle to traverse a particular piece of terrain, are:

(1) Vehicle type and loading conditions - especially running gear properties and characteristics.

(2) Surface cover and surface layer properties.

(3) Geometric terrain features - e.g. roughness, obstacles, slopes, ditches, etc.

For a specific vehicle with particular running gear characteristics, mobility capability and efficiency of performance will be controlled by items (2) and (3). Changing the running gear could cause immobilization or increase mobility - dependent on the nature of the interactions developed between the running gear and the supporting terrain.

Trafficability refers to the capability of the particular terrain unit to support vehicle mobility. A piece of terrain could prove to be trafficable for one type of vehicle and not for another - dependent again on the particular sets of interactions produced in the production of mobility of the vehicle.

The properties of terrain patches (i.e. characteristic features of the terrain), will dictate the extent and types of interactions produced - consistent with the loading conditions and the types of running gear systems. These interactions will in turn describe vehicle mobility characteristics and terrain trafficability. Thus, whilst a piece of ground might support the mobility of a particular type of vehicle, it could be said that changing the vehicle characteristics could indeed render that same vehicle immobile. To travel from point A to point B over a particular area would require one's ability to determine if the chosen vehicle could prove "mobility capability" over the various terrain

patches lying in-between the two points. Alternatively, one could say that it is required to determine whether the terrain patches lying in between A and B are trafficable to the vehicle chosen to traverse from point A to point B. In essence, what is required is the development of one's capability to determine the conditions which would render the terrain untrafficable - or the conditions whereby mobility can be increased.

1.5.1 Traction mechanisms

The mechanisms of interaction established between the running gear and the supporting terrain depend not only on the type of running gear contact element, e.g. track-grouser or tyre type, but also on the properties of the surface layer material. In addition, the manner of load application imposed by the vehicle is an important element in the development of the kind of mechanisms of interaction at the interface between the running gear and the supporting surface layer.

The questions that can easily be posed are:

(1) What is traction, and how is it produced?

(2) What are the principal characteristics of interaction between traction elements and the surface layer?

(3) What is the role of traction in relation to mobility and trafficability?

The items of pertinent interest and concern relate to: thrust, slip, drawbar-pull, traction coefficient, sinkage, shear and friction.

The manner in which traction is established is a function of the characteristics of the running gear contact patch and the manner in which load transfer is implemented. The choice between tyres and tracks, i.e. a wheeled vehicle or a tracked vehicle, depends on several controlling issues. The first set of issues concerns speed and capability of operation. A wheeled vehicle can generally travel faster and is more manoeuvrable in comparison to a tracked vehicle - provided that the supporting surface layer is competent and non-yielding, such as highways and secondary roads. However, when the supporting surface and sub-surface layers are soft or yielding, as is the case for most unprepared natural ground, the speed and manoeuvrability characteristic features of the wheeled vehicle become degraded. The more yielding the supporting terrain is, the more attractive the tracked vehicle becomes as an alternative consideration.

However, other factors now become important in the consideration of choice of type of vehicle. These relate to: economics of operation, payload requirements, mission profile, terrain envelope, operational envelope, reliability, speed, etc.

The mechanisms of traction production differ in detail between tyres and tracks, and can be influenced considerably by (a) detailed changes in the types of grousers, spacing, geometry, track type, road wheels, suspension, etc. for tracked vehicles, and (b) tyre type, carcass properties, tread design, etc. for wheeled vehicles. Thus efficiency of operation requires all these factors to be

integrated into the decision-making mechanism at the proper time.

Development of traction is fundamental to the production of successful vehicle mobility - provided that flotation is available. A vehicle can be immobilized in a combination of ways:

- (a) sinkage due to lack of flotation,
- (b) excessive slip, even though adequate flotation exists,
- (c) slip-sinkage where continued slip serves to degrade flotation, resulting in total sinkage immobilization.

The elements of traction mechanics consist of principles which can be utilized to analytically model the mechanisms of interaction for evaluation of traction - with a view to prediction of mobility. The items for consideration include basic correlative empirical techniques, limit equilibrium theories and application, plasticity techniques, and other principles of mechanics.

Chapter 2

TERRAIN MATERIAL AND INTERFACE REACTION

2.1 INTRODUCTION

Terrain (i.e. ground) can be described in geometric, as well as physical terms insofar as vehicle mobility or trafficability is concerned. One can describe a terrain in broad terms such as "rough, rocky, hilly, etc.", or in more specific terms such as "soft organic, loose granular, wet clayey, etc.". We observe therefore that the term "terrain" is used very loosely as a descriptive term, covering not only geometric features at times, but also physical characteristics and properties of the immediate surface layer material. The broad types of surface layer material (other than vegetative cover) can be viewed as:

- (a) inorganic, such as granular soil (sand), cohesive soil (clay), or mixed soil type material,
- (b) organic, such as muskeg or peat,
- (c) snow,
- (d) rock outcrop.

In regard to vehicle mobility, immobilization (of a vehicle) can occur due to:

(a) Physical impediments derived from the mechanical characteristics and properties of the terrain, i.e. excessive sinkage of the vehicle due to lack of flotation, or insufficient traction due to slip.

(b) Physical impediments due to obstacle geometric characteristics, i.e. vehicle profile-obstacle interference.

(c) Terrain roughness, which would severely limit the speed of the vehicle because of excessive vibrations - leading to total immobilization.

2.2 INORGANIC TERRAIN

Inorganic terrain material generally consists of mineral soils. Since these soils vary widely, they need to be classified in some rational fashion to allow for proper identification. There are many methods available for classifying mineral soils. The choice of method depends upon the specific use intended for the soil. For engineering purposes, the classification methods rely primarily on the grain size and its gradation within the soil mass, its consistency, and probably its relation to frost effects. These methods are outlined in various books on soil engineering.

While it is possible to grossly estimate or to infer the water-holding capacity of soils, strength and compressibility, etc., from particle-size distribution, there is no substitute for actual measurements and evaluation of the

properties of the soil. It is not possible, however, to include these actual measurements in classification methods, since they involve tedious laboratory studies. There is no universal standard classification system for trafficability purposes. However, the most common one in present-day use is the one developed by the Waterways Experimental Station (WES), which is concerned primarily with soils limited to the first 60 cm from the surface.

2.2.1 Particle-size composition of soils

The particle-size distribution of a soil influences chemical, physical and biological properties of soils. Separates consisting of larger particles, the sands and gravels, form the skeleton of the soil and determine many of its mechanical properties, (Yong and Warkentin, 1975). The clay content in soils determines most of the chemical and physical-chemical properties of the soils. Particle-size distribution in soils and density can influence the type and weight of the off-road vehicles operating on the soil, the susceptibility of the soils to erosion, the water-holding capacity and hence the water supply to plants, spacing of irrigation and drainage ditches, types of drainage, and irrigation systems required. It also influences the strength and compressibility of soils, both of which are important in the consideration of flotation for vehicle mobility.

Various systems have been used to group soils according to the proportion of different sizes of the constituent particles. The size limits used for sand, silt, and clay vary slightly in different systems. The Atterberg or International system, the Massachusetts Institute of Technology, the International Society of Soil Sciences, U.S. Bureau of Public Roads, and the U.S. Department of Agriculture systems are all used (see Fig. 2.1). Figure 2.2 is a triangle used in soil science giving textural classes corresponding to different proportions of sand, silt and clay. Sometimes a size-distribution curve (Fig. 2.3) is used to show the results of particle-size analysis. This does not require an arbitrary division of particles into separates based upon size, but for many purposes it is easier to work with the numbers obtained by considering sizes such as sand, silt and clay.

In the WES classification of soil for trafficability purposes (Knight and Rula, 1961) the following scheme is used:

- (a) Fine-grained soil. A soil of which more than 50% of the grains, by weight, will pass a No. 200 U.S. Standard sieve (smaller than 0.074 mm in diameter).
- (b) Coarse-grained soil. A soil of which more than 50% of the grains, by weight, will be retained on a No. 200 U.S. Standard sieve (larger than 0.074 mm in diameter).

This type of classification, accompanied by Soil Cone Index and Vehicle Cone Index makes it possible to estimate (from empirical information), trafficability of soil (see Chapter 9).

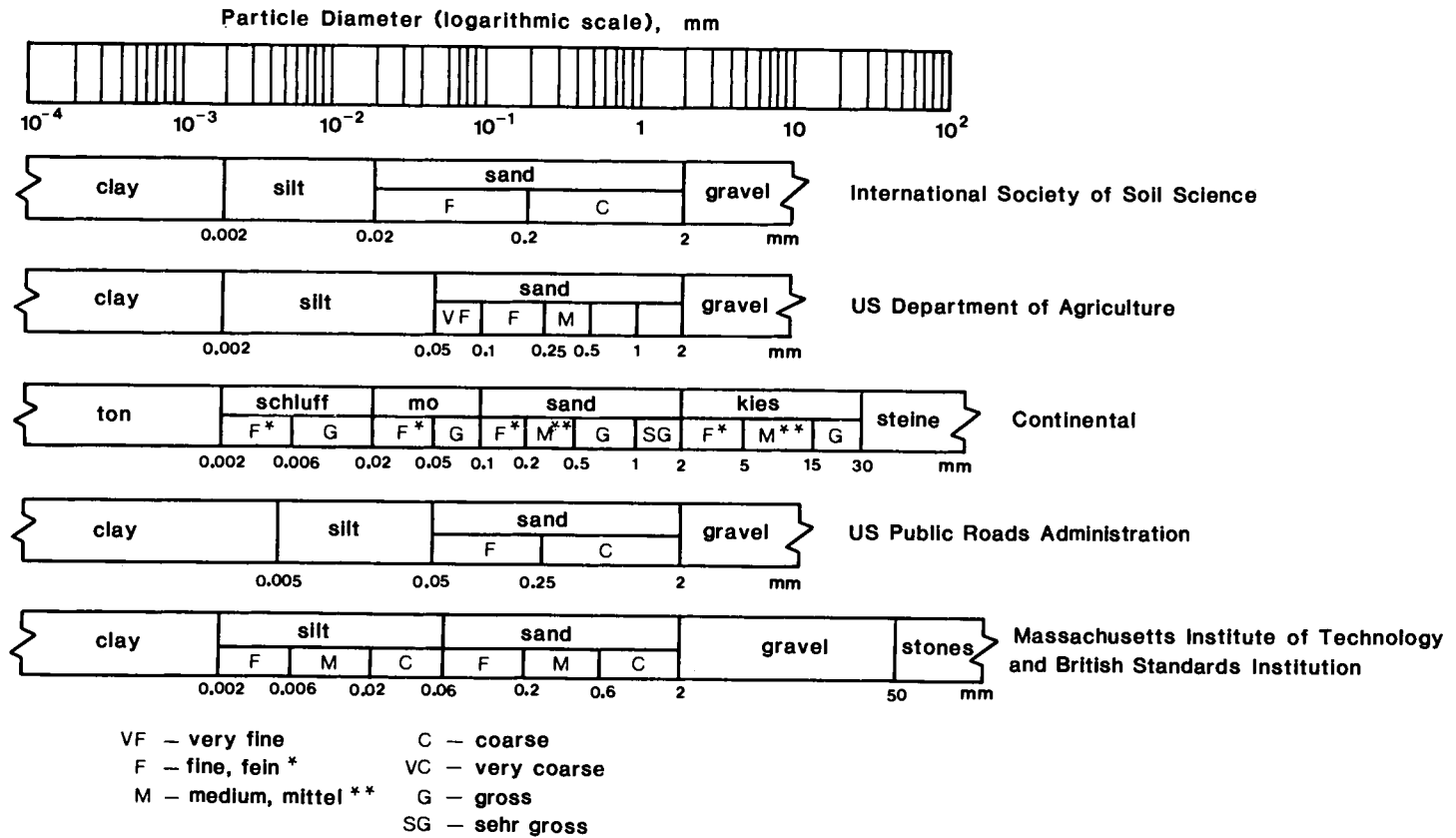


Fig. 2.1. Principal particle-size scales (from Yong and Warkentin, 1975).

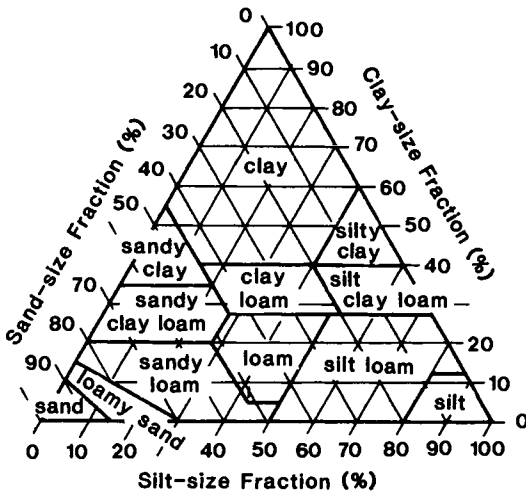


Fig. 2.2. Chart showing percent clay, silt, and sand in the soil textural classes of U.S. Department of Agriculture.

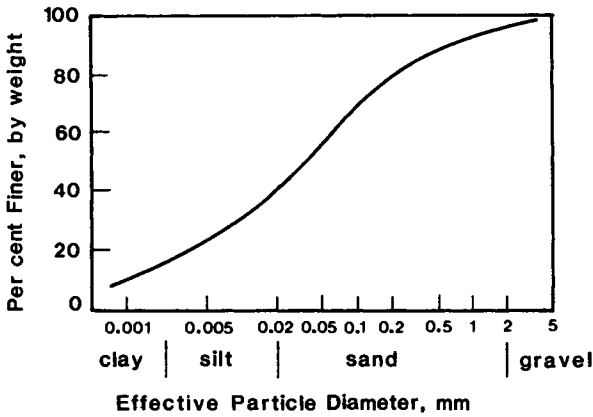


Fig. 2.3. Particle-size distribution curve.

2.2.2 Basic soil properties

(i) Weight and volume. The basic soil properties may be easily defined by visualizing soil in terms of the three component phases in the soil - namely, solid, liquid, and gaseous. Consider the schematic diagram in Fig. 2.4. By separating the phases into three distinct parts, we may obtain relationships to define the basic soil properties.

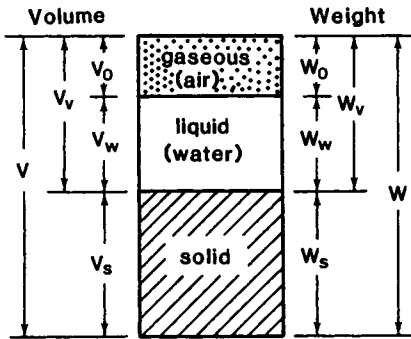


Fig. 2.4. Idealized three-phase soil system.

Void ratio e is defined as the ratio of volume of voids V_v to volume of solids V_s :

$$e = V_v/V_s \quad (2.1)$$

The ratio of volume of voids V_v to total volume V is defined as the porosity, n :

$$n = V_v/V \quad (2.2)$$

But $V = V_v + V_s = (1 + e)V_s$. Hence:

$$n = \frac{V_v}{V_s(1 + e)} = \frac{e}{1 + e} \quad (2.3)$$

The water content, ω , is given as $W_w/W_s \cdot 100\%$. For a fully saturated soil-water system, since all the voids will be completely filled with water:

$$V_v \gamma_w = W_w \quad (2.4)$$

where W_w = weight of water, and γ_w = density of water. For partial saturation:

$$V_w \gamma_w = W_w, \text{ or } (V_v - V_a) \gamma_w = W_w \quad (2.4a)$$

Hence, the relationship for S_r , the degree of saturation, is given as:

$$S_r = \frac{(V_v - V_a)\gamma_w}{V_v\gamma_w} \cdot 100\%$$

i.e.

$$S_r = \frac{V_v - V_a}{V_v} \cdot 100\% = \frac{V_w}{V_v} \cdot 100\% \quad (2.5)$$

The unit weight γ , of the saturated soil-water system, is defined as W/V , i.e. total weight divided by total volume. It is frequently more desirable to express unit weight relationships in terms of a dry, or bulk density, γ_d , i.e.

$\gamma_d = W_s/V$. Since:

$$\gamma = \frac{W}{V} = \frac{W_w + W_s}{V}$$

$$\gamma = (1 + \omega) \frac{W_s}{V}$$

But since $W_s/V = \gamma_d$, we have $\gamma = (1 + \omega)\gamma_d$, or:

$$\gamma_d = \frac{\gamma}{1 + \omega} \quad (2.6)$$

In a submerged state, because of the buoyancy effect of water, the submerged or buoyant density γ' is given by $(\gamma - \gamma_w)$.

(ii) Consistency limits. The definitions of the various states of consistency (Fig. 2.5) depend upon laboratory tests for establishing the limits of consistency. These limits are by no means absolute and are sensitive to several environmental and operative factors.

The generalized relationship between water content and volume as a proportion of oven-dry volume is shown graphically in Fig. 2.6.

Points 1, 2 and 3 in Fig. 2.6 represent the liquid limit ω_L , plastic limit ω_p and shrinkage limit ω_s respectively. In terms of a water content-volume change definition, only the shrinkage limit can be rigorously defined. The shrinkage limit ω_s defines the water content at which volume change is no longer linearly proportional to change in water content. The relationship shown in Fig. 2.6 is linear until the shrinkage limit is reached. Beyond this stage, any decrease in water content will not cause a proportional decrease in volume. If the straight line is projected until it intersects the abscissa (water content line), point 4,

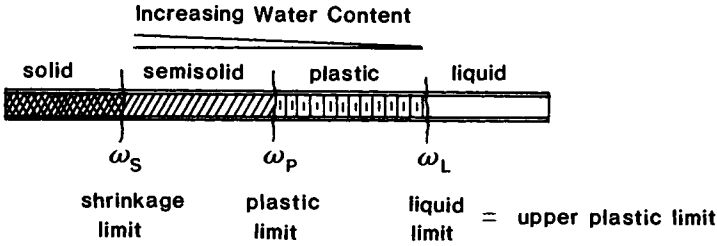


Fig. 2.5. Consistency states of soil.

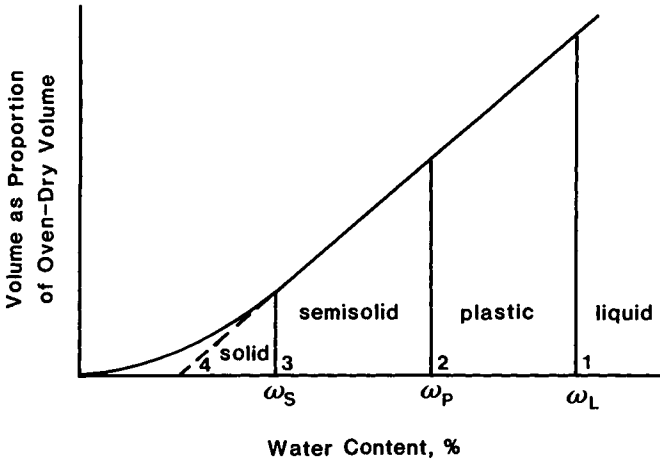


Fig. 2.6. Consistency states during drying of an initially saturated clay.

as shown in Fig. 2.6, is reached. This represents the total shrinkage of the soil sample.

The actual measurement of both the liquid and plastic limits depends on standardized laboratory tests. The liquid limit ω_L is that water content at which a groove cut in a standard liquid limit device is closed after 25 taps. The plastic limit ω_P is that water content at which a 3 mm diameter thread of soil begins to crack and crumble under continued rolling by hand. The standardized laboratory procedures may be found in the American Society for Testing Materials (ASTM) specifications.

2.2.3 Basic soil behaviour

Since the loading of soil in vehicle mobility and traction application is to all intents and purposes a relatively quick type of transient loading, it can be safely assumed that total stress approach can be adopted for studying subsoil response, i.e. the developed pore-water pressures will not have sufficient time to dissipate. The role of water in the soil can be limited to its effect on the strength of the soil. It can also be assumed that the Mohr-Coulomb theory of failure (Yong and Warkentin, 1975) can be adopted since, by and large, traction production in the soil will in all likelihood render a limiting state of equilibrium in the zone of interest. The application of the Mohr-Coulomb failure theory allows us to identify two strength parameters of the soil, namely, cohesion C , and angle of internal friction, ϕ .

(i) Coarse grained soil. In granular soils, since no measurable "cohesion" exists, the behaviour under load will be influenced solely by the friction properties of the soil. If σ = total normal stress, then the shear strength τ of the granular soil is given by

$$\tau = \sigma \tan \phi \quad (2.7)$$

where ϕ = angle of internal friction.

This relationship is the basic Mohr-Coulomb failure criterion for non-cohesive ($C = 0$) soils - where only frictional resistances control the response shear performance of the soil. By definition, these are generally identified as frictional soils, and sands and gravels are said to fall into this class of soils. These soils are sometimes called cohesionless soils.

Since the frictional property of granular soils is the primary physical component governing the development of shear strength, intimate contact between particles is established during shear. The physical process contributing to resistance to shear motion includes both sliding of particles and removal or displacement of particles from interlocking action between adjacent particles. Figure 2.7 shows the difference between the two.

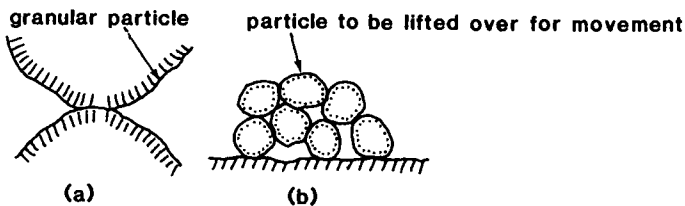


Fig. 2.7. Friction between soil grains. (a) Microscopic interlocking (surface friction). (b) Macroscopic interlocking (mechanical locking).

(ii) Stress and strain. The constitutive performance of a soil is generally expressed in terms of the deformation under load. Soil will strain and finally fail in response to tractive forces. It is important to be able to describe the constitutive performance of soil in terms of stress-strain relationships. To do so, strength tests are performed either with the soil subject to confining stresses - as in the triaxial test - or in the unconfined mode. (See Yong and Warkentin, 1975 for a detailed description of soil strength tests and failure theories.)

The stress-strain relationships for soils obtained in triaxial testing will depend on the initial density of the materials and the degree of stress confinement. Note that the use of stress confinement is meant to simulate the confinement of the soil in the pressure zone beneath the vehicle, i.e. the three-dimensional stress confinement effect due to super-imposed loads. Particle packing (density) is a critical consideration since the denser the packing, the greater is the need for energy input to create shear distortion and volume change.

The range in stress-strain curves shown in Fig. 2.8 depicts the influence of state of particle packing of the cohesionless material. The stress-strain performance of the dense granular soil can be approximated by elastic strain softening theories, whilst loose granular soil would be identified with work hardening concepts.

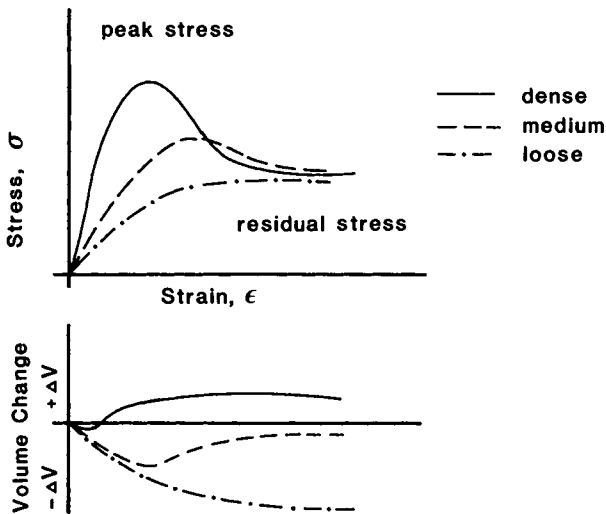


Fig. 2.8. Stress-strain and volume change relationships as a function of initial density. Note that the residual (large strain) stress is the asymptote at large strains. (Yong and Warkentin, 1975).

The effect of moisture content on load (shear) resistance of sand is small, unless the sand contains small percentages of fines (5-8%), which act as a cementing agent between the sand grains at low moisture content. Figure 2.9 shows the effect of moisture content on the penetration shear resistance for sand at different densities.

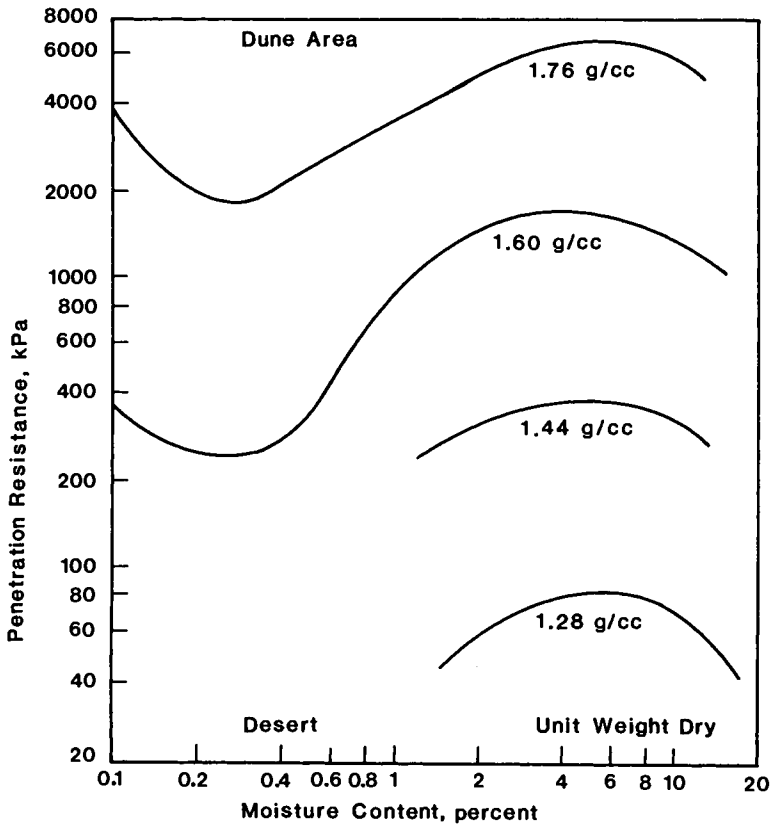


Fig. 2.9. Effect of moisture content on penetration shear resistance of sand. (Traffic Research Team, 1961).

(iii) Mixed cohesive soil (soft soil-fine grained soil). A mixed cohesive soil is one which possesses physical properties of friction and cohesion. These soils are fine-grained in texture, in contrast to sands which are coarse-grained soils. The two properties of cohesion and friction participate in demonstration of shearing resistance. If σ = normal stress, then the shear strength τ is given by

$$\tau = C + \sigma \tan \phi \quad (2.8)$$

where ϕ = angle of internal friction, and C = cohesion.

For simplicity in communication, a mixed cohesive soil is generally referred to as a "cohesive" soil, whereas when the frictional resistance is zero, i.e. $\phi = 0$, the soil is referred to as a " $\phi = 0$ cohesive" or "purely cohesive" soil. Cohesive soil strength can be attributed to interparticle forces (i.e. forces developed between the soil particles) which interact in resisting shear deformation and lead to specific arrangements of soil particles (fabric) and stability. Disruption of soil fabric occurs as the soil develops resistance to shear. A demonstration of the strength of cohesive soil and the specific contribution by structural bonds which are formed as part of a natural soil, linking fabric units and particles to each other, may be seen in Fig. 2.10.

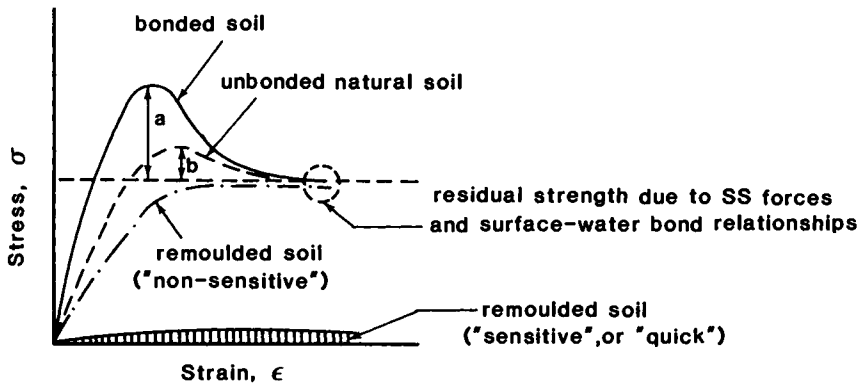


Fig. 2.10. Comparison of stress-strain curves for bonded and unbonded clays. Magnitude of 'a' is due to structural bonds plus interparticle force plus mechanical resistance. Magnitude of 'b' is due to interparticle force bonds plus mechanical interference.

It should be noted that the principal influence on the strength of the fine-grained soils (i.e. cohesive soils) is the amount of water it contains. Almost any cohesive soil in a comparatively dry state is trafficable to all off-road vehicles. However, if its moisture content is increased, its strength may be reduced to the point where only certain vehicles can traverse it. A point can be reached where further increases in moisture may render the soil untrafficable to all vehicles.

2.3 ORGANIC TERRAIN

2.3.1 Muskeg

Muskeg is a term commonly used to describe "organic terrain". It consists of living vegetation such as lichens, sedges and/or grasses, with or without tree and shrub growth. Usually, a combination of these plant forms are found (Radforth, 1969). Underneath this vegetation there is a mixture of decomposed organic material derived from past vegetation but currently chemically changed and fossilized. This material is commonly known as "peat", (Fig. 2.11).

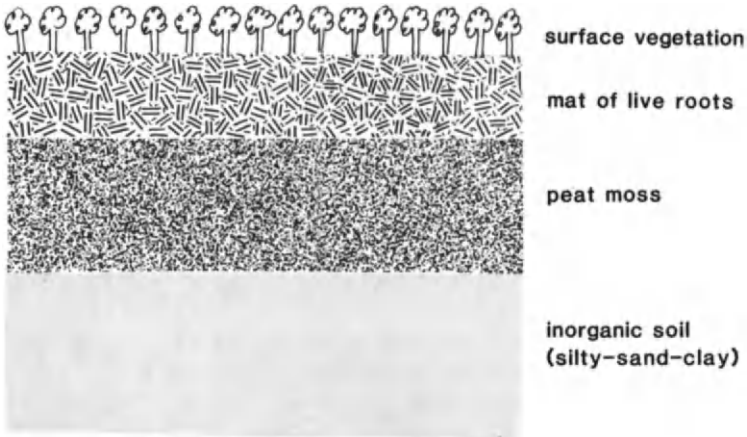


Fig. 2.11. Typical muskeg terrain profile.

The subsurface material "peat" is highly compressible (MacFarlane, 1958) in comparison with most mineral soils, and is generally characterized by very high water content and extremely low bearing capacities. Peat varies in colour from straw through golden brown to chocolate and black. It may be coarse or fine, depending upon the structure of the proportionate components of past cover that became fossilized successionaly. The thickness of the peat mat varies between 5 cm to 27.5 cm, (Radforth, 1969). The peat may be so dry as to show no evidence of free water even when the sample is subjected to pressure, or it may give up sufficient water under its own weight.

Although peat is by nature fluid and compressible, its properties are variable and are largely determined by the living matter from which it originates, (Adams, 1965). The correlation of the living layer with the co-existing peat layer was observed by Radforth (1952) and formed the basis of his engineering classification of muskeg.

2.3.2 Classification of muskeg cover

The object of classification of muskeg vegetal cover using visual inspection is to develop an appreciation of the subsurface terrain characteristics, since there are approximate relationships between living cover and the characteristics of the peat beneath the surface. Radforth (1969) combined his approach for classification of muskeg cover with that of the British Mires Research Group and obtained Table 2.1. The Table contains nine classes of vegetal cover referred to in column two by the letters A to H. The symbols relate to functions of the structure, i.e. shape and texture of the individual elements making up the composition and size. They also have reference to habit, the equivalent of arrangements (Radforth, 1969). The occurrence of pure classes in nature is rare; association of classes is more normal. The predominating class of cover is usually, but not necessarily, the tallest. If the estimated percentage of cover for any class is less than 25%, it should not be considered in the estimation, hence no assessment of total vegetal cover will show more than three classes. In many instances only two classes will be dominant issues in a vegetal cover. Each cover class indirectly signifies the occurrence of prevailing conditions which may be taken into account for purposes of engineering design. For a further study of these conditions, the reader is referred to Radforth (1969).

2.3.3 Structure and properties of peat

Generally, peat consists of two structural types: one fibrous, the other granular. Both fibres and granules have an influence on the mechanical properties of the peat and on the behaviour of the peat continuum under load. A proper method for assessing and distinguishing the factors which contribute to strength and other mechanical properties of peat has yet to be established.

2.3.4 Physical and chemical characteristics of peat

The physical properties which characterize the engineering properties of peat are: water (or moisture) content, shrinkage, permeability, void ratio, gas content, unit weight, specific gravity, size of fibres and percent of ash (MacFarlane, 1969). Acidity is the chemical property of peat most relevant for engineering purposes.

(i) Water content. This is defined as the amount of water contained in the voids of a peat in its natural state. Because of its compositional nature peat has a great affinity for water. Water content ranges between wide limits, depending on the origin and the thickness of a peaty deposit. Whilst the water content of the crust or the living mat may be as low as 100% (by dry weight), the peat beneath the surface crust may possess water content in excess of several hundred percent. Since peat, as a rule, has only a negligible submerged weight,

TABLE 2.1

Structural classification of vegetal cover of muskeg (peatland). (Integration of British and Canadian Systems).

British Mires Research Group*	Radforth system			
	Class symbol	Texture	Stature	Form
Trees over 5 m	A	Woody	15 ft or over (4.5 m or over)	Tree form
Trees under 5 m	B	Woody	5-15 ft (1.5-4.5 m)	Young or dwarfed tree or bush
Shrub habit 50 cm to 2 m	D	Woody	2-5 ft (0.6-1.5 m)	Tall shrub or very dwarfed tree
Shrub habit up to 50 cm	E	Woody	Up to 2 ft (up to 0.6 m)	Low shrub
Creeping shrub up to 50 cm	G	Non-woody	Up to 2 ft (Up to 0.6 m)	Singly or loose association
Broad-leaved herbs				
Sedge-graminoid habit 1-3 m (a) mats (b) hummocks	C	Non-woody	2-5 ft (0.6-1.5 m)	Tall, grasslike
Sedge-graminoid habit under 1 m (a) mats (b) hummocks	F	Non-woody	Up to 2 ft (up to 0.6 m)	Mats, clumps, or patches sometimes touching
Moss habit	I	Non-woody	Up to 4 in. (up to 10 cm)	Often continuous mats, sometimes in hummocks
Lichen habit	H	Non-woody	Up to 4 in. (up to 10 cm)	Mostly continuous mats

Note: Following classification, observer states percentage of cover class within 20%.

*Adapted by Radforth.

the decrease in water content with depth is barely perceptible. (Casagrande, 1966). Figure 2.12 shows a typical water content profile for a representative muskeg site in Ontario, Canada.

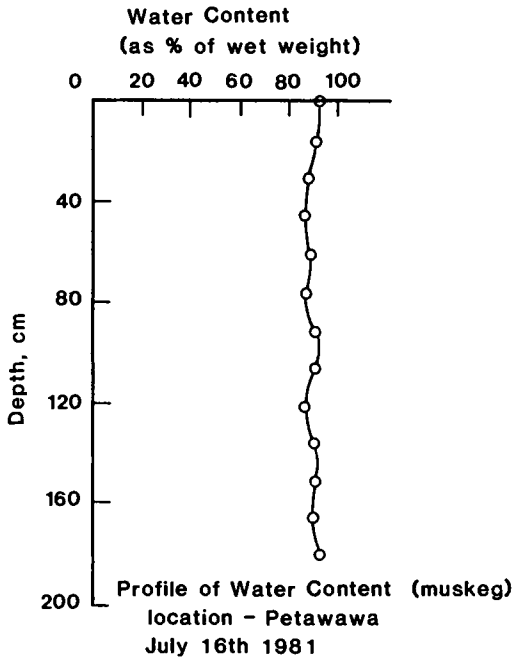


Fig. 2.12. Typical water content profile for muskeg, Petawawa, Ontario.

(ii) Plasticity. The plasticity of peat ranges from a low plasticity for thoroughly weathered deposits to non-plastic for highly fibrous deposits (Casagrande, 1966), as shown in the plasticity chart in Fig. 2.13. Although only a few investigations have been concerned with the plasticity of peat, it is believed that such tests would provide the user with a simple method for estimating the character and the engineering properties of peat deposits.

(iii) Void ratio and permeability. The void ratio, i.e. ratio of the volume of voids to volume of solids, gives an indication of the compressibility of a material: the higher the initial void ratio, the greater the potential compressibility. The void ratios and the coefficients of permeability for peaty soil are highly variable and range between wide limits. Surface layers and shallow peat deposits which are subjected to air drying may possess void ratios between two and five. Or, on the other hand, deep deposits will likely possess void ratios ranging from between five to twenty, with some cases reported as high as thirty.

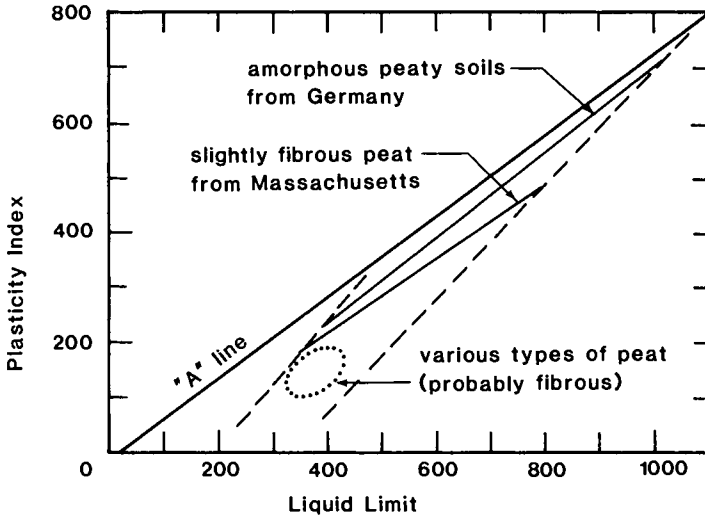


Fig. 2.13. Plasticity chart for peat. (After Casagrande, 1966.)

The permeability of peats varies widely, depending upon (a) the amount of mineral matter present in the peat, (b) the degree of consolidation, and (c) the extent of decomposition. The coefficient of permeability ranges between 10^{-2} and 10^{-4} cm/sec. Upon application of even small loads the permeability decreases rapidly. Extensive investigations by Lea and Brawner (1963) resulted from a log-log plot, (Fig. 2.14), in a straight line relationship between void ratio and permeability.

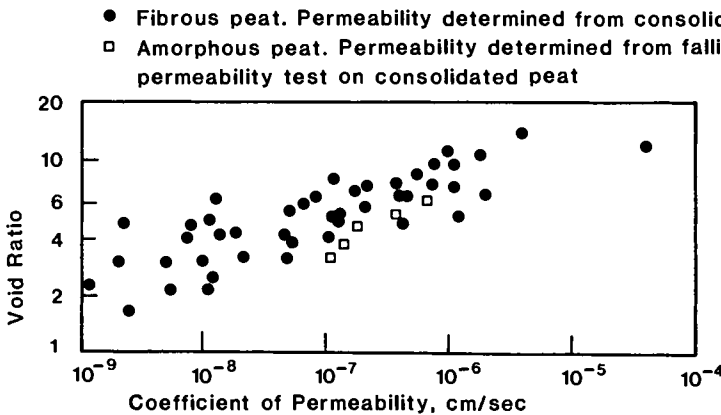


Fig. 2.14. Void ratio-coefficient at permeability relationship.

(iv) Unit weight. The natural unit weight depends upon the water and organic content of the peat: for a saturated pure peat, this weight is usually about the same as that of water and increases with increasing inorganic content. Natural unit weights of peat range from 0.4 g/cc for a moss peat to 1.29 g/cc for amorphous peat. Dry unit weight ranges from 0.08 g/cc to 0.32 g/cc for the case of a peat containing a high mineral soil content.

(v) Specific gravity. The range of specific gravity for peat is from 1.1 to 2.5, with the average about 1.5 or 1.6. Specific gravity values greater than two indicate a peat with considerable amounts of mineral soil content. It should be noted that an accurate determination of the specific gravity of peat can be very difficult because of the presence of entrapped air or gases. This can be minimized by pulverizing the oven-dried peat, following which the specific gravity can be obtained using standard procedures. In this particular case kerosene, with a known specific gravity, is used as the displacement fluid.

(vi) Size of fibres. As might be expected, long fibres make the peat continuum much stronger in comparison to peat with short fibres. Peat with long fibres can act as a mat layer resting on soft soil (Fig. 2.11). In the case of peat composed of short fibres or granules, the material will respond differently depending on whether the granules are colloidal in size or as particles in a mechanical mixture. Both colloidal or particle mechanisms can exist in the same sample.

(vii) Acidity and ash content. The acidity of peat has been reported to range between 3.8 and ten, while the ash content may vary between zero and 95%. (MacFarlane, 1969).

2.3.5 Strength characteristics of muskeg terrain

As stated in Chapter 3, the two prime criteria which control trafficability are flotation and traction. As shown in Fig. 2.11, the general muskeg terrain consists of a surface mat of living material supported on soft peat deposits which overlie soft soil. Due to the excessive deformation of muskeg terrain under applied load, (Fig. 2.15), and because of the fibrosity of the living mat, tensile stresses will develop in the living mat layer. Failure under load may occur at a plane perpendicular to the edge of the loading tool (wheel or plate-terrain contact perimeter) due to edge-cutting effects, or to yielding of the material because of excessive tensile stresses. The former is generally referred to as the "punching" effect. It is not unlikely that both punching failure and yielding due to excessive tensile stresses could occur in concert. In the case of a vehicle mobility problem, failure under load represents a lack of flotation. In terms of traction mechanics this will represent a failure in the mat to provide the means for development of thrust. Traction failure in the muskeg may be

developed due to repeated loading of the muskeg - e.g. multi-vehicle pass. The high permeability and compressibility of the live mat and peat layer are particularly susceptible to the resultant pumping effect created by the repeated loading. In consequence, the live mat will sink into the peat layer and a colloid of amorphous fine organic material will propagate to the surface, thus creating the situation for a lack of traction.

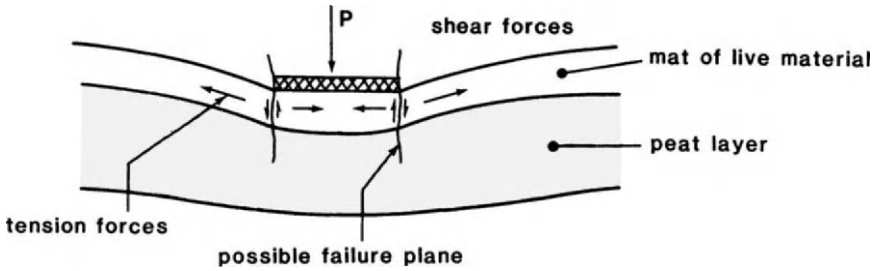


Fig. 2.15. Schematic representation of failure in muskeg under loading action.

There are some field instruments available which can be used to "more-or-less" evaluate the strength characteristics and/or parameters of a terrain for trafficability purposes, such as plate loading (Bekker, 1969), annular ring (Bekker, 1969), vane-shear (Irwin and Yong, 1980), cone penetrometer (Knight and Meyer, 1961), and vane-cone (Yong et al., 1975). Some of these have been adapted for use in muskeg "trafficability" assessment - with various degrees of success. Much obviously depends on the ability of the field instrument to properly and fully evoke all the response performance characteristics of the material - especially the tensile capability of the living mat.

The plate load technique is one such method which has been adopted in muskeg field testing to establish a flotation criterion. Typical load-sinkage curves for different plate sizes under load are shown in Figs. 2.16 and 2.17 (Lee and Jarrett, 1977). The results also show the effect of plate size and the tensile strength of the surface mat on the plate penetration results. The highly compressible nature of the muskeg, especially at the early stages of loading and at failure, can be noticed.

Bekker (1969) suggested the following empirical formula for evaluation of punching pressure P_p for a circular plate.

$$P_p = \frac{2\pi b t_o \tau_v + \pi b^2 p''}{\pi b^2} \quad (2.9)$$

where b = plate;

t_0 = surface mat thickness;

τ_v = mat shear strength and

p'' = bearing pressure at the sublayer.

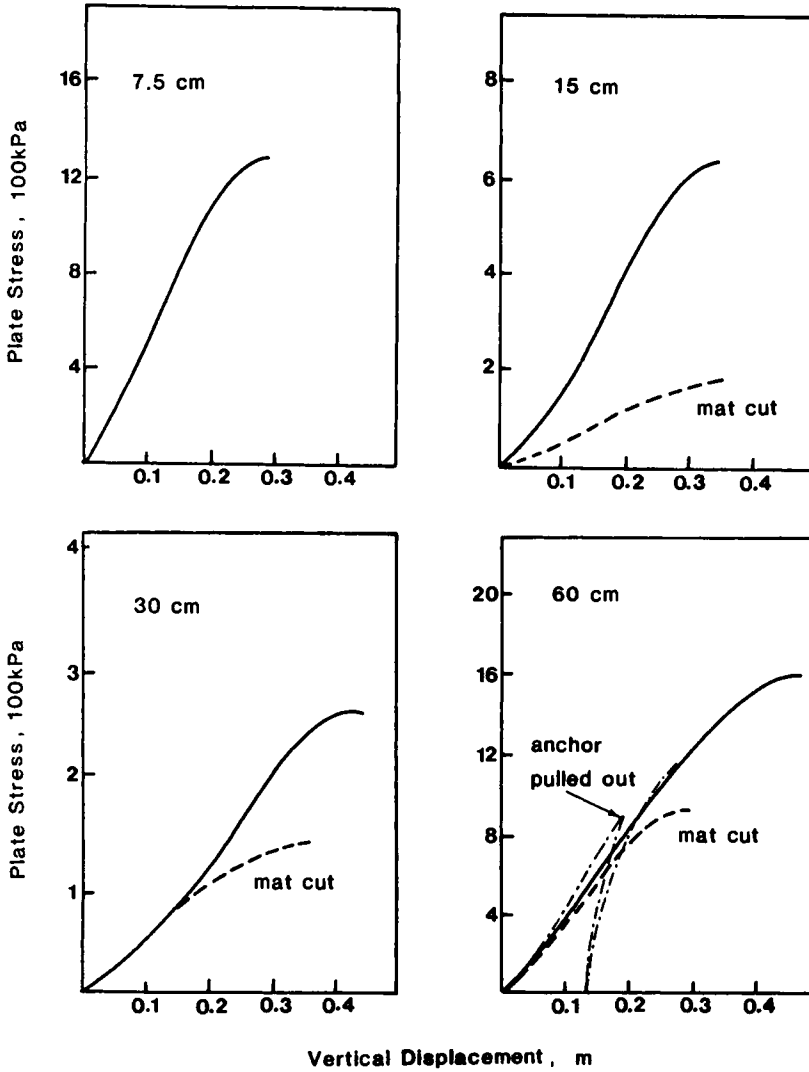


Fig. 2.16. Plate bearing test results. (Lee and Jarrett, 1977).

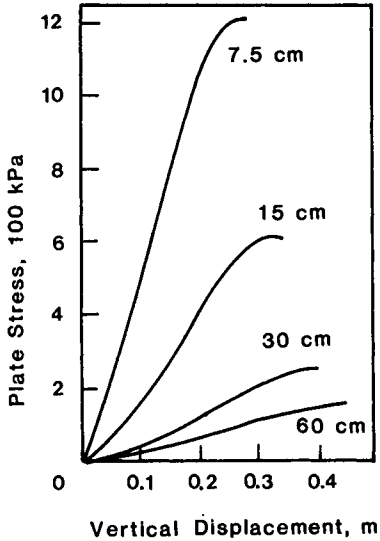


Fig. 2.17. Averaged results for plate bearing test. (Lee and Jarrett, 1977).

Lee and Jarrett (1977) suggest the following model, for bearing capacity of muskeg, Fig. 2.18.

$$Q = P + T$$

$$T = f_t \cdot \pi(D + h) \cdot h \quad (2.10)$$

$$P = 5.5 \cdot \tau_f \cdot \pi(D + h)^2 / 4$$

where Q = total plate load at failure;

T = tensile load in surface mat at failure;

P = bearing capacity of the underlying peat at failure;

f_t = direct tensile strength of the live mat and

τ_f = vane shear strength of the peat layer.

It should be noted that muskeg is anisotropic: thus it is important to note both characteristics and properties of the mat in terms of a referential set of axes since this is important in determining the directional strength of the mat.

Traction properties at the tractive element-terrain surface interface can be obtained by using an annular shear ring (Wong et al., 1979). Typical shear stress-displacement relationships are shown in Fig. 2.19. These relationships are seen to be a function of annular ring geometrical dimensions, grouser spacings in the annular ring and heights of the grousers, normal pressure and annular ring material type. The use of the plate and annular ring techniques for prediction of vehicle performance is discussed in Chapter 4.

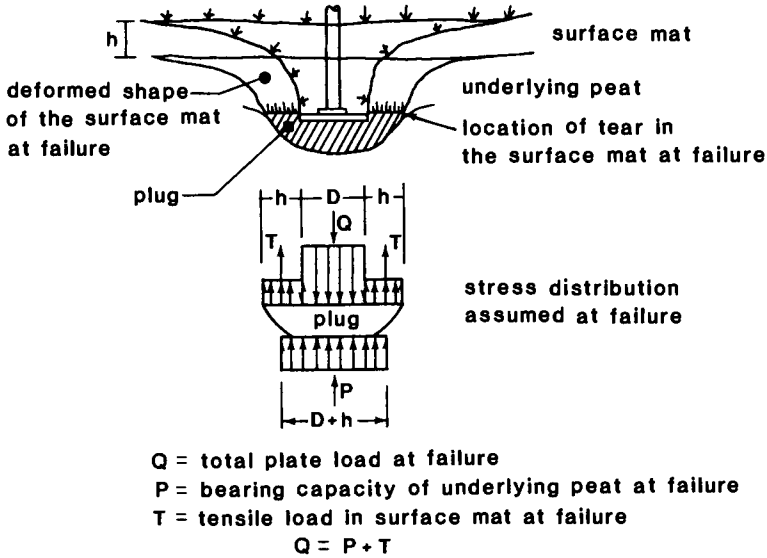


Fig. 2.18. Lee and Jarrett (1977) model for calculation of bearing capacity of muskeg.

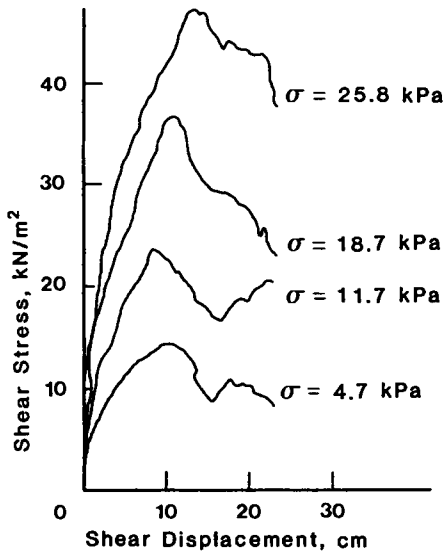


Fig. 2.19. Shearing characteristics of muskeg mat using an annular shear plate with grouser height of 1 cm and grouser spacing of 30°.

The standard size shear vanes used in soil engineering cannot be used for determining the shear strength behaviour of the living mat, not only because of its small size but principally because the action of the shear vane in the shear process does not develop the means for sensing the tensile capability of the fibres in the living mat. On the other hand, if the peat layer beneath the mat consists of soil particles to the extent that this layer behaves as a soil-type layer, the vane shear device could be usefully employed to sense the shear strength of this layer. Under these circumstances, it is important to note that the measured strength of the peat layer is a function of vane size (Radforth, 1969), as shown in Fig. 2.20.

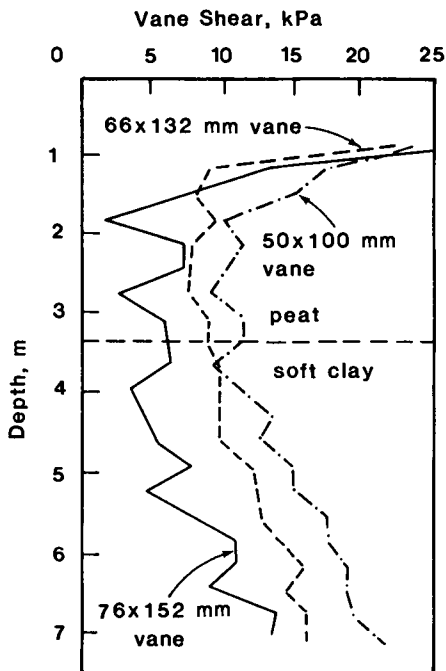


Fig. 2.20. Vane shear profiles for three vane sizes.

Whilst the standard cone penetrometer has been used to provide trafficability predictions on muskeg, we should note that the same limitations cited for the shear vane apply equally well for cones. It is indeed not possible for the cone to test the tensile strength capability of the living mat. Values obtained as cone indices do not provide any real insight into the mechanisms generating the value measured. In that sense, and because the test is not a rational test - when used indiscriminately on the fibrous living mat - the technique can only be used with empirical correlations.

It should be stated that the cone index is only an empirical indication and not a measure of the shear strength of the muskeg terrain. If the peat layer below the living mat behaves as a soil layer, the cone might be used as a sensing tool. Figure 2.21 shows a typical cone index profile for a muskeg terrain. Note that whilst the high penetration resistance measured shows the presence of the living mat, we have no proper indication of the strength of the fibres. Since the peat layer below shows characteristics not unlike that of a cohesive soil, the peat layer shows a constant cone index with depth, confirming the fact that this layer behaves like a soft cohesive soil.

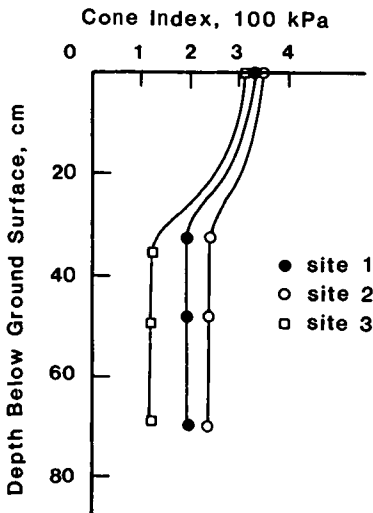


Fig. 2.21. Typical cone index profile for a muskeg terrain, Petawawa, Ontario.

2.4 SNOW TERRAIN

For proper, continuous, vehicular travel on snow-covered terrain, the following conditions need to be fulfilled:

- (a) stable snow compression, i.e. stable compression of the underlying (supporting) snowpack to provide for support (flotation) of the vehicle, and
- (b) integral traction (minimal slip) between the vehicle tractive element (track or wheel) and snow to allow for generation of propulsion.

Apart from terrain impedances such as obstacles, terrain roughness and topographic slope, the snow parameters which affect vehicle trafficability are generally the same as those which affect the strength and deformation of snow. From an engineering point of view, snow may be classified into four types. These are (a) fresh snow, (b) granular snow, (c) semi-bonded snow, and (d) sintered snow,

as shown in Fig. 2.22. These types of changes in snow type occur with time and temperature, as shown in Fig. 2.23. The significant point to note is the bonding which develops as snow matures. Fresh snow becomes sintered with time. The granularity of snow develops with time - defined as ageing - and the particles become semi-bonded, as shown in Fig. 2.22c. With increasing time, this snow becomes sintered snow, as seen in Fig. 2.22d. This transformation of snow type which is often accompanied by changes in density and grain characteristics is seen to be a function of time, temperature and pressure.

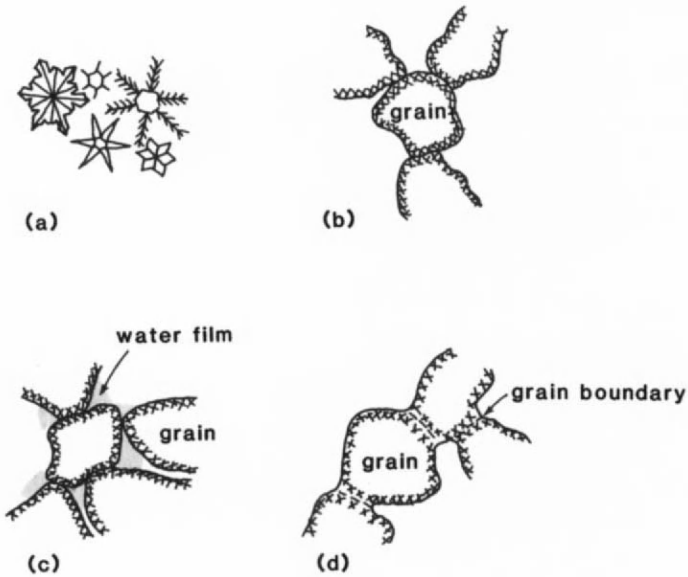


Fig. 2.22. Various snow models, showing (a) fresh snow with original crystal shape, (b) granular snow, (c) semi-bonded snow with water film, and (d) sintered snow.

Figure 2.23 illustrates the various stages and processes of snow ageing. This type of rough classification provides one with an initial idea of the strength, deformation and likely response characteristics of the snow. Obviously for detailed and more precise information, both field and laboratory tests are needed to derive the appropriate mechanical properties of the snow being studied.

The snow parameters which could affect trafficability of vehicles on snow are:

(i) Density. Snowpack density is a very popular measurement in snow classification schemes but tells little about the snowpack without knowledge of grain size, in situ temperature and thermodynamic history. Deposited snow ranges in density from less than 0.1 g/cm^3 for fresh, fluffy masses to dendritic crystals, to more than 0.7 g/cm^3 for snow which has been soaked with water or densified.

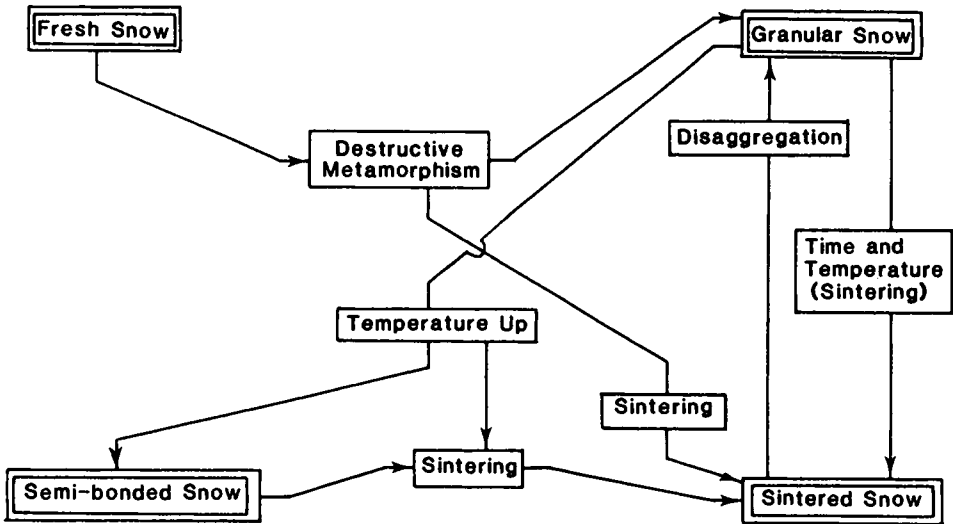


Fig. 2.23. Transformation diagram for snow type.

Density of snow is defined as:

$$(\text{g/cm}^3) = \frac{\text{snow mass}}{\text{volume of snow mass}}$$

By and large, snowpack density varies with age and normally has a profile of values increasing from the surface downward. A knowledge of this is important not only from the density variation point of view, but also from the viewpoint of detailing with respect to stratigraphy. Since initial vehicle flotation relies on snowpack stability vis-a-vis bearing support, structural configurations in the snowpack are important considerations. Figure 2.24 shows the normal stress-density relationship for confined compression with controlled deformation rates (Yong and Harrison, 1978). Curve A indicates the typical deformation rate compression test on initially semi-bonded loose snow, while curve B shows a typical result obtained from high compression rates.

Figure 2.25 shows the stress-density relationship for snows with varying initial density, tested at a common constant strain rate of 0.075% per second and at a temperature of -13°C . Figure 2.26 shows a typical relationship for the effect of snow density on the unconfined compressive strength of snow. The inter-relationships from these Figures, described between stress, strain-rate, initial and threshold densities, are seen in the three-dimensional representation shown in Fig. 2.27. Note that there is a limiting density developed in the snow, under compression, which is a direct function of the snow type and the load applied. This is identified as the threshold density. Quite obviously, the density

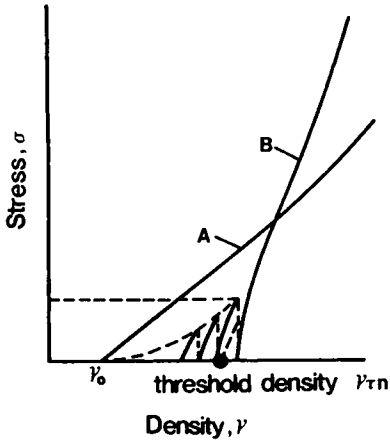


Fig. 2.24. Typical stress-density relationships for confined compression under controlled deformation rates. (A) No-fracture performance at low deformation rates. (B) Micro-fracture region preceding threshold density at high deformation rates.

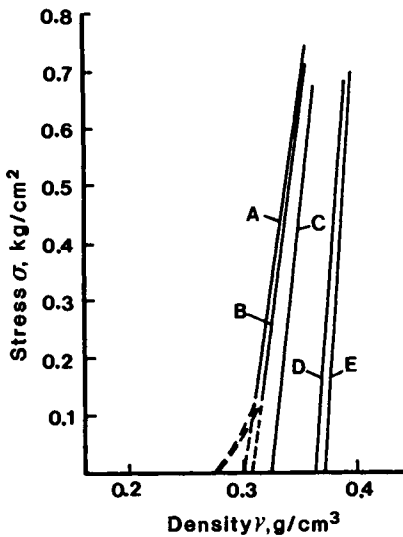


Fig. 2.25. Stress-density change curves as a function of initial density; constant test strain rate of 0.075% per second at -13°C temperature. Initial densities: A and B = 0.281 g/cm^3 ; C = 0.323 g/cm^3 ; D = 0.364 g/cm^3 ; E = 0.371 g/cm^3 .

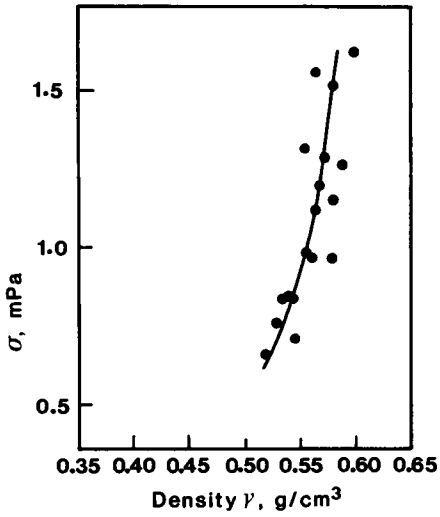


Fig. 2.26. Unconfined compressive strength as a function of density for Peter snow aged 13 days or more.

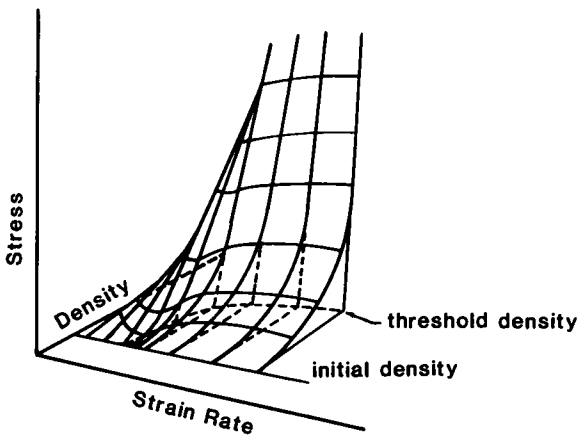


Fig. 2.27. Threshold density surface.

increase with load becomes lesser as the limit density approaches that of ice. Thus the threshold density in actual fact really reflects a limit value of density dependent specifically on the type of snow. The shape of the surface shown in Fig. 2.27 can therefore be said to be indicative of the type of snow being examined.

(ii) Grain size distribution. This is an important factor relative to shear strength and potential or actual bonding. It is also a factor in the density of the pressure bulb which forms beneath the vehicle traction element. The grain size distribution characteristics of a snow pack are affected by age, temperature variations, climatic conditions during and after deposition, and pressure due to snow selfweight or external loads. Table 2.2 (Harrison, 1981) shows a grain size range of deposited snow. Practical experience indicates that the highest strengths are achieved when the snow is well-graded - not unlike the situation of coarse-grained soils (i.e. sand). However, if the snow becomes coarse-grained, the snow will likely be cohesionless and weak (Mellor, 1964).

TABLE 2.2

Grain size definitions of snow

Term	Symbol	Grain size range (mm)
Very fine	a	less than 0.5
Fine	b	0.5 to 1.0
Medium	c	1.0 to 2.0
Coarse	d	2.0 to 4.0
Very coarse	e	greater than 4.0

(iii) Temperature. Local temperature has a pronounced effect on the strength properties of snow. Because of day/night effects it is not uncommon for the near surface layer in a snowbank to vary 20°C in a 24-hour period. In conjunction with elapsed time, the variations in temperature which contribute to the thermodynamic history of snow pack will thus create related changes in snow resistance properties.

(iv) Depth. Whilst a knowledge of the depth of the snow pack gives only documentary information by itself, it becomes extremely important when coupled with the size of the loading (tractive) elements associated with a vehicle. In vehicle operation in a snow pack, the effects of vehicle sinkage compress the snow significantly. This compressed layer can act as a proper bearing layer if the bottom boundary is significantly distant from the loading boundary. On the other hand, if the bottom boundary is a near-boundary, the snow layer becomes significantly confined and bearing (flotation) is provided by both the immediate snow layer and the substrata below. Vehicle performance under the two preceding conditions are identified as oversnow and throughsnow respectively. The performance characteristics of vehicles vary widely between oversnow and throughsnow because of the mechanisms developed in the production of traction.

In deep snow, the pressure bulb formed from tractive element loading will not extend into the bottom boundary (ground) as seen in Fig. 2.28. This situation

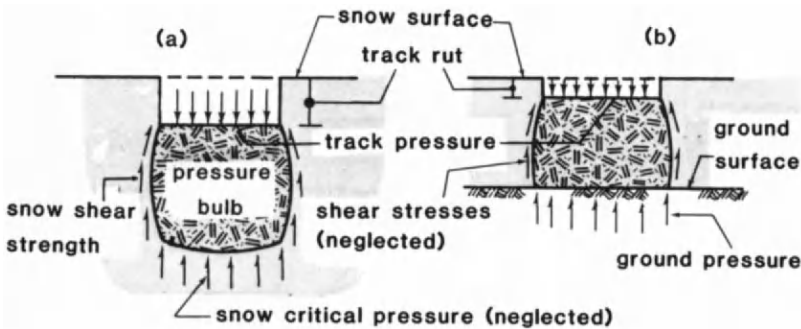


Fig. 2.28. Pressure bulb beneath a tractive element (track). (a) Deep snow. (b) Shallow snow.

identifies the oversnow performance of a vehicle. The compression pressure bulb will extend downward to the point at which snow pressure reaches a critical value indicative of the snow response property - i.e. that load which the snow can support without significant plastic deformation. Since only small pressures are required to produce plastic compaction, the snow critical pressure is generally small in comparison to the loading transmitted by the tractive element. Consequently the compression stresses developed in the pressure bulb are supported primarily by the shear stresses on the bulb walls (Brown, 1981).

In the case of throughsnow performance of a vehicle, the snow layer is relatively shallow, and the compression pressure bulb extends into the bottom boundary. Thus, the pressure bulb receives a significant amount of bearing support from the ground, and the shear stress support from the bulb walls becomes a lesser significant consideration. The effect of shear stresses on the bulb wall can thus be neglected, especially when the tractive element width is larger than the snow layer.

2.5 OTHER TERRAIN EFFECTS

2.5.1 Terrain cover

If the strength and deformation of terrain material can provide the necessary flotation and traction to keep a vehicle in constant travel and produce the required pull force, terrain cover characteristics can constitute another factor which could restrict vehicle travel speed, or even cause total vehicle immobilization. Terrain cover factors can be identified as (Fig. 2.29), (i) ground slope, (ii) obstacles (mounds and ditches), (iii) vegetation, (iv) visibility, and (v) roughness.

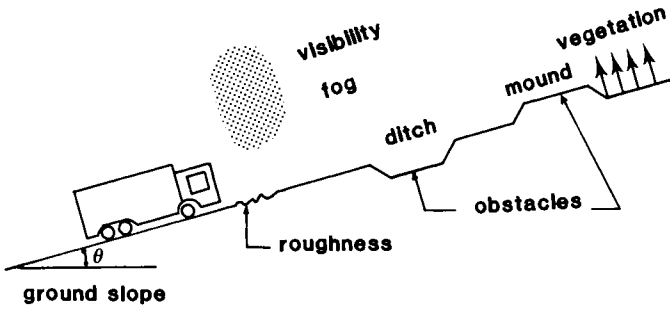


Fig. 2.29. Types of terrain cover.

(i) Ground slope. The maximum ground slope which a vehicle can climb is an important performance criterion, especially for off-road vehicles operating in mining areas or construction sites where significant ground slopes can be encountered. Vehicle motion resistance increases because of the gravitational component of the vehicle along the slope (Fig. 2.30), where redistribution of vehicle weight on its tractive elements results. The overturning moment due to vehicle weight component along the slope and the height of the vehicle centre of gravity can be cited as the cause for redistribution of the vehicle weight on its tractive elements.

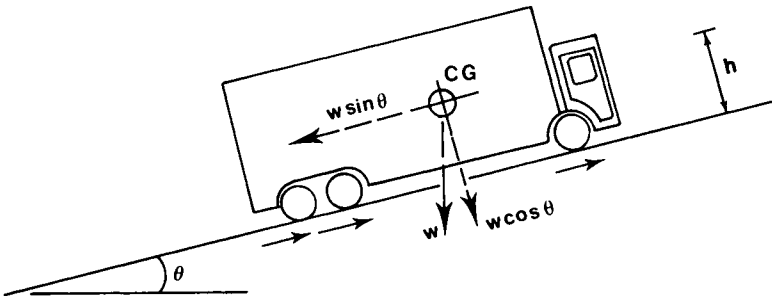


Fig. 2.30. Vehicle body forces.

(ii) Obstacles. These include surface features such as boulders, stumps, logs, dikes, potholes, mounds, ditches, etc., which cause impediments to vehicles. These will cause a vehicle to over-ride slowly or implement procedures to circumvent the obstacle. Manoeuvring around obstacles will generally require additional traction forces to account for steering, in particular for any dis-

tance between any two obstacles not less than two vehicle lengths.

Two criteria are required for a vehicle to over-ride an obstacle. These are:

(1) The requirement that there be no interference between the obstacle and the bottom profile of the vehicle.

(2) The requirement that there is enough traction at the tractive element-soil interface (assuming that the vehicle engine has unlimited power). Figure 2.31 shows a schematic representation of how some of these obstacles might appear in a vehicle-ride situation.

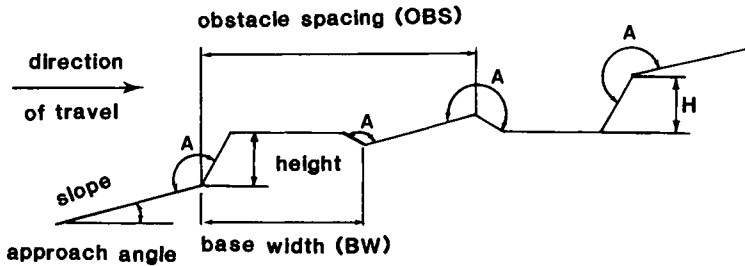


Fig. 2.31. Obstacle dimensions.

(iii) Vegetation. This may be considered as a type of obstacle. Resistance to vehicle motion is caused by vegetation when the vehicle attempts to over-ride it, and it is generally categorized on the basis of stem diameter. Alternatively, as in the case of obstacles, manoeuvring around vegetation will be required, thus necessitating additional traction forces.

(iv) Visibility. This is also referred to as driver recognition distance, and is a weather characteristic for the terrain under consideration. Visibility controls the maximum speed at which a driver may proceed, subject to any one of these factors, (a) vehicle braking force, (b) vehicle tractive force on the corresponding terrain surface, (c) vehicle deceleration of not more than twice the gravitational acceleration.

(v) Roughness. This can be defined as ground surface irregularities. When a vehicle travels on such ground surfaces, the resultant vibrations generated are generally felt in the vertical direction. The magnitude of the vibrations is measured in terms of "instantaneous" acceleration, or calculated from accelerometer readings in terms of the generated power. The generated vibrations are a function of terrain roughness, terrain material dynamic properties, vehicle dynamic characteristics and translational speed. From human engineering tests on power absorbing capabilities of drivers of vehicles, it has been established that there is a limiting power which the human body can absorb, beyond which sensible conduct will no longer prevail. Translated into vehicle terms, we note

that the maximum speed which a vehicle can travel on a rough terrain is the speed at which the generated absorbed power at the driver seat is six watts (Murphy and Ahlvin, 1976).

Surface roughness can be described using statistical methods for reducing data of continuous profile of ground surface (power spectral density). Terrain data are collected in terms of elevation and regular station intervals using land survey or aerial photography techniques. Figure 2.32 shows a technique for calculating the root mean square (RMS) of a rough terrain.

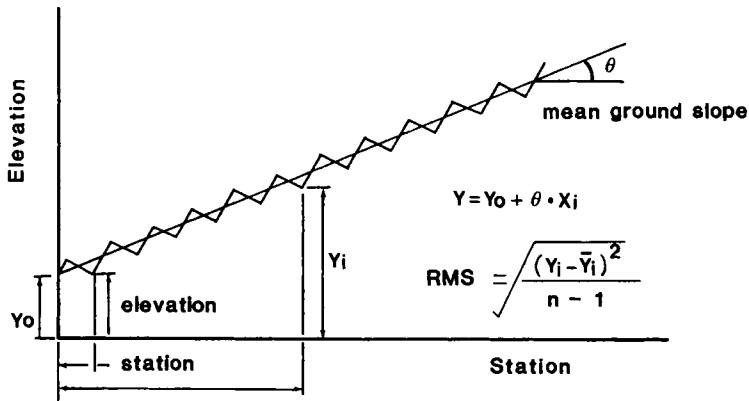


Fig. 2.32. Example of terrain roughness characterization for RMS.

2.6 SUMMARY

There are five major classes of soil types for trafficability purposes. These are (a) cohesive, (b) cohesionless, (c) mixed soil, (d) muskeg, and (e) snow. The characteristics of these types of material for trafficability purposes differ widely and must be assessed if proper performance of the vehicle is to be desired. Methods for calculating their basic properties together with the methods for soil, muskeg and soil classification are presented in this Chapter to permit one to evaluate the terrain characteristics. In addition to terrain cover properties and characteristics, we should note that the types of impediments which could immobilize the vehicle or limit its performance are terrain roughness, obstacles, and visibility.

REFERENCES

- Adams, J.I., 1965. The engineering behaviour of a Canadian muskeg. Proc., 6th Int. Conf. on Soil Mech. and Found. Eng., 1:3-7.
- Bekker, M.G., 1969. Introduction to Terrain Vehicle Systems. University of Michigan Press, 846 p.
- Brown, R.L., 1981. Application of energetics to vehicle trafficability problems. ISTVS Workshop on Snow Traction Mechanics, Alta, Utah, CRREL SR 81-16, pp. 25-38.
- Casagrande, A., 1966. Construction of embankments across peaty soils. J. Boston Soc. Civ. Engrs., 53:3, pp. 272-317.
- Harrison, W.L., 1981. Snow measurements in relation to vehicle performance. ISTVS Workshop on Snow Traction Mechanics, Alta, Utah, CRREL SR 81-16, pp. 13-24.
- Irwin, G.J. and Yong, R.N., 1980. Demonstration of a portable device for predicting vehicle tractive performance in snow. J. Terramechanics, 17:4, pp. 197-206.
- Knight, S.J. and Rula, A.A., 1961. Measurement and estimation of the trafficability of fine-grained soils. Proc., 1st Int. Conf. Mech. Soil-Veh. Systems, Torino, pp. 371-386.
- Knight, S.J. and Meyer, M.P., 1961. Soil trafficability. Classification scheme. Proc., 1st Int. Conf. Mech. Soil-Veh. Systems, Torino, pp. 567-574.
- Lea, N.D. and Brawner, C.O., 1963. Highway design and construction over peat deposits in lower British Columbia. Highway Research Record No.7, Nat. Res. Council, Pub. 1103, pp. 1-33.
- Lee, R.A. and Jarrett, P.M., 1977. Plate bearing tests on a fibrous peat. Proc., 17th Muskeg Research Conf., pp. 151-164.
- MacFarlane, I.C., 1958. Guide to a Field Description of Muskeg. Nat. Res. Council ACSSM Tech. Memo 44, 36 p.
- MacFarlane, I.C., 1969. Engineering characteristics of peat. Muskeg Eng. Handbook, Ed. I.C. MacFarlane, University of Toronto Press, pp. 78-126.
- Mellor, M., 1964. Properties of snow. Cold Regions Science and Engineering, Part III, Engrg. Sect. A., Snow Engrg. U.S. Army Material Command, CRREL, pp. 528-559.
- Murphy, N.R. and Ahlvin, R.B., 1976. AMC-74 Vehicle dynamics module. Tech. Rept. M-76-1, U.S. Army WES, Vicksburg, 76 p.
- Radforth, N.W., 1952. Suggested classification of muskeg for the engineer. Eng. J., 35:11, pp. 1199-1210.
- Radforth, N.W., 1969. Muskeg as an engineering problem. Muskeg Engrg. Handbook, Ed. I.C. MacFarlane, University of Toronto Press, pp. 3-30.
- Traffic Research Team, 1961. Forecasting the trafficability after traffic for sand-possessing structures. Proc., 1st Int. Conf. Mech. Soil-Veh. Systems, Torino, pp. 87-96.
- Wong, J.Y., Graber, M., Radforth, J.R. and Dowell, J.T., 1979. Characterization of the mechanical properties of muskeg with special reference to vehicle mobility. J. Terramechanics, 16:4, pp. 163-180.
- Yong, R.N. and Warkentin, B.P., 1975. Soil Properties and Behaviour. Elsevier Scientific Publishing Co., Amsterdam, 451 p.
- Yong, R.N. and Harrison, W.L., 1978. On vehicle mobility in snow-covered terrain - 1. Problem development and requirements for analysis. J. Terramechanics, 15:4, pp. 223-235.
- Yong, R.N., Youssef, A.F. and Fattah, E.A., 1975. Vane-cone measurements for assessment of tractive performance in wheel-soil interaction. Proc., 5th Int. Conf. Int. Soc. Ter. Veh. Systems, Detroit, 3:769-788.

NOMENCLATURE

C	cohesion
P	bearing capacity at failure
Q	total plate load at failure
S_r	saturation degree (%)
T	tensile load at failure
V	total volume
V_a	volume of gas
V_s	volume of solids
V_v	volume of voids
W	total weight
W_w	weight of water
b	plate radius
e	void ratio
f_t	direct tensile strength of the live mat
n	porosity
p''	bearing pressure of the sublayer
t_o	surface mat thickness
γ	unit weight of soil
γ_d	dry density of soil
γ_{tn}	threshold density
γ_w	density of water
σ	total normal stress
τ	shear strength
τ_f	vane shear strength of the peat layer
τ_v	mat shear strength
ω	water content

Chapter 3

MOBILITY ELEMENTS AND REQUIREMENTS

3.1 ELEMENTS OF VEHICLE TERRAIN INTERACTION

The primary purpose of a vehicle tractive element is to provide sufficient (a) flotation and (b) traction required for moving a vehicle between two points. For conventional off-road vehicles, tractive elements provide traction and flotation as driven tyres or tracks, or provide flotation only as towed tyres or tracks.

For non-conventional vehicles - such as hybrid air cushion systems, flotation is provided by an air cushion and propulsion is provided by either driven wheels or propellers. For screw-type swamp vehicles, traction and flotation are provided by Archimedes' screw. Figure 3.1 illustrates the different types of vehicle-terrain interaction elements.

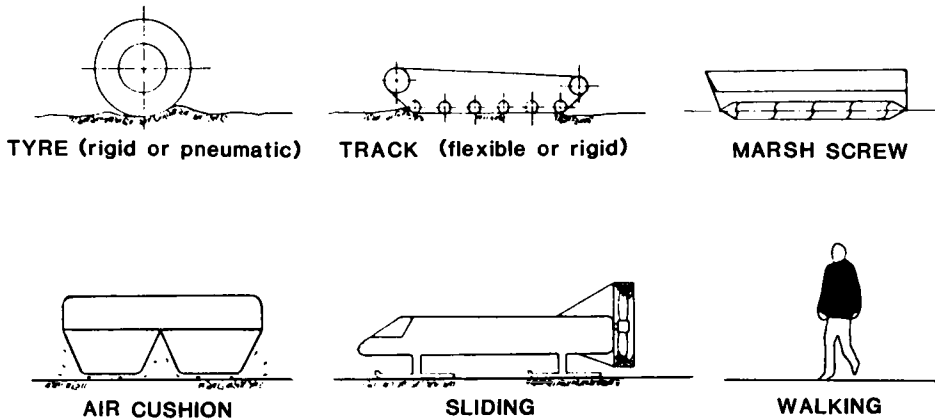


Fig. 3.1. Types of tractive elements.

3.1.1 Flotation

Flotation is defined as the ability of a vehicle to travel without excessive sinkage. Sinkage is controlled by vehicle clearance, beyond which the drag forces become excessively large, and the vehicle will be immobilized. The amount of allowable sinkage is controlled by the condition under which the vehicle operates. For example, agricultural or forestry sinkage should be minimal to avoid any change in the physical characteristics of soil. Swamps, desert or snow terrains have no set criteria to define the permissible amount of sinkage. In gen-

eral, the amount of sinkage should be minimal to avoid any unexpected environmental detrimental effects.

3.1.2 Traction

Traction can be defined as the ability of the vehicle tractive element to generate enough forces to overcome all types of vehicle resisting forces. These tractive forces should be generated without excessive slip or terrain surface damage, and should be in equilibrium with the torque produced at the wheel hub or track driving sprocket. The objectives of tractive elements, in addition to flotation and traction, are to provide (a) braking, (b) steering, (c) obstacle or slope climbing ability, and (d) a mount to absorb shocks.

3.2 FLOTATION AND TRACTION ELEMENTS

Different types of tractive elements are used with off-road vehicles. These are:

3.2.1 Rigid wheels

Rigid wheels have been used since ancient civilization as a means of transferring vehicle load to ground during travel. They require a minimum amount of maintenance, but are generally penalized by their heavy weight, and high noise and vibrations when used on rough surfaces. Rigid wheels have been used for early models of agricultural tractors and are still being used for some construction equipment (roller-compaction) where the vehicle velocities are very low. For high speed vehicles, rigid wheels cannot be used since the shock and vibration generated from the uneven roughness of the terrain surface can be detrimental to the vehicle and on ride comfort. Nowadays, rigid wheels are by and large limited only to railways where the smoothness of rail and wheel surface provide a situation where high speed with ride comfort can be achieved.

3.2.2 Tyres

A tyre forms a torus of a complex flexible reinforced composite material surrounding a steel hub and filled up with air under pressure. It has more or less expanded ribs on the rolling tread. The different types of torus shapes and construction are selected according to the type of tyre application. In general, a tyre is characterized by the tyre construction type, (Fig. 3.2), mounting data, ply rating and other dimensions such as that shown in Fig. 3.3.

The type of application (of tyres as traction elements) can be divided into four broad categories, each of which is comparatively unique (Finney, 1961).

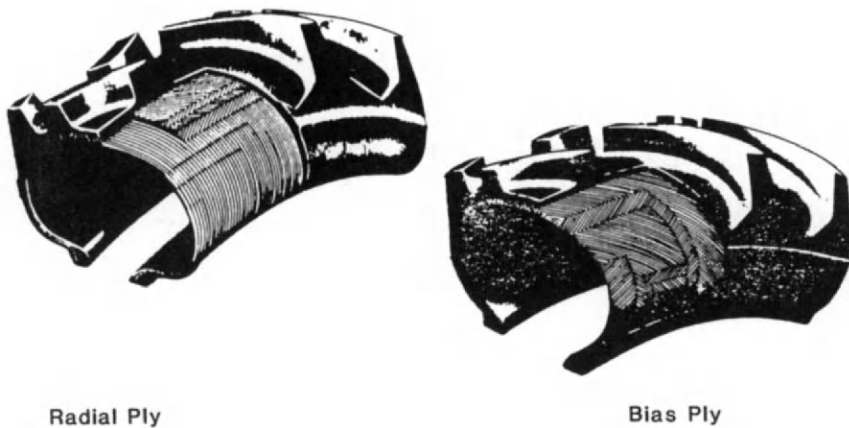


Fig. 3.2. Tyre construction type (Turnage, 1978).

(1) In the construction field, as typified by dam, waterway and highway projects which require movement of large quantities of earth and rock. In this type of service, speeds as high as 40 to 80 km/hr, length of haul to 16 km, and size of loads and equipment to 75 cu. m capacity, are generally expected.

(2) In the logging, mining and petroleum industries - heavier units such as mobile cranes and self-contained pumps and power plants, are used. This demands tyre types with high flotation characteristics and load-carrying capacities.

(3) In military operations. In this field the various types of tyred vehicles are expected to operate over a great variety of surfaces in cross-country transport. Reliability is of particular importance.

(4) In general transportation into newly developed areas without adequate highways or railways - such vehicles must have flotation and mobility capability under heavy loads, without the need for extensive preparation and maintenance of roads or tracks.

3.2.3 Tyre sizes and types

The growth of off-road operations has brought about a great diversification in tyres to meet all service requirements.

(i) Number of sizes. Tyres have become larger both in cross-section and in rim diameter. Larger tyres permit higher loads per tyre without sacrificing flotation.

(ii) Conventional vs wide base. Two types of tyres now exist (D'Avello, 1964) namely, conventional and wide base. Figure 3.4 illustrates the differences between these two types of tyres. Without changing rim diameter or tyre overall diameter, the cross-section width can be increased by using a wider rim. With

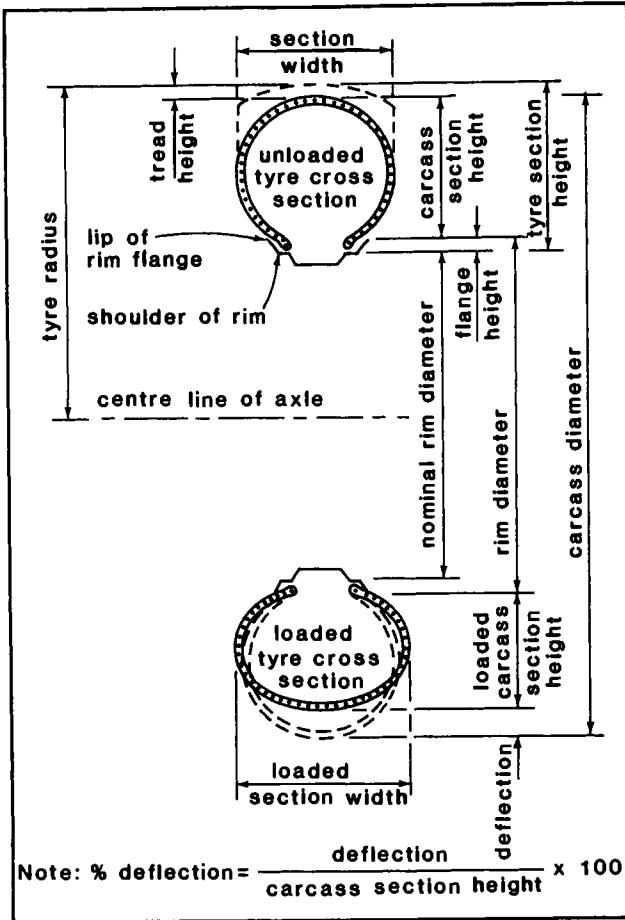


Fig. 3.3. Tyre geometrical characteristics (adapted from Meyer, 1977).

the same tyre loadings, inflation pressures on the wide-base tyre can be reduced. The wider cross-section gives improved traction and flotation and the lower unit ground pressure can improve the resistance to damage from stones and other objects.

(iii) Low section-height tyres. The wide base principle can be extended into low section-height tyres. Figure 3.5 compares two tyre types. The low section-height shape makes possible a wider cross-section for improved flotation without increasing overall diameter or tyre weight, as would have been necessary if conventional tyre shapes had been maintained.

(iv) Single vs dual. Another application of the low-section height principle is in the use of larger single tyres to replace dual tyres, (Fig. 3.6). Although

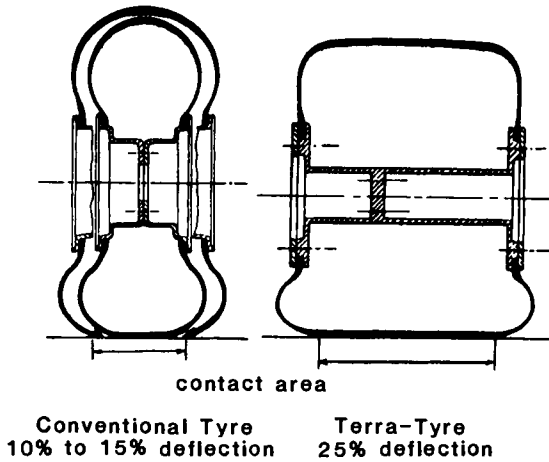


Fig. 3.4. Conventional and wide-base tyres. (D'Avello, 1964).

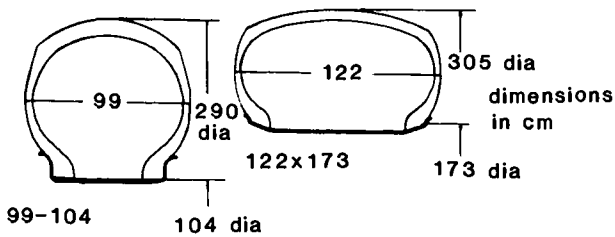


Fig. 3.5. Example of low section-height off-highway tyre. (Finney, 1961).

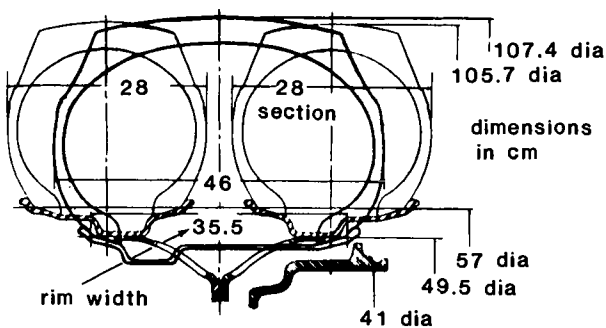


Fig. 3.6. Sand tyre. Single to replace dual. (Finney, 1961).

the change from dual tyres to one large single tyre reduces total ground contact area, experience has shown that flotation and mobility are improved without reduction in total load-carrying capacity, (Finney, 1961).

(v) Tread pattern. All off-highway operations do not need the same degree

of traction. As a result, separate tread designs are used for different degrees of tractive effort.

3.2.4 Tyre traction

(i) Maximum traction. Figure 3.7a shows a representative tread pattern designed for maximum traction requirements, as in agricultural tractors, earth moving or excavation operations. Figure 3.7b shows a variation of this pattern in which deep grooves have been added to the traction elements to reduce rubber mass and provide lower tyre operating temperatures in high-speed service.

(ii) Medium traction. Figure 3.7c illustrates a medium traction design used mainly in military operations, and Fig. 3.7d shows a design which is supposed to provide extra traction in off-road operations whilst still performing satisfactorily if used part of the time on the highway.

(iii) Free-rolling. Figures 3.7f and 3.7g show two types of tread design widely used on free-rolling wheels.

(iv) Special requirements. Unusual service conditions sometimes demand a special choice of tread pattern. In muskeg and deep snow operation, high flotation and traction are required and hence terra tyres (Fig. 3.7e) are used. In desert operations maximum traction is necessary but the use of an aggressive design is not always recommended because the tyre may tend to "dig in", and become stuck when a "no-go" situation is encountered (in soft sand). In this case, a ribbed design, such as in Fig. 3.7h, could be used where the lack of traction elements is offset by the large ground contact area. Snow has problems similar to soft sand. Figure 3.7i illustrates a shallow-depth design which has been successful on powered as well as free-rolling wheels.

Tyres must possess the characteristics of durability, load carrying ability, speed capability and low operating temperature - to the degree which service requirements demand. High tensile cord materials must be used as reinforcement to provide sufficient strength and flexibility to the tyres, and tyre material should be characterized by toughness and high abrasion resistance and low heat generation during operation.

3.2.5 Tracks

Tracked vehicles are the ones which transmit loads to the ground through a system of wheels running over a mobile road which is the track. The track is simply an endless belt or chain driven by a sprocket (front or rear). Generally, there are two types of stiffness classification for tracks, (a) flexible, and (b) rigid. This stiffness is a function of track construction material (steel-rubber), tension in the track belt, road wheels characteristics, spacings and suspension system. Tracked traction systems are generally used in vehicles which



(a)



(b)



(c)



(d)



(e)



(f)



(g)



(h)



(i)

Fig. 3.7a-d and f-i. Offroad tyre types (Finney, 1961). Fig. 3.7e. Terra tyre for muskeg and snow (Gasslander, 1982).

have to operate on very soft soils whilst carrying large loads. Tracks have adverse characteristics when compared with wheels from the point of view of steerability, manoeuvrability, noise, maintenance and limited speed. They do however, have the advantage of high flotation and traction.

For construction equipment such as cranes and excavators supported on smooth rigid tracks with maximum contact length, (angles of attack and escape are minimum), better stability and flotation are required since they are more critical in these types of services than high traction or speed. Earth-moving vehicles are generally required to generate high drawbar-pull forces. Hence they are equipped with tracks which can provide high flotation and traction. In this case, tracks are equipped with grousers with different patterns in order to provide high traction. Vehicles operating on snow or muskeg are equipped with light rubber flexible tracks for high flotation and traction. Vehicles operating in various terrain conditions which require mobility and high speed have tracks which are characterized by flexible tracks with small pitch, high abrasion resistance and toughness to minimize the effect of noise and vibrations on the vehicle body. Tracks should have high durability, minimum joint friction resistance, and have different surface tread patterns, grouser shapes for better traction and flotation.

3.2.6 Air cushion vehicle

These types of vehicles are supported on a cushion of air, by forcing it through special skirts mounted beneath the vehicle. In this case the ground pressure and the air escape velocity beneath the vehicle skirts are in the range of 4 kPa and 50 m/sec respectively.

Air cushion vehicles can be operated successfully over swamps, snow, or cohesive soil, but cause excessive dust generation and soil erosion on loose soil. For forward motion, steerability and braking, these vehicles should be equipped with other systems for traction such as tyres, tracks or propellers. Figure 3.8 illustrates these types of hybrid air cushion vehicle.

3.2.7 Walking elements

Whilst walking locomotion is the most efficient method for traction, its direct use as a vehicle-ground surface tractive mechanism is still in the research stage. The difficulty of obtaining uniform stable motion using walking mechanisms is due to (a) difficulty of synchronization between the different legs, (b) stability of the vehicle, especially if the number of legs is small, (c) different directions of mass forces of the different vehicle legs, (d) impact effect when the feet contact the ground and the momentum generated when leaving the ground, (e) high torque required for moving leg joints, (f) braking, and (g) steering. Figures 3.9a and 3.9b show the available suggested walking mechanisms.

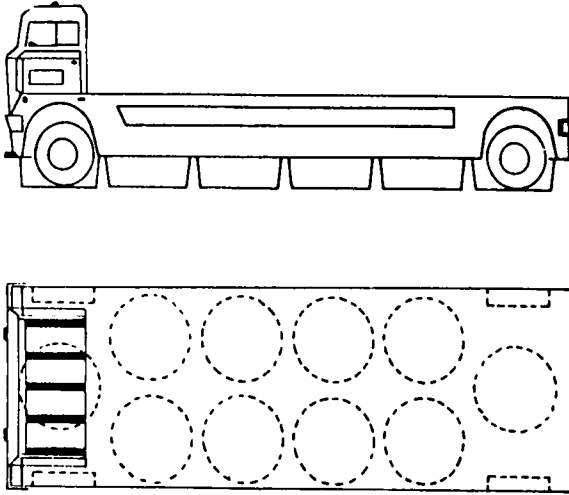


Fig. 3.8. Hybrid air cushion-wheeled vehicle (Adapted from Bertin and Berthelot, 1967).

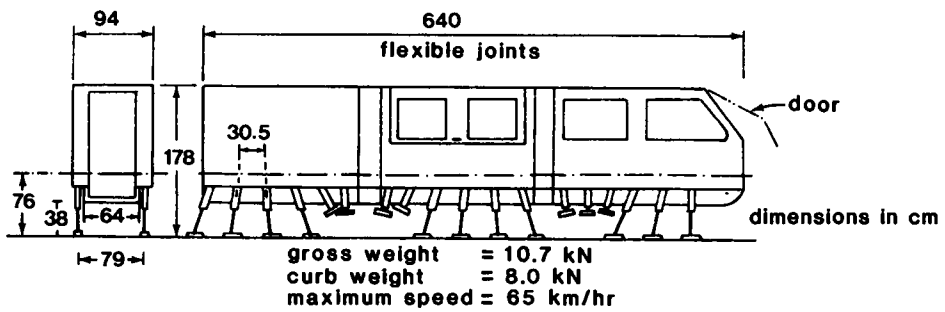


Fig. 3.9a. Proposal for a multi-legged walking vehicle (Siddall, 1964).

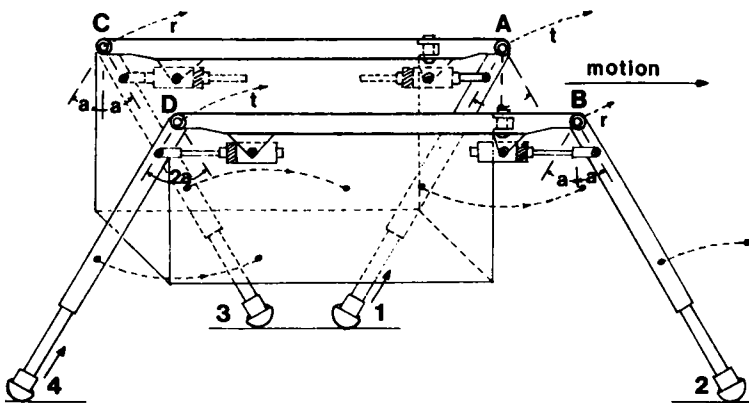


Fig. 3.9b. Schematic diagram of Maratori's 'Golden Horse' (Liston, 1964).

3.3 TERRAIN SUPPORT AND INTERFACE REQUIREMENTS

Interaction between vehicle and terrain which is achieved through the running gear system - wheel system, track/device, or some other equivalent system - will produce reaction and responses at the terrain interface. For optimum mobility purposes, it is desirable that the vehicle be able to move from one point to another with the least amount of wasted motion and energy input. To achieve this, the vehicle must not only be supported by the terrain (flotation) but must also provide sufficient resistance capability wherein thrust can be developed between the running gear and terrain material itself with minimal slip loss. The greater the ability of the terrain material and the interactions at the interface to transfer the thrust action into the substrate - the better is the capability of the vehicle to achieve maximum tractive effort.

Immobilization of a vehicle can arise as a result of lack of ground support or lack of strength in the terrain to provide the means for development of thrust. The result of these deficiencies can be demonstrated in terms of (a) sinkage immobilization, i.e. lack of flotation, where the vehicle sinks into the supporting terrain because of its inability to support the vehicle, and (b) slip immobilization where the vehicle cannot propel itself forward because of its inability to transfer the thrust from surficial slip motion to substrate thrust. Note that with proper design considerations, slip immobilization can be minimized - provided that terrain support capability is available. One should also observe that there are obviously combinations between the two primary mechanisms for immobilization - e.g. the phenomenon of a vehicle "digging" itself into the ground because of initial excessive slip development.

In the assessment of trafficability of a particular piece of terrain, the need to be able to determine the ability of the terrain to provide flotation and traction thrust capability is apparent. In organic terrain, the ability of muskeg, for example, to support loads cannot necessarily be taken as an indication of the muskeg to provide for traction capability. The action of thrust applied at the surface, if not properly addressed, may tear the surface cover and hence degrade the cover to the extent that load support capability can no longer be available. Thus, if optimum mobility is to be achieved on such terrain units, the interactions that must occur at the terrain surface must ensure that no disruptive shearing forces or mechanisms are allowed to dominate the energy transfer mechanics.

3.4 MECHANISMS OF TRACTION

Traction is the ability of the vehicle tractive element (wheel-track) to generate enough forces to overcome all types of vehicle resisting forces, and hence keep the vehicle in constant travel. The traction mechanism is dependent on the tractive element type (a) wheel or track, and (b) ground support type which

could be classified as:

- (1) cohesive soil (soft clays, swamps),
- (2) granular soil (sand beaches, desert),
- (3) mixed soil (cohesive/friction - loam, till),
- (4) muskeg (organic fibres - live, decomposed, organic material supported on soft soils), and
- (5) snow, which possesses "cohesive and frictional" properties varying with time and temperature, accompanied by high compactibility, (Chapter 2).

Soft cohesive soils represent a severe condition for the tractive performance, whilst cohesive-frictional soils perhaps represent the more commonly encountered soils. Muskeg represents severe condition for the tractive performance, where the traction should be generated at the surface of the mat layer without tearing it (minimum slip). The mat works as a flotation raft over the soft clays. Thus, destroying it severely limits the capability of the muskeg terrain to support the vehicle.

3.4.1 Wheel-soft clay traction mechanism

Assume that a constitutive equation of the form $\tau_s(p, I)$ can be postulated for the yield point in shear of the soil at the wheel-soil interface. I is the strain-rate invariant and p is the pressure. The tangential stress, τ , can then be defined in the following manner:

$$[\tau] < \tau_s(p, I) \quad (3.1)$$

This follows because the shear stress at a point in the thin surface layer of soil (or in a layer parallel and close to the surface) is less than on the slipping surface at this point. The equality holds if the surface of contact is a slip surface, that is, the maximum value of the tangential stress is given by the relation:

$$[\tau] = \tau_s(p, I) \quad (3.2)$$

Prandtl (1949) has shown for an ideal plastic material moving between rough platens that the flow boundary is a slip plane, and that on this slip plane the tangential stresses reach the value $\tau_s = k$, i.e., the shear stress of the material. It is essential, however, that the normal pressure p on the surface be greater than a certain value p_s . This condition is satisfied when the contact pressure is a few times larger than the yield stress of the material.

3.4.2 Wheel-sand traction mechanism

One of the basic mechanisms of dry surface friction is the plastic deformation of a thin layer. In metals, it is customary to talk about projections on the surface. These projections act independently at small pressures and the effective cross-sectional area is the sum of these projections. Since the effective area in shear which determines the capacity of these projections for a shearing stress is directly proportional to the area of the projections, the frictional stress will be directly proportional to the pressure p . This relation is usually expressed as Coulomb's law, and can be written at:

$$[\tau] = \mu p \quad (3.3)$$

where μ = coefficient of friction.

The frictional stress can have the values given in eqs.(3.1) and (3.3) only at points of contact of the surface where there is relative velocity, i.e. the rim velocity ($r.\omega$) must be different from the soil velocity V (carriage velocity plus instantaneous soil velocity). Points on the contact surface where the true slip velocity $V_s = r.\omega - V = 0$, are zones of adhesion, and in these zones static friction applies. These zones of adhesion can be looked upon as changes in the sign of μ . Equations (3.1) and (3.2) are the approximate laws of surface friction which can be used in the total deformation theory.

3.4.3 Wheel-mixed soil traction mechanism

The traction mechanism at the wheel-soil interface for mixed soil can be visualized as a combination of both cohesive soil reacting mechanisms, which are strain rate dependent, and frictional soil reacting mechanisms which are mainly Coulomb friction. In this situation the wheel-soil tangential forces are a function of soil strength parameters (cohesion C and friction angle ϕ), relative slip at the wheel-soil interface, and slip velocity.

3.4.4 Wheel-snow traction mechanism - shallow snow

The traction characteristics developed at the wheel-snow interface are complex because of the highly compressible nature of snow and also because its properties are time, pressure and loading rate dependent. For shallow snow, application of load from wheel motion compresses the snow in a front-to-rear mode consistent with wheel travel and a rate governed by wheel travel speed and sinkage. Maximum compression occurs at the bottom dead centre of the wheel. Compression of snow increases its density. By and large, because of the rigid bottom boundary condition, no general shear failure occurs - i.e. only localized shear failure occurs at the interface.

3.4.5 Wheel-muskeg traction mechanism

As previously discussed, a muskeg mat consists of live vegetation with relatively high tensile strength. The vegetation rooted through a live mat consists mainly of organic fibrous material followed by a decomposed organic material mixed with silt and clay. The water table is generally always at or above the ground surface and the live mat, to all intents and purposes, floats on the top of its sublayer. Thus development of traction mechanisms should rely mainly on the friction stresses between the tyre and the vegetative cover without severe tearing of the mat layer. Destruction of the mat layer through tearing of the root system, or bunching, will generally result in sinkage or immobilization because of the lack of flotation. A low ground pressure is desirable to minimize the amount of tyre sinkage.

3.4.6 Factors affecting tyre-ground surface traction coefficients

The traction coefficient for a tyre can be defined as the ratio between its driving force and load. The driving force is the sum of the tangential forces at the wheel-soil interface. For a rigid tyre, it is equal to the driving torque divided by its radius. For a pneumatic tyre moving on a rigid, non-yielding, surface, it is equal to the driving torque divided by the tyre rolling radius, (Fig. 3.10).

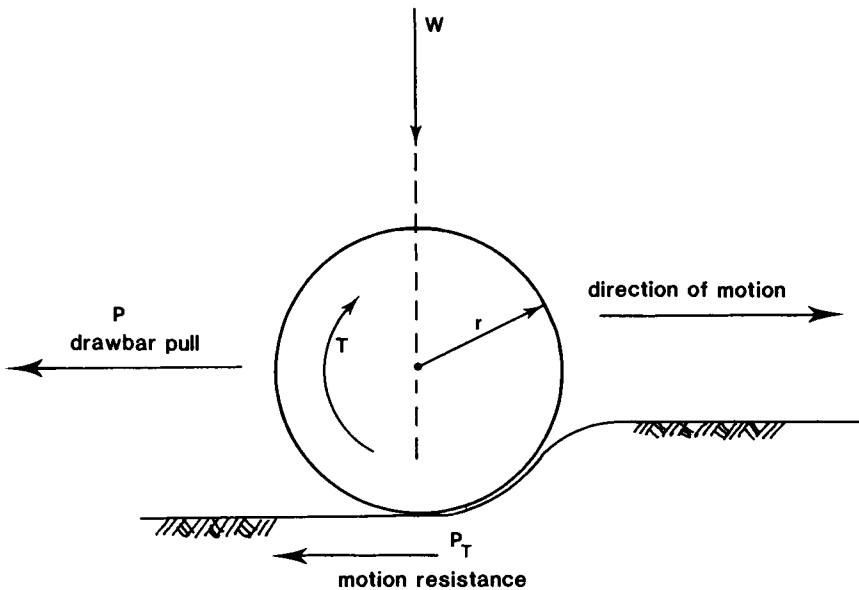


Fig. 3.10. Forces acting on a moving tyre.

The significant factors influencing the traction coefficient of a tyre are soil type, tread configuration, diameter, width, wheel load, inflation pressure, and tyre structure.

(i) Tread configuration. Improvement of traction through the "suitable design" of tyre tread configuration has always been conceived as being one of the principal contributors. Tyre treads with varying degrees of "aggressive" action have been tested (continuously) to determine their direct influence on traction production. Whilst no real analysis formulations have been derived to specifically quantify the degree of tread "aggressivity" in relation to traction production, much experience with tread design and geometry on tyre performance has been gained in recent years - through systematic tests. Figure 3.11, for example, demonstrates the effect of a simple wheel surface condition for wheels moving on soft cohesive soil, (Yong et al., 1980). Similar types of curves can obviously be generated for various types of surface features (tread design). However, we should note that unless a means for quantitatively relating tread features to traction production is developed, the only recourse available for choice of tread pattern for traction production remains one of direct experience and corroborative testing.

Special tyres with aggressive tread configuration are used in marshy ground with wet and slippery surface conditions. Tyre chains, additional grip tyres, and spade wheels, are commonly used to increase traction forces on soft surfaces. Increased traction is achieved through the development of tyre-soil tangential forces which depend on soil cutting, and not on tyre material-soil interfacial characteristics, as is the case of interaction with smooth wheel surface.

(ii) Tyre diameter. This has a significant effect on the development of traction forces. For the same tyre characteristics (width, inflation pressure and load), the traction coefficient increases with increasing tyre diameter and load. The increased length of the tyre contact patch serves as a beneficial factor in the transfer forces from tyre-into-ground whilst keeping motion resistance at a minimal value.

(iii) Tyre width. For the same nominal ground pressure, increasing tyre width increases the flexibility of the tyre and generally assists in the development of uniformity of pressure application. Whilst this might increase traction capability, the increased width of the tyre could produce more motion resistance. The trick in establishing a width and diameter characteristic insofar as traction production is concerned, is to optimize the width:diameter ratio to achieve (a) contact patch properties to ensure the greatest uniformity in pressure distribution, and (b) lowest motion resistance through effects resulting from sinkage, side walls and ploughing.

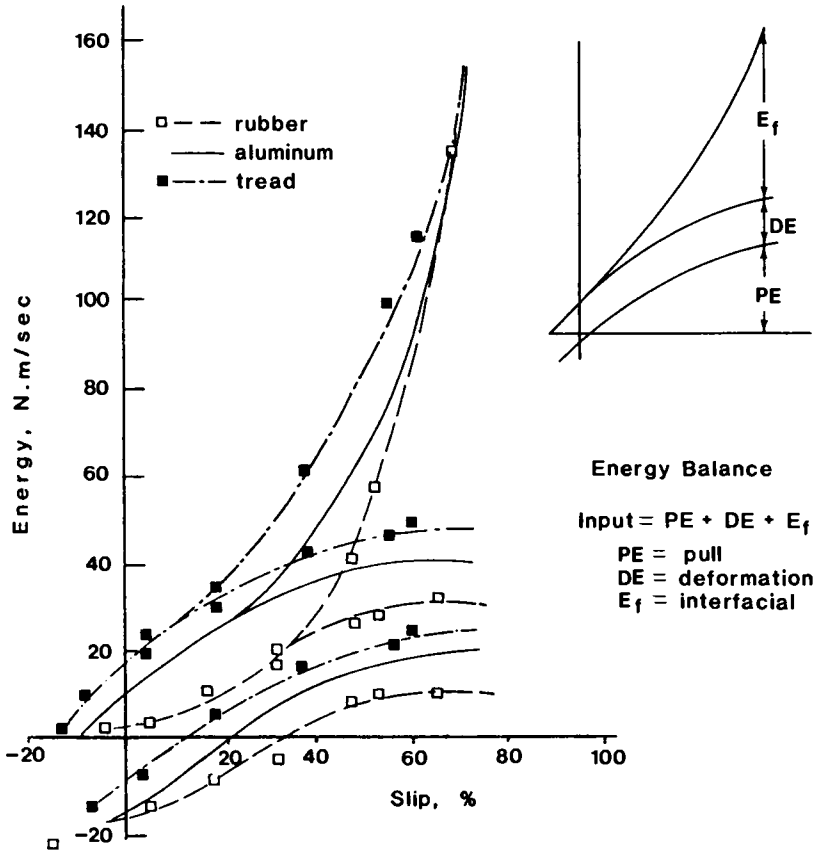


Fig. 3.11. Energy balance per unit wheel width-wheel load 150 Newton.

(iv) Inflation pressure. This contributes directly to stiffness of the tyre and hence controls (a) tyre contact area, and (b) tyre-soil ground pressure distribution, both of which influence the traction capability of the tyre. In general, for traction in loose or soft soils, a decrease in inflation pressure results in an improvement in the distributions of both normal and tangential interfacial stresses, (Fig. 3.12), in the tractive performance of the tyre. However, there is a limit to which the inflation pressure could be reduced. This is governed mainly by the amount of deformation permissible in the tyre carcass. Excessive deflection (a) causes high motion resistance, (b) overheats the tyre and (c) accelerates tyre surface wear. Hence the gain in traction may be lost due to an increase in tyre motion resistance. It should be noted that a significant decrease in inflation pressure may not result in excessive tyre deflections when the tyre is operating on loose or soft soils. Figure 3.13 shows the effect of inflation pressure

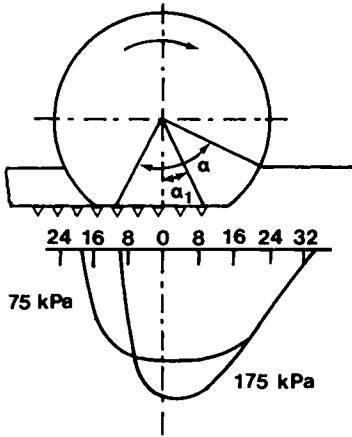


Fig. 3.12. Contact pressure distribution diagram for tyre surface. (Kolobov, 1966).

on the amount of the developed torque for different tyres operating on soft soil, (Yong et al., 1980).

(v) Tyre load. This influences its traction coefficient, and hence its pulling capacity according to the type of soil. The traction coefficient decreases when the load on the tyre is increased for loose or soft soils, and increases for stiff types of soils. Figure 3.14 shows torque to weight ratios as a function of slip for rigid wheels moving in soft soils. For certain types of soils (stiff frictional) the traction coefficient remains constant, or nearly constant, when the tyre load changes for the same inflation pressure, Fig. 3.15, (Kliffoth, 1966).

3.4.7 Track-ground surface traction mechanism

In tracked vehicles, the interaction between the vehicle and the ground is maintained through the track/grouser system which, together with the road wheels, sprockets and associated suspension arrangement constitutes the running gear of the tracked vehicle. Under present-day concerns and priorities, we need to pay attention to at least two requirements in the evaluation of grouser/track-soil traction mechanisms. These are:

- (1) the requirement for protection of the surficial environment from excessive surface disturbance (since tracks are generally used in marginal terrains) - especially in the more fragile environments, and
- (2) the need for obtaining the greatest amount of useful work for the least expenditure of fuel energy.

In response to the first of these concerns, recent experiments such as those by

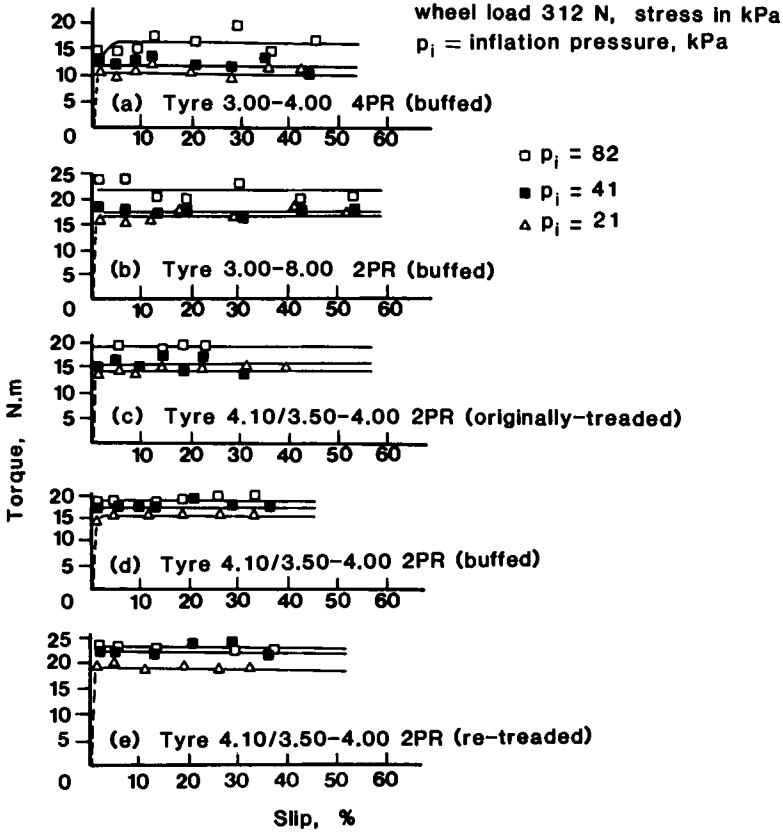


Fig. 3.13. Relationship of torque and slip velocity in clayey sand.

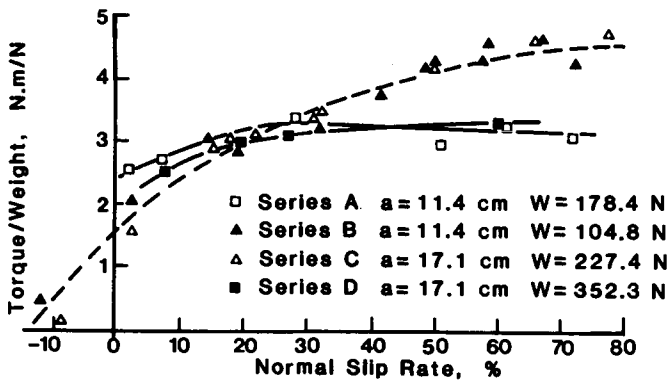


Fig. 3.14. Torque/weight versus normal slip rate for rigid wheel moving on soft clay.

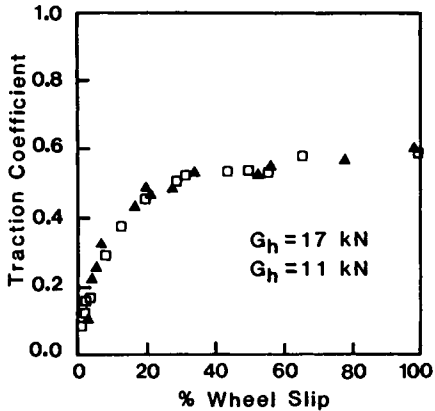


Fig. 3.15. Traction-coefficient on "friction soil" at two different wheel slip loads.

Yong et al. (1976) have examined the development of a passive track system where the grousers used have been designed so that their interaction with the terrain surface for production of traction is not in any way destructive. These will not be discussed herein since this is not the intent of this book.

Whilst it may be reasonably assumed that the requirement for optimum production of thrust in a grouser/track system is such that the full reaction of the supporting terrain needs to be developed, it is apparent that there needs to be certain rational guidelines for establishment of optimum spacing of grousers in relation to grouser shape, size and other parameters, to assist in establishing an optimum performance. A knowledge of the shear and deformation performance (traction mechanism) of the reacting terrain in the wake of grouser thrust would be most useful.

The track-soil developed traction force is a function of soil type (cohesive and frictional) and track parameters, such as:

- (1) grouser shape, geometrical dimensions, and spacing,
- (2) track weight,
- (3) angle of attack,
- (4) track belt flexibility (number of road wheels, track tension), and
- (5) driving sprocket position.

An increase in the traction force can be achieved by involving deeper layers of soil for development of the reacting shear stresses. This requires the deformation of the soil until general shear failure instead of forced shear failure along the track-soil contact area (Cho et al., 1969). Two causes can be attributed for the increase in track traction, (1) uniform pressure distribution at the grouser-soil interface, and (2) support obtained from the soil mass behind each grouser. The soil involved in developing the traction force extends to a

considerable depth after significant slip-sinkage has taken place over and above the static sinkage. The increase in track slip required to extend the soil failure pattern into the space left by the trailing grouser tends to nullify the gain in tractive effort obtained when operating on cohesive soils (Fig. 3.16), Cho et al., 1969.

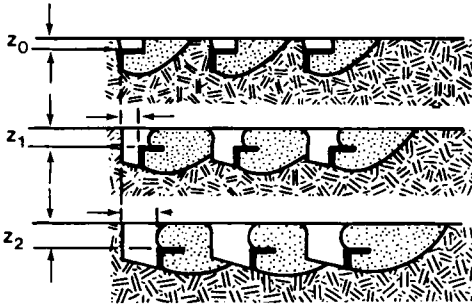


Fig. 3.16. Shear zones of grousers at different deformations. On strong soils the shear failure cannot develop completely when sinkage z and deformation j increase. Shear failure finally occurs in the plane of the grouser tips.

The above-mentioned track parameters which affect the performance in terms of traction force are discussed in the following Section.

(a) Grouser shape and spacing.

Figure 3.17 demonstrates the effect of grouser shape and spacing on the force developed by a second grouser in a multi-grouser moving in soft soil (after excluding the effect of the first grouser - Fig. 3.18). While it is shown that the aggressive grouser system produces the larger force due to its exaggerated height, one should also consider the grouser spacing associated with the maximum thrust developed by the grousers. Figure 3.17 shows that the horizontal force increases as the spacing between grousers increases, until an optimum spacing is reached at which the maximum force per unit spacing is obtained - as indicated from the gradient of the force.

(b) Track belt flexibility. (multi-grouser system)

Figure 3.19 illustrates the mobilized horizontal force variation with grouser displacement for one rigid and two flexible tracks with different flexibilities. The horizontal force increases with increased belt rigidity for any specific spacing. This result is due to upward soil movement. As the belt rigidity is relaxed, the upward soil movement causes distortion in the "in-between-the-grousers" region, thus reducing the thrust enhancement obtained in the rigid element situation. For the rigid boundary condition, the soil between the grousers is restricted to move as an integral part of the grouser system and hence, the grouser effect extends further into the ground.

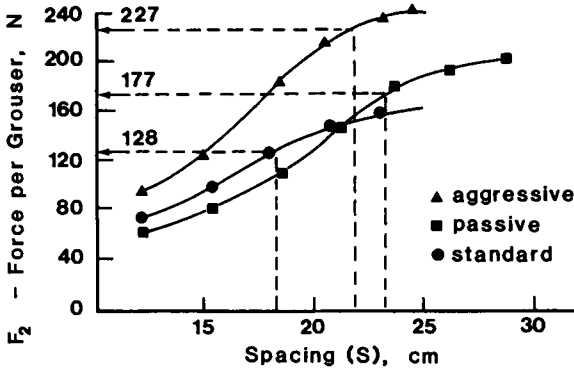


Fig. 3.17. Effect of spacing and grouser shape on the mobilized soil resistance.

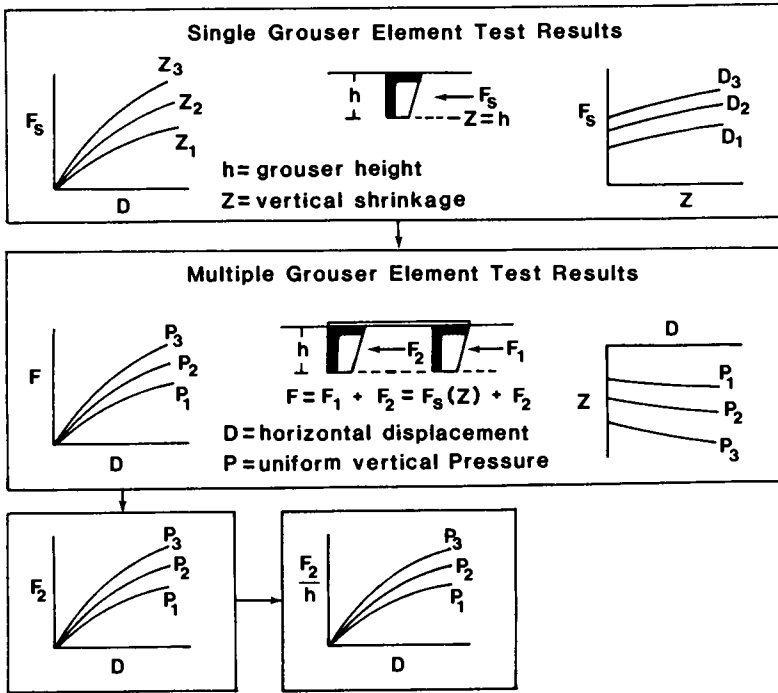


Fig. 3.18. Method of force calculation, F_2 , on second grouser.

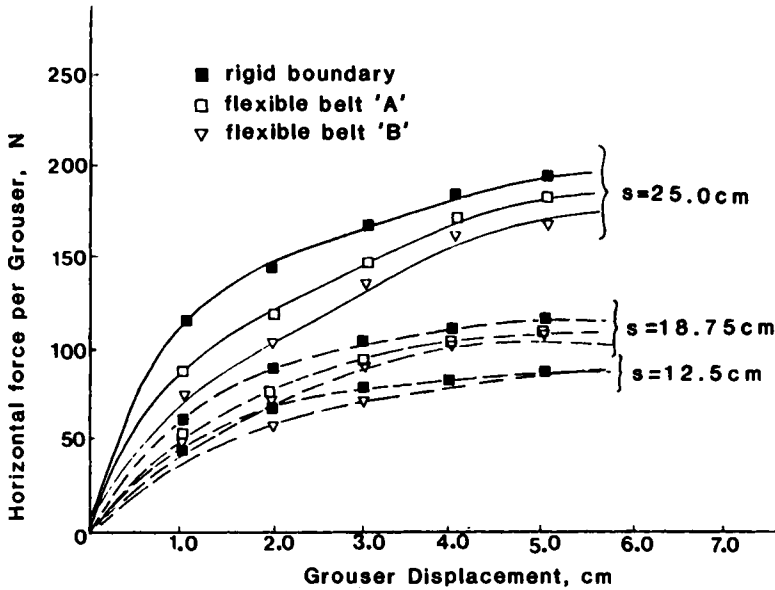


Fig. 3.19. Effect of spacing and boundary condition on the mobilized horizontal force of the passive grouser element.

In order to specify the optimum spacing between grousers, at which optimum performance of rigid and flexible tracks is obtained, the measured horizontal forces are normalized to correspond to both unit grouser height and spacing as shown in Fig. 3.20 for three different grouser shapes. Optimum spacing (indicated by arrows in Fig. 3.20) reduces as the belt flexibility increases. This behaviour is consistent with expectations, since under rigid belt conditions a larger spacing is necessary in order to develop a higher mobilized thrust.

(c) Boundary (track) pressure. (multi-grouser)

According to the limit equilibrium model for prediction of the mobilized traction force for a grouser moving on soil (Chapter 4), the force increase resulting from an increase in the boundary pressure together with the rate of increase of the traction force are a function of the soil frictional strength parameter (ϕ) and grouser surface-soil frictional parameter (δ). Because of grouser sinkage under the effect of the normal pressure, and also because of horizontal displacement, it is not unusual for the measured mobilized traction force to be higher than the predicted force. Figure 3.21 shows the measured horizontal force for a grouser moving in kaolinite clay under the effect of different normal pressures, whilst Fig. 3.22 shows the corresponding grouser sinkage as a function of horizontal displacement.

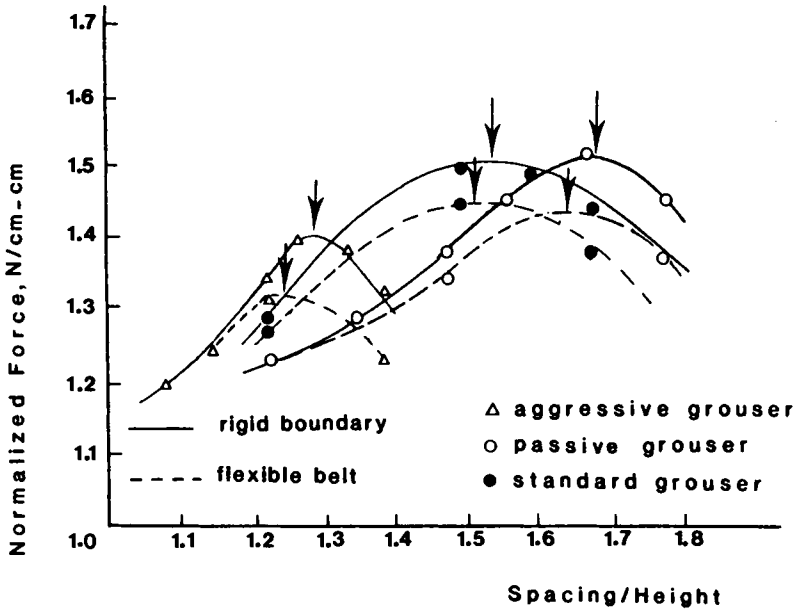


Fig. 3.20. Normalized force per unit spacing per unit grouser height versus the spacing/height ratio for the three grouser types.

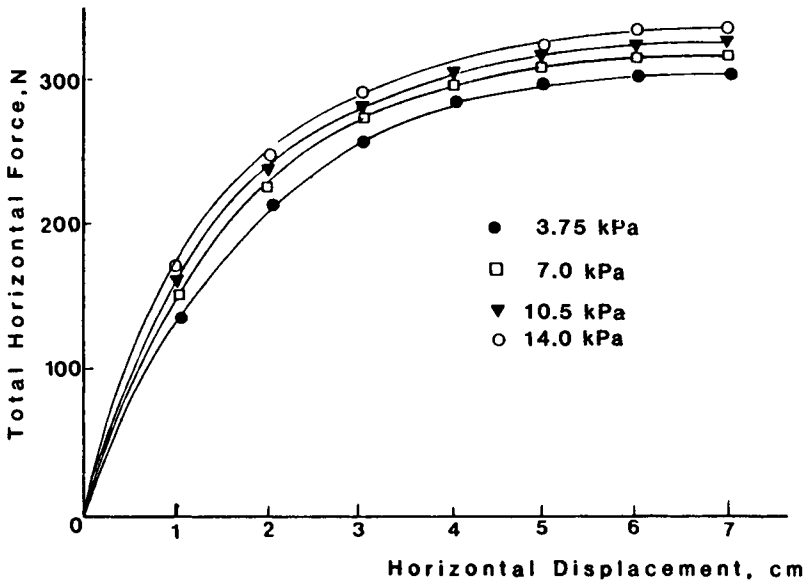


Fig. 3.21. Total horizontal force versus displacement for the passive MGE. Spacing = 12.5 cm.

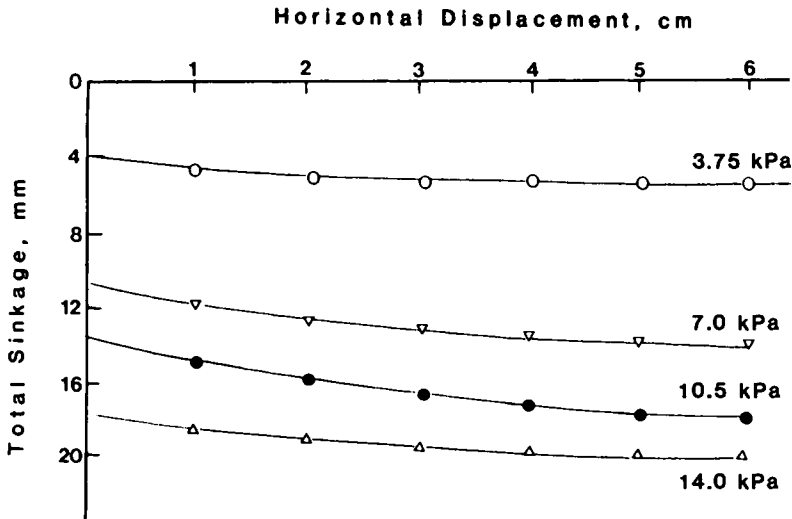


Fig. 3.22. Total sinkage versus displacement for the passive MGE. Spacing = 12.5 cm.

3.4.8 Track performance

We have discussed, in the previous Section, the factors affecting the performance of a grouser in a multi-grouser system. These kinds of studies are generally performed to assist one in the selection of suitable grouser shapes and spacing for an actual track. In the following discussion in this Section, the effect of track parameters on tracked vehicle performance is discussed.

(a) Degree of slip.

Figure 3.23 shows the various distributions of tractive force developed by a track as a function of slip. With high values of slip, a greater portion of the tractive effort is supplied by the front part of the track, whereas at small slips the rear part of the tracks contribute the greater part of this force. However, under average conditions a considerable part of the tractive force is generated in the second half of the track. This is because with the increase in drawbar-pull there is a redistribution of contact pressure, and the centre of pressure moves towards the rear of the tracks or, in other words, the increase in contact pressure moves into the zones where the deformation is greatest.

(b) Effect of grouser shape and vertical weight.

Figures 3.24 and 3.25 show the measured traction and drawbar-pull as a function of slip for all the grouser types and two different track weights. The belt tension is such as to produce a rigid track situation. From the results shown, we note that the aggressive track develops the highest traction but at the expense of higher sinkage (Fig. 3.26), and consequently, higher resistance and

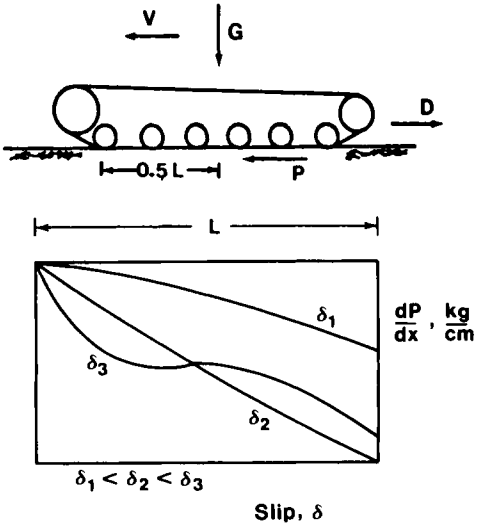


Fig. 3.23. The variation of the distribution of tractive force with slip in a track-laying tractor.

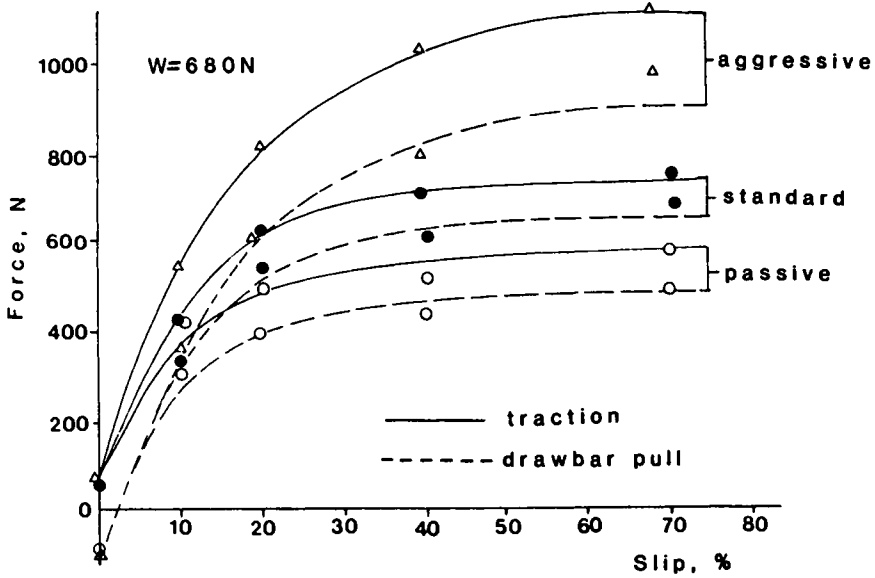


Fig. 3.24. Traction and drawbar-pull-slip relationships for the three grouser-track system. $W = 680 \text{ N}$ (soft kaolinite clay).

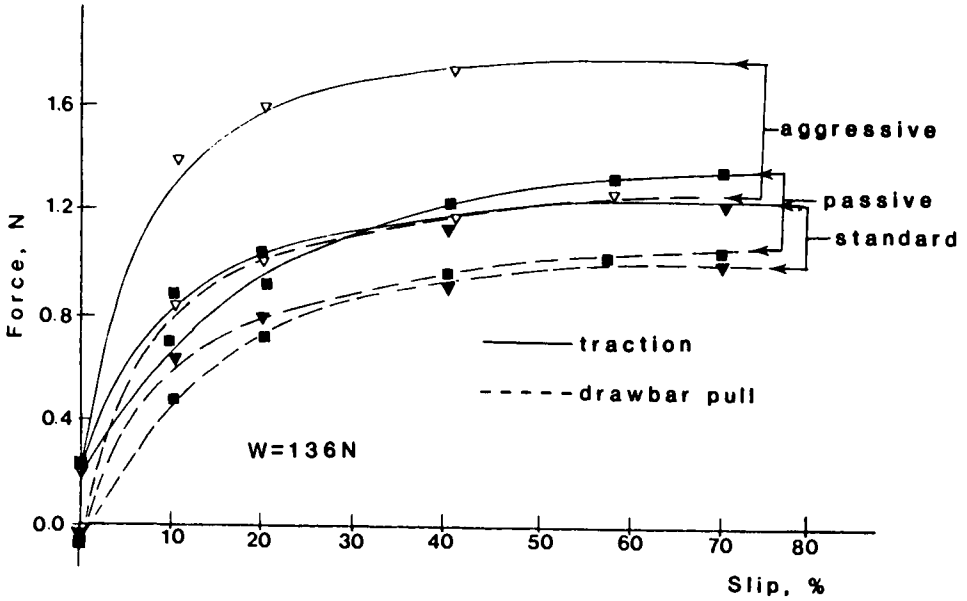


Fig. 3.25. Track and drawbar-pull-slip relationship for the three grouser-track systems. $W = 136\text{ N}$ (soft kaolinite clay).

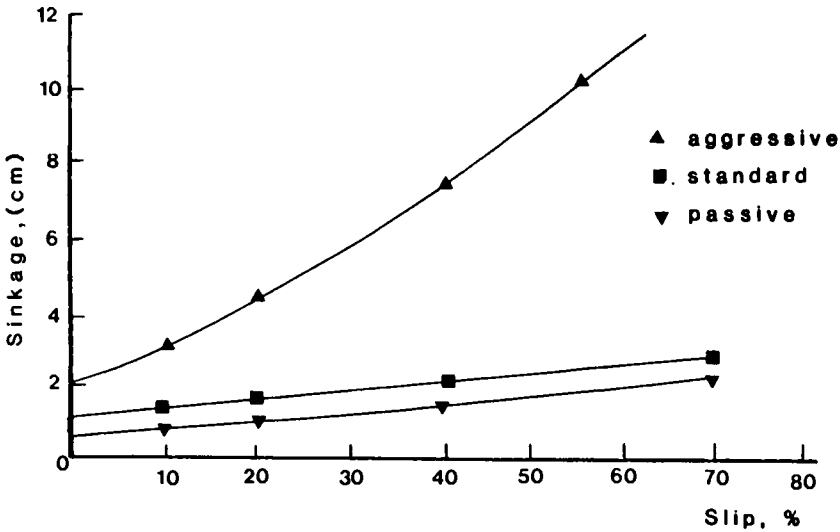


Fig. 3.26. Sinkage slip relationships for the three track systems. $W = 680\text{ N}$ (soft kaolinite clay).

energy losses. The passive track in the test series shown, produced the lowest traction and drawbar-pull, especially under a light weight condition. This is due to the partial embedment of the passive grousers into the soil (because of wider bearing area) thus, in essence, forfeiting a significant capability for thrust development, - i.e. if greater sinkage occurs, more thrust can be developed. However, in the specific role design for the passive track, the results show that it experienced the lowest sinkage (Fig. 3.26) thus fulfilling the requirement for protection of the surficial environment from excessive surface disturbance.

Figure 3.27 shows the developed drawbar-pull for different tractor weights operating on loam and peat soils. As shown in Fig. 3.27, the value of the tangential tractive force increases at first with slip, but after reaching a certain peak it falls off, (Kacigin and Guskov, 1968). Test results show that the maximum tractive force for a track occurs at 20-26 percent slip for mixed cohesive soils, at 30-40 percent for marshy soil, and at 40 percent for soft cohesive soils.

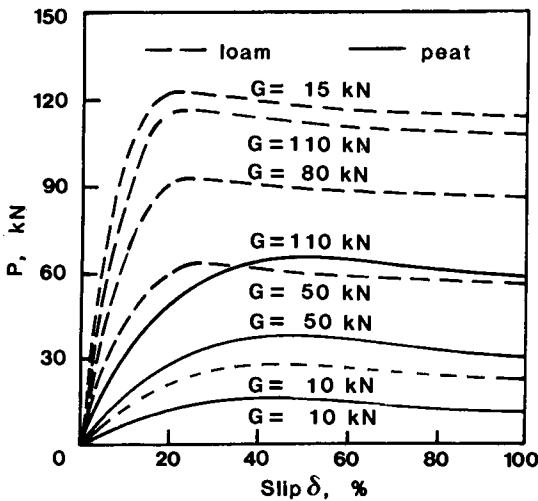


Fig. 3.27. The influence of tractive effort on slip at different tractor weights for a track-laying tractor. Fixed contact area $S = 13,200 \text{ cm}^2$.

(c) Effect of centre of gravity position.

Brusentsev (1967) studied the effect of displacing the centre of gravity of a bulldozer on its performance. Table 3.1 and Fig. 3.28 show the summary of field test for a bulldozer operating on stiff soil. The results show a change in load between -10 and 20 kN respectively. There appeared to be a fall-off in the effective use of engine power and tractive efficiency with an increase in fuel

consumption. A reduction in the tractive force of the bulldozer was accompanied by an increase in the rolling resistance and the coefficient of rolling resistance, (Brusentsev, 1967).

TABLE 3.1

Summary of field tests for a bulldozer operating on stiff soil.

Distance of the centre of pressure of the track contact area from the driving sprocket centre (mm)	1342	1521	1678	1825	1122
Load (kg)	-1000	0	+1000	+2000	-
Tractive force (kg)	8400	7500	6200	4600	8550
Speed (km/hr)	3.26	3.25	3.24	3.22	3.09
Power (h.p.)	101.5	90.4	74.4	54.9	98.0
Specific fuel consumption (g/hp-hr)	244	274	329	451	-
Rolling resistance (kg)	1250	2230	3580	5280	1250
Coefficient of rolling resistance	0.092	0.15	0.23	0.33	0.085
Tractive efficiency	0.76	0.67	0.55	0.41	0.73

The results shown in Fig. 3.28 indicate that the increase in rolling resistance of the tractor is caused by the redistribution of the load between the track rollers. This is caused by the formation of a zone of pressure concentration under the track and the manner in which the front idler sprocket interacts with the track itself.

(d) Belt tension and number of wheels effect.

The effects of the belt flexibility on the track performance can be studied by conducting tests where both the belt tension and number of road wheels are reduced, (Yong, 1982) so that more flexibility and upward movement of the track belt portion interacting with the underlying soil is allowed. Figure 3.29 presents the results of the measured traction and drawbar-pull for different degrees of slip and three levels of belt tension (very rigid, relatively rigid, relatively loose) cases. Both the measured input and output forces increase as the track belt tension is increased. However, since a very tight belt may cause extra losses at the track wheels and waste energy inside the track system, a less-than-maximum belt tension is recommended for development of high track efficiency.

Similar kinds of results can be obtained by reducing the road wheels - say, from five to three. For a rigid track (tight belt, no upward flexing), the effect of the number of road wheels becomes minimized. For a loose track, a reduction in the number of road wheels causes a reduction in track performance capability due to pressure concentrations under the position of the wheels. These pressure concentrations cause higher sinkages which in turn will reduce track efficiency, as demonstrated in Fig. 3.30.

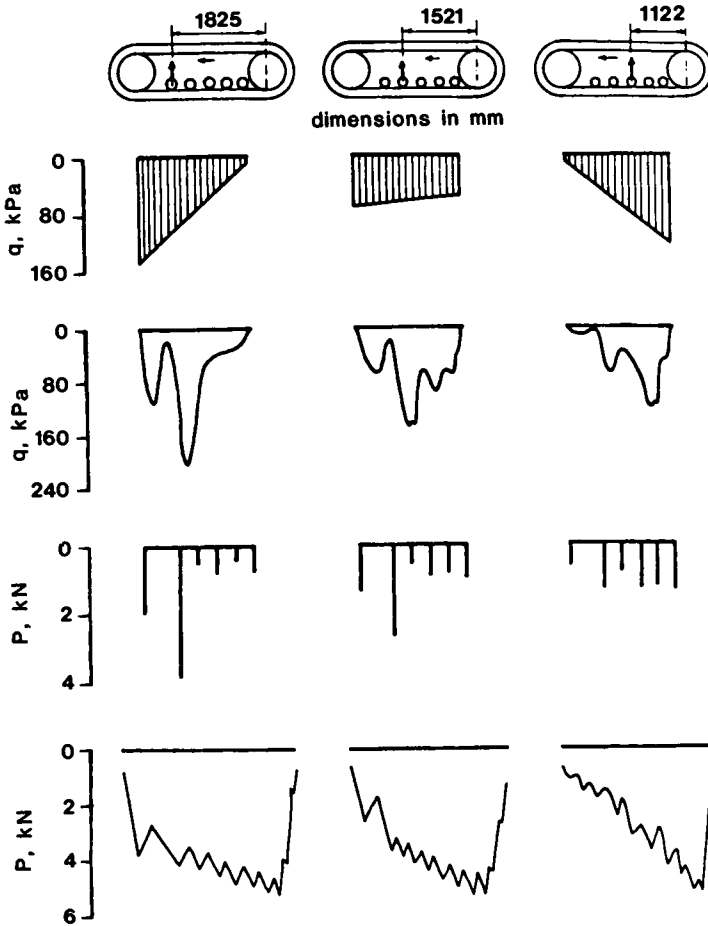


Fig. 3.28. Analysis of track forces. The computed contact pressure distribution (a) is compared with the following experimental results, (b) contact pressure under track rollers, (c) track roller reactions on links, and (d) track tension.

(e) Sprocket wheel position and angle of attack effect.

Figure 3.31 shows experimentally measured tractive performance results for different sprocket wheel positions (rear and front). The position of the front sprocket wheel determines the angle of attack obtained at two different belt tensions. Under tight belt conditions the sprocket wheel position effects are negligible. However, a more pronounced reduction in input and output forces is measured when the sprocket wheel is transferred towards the front of the track in

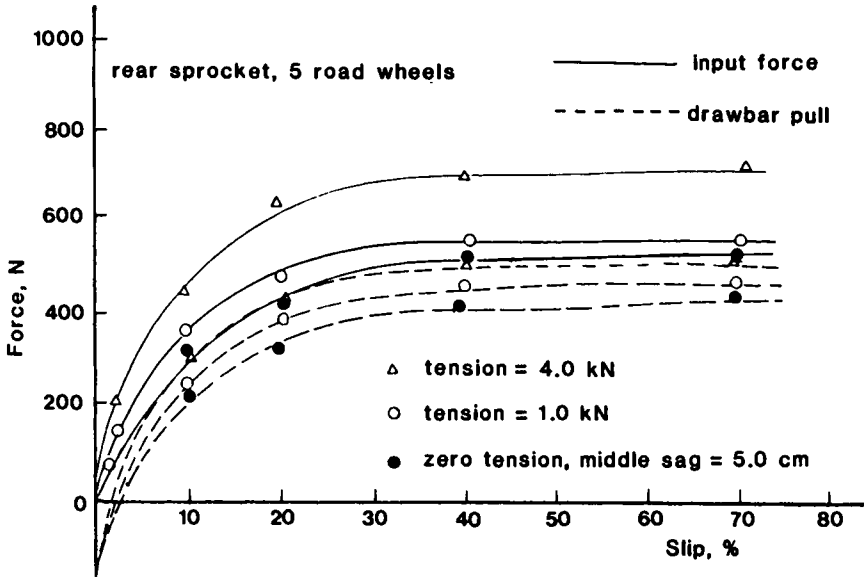


Fig. 3.29. Effect of belt tension on the input traction and output drawbar-pull of the passive track system ($W = 680 \text{ N}$).

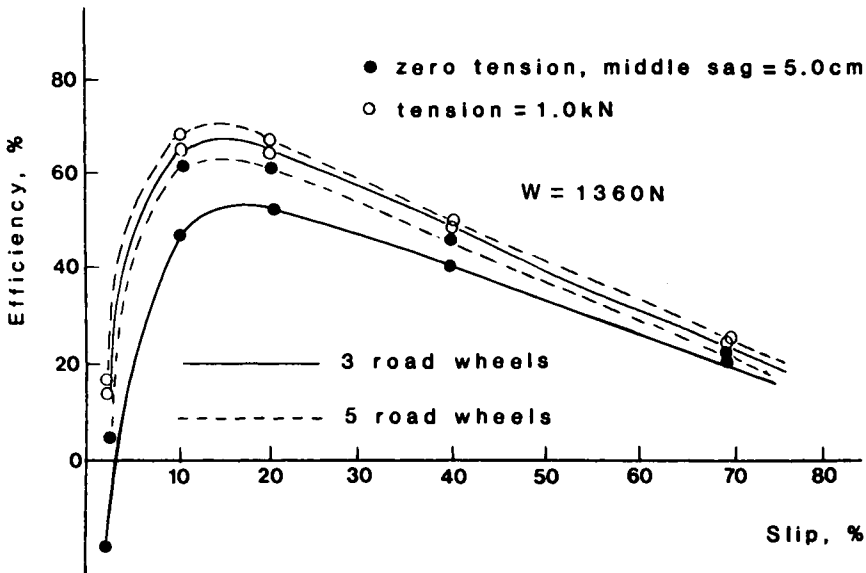


Fig. 3.30. Effect of road wheels number on the passive track efficiency at two different belt tensions.

the case of flexible belt tracks. This is attributed to the associated large powered length of the belt which increases the possibility of additional belt flexing at the contact level, and causes energy losses and associated track reduction performance.

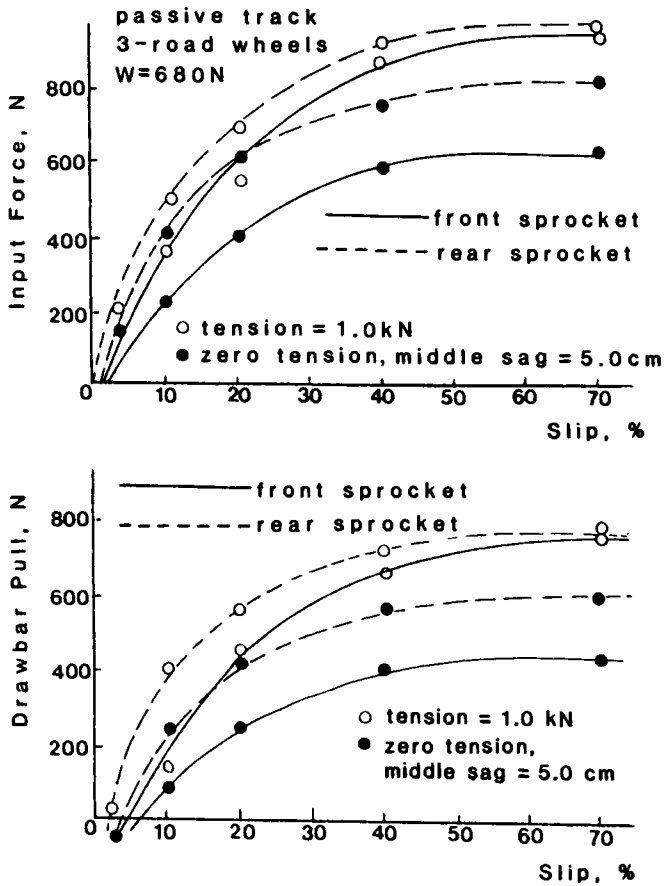


Fig. 3.31. Measured input and drawbar-pull forces for front and rear sprocket positions.

3.5 PREDICTION OF TRACTIVE EFFORT

The prediction of tractive effort (forces) is an essential part of the requirement for vehicle performance simulation. Realistic soil values and tractive element-soil parameters are basic requirements for exact simulation of the wheel or track performance. In this Section the methods available for prediction of the tractive forces for tyred or tracked vehicles are discussed.

3.5.1 Tyres

Two approaches can be used for prediction of the traction driving force for a wheel moving on a soil; (i) dimensional analysis, and (ii) mathematical modelling of the traction behaviour at the tyre-soil interface.

(i) Dimensional analysis. In this approach, the behaviour of tyres is observed through extensive experimental and field test programs. The performance of the test tyres is plotted in non-dimensional terms as a function of tyre-soil parameters. If the plotted relationships are unique for certain classes of tyres and soil, and can be modelled mathematically, these relationships will constitute the performance equations.

The complete spectrum of performance of a tyre moving on soil from the towed point to standstill and spinning (100% slip), is shown schematically in Fig. 3.32.

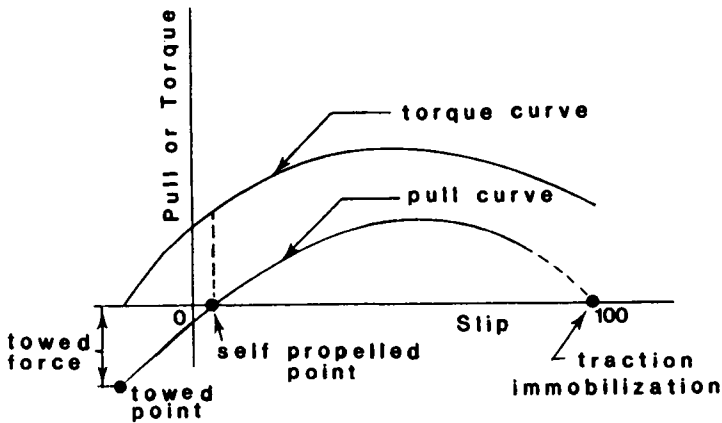


Fig. 3.32. Pull and torque-slip relationships.

Torque or pull performance equations should be valid for specific, or all, degrees of slip. A typical non-dimensional relationship for a pneumatic tyre moving in saturated clay is shown in Fig. 3.33. This relationship shows that (a) the towed force/load ratio (TF/W) decreases hyperbolically with increasing values of the soil-wheel numeric ($Cibd/W$), and (b) the traction coefficient (Q/rW) and pull coefficient (P/W) increase with increasing numeric values, and appear to approach an asymptotic value. The relationships between the tyre performance and its parameters can be expressed non-dimensionally as:

$$\frac{TF}{W}, \frac{P}{W}, \frac{Q}{rW} = f\left(\frac{Cibd}{W}, \frac{b}{d}, \frac{r}{d}, S\right) \quad (3.4)$$

where

TF = towed force;

W = tyre load;

P = drawbar-pull;

Q = input torque;

r = tyre rolling radius;

CI = soil cone index;

b = tyre section width;

d = overall tyre diameter;

S = tyre slip;

s = $(1 - Va/r\omega)$;

Va = tyre translational velocity and

ω = angular velocity of the tyre.

The following are some typical equations for a pneumatic tyre moving on soft soil (Turnage, 1972).

$$\frac{P_T}{W} = 0.04 + \frac{0.20}{\beta - 2.50} \quad (3.5)$$

$$\frac{P_{20}}{W} = 0.80 - \frac{1.31}{\beta - 2.45} \quad (3.6)$$

$$\beta = \frac{CIbd}{W} \left(\frac{\delta}{h}\right)^{1/2} \left(\frac{1}{1 + b/2d}\right) \quad (3.7)$$

Wismer and Luth (1973):

$$\frac{TF}{W} = \frac{1.2}{C_n} + 0.04 \quad (3.8)$$

$$\frac{P}{W} = 0.75 (1 - e^{-.3C_n S}) - \left(\frac{1.2}{C_n} + 0.04\right) \quad (3.9)$$

$$C_n = \frac{CIbd}{W} \quad (3.10)$$

where

$P_{T,TF}$ = rolling resistance;

δ = tyre deflection on rigid surface;

h = tyre section height;

S = degree of slip;

P_{20} = pull force at 20 percent degree of slip and

P = pull force at any degree of slip.

Both relationships are shown in Fig. 3.34 (Wisner and Luth, 1973), for comparison. It should be noted that these equations were developed for vehicles operating in cohesive soils where the cone index is used as a measure of soil strength.

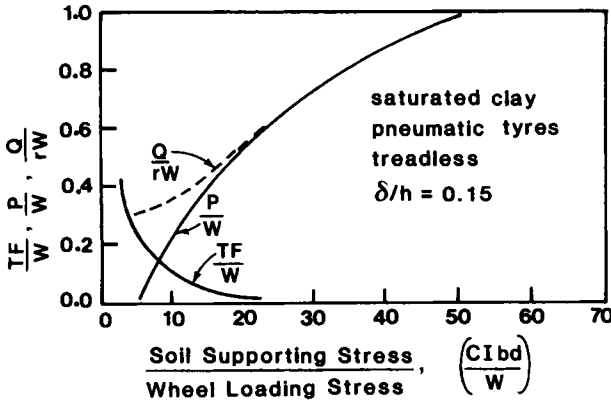


Fig. 3.33. Effect of soil-wheel stress ratio on traction.

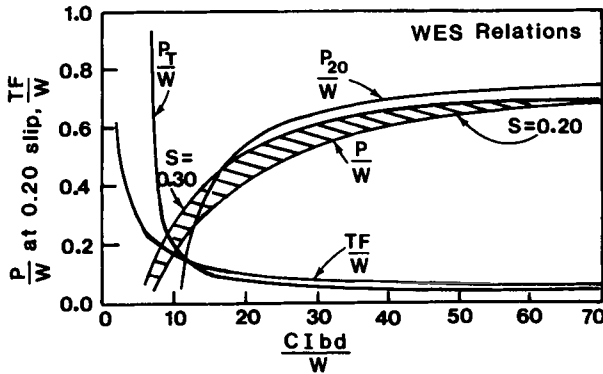


Fig. 3.34. Comparison of WES and Deere traction relations.

(ii) Traction mathematical modelling. The state of failure in soils is generally expressed by the well-known Mohr-Coulomb failure criterion (Yong and Wakrentin, 1975), and can be written as:

$$\tau = C + \sigma \tan \phi \tag{3.11}$$

where

τ = shear stress;

σ = normal stress and

C and ϕ = mathematical constants which can be interpreted as soil shear strength parameters: C for cohesion and ϕ for friction.

Assuming a uniform pressure distribution at the tyre or track-soil interface, the maximum traction forces can be calculated as:

$$F = CA + W \tan \phi \quad (3.12)$$

where

A = tyre or track-soil contact area and

W = tyre or track load.

Generally speaking, one is interested not only in the maximum traction developed but also in the development of traction at specific degrees of slip (deformation). Soil displacement along the interface contact with the tyre (track) depends on the degree of slip and the distance from the first contact point of the tyre (track) and the ground.

$$\delta = i x \quad (3.13)$$

where

i = degree of slip;

x = distance from the first contact and

δ = tyre (track)-soil shear displacement.

In order to mathematically express the soil shear stress-shear deformation relationship, the general behaviour of the soil needs to be established. It is known that soil-shear diagrams either increase monotonously toward a horizontal asymptote (cohesionless soil) or increase to a local maximum and drop toward a horizontal asymptote (cohesive soils), Fig. 3.35.

Bekker (1956) suggests an equation for the description of shear diagrams of a "humped" form, similar to the form of an aperiodic damped vibration:

$$\tau = \frac{C + \sigma \tan \phi}{\gamma_{\max}} \left[e^{(-k_2 + \sqrt{k_2^2 - 1})k_1 \delta} - e^{(-k_2 - \sqrt{k_2^2 - 1})k_1 \delta} \right] \quad (3.14)$$

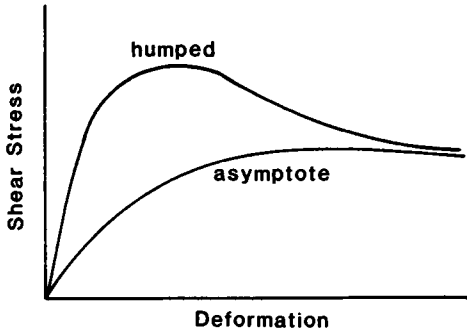


Fig. 3.35. Shear deformation diagram.

where

- τ = shear stress (kPa);
- C = soil cohesion (kPa);
- σ = mean ground pressure (kPa);
- ϕ = internal friction angle;

k_1, k_2 = soil parameters and

Y_{\max} = maximum value of the expression in the brackets.

Kacigin and Guskov (1968) suggest the following formula for general shear diagram:

$$\frac{\tau}{\sigma} = f_m \left[1 + \frac{a}{\cosh \delta/k_\tau} \right] \tanh \delta/k_\tau \quad (3.15)$$

This function is illustrated in Fig. 3.36. This expression contains three parameters which describe the shear-deformation curve; (a) the ratio f_m of the residual shear strength to the contact stress at large displacements (coefficient of residual strength), (b) the displacement k_τ required to reach the peak shear stress, and (c) the constant a which depends on the ratio of residual to peak strength. The magnitude of a is given by:

$$a = 2.55 \left(\frac{f_s - f_m}{f_m} \right)^{0.825} \quad (3.16)$$

In the case of an asymptotic shear curve, Fig. 3.36b, $\tau_s = \tau_m$ and hence $a = 0$

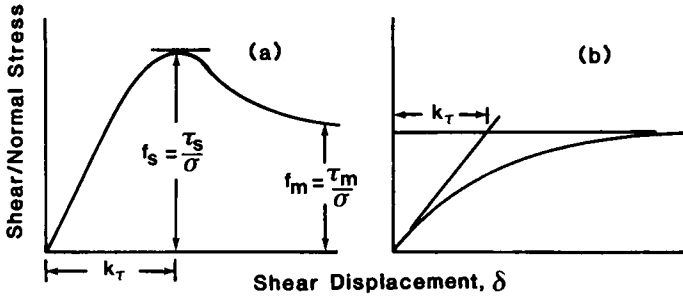


Fig. 3.36. Typical shear stress deformation curves.

and eq.(3.15) reduces to:

$$\frac{\tau}{\sigma} = f_m \tanh \delta/k_\tau \quad (3.17)$$

The different soil parameters identified by Kacigin and Guskov (1968) are defined schematically in Fig. 3.36. It should be noted that according to the Mohr-Coulomb failure criterion, the peak shear strength can be calculated from eq.(3.11), and hence

$$f_m = \frac{\tau_s}{\sigma} = \frac{C + \sigma \tan \tau}{\sigma} \quad (3.18)$$

Janosi and Hanamoto (1961) recommended a simpler equation for describing asymptotic shear curves (Fig. 3.37), since in the majority of cases the soil does not exhibit a hump followed by a drop in the shear stress-strain curve.

$$\tau = (C + \sigma \tan \phi) (1 - e^{-\delta/k}) \quad (3.19)$$

For very large deformations eq.(3.19) approaches Coulomb's equation:

$$\tau = C + \sigma \tan \phi \quad \text{as } \delta \rightarrow \infty$$

Differentiating both sides of eq.(3.19) and setting j equal to zero:

$$\left(\frac{d\tau}{dJ}\right)_{j=0} = \frac{C + \sigma \tan \phi}{k} \quad (3.20)$$

Equation 3.20 represents the slope of the tangent drawn at the origin,

Fig. 3.37. k , which is called the deformation modulus of a soil shear stress-strain curve, may be obtained from the experimental shear stress-strain curve as the distance between the intercept of the tangent drawn at the origin and the line given by $\tau = C + \sigma \tan \phi$ and the τ -axis, (Janosi and Hanamoto, 1961).

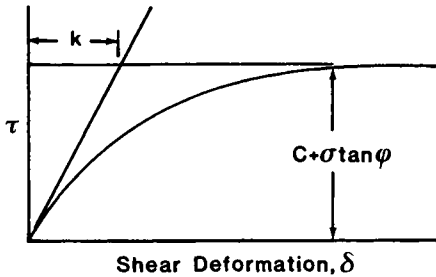


Fig. 3.37. Evaluation of ' k ' from a typical soil shear stress-strain curve.

Observation of shear-deformation diagrams at different normal pressures reveals two different types of diagrams, Fig. 3.38, (a) characterized by a constant deformation modulus k , as in Fig. 3.38a, and (b) characterized by a constant slope k_T , as shown in Fig. 3.38b. For a constant deformation modulus, the shear-deformation relationship is the same as Janosi and Hanamoto (1961), eq. (3.19). For the constant slope modulus, k_T , the relationship can be written as -

$$\tau = (C + \sigma \tan \phi) \left(1 - e^{-\delta k_T / \sigma} \right) \quad (3.21)$$

where

k_T = initial tangent modulus for shear-deformation diagram.

In the case of pneumatic tyres or smooth rigid tracks, it is assumed that the shear deformation at the tractive element-soil interface changes linearly with slip, Fig. 3.39. The tangential stresses at any point of the interface can be calculated using eqs.(3.19 or 3.21), provided that the following pieces of information are known: (a) degree of slip, (b) contact length at tyre (track)-soil interface (FPL), (c) tyre (track) surface-soil parameters, (C and ϕ), and (d) normal pressure distribution at the tyre-soil interface. The total tractive force can be predicted by integrating the tangential stresses along the tyre (track)-soil contact area.

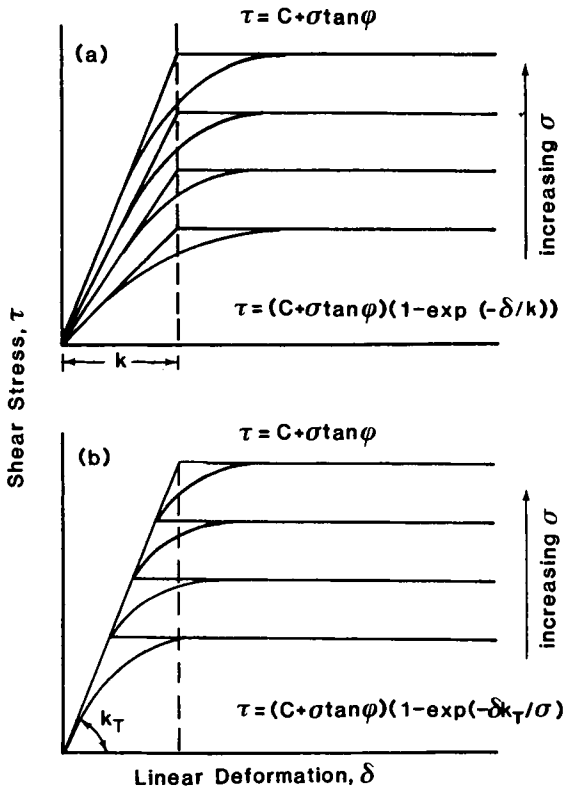


Fig. 3.38. Idealization of shear-deformation diagrams.

In the case of uniform pressure distributions, the tractive force can be written (Janosi and Hanamoto, 1961) as -

$$H = (AC + W \tan \phi) \left[1 - \frac{1}{J} (1 - e^{-J}) \right] \quad (3.22)$$

where

H = tractive force;

A = contact area = $b\ell$;

b = contact area width;

ℓ = contact area length;

W = track or tyre load;

σ = tyre(track)-soil contact pressure;

$$J = \frac{i_0 \ell}{k};$$

i_0 = degree of slip and

k = deformation modulus.

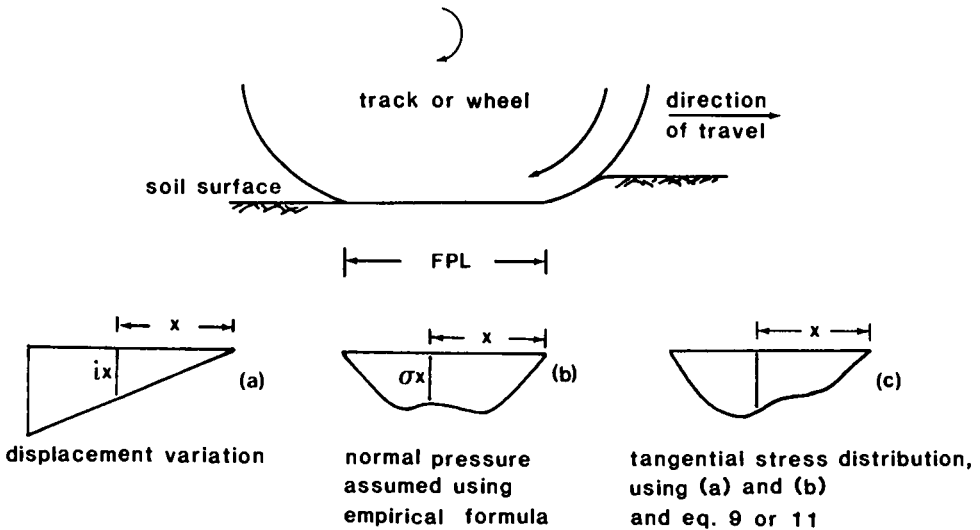


Fig. 3.39. Schematic for deformation and interfacial stresses at tyre(track)-soil interface.

The 'sled' parameters C , ϕ , k , k_T , can be obtained experimentally in the laboratory using an annular ring or a sled plate where the bottom surface is rendered similar to that of the tyre. Methods for sled parameters determination are illustrated in Figs. 3.40 and 3.41. It should be noted that the C and ϕ parameters shown in Figs. 3.40 and 3.41 bear no correspondence to the Mohr-Coulomb cohesion and friction parameters, and should not be confused with the standard Mohr-Coulomb strength parameters.

Figure 3.42 shows the measured and predicted performance for a 5.44 kN loaded tyre moving on silty loam soil. Equation 3.21 can be used to predict the tangential stresses at any degree of slip. It is assumed that the normal pressure possesses a trapezoidal distribution with its top length equal to half its base. The finite element method (Chapter 7) can be adopted to predict the tyre-soil motion resistance. Close agreement between the measured and predicted input energy which is directly related to the tractive effort can be obtained. Details of the calculation procedures are presented in Chapters 5 and 7.

3.5.2 Track

The procedure for determining the track tractive forces is similar to that for pneumatic tyres and is summarized as follows:

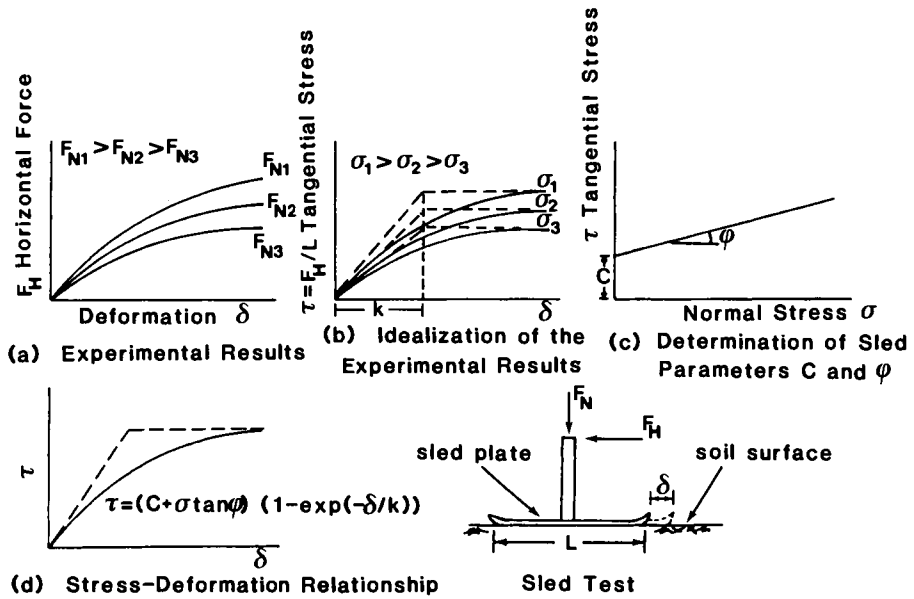


Fig. 3.40. Sled parameters determination - constant deformation modulus.

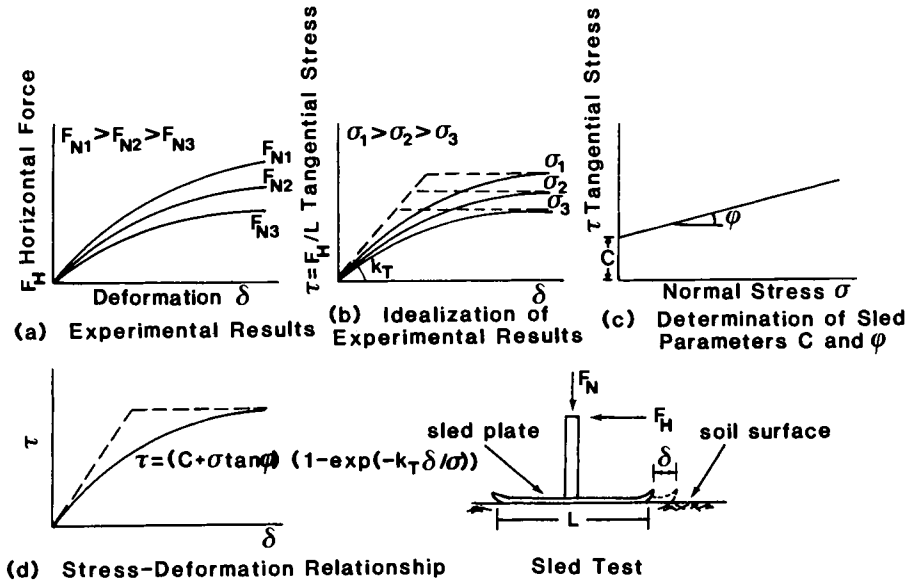


Fig. 3.41. Sled parameters determination - constant slope K_T .

Tyre type: LA 78 x 15
 Load = 5.44 kN; Inflation pressure = 174 kPa
 Contact area = 20.25-19 mm; Rolling radius = 328 mm
 Soil type: silty loam
 Density = 1.8 Mg/m; Moisture content = 12.2%
 S3 = 103.5 kPa (S1-S3) ULT = 352 kPa
 E1 = 2300 kPa Shape factor = 1
 Sled parameters: $C = 8.3$ kPa; $\phi = 2.6^\circ$; $k_T = 3450$ kPa
 Observation: Vane shear maximum = 85 kPa

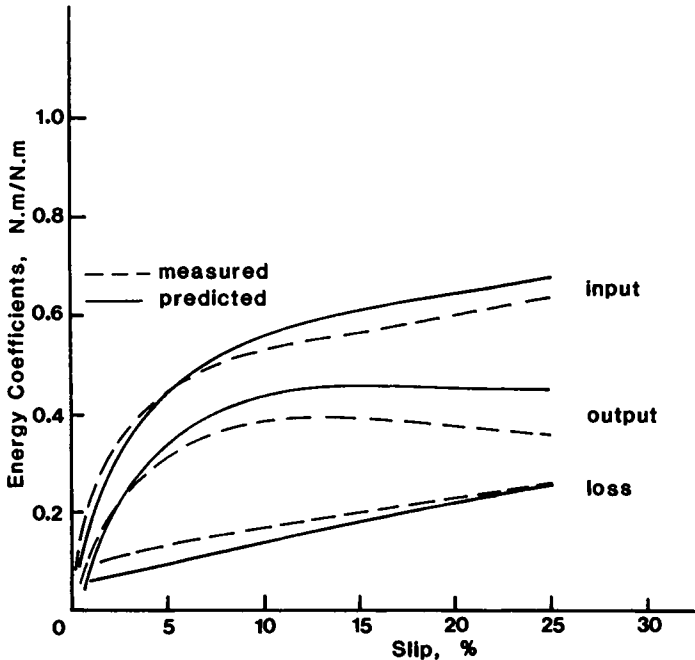


Fig. 3.42. Wheel performance in terms of energy coefficients.

(1) Determine the sled parameters k (k_T), C and ϕ from multi-grouser tests according to the procedure shown in Figs. 3.40 and 3.41.

(2) Use eqs.(3.19 or 3.21) and, provided that the normal pressure distribution and the degree of slip are known, the tangential stresses can be predicted.

(3) Integrate the tangential stresses along the track contact area. The traction force can be predicted for specific degree of slip.

Figure 3.43 shows the results of multi-grouser sled tests moving in a soft soil under different normal pressures. The results show that the curves demonstrate a constant deformation modulus $k = 3.33$. Figure 3.44 shows the effect of surface conditions of the sled plate on the values of sled parameters. In spite of the fact that all the grousers act on the same type of clay, the sled parameters derived are different because of (a) different modes of failure due to

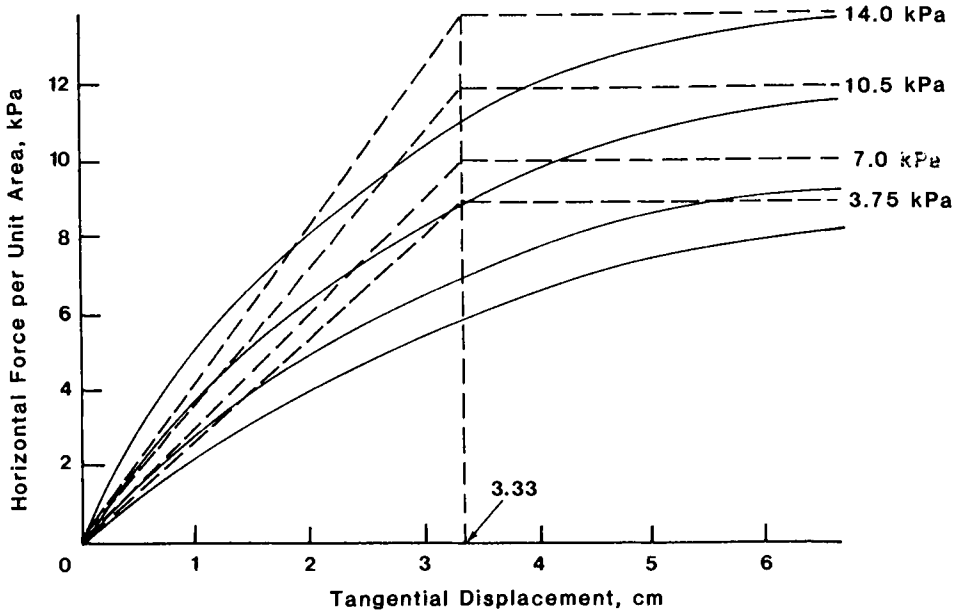


Fig. 3.43. Tangential stress-displacement relationship for the aggressive MGE ($s = 12.5$ cm).

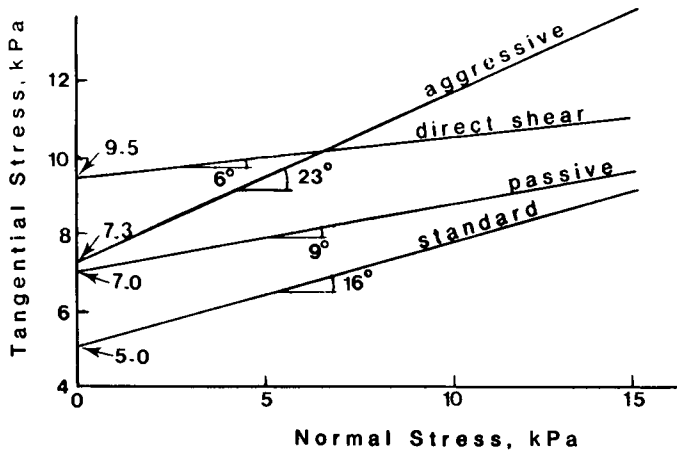


Fig. 3.44. Tangential - normal stress relationships.

dimensions, and (b) different grouser surface conditions. Table 3.2 shows the sled parameters for different types of grousers mounted on various sled plates.

TABLE 3.2
Sled parameters

Test description	C kg/cm ²	ϕ degrees	k cm
Direct shear	0.095	6.0	0.16
MGE - Aggressive	0.073	23.0	3.33
MGE - Standard	0.05	16.0	2.60
MGE - Passive	0.07	9.0	3.33

Figure 3.45 shows comparison between the measured and predicted input energy coefficients for two-dimensional track section tests conducted in the laboratory. It is interesting to note that at low degrees of slip there are differences between the predicted values using direct shear test and aggressive grouser sled tests, while at high degrees of slip both types of tests give the same results because the mode of failure becomes similar for all types of tests. The slip surface becomes parallel to the track belt. The discrepancy between the predicted and the calculated tractive effort can be attributed to the following:

- (a) difference in flexibility between the sled plate and the track,
- (b) no consideration for the effect of sled plate dimensions on the tangential stress-deformation relationship (eqs.3.19 or 3.21).
- (c) difference in the rate of shearing the soil between the sled test and the actual track.

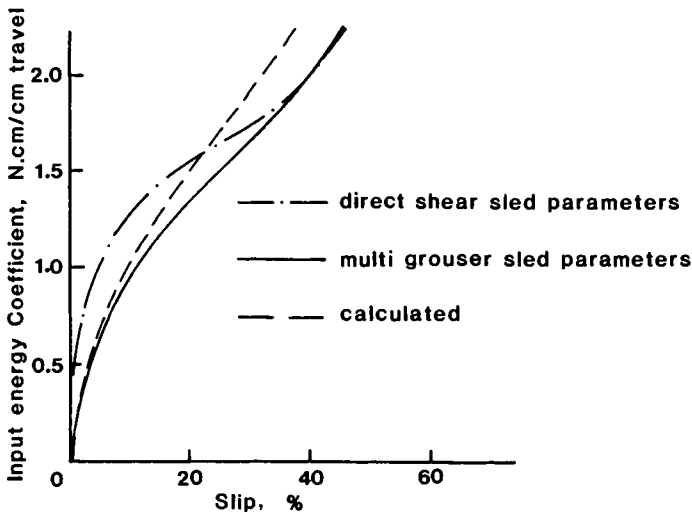


Fig. 3.45. Input energy coefficient prediction. Aggressive track.

3.6 SUMMARY

The mechanics of interaction between traction elements and supporting ground are essentially similar between tyres and tracks, and boil down to the action of the most basic element within the system which can develop thrust in the ground. Flotation provides the support bearing capability of the vehicle, whilst "thrust" provides the driving force.

In developing an efficient traction element, it is important to provide thrust without immobilization resulting from loss of flotation or insurmountable motion resistance due to bulldozing effects. Excessive slip generation at the interface between traction element and ground is a demonstration of shear failure of the ground near the surface. This degrades from thrust development and (a) reduces tractive efficiency, and (b) can cause immobilization if flotation is destroyed by ground degradation.

REFERENCES

- Bekker, M.G., 1956. Theory of Land Locomotion. The University of Michigan Press, Ann Arbor, Michigan, 520 p.
- Bertin, J. and Berthelot, M., 1967. A transport philosophy for developing countries. *J. Hovering Craft and Hydrofoil*, 7-2:24-35.
- Brusentsev, F.S., 1964. The tractive performance of tractors with bulldozers. *J. Terramechanics*, 4-4:9-16.
- Cho, S.W., Schwanghard, H. and Sybel, V.H., 1969. The spacing effect of track shoes on loose soils. *J. Terramechanics*, 6-3:21-45.
- D'Avello, F.S., 1964. Terra tires. *J. Terramechanics*, 1-4:107-116.
- Finney, A., 1961. Special application of high mobility tires. Proc. 1st Int. Conf. Mechs. Soil-Veh. Systems, Torino, Italy, pp. 465-485.
- Gasslander, J.E., 1982. State-of-the-Art Report in Forest Engineering, 19-1:71-82.
- Janosi, Z. and Hanamoto, B., 1961. The analytical determination of drawbar-pull as a function of slip for tracked vehicles in deformable soils. Proc. 1st Int. Conf. Mechs. Soil-Veh. Systems, Torino, Italy, pp. 707-736.
- Kacigin, V.V. and Guskov, V.V., 1968. The basis of tractor performance theory. *J. Terramechanics*, 3-2:71-84.
- Kliffoth, F., 1966. The determination of traction coefficient curves for synthetic farm tractor field tests. *J. Terramechanics*, 3-2:71-84.
- Kolobov, G.G., 1966. Soil pressure measurements beneath tractor tires. *J. Terramechanics*, 3-4:9-15.
- Liston, R.A., 1964. Walking machines. *J. Terramechanics*, 1-3:18-31.
- Meyer, M.P. et al., 1977. International Society for Terrain-Vehicle Systems standards. *J. Terramechanics*, 14-3:153-182.
- Prandtl, L., 1949. *Fuehrer Durch Die Stroemungslehre*. 3rd ed. Friedrich Vieweg and Sohn, Braunschweig, Germany, 407 p.
- Siddall, J.N., 1964. The wave mode of walking locomotion. *J. Terramechanics*, 1-4:54-73.
- Turnage, G.W., 1978. A synopsis of tire design and operation considerations aimed at increasing in-soil tire drawbar-pull performance. Proc. 6th Int. Conf. Int. Soc. Terr. Veh. Systems, ISTVS, Vienna, Austria, 2:757-810.
- Turnage, G.W., 1972. Tire selection and performance prediction for off-road wheeled vehicle operations. Proc. 4th Int. Conf. Int. Soc. Terr. Veh. Systems, Stockholm, Sweden, 1:61-82.
- Wisner, R.D. and Luth, H.J., 1973. Off-road traction prediction for wheeled vehicles. *J. Terramechanics*, 10-2:49-61.
- Yong, R.N., 1982. Track/grouser-soil interaction studies. Vehicle Mobility Laboratory, McGill University, Montreal. Technical report submitted to the Defence Research Establishment, Suffield, 125 p.

- Yong, R.N., Boonsinsuk, P. and Fattah, E.A., 1980. Tyre flexibility and mobility on soft soils. *J. Terramechanics*, 17-1:43-58.
- Yong, R.N., Fattah, E.A. and Youssef, A.F., 1976. Performance of a passive grouser track system. *Soc. Auto. Engrs.*, 85-3:2045-2052.
- Yong, R.N. and Warkentin, B.P., 1975. *Soil Properties and Behaviour*. Elsevier, Amsterdam, 449 p.

NOMENCLATURE

A	contact area
C	cohesion
CI	soil cone index
F	traction force
H	tractive force
I	strain-rate invariant
P	drawbar-pull
P_T	rolling resistance
P_{20}	pull force at 20 percent degree of slip
Q	input torque
S	degree of slip
TF	towed force or rolling resistance
V	soil velocities
V_a	tyre translational velocity
V_s	tyre slip velocity
W	tyre or track load
b	tyre section width
$b\ell$	contact area
d	tyre diameter
h	tyre section height
i, i_0	degree of slip
k	deformation modulus
k_T	initial tangent modulus
k_1, k_2	soil parameters
ℓ	contact area length
p	pressure
r	tyre rolling radius
s	tyre slip
γ	tyre deflection or shear displacement
μ	coefficient of friction
σ	normal stress, mean ground pressure or tyre(track)-soil contact pressure
τ	tangential or shear stress
ϕ	soil friction angle
ω	angular velocity

Chapter 4

ANALYTICAL METHODS

4.1 GENERAL

Off-road vehicle-ground mechanics is a relatively new field. The need for development of analytical methods to predict vehicle performance over a certain terrain is indeed obvious. To accomplish this most effectively, the characteristics of the vehicle's tractive element and terrain material need to be considered as active partners in the production of vehicle traction.

Plate and cone penetrometers which have been used extensively in the field of soil mechanics to evaluate the bearing capacity of soil and/or load-settlement relationships were first adopted in the field of off-road mechanics to determine soil "property" values for use in prediction of motion resistance of moving rigid cylindrical wheels or tracks. These predictions which are based on the questionable assumption that the radial pressure beneath a statically loaded narrow rectangular plate and a point at wheel-soil ground interface are the same for the same ground sinkage, neglect the many obvious differences in stress regimes developed between statically and dynamically loaded systems, and the problem of physical boundary conditions. Bekker (1956, 1960, 1969) eliminated the problem of influence of plate size by using circular plates of different diameters (Bevameter). By assuming that the pressure-sinkage relationship is linear on a log-log scale, he obtained three dimensionless parameters k_c , k_ϕ , n , which are known as soil values. As will be seen later in this Chapter, prediction methods based on the plate penetration approach are simple and can utilize a programmable calculator to develop computational procedures to predict the motion resistance and sinkage.

Mobility or trafficability prediction methods based on the use of cone penetration results are based on a curve fitting correlation between dimensionless numbers for (a) certain performance characteristics (drawbar-pull/motion resistance), and (b) element parameters which include material cone index. Whilst methods of analysis or prediction based on the use of plate and cone terrain results are generally accepted as being "rough and ready" methods for prediction of "mobility", they cannot be used to differentiate between the performance of variable tractive elements (e.g. tread pattern, inflation pressure, ... etc.) or to evaluate subsoil response beneath the tractive element.

With the advance of electronic computational tools and numerical methods for solving large numbers of linear or nonlinear equations, research which has concentrated on the modelling of tractive element-soil systems interaction falls into two separate categories:

(a) Methods of limit equilibrium which assume that the continuum beneath the tractive element is in a state of limit equilibrium, hence performance prediction is valid only at this state.

(b) Application of finite element methods (FEM) to predict the performance of the tractive element without consideration of a limiting state, and also the material or soil response beneath the tractive element at any state of loading stress.

Since the efficiency of the tractive element is a prime factor in the operational cost of off-road vehicles, evaluating the performance of the element in energy terms can give a vivid picture of the power required to move the tractive element and the energy wasted in the tractive element-soil system. Hence, a computational technique for optimizing element parameters constitutes an important requirement in seeking an energy efficient traction system.

In this Chapter some of the different methods of analysis are discussed. The energy approach for analysis of interaction between a tractive element and the supporting terrain material is given in Chapter 5, whilst the FEM of application to traction problems is discussed in Chapters 6 and 7.

4.2 REQUIREMENTS FOR PREDICTION

The general requirements for constructing a model for an engineering problem to analyse or predict the behaviour under the effect of certain boundary conditions are:

(i) Idealization. There are different types of idealization such as

(a) geometrical idealization, in which all the physical components of the problem can be identified using analytical geometry,

(b) material idealization, in which the material can be idealized as elastic, nonlinear elastic, elasto-plastic, plastic, ... etc. This type of idealization influences the derivation of constitutive relationships for the material, and

(c) continuum idealization, which is performed when an exact solution for the problem cannot be obtained. In this idealization, the continuum is represented by nodal points at regular intervals or assembly of finite elements according to the numerical method adopted.

(ii) Governing equations. The requirements for developing the governing equations which define the state of stress and/or the state of strain at any point of the continuum are generally a function of the method of analysis adopted. For example, the limit equilibrium approach requires (a) conditions of equilibrium, and (b) yield criteria.

The FEM, on the other hand, requires (a) constitutive relationships, (b) conditions of equilibrium, (c) displacement functions, (d) strain-displacement relationships, and (e) applicable energy principle.

(iii) Method of solution. Once the governing equations for the problem are developed, they can be solved to obtain the required information, using the established boundary conditions. A computer is a must for carrying out the tedious computations.

From the above discussion it can be concluded that methods of analysis or prediction based on the plate approach do not satisfy all the requirements for establishment of a rational model, and hence they are called semi-empirical methods. Methods based on the cone approach are seen not to satisfy any of the requirements, and hence are identified as empirical methods.

In general, a successful rational analytic model should satisfy the following requirements:

(1) The model should represent physically and analytically the response behaviour of the system due to the effect of the operating conditions.

(2) The parameters required for operating the model should be realistic and easy to obtain.

(3) The data required for operating the model should be minimal.

(4) The model should be suitable for the purpose it serves, i.e. simple model for field predictions or detailed model for design purposes.

(5) Economic - this involves the time required to obtain the data, preparation time and the computer time for running the model.

The next Section presents the discussions involving parameters and factors which affect conventional tractive element-soil system modelling.

4.3 PARAMETERS AND FACTORS

The parameters and factors which can affect physical/analytical modelling of tractive element-soil systems can be classified as follows:

(a) parameters concerned with the tractive element,

(b) parameters concerned with the tractive element-soil characteristics,

(c) parameters concerned with the supporting terrain material,

(d) factors involved in the type of measurements made, and

(e) factors associated in the production of the required output information.

A complete solution of the problem requires proper consideration of all the pertinent parameters. In most instances however, we note that in considering all the parameters and factors in the development of the solution, a considerable expenditure of time and money may result, without a significant increase in the accuracy of the model. It would then be wise to limit one's consideration to the more influential items in the development of the analytical model chosen to represent the problem at hand.

4.3.1 Tractive element parameters

The basic parameters involved in wheel and track-soil interactions are illustrated in Fig. 4.1. Whilst the basic interaction mechanics are similar in many ways between wheel-soil and track-soil interactions, morphological considerations require somewhat different approaches for performance prediction and evaluation - since the outputs required are not necessarily similar.

4.3.2 Tractive element-soil characteristics

The tangential stress-strain relationship at the tractive element-soil interface contributes significantly in the development of the ground response beneath the tractive element. It also affects the type of idealization of the ground material continuum.

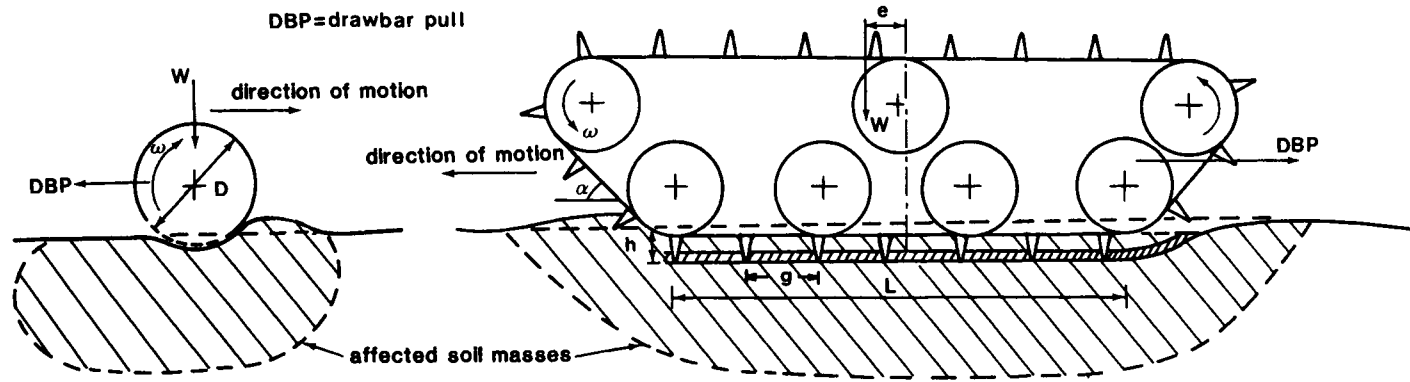
4.3.3 Supporting terrain material parameters

The supporting terrain material parameters which could affect the type and formulation of the governing equation (of the analytical model) are:

- (a) homogeneity of the material in terms of isotropic characteristics and layering,
- (b) material fabric such as particulate-unbonded (sand) or bonded (snow), continuous (remoulded soft clays or unconsolidated clays), and fibrous, such as muskeg and peat, and
- (c) the load-unload deformation characteristics of the material.

4.3.4 Type of measurements

The terrain material characteristics can be determined through different types of field or laboratory test measurements. These will be discussed in detail in Chapter 9. For the purposes of modelling, the direct shear test can be used for determining material strength parameters - if the supporting material is soil - for direct application in limit equilibrium models (Yong et al., 1981). If proper stress-strain relations (of the material) can be obtained, models based on continuum mechanics can be used with solutions sought through application of the finite element method (Yong and Fattah, 1976, and Yong et al., 1978). In the case where cone penetrometers are used, since only penetration resistance is measured, models based on direct or indirect correlations or models relying on dimensional analysis applications, are used. When only plate penetration measurements are available, models based on semi-empirical relations and correlations appear to be favoured for use in predicting vehicle mobility. Vane-cone measurements have also been used to predict mobility and motion resistance (Yong et al., 1975).



VARIABLES ENCOUNTERED IN WHEEL-SOIL INTERACTION PROBLEM:

1. Wheel diameter "D", width and cross-sectional shape.
2. Vertical load "W".
3. Wheel rigidity.
4. Wheel surface roughness and tread configuration.
5. Slip rate value.
6. Rotational velocity " ω ".
7. Soil properties and profile.
8. Wheel type (towed or driven).
9. Inflation pressure.
10. Carcass stiffness and mechanical properties.

VARIABLES ENCOUNTERED IN TRACK-SOIL INTERACTION PROBLEM:

1. Grouser shape and geometry.
2. Grouser height "h".
3. Grouser spacing "g".
4. Contact length "L".
5. Slip rate value.
6. Angle of attack " α ".
7. Driving sprocket position.
8. Drawbar-pull position.
9. Vertical load "W" and its eccentricity "e".
10. Number and spacing of road wheels.
11. Rigidity of the track belt.
12. Soil properties and profile.
13. Road wheels stiffness characteristics.
14. Suspension stiffness.
15. Track tension.
16. Grousers geometrical configuration.
17. Grousers-track connection type.

Fig. 4.1. Basic elements involved in wheel-soil and track-soil interaction.

4.3.5 Required output results

An ideal analytical/computer model should accurately describe, in mathematical terms, the tractive element-soil interaction mechanics, the tractive element motion, and predict its performance and associated soil response. The term "soil" is used in most instances as a general term to identify the substrata material. It is understood that the material under consideration may be some other type of "material". When it is not required to predict individual tractive element-soil system performance, it may be more suitable to use a model which can fit the overall system performance. For example, for design purposes, a detailed component model is needed to differentiate between the different types of tractive elements, whilst for trafficability or mobility prediction purposes, a simple model describing motion capability would be more suitable.

4.4 PLATE APPROACH

The plate penetration test has received a great deal of attention as a means of measuring soil characteristics. In civil engineering, loading tests on large plates (30-60 cm diameter) are frequently used to assess the bearing capacity of soil for foundations where the analogy is obviously close, i.e. the subsoil response beneath the plate and foundations are similar. Usually in plate bearing tests, the loads are applied slowly and sinkage is measured.

Models based on plate penetration results have been used to predict the performance of a moving running gear. The plates used are generally less than 15 cm diameter or width, and are allowed to sink several inches into the soil.

Most prediction models based on the plate sinkage approach have been primarily experimental and are employed as follows:

(1) Plate load tests, using different plate sizes, are conducted to provide basic pressure-penetration relationships which are thought to be characteristic of the terrain material mechanical response performance.

(2) By means of essentially curve-fitting techniques, parameters of the prediction equation are calculated. The basis for calculation originates from the application of limit equilibrium theory to a bearing capacity problem not unlike that used in the Prandtl rigid-plastic indenter problem.

(3) These parameters are then employed in the prediction model to predict penetration characteristics of the running gear.

The pressure-sinkage relationship for a plate load penetration test is generally plotted in the form of an exponential curve, as:

$$P = kz^n \tag{4.1}$$

where P = pressure on the plate;

z = depth of plate penetration;

k = function of soil and plate geometry and
 n = property of soil.

The basic idea of correlating the sinkage beneath the plate and the running gear for the same pressure begins with consideration of the general Bernstein equation:

$$P = kz \quad (4.2)$$

In applying the limit equilibrium approach to evaluation of the bearing capability of the loaded plate, Bekker (1960) proposed a modification of the Bernstein relationship as follows:

$$P = \left(\frac{k_c}{b} + k_\phi \right) z^n \quad (4.3)$$

where k_c , k_ϕ and n are empirically measured soil-describing constants, and b is the minor dimension of the loaded area.

To predict the running gear drawbar-pull (Fig. 4.2) plate loading models utilize the condition of equilibrium in the horizontal direction as follows:

$$DBP = H - RT \quad (4.4)$$

where DBP = drawbar-pull;

H = tractive effort and

RT = motion resistance.

The methods for calculation of tractive effort at the running gear-soil interface can be found in Chapter 2. In this Section, we will address methods for calculating running gear motion resistance.

4.4.1 Running gear motion resistance

The motion resistance of a running gear can be considered as a summation of the following:

(a) motion resistance encountered due to compaction of the bearing substrate material (soil) in the vertical direction,

(b) motion resistance due to bulldozing efforts in the horizontal direction, and

(c) motion resistance due to flexing of the running gear.

In using the plate model to calculate the vertical motion resistance component for a rigid wheel or track moving on soil, it is assumed that the radial stresses at any point at the soil-running gear interface is the same as that of a plate of the same width as the running gear. It is further assumed that the plate penetration is the same as the sinkage produced by the running gear (Fig.

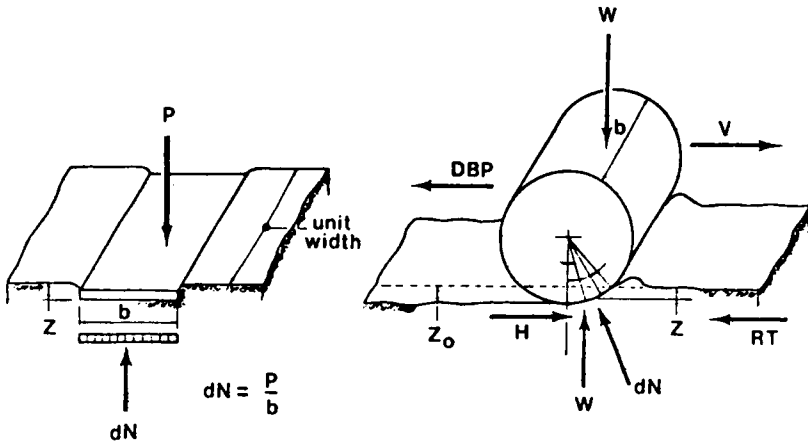


Fig. 4.2. Wheel and plate - soil force system.

4.2). Utilizing the stated assumptions and eq.(4.3), the sinkage Z_0 and compaction resistance R_c of a rigid wheel can be written as:

$$Z_0 = \left[\frac{3W}{bk D (3-n)} \right]^{2/(2n+1)} \tag{4.5}$$

$$R_c = \frac{bk}{n+1} \left[\frac{3W}{bk D (3-n)} \right]^{(2n+2)/(2n+1)} \tag{4.6}$$

where $k = \left(\frac{k_c}{b} + k_\phi \right)$

In the case of rigid track the compaction resistance can be written, (Bekker, 1960) as:

$$R_c = \frac{1}{(n+1)(k_c + bk_\phi)^{1/n}} \left[\frac{W}{\ell} \right]^{(n+1)/n} \tag{4.7}$$

where ℓ = track contact length;

W = track or wheel load;

b = track or wheel width;

D = wheel diameter and

k_c, k_ϕ, n = soil values.

Bulldozing resistance is difficult to calculate since it is difficult to distinguish between compaction and bulldozing. If it is defined as the force re-

quired to push the (terrain) soil mass at a sinkage z ahead of the track or wheels, the bulldozing resistance can be calculated using passive earth pressure theories as follows:

$$R_b = \frac{b \sin(\alpha + \phi)}{2 \sin \alpha \cos \phi} \left[2zck_c + \gamma z^2 k_\gamma \right] \quad (4.8)$$

where $k_c = (N_c - \tan \phi) \cos^2 \phi$;

$k_\gamma = (2N_\gamma / \tan \phi + 1) \cos^2 \phi$;

α = angle of attack for the track

$\approx \cos^{-1} (1 - 2z/D)$, for the wheel;

z = track or wheel sinkage;

N_c, N_γ = bearing capacity factors (Fig. 4.3);

γ = unit weight of soil and

c, ϕ = soil strength parameters.

It should be noted that in some instances there is no displacement of soil in front of the wheel or track, hence the value calculated using eq.(4.8) overestimates the real values.

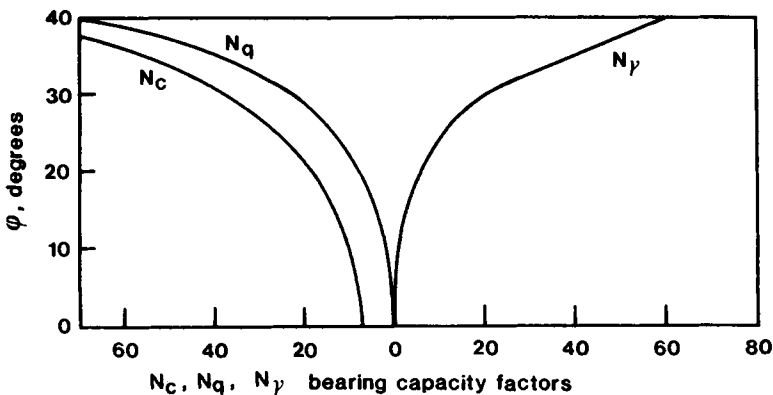


Fig. 4.3. Soil bearing capacity.

Motion resistance due to flexing of the tractive element is a function of many factors (in the case of a wheel), such as:

- (1) number of plies,
- (2) thickness of carcass,
- (3) tread design,
- (4) tyre interface resistance characteristics,
- (5) inflation pressure,

(6) all the various other factors that go into the characterization of tyre stiffness and flexibility, and

(7) wheel-soil relative stiffness.

In the case of a track, the flexing resistance is a function of:

(1) road wheel characteristics similar to those involved in control of tyre properties and performance,

(2) road wheel spacing,

(3) track tension,

(4) track flexibility/stiffness, and

(5) track-soil relative stiffness.

Experimentally, the flexing resistance can be determined with respect to rigid surfaces only, which will be an upper value for the tyre, and an intermediate value for the track. In the case of a pneumatic tyre, the flexing resistance on rigid surfaces can be evaluated as:

$$R_t = W \cdot f_t \quad (4.9)$$

$$\text{where } f_t = u/P_i^a; \quad (4.10)$$

u and a = empirical fitting constants obtained from laboratory experiments and

P_i = tyre inflation pressure.

Thus the total motion resistance can be calculated as:

$$RT = R_c + R_b + R_t \quad (4.11)$$

The application of the plate model to predict the motion resistance of pneumatic tyres is not entirely accurate since the model does not physically represent the loaded deflection shape of the tyre at the tyre soil interface. Figure 4.4 shows the physical model for a pneumatic tyre (Bekker, 1960), and the actual deflected tyre surface (Freitag and Smith, 1966).

If the tyre is physically idealized as shown in Fig. 4.4 and if the pressure is assumed to be distributed uniformly along the flat contact surface, the compaction resistance can be calculated as:

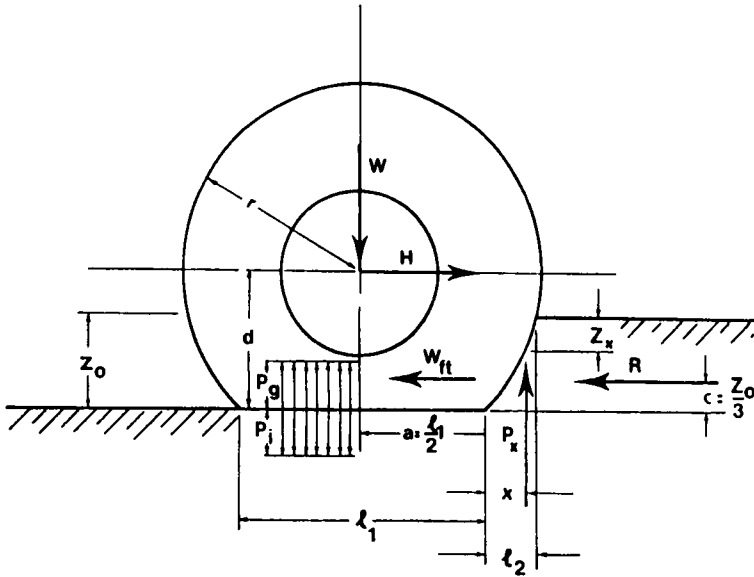
$$R_c = \frac{[b(P_i + P_c)]^{(n+1)/n}}{(k_c + bk_\phi)^{(n+1)}} \quad (4.12)$$

where P_i = tyre inflation pressure;

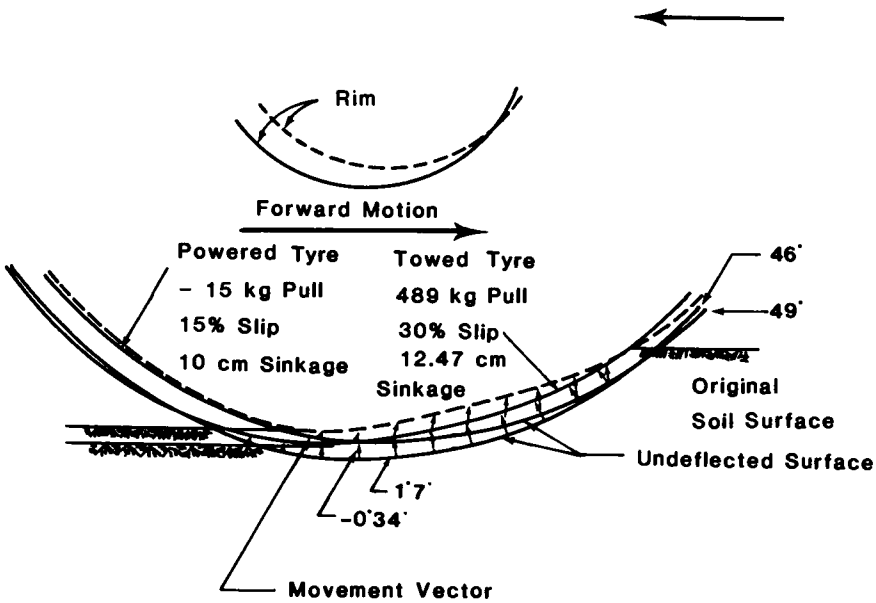
P_c = carcass pressure and

$P_g = (P_i + P_c)$ = ground pressure.

and the dynamic sinkage Z_0 can be calculated as:



(a) Pneumatic tyre moving over soft ground (Bekker, 1960).



(b) Shape of a moving tyre, powered and towed wheel (Freitag and Smith, 1966).

Fig. 4.4. The physical model and actual measurements for a pneumatic tyre.

$$Z_o = \left[\frac{P_i + P_c}{k_c/b + k_\phi} \right]^{1/n} \quad (4.13)$$

An inflated tyre can behave as a rigid tyre if the supporting terrain is soft. The relationship for differentiation between flexible and rigid tyre action was established by Bekker (1960) using static equilibrium consideration. If the contact length l_1 is equal to zero, the following relationship is obtained (Bekker, 1960):

$$P_{cr} = \frac{W(n+1)}{b \left[\frac{3W}{(3-n)bk\sqrt{D}} \right]^{1/(2n+1)} \sqrt{D} - \left[\frac{3W}{(3-n)bk\sqrt{D}} \right]^{2/(2n+1)}} - P_c \quad (4.14)$$

where P_{cr} = inflation pressure above which the tyre will behave as a rigid wheel.

4.4.2 Tractive effort

Tractive effort can be defined as the tractive force which can be mobilized at the terrain interface at a certain degree of slip. This force is a function of all the parameters and factors shown in Fig. 4.1. We recall that the characteristics of this force, the parameters affecting it, and the methods of calculation have been presented in Chapter 2. If it is assumed that (a) the maximum mobilized force occurs between soil and soil, (b) the Mohr-Coulomb failure criteria is valid and applicable, and (c) the tractive element acts on a flat ground surface, then the soil strength parameters (c, ϕ) , can be used to determine the maximum mobilized force as:

$$H = A \left(c + \frac{W}{A} \tan \phi \right) \quad (4.15)$$

where c and ϕ = soil strength parameters determined from standard triaxial test, or direct shear test;

W = tractive element load and

A = tractive element-ground contact area.

In tractive element tests performed on soil, a relationship between applied shear stress and shear displacement can be obtained as a function of the normal load applied to the tractive element. There are different curve fitting techniques which permit us to relate the shear stress τ to the shear deformation Δ , (Kacigin and Guskov, 1968), as:

$$\frac{\tau}{\sigma} = f_m \left[1 + \frac{a}{\cosh(\Delta/k_\tau)} \right] \tanh(\Delta/k_\tau) \quad (4.16)$$

where Δ = shear deformation;

k_r = displacement at peak shear stress and

a = constant.

This function, which is illustrated in Fig. 4.5, contains three constants describing the soil characteristics:

- (a) the ratio f_m of the residual shear strength to the contact stress at large displacements, (this can be represented by the Coulomb parameters c and ϕ),
- (b) the displacement k_r required to reach the peak shear stress, and
- (c) the constant "a" which depends on the ratio of the friction coefficients at the peak and residual stresses. The magnitude of "a" is given with sufficient accuracy by the expression:

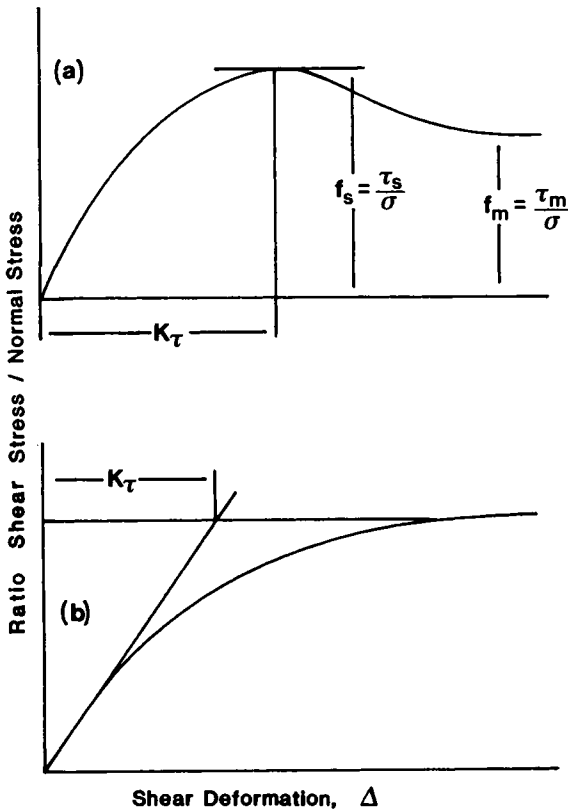


Fig. 4.5. Typical shear stress deformation curves for (a) loam, dense sand, sensitive soil, and (b) loose sand, remoulded clay.

$$a = 2.55 \left(\frac{f_s - f_m}{f_m} \right) 0.825 \quad (4.17)$$

In the case of certain simple soils such as dry sand, and a saturated clay there is no peak shear stress as shown in Fig. 4.5b. In this case $\tau_s = \tau_m$ and hence $a = 0$, and the expression reduces to :

$$\frac{\tau}{\sigma} = f_m \tanh (\Delta/k_\tau) \quad (4.18)$$

where k_τ is the tangent modulus of the stress-deformation curves as shown in Fig. 4.5, and σ is the normal stress.

The tractive force can be calculated by integrating the tangential stress τ over the tractive element-soil interface. Details of the calculation procedure for specific cases are presented in Chapter 3. Once the tractive force at any degree of slip, and the motion resistance are calculated, the drawbar-pull can be determined using eq.(4.4).

4.5 SEMI-EMPIRICAL TECHNIQUES

4.5.1 Dimensional analysis

The method of dimensional analysis, as the name implies, evolves from a consideration of the variables in the problem and the dimensions of these variables. For example, acceleration has dimensions of a length divided by the square of time, unit weight has the dimensions of force divided by length cubed, etc. Therefore, to apply dimensional analysis to a problem it is only necessary to determine the variables and their basic dimensions. Application of the Buckingham Pi Theorem then leads to a set of dimensionless parameters from which modeling laws can be derived. It should be noted that whilst a partial solution to nearly any problem can generally be obtained with this technique, a complete solution may not be easily obtained, nor is the inner mechanism of a phenomenon revealed by dimensional reasoning alone.

In studies by the Waterways Experiment Station (WES), the method of dimensional analysis was used to model the running gear (wheel or track)-soil interaction system. This was done by performing numerous tow-bin and field tests for different characteristics of running gear on different types of soils. The measured running gear performance and the characteristics of the tested elements were then evaluated in terms of dimensionless numbers for each class of soil type. The relationship obtained thereby between the dimensionless characteristics and the performance of the running gear can be used to predict the performance of different gear characteristics.

4.5.2 Method of analysis

In running gear-soil systems the independent and dependent parameters can be listed as seen in Tables 4.1 and 4.2.

TABLE 4.1
Independent gear-soil system parameters

Parameters	Symbol	MLT units
<u>Soil:</u>		
Friction angle	ϕ	-
Cohesion	c	$ML^{-1}T^{-2}$
Specific weight	γ	$ML^{-2}T^{-2}$
Penetration resistance	C	$ML^{-1}T^{-1}$
<u>Tyre:</u>		
Diameter	d	L
Section width	b	L
Section height	h	L
Deflection	δ	L
<u>Track:</u>		
Length	L	L
Width	b	L
Deflection	δ	L
Grouser height	h	L
<u>System:</u>		
Load	W	MLT^{-2}
Translational velocity	V	LT^{-1}
Slip	S	-
Gear-soil interaction coefficient	μ	-
Acceleration	g	LT^{-2}

TABLE 4.2

Dependent gear-soil system parameters

Parameters	Symbol	MLT units
Drawbar pull	P	MLT ⁻²
Towed force	P _T	MLT ⁻²
Torque	T	ML ² T ⁻²
Sinkage	Z	L

In the tyre-soil system (WES) seventeen variables are identified with three basic dimensions indicating that $17-3 = 14$ Pi terms would compose a complete set of linearly independent solutions of the dimensional equation. The Pi terms which were derived by a combination of inspection and matrix solution techniques should be physically meaningful. In addition, it is necessary that these can be tested conveniently, and can be redefined or combined by multiplication, division or raised to a power as long as the total number of Pi terms remains the same - i.e. 14 in this case. The resulting Pi terms by WES for their study were:

$$\begin{aligned}
 \pi_1 &= P/W & \pi_2 &= P_T/W & \pi_3 &= T/dW & \pi_4 &= Z/d & \pi_5 &= \mu \\
 \pi_6 &= \phi & \pi_7 &= S & \pi_8 &= b/d & \pi_9 &= h/d & \pi_{10} &= \delta/h \\
 \pi_{11} &= cd^2/W & \pi_{12} &= d^3/W & \pi_{13} &= Cd^2/W & \pi_{14} &= gd/V^2
 \end{aligned}$$

The functional relationship between the Pi terms is:

$$\frac{P}{W}, \frac{P_T}{W}, \frac{T}{dW}, \frac{Z}{d} = f\left(\mu, \phi, S, \frac{b}{d}, \frac{h}{d}, \frac{\delta}{h}, \frac{cd^2}{W}, \frac{Cd^2}{W}, \frac{d^3}{W}, \frac{gd}{V^2}\right) \quad (4.19)$$

If analysis is performed with respect to a constant degree of slip (e.g. $S = 20\%$), one term can be omitted. Under normal operating speeds, the effect of speed on the dependent parameters can be neglected, thus all terms incorporating speed can be omitted. If tractive failure occurs between soil and soil, the running gear-soil interaction coefficient μ has no effect on performance. For cohesive soils the average cone index C is equivalent to cohesion c , (WES), thus density is not a significant factor. For sands, the cone index gradient G is a function of the density γ and angle of internal friction ϕ , thus the term which includes C can be neglected, and G can be used instead of γ and ϕ . For tyre size variables, the Pi variables are b/d , h/d , δ/h . Experiments conducted (WES) show

that the influence of (h/d) can be considered as insignificant. The Pi term functional relations can be written as:

$$\text{For clay: } P/W, P_T/W, T/dW, Z/d = f\left(\frac{Cd^2}{W}, \frac{b}{d}, \frac{\delta}{h}\right) \quad (4.20)$$

$$\text{sand: } P/W, P_T/W, T/dW, Z/d = f\left(\frac{Gd^3}{W}, \frac{b}{d}, \frac{\delta}{h}\right)$$

Freitag (1966) developed two dimensionless prediction terms for treadless (buffed smooth), thin-walled, low-ply tyres as follows:

$$\text{For cohesive soils: } N_c = \frac{Cbd}{W} \cdot \left(\frac{\delta}{h}\right)^{1/2} \quad (4.21)$$

and

$$\text{frictional soils: } N_s = \frac{G(bd)^{3/2}}{W} \cdot \frac{\delta}{h} \quad (4.22)$$

Turnage (1978) modified eq.(4.21) to account for the effect of tyre cross-sectional shape, (circular or rectangular):

$$N_c = \frac{Cbd}{W} \cdot \left(\frac{\delta}{h}\right)^{1/2} \cdot \frac{1}{1 + b/2d} \quad (4.23)$$

where N_c = clay-tyre numeric;

N_s = sand-tyre numeric;

C = cone index for clay (50 → 470 kPa) and

G = sand penetration resistance gradient (slope of C versus depth).

Figure 4.6 shows a typical relationship between cone index (0.5 in.² base area and 30° apex angle) and depth of penetration for cohesive and sandy soil. For a tyre moving in cohesive-frictional ($c-\phi$) soil, Wismer and Luth (1972) developed the following dimensionless number:

$$N_{CS} = \frac{Cbd}{W} \quad (4.24)$$

For $c-\phi$ soils, the soil penetration resistance C varies with depth of penetration (Fig. 4.7). It should be noted that many independent parameters are neglected in developing the numeric numbers (N_s , N_c , N_{CS}) such as tyre-soil friction (μ) and translational velocity (V) whilst some parameters are implicitly expressed by others, such as tyre stiffness expressed through deflection δ . The effect of tyre type (radial or bias-ply) is not considered in the previous numeric numbers. Figures 4.8 to 4.10 show the experimental relationship between the four basic tyre performances, and the tyre numeric number.

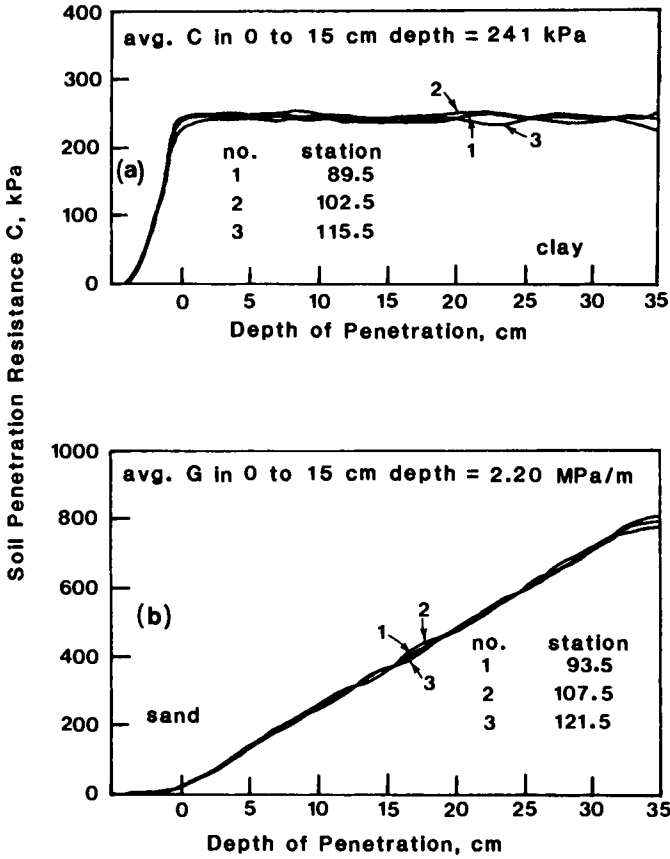


Fig. 4.6. Sample recordings of cone penetration tests in purely cohesive soil and in purely frictional sand. (Turnage, 1978)

We should observe that whilst models based on dimensional analysis may not be used to differentiate between the performance of two different tyre types, they can however be used as a simple technique for prediction of the performance of the running gear, since the relation between a numeric number and certain performance can be expressed by a mathematical formula using a curve-fitting technique, (Figs. 4.9 and 4.10).

4.6 LIMIT ANALYSIS

Mathematical models based on limit equilibrium have been adopted in the field of machine-soil interaction by several investigators. Ohde (1938), Siemens et al. (1964), Osman (1964), Reece (1965), and Yong et al. (1969a, 1969b, 1970), used limit equilibrium procedures to predict the forces on two-dimensional cutting blades. Bekker (1960), Haythornthwaite (1961), Yong et al. (1969a), have also applied these procedures to predict grouser driving forces. In addition, Yong et

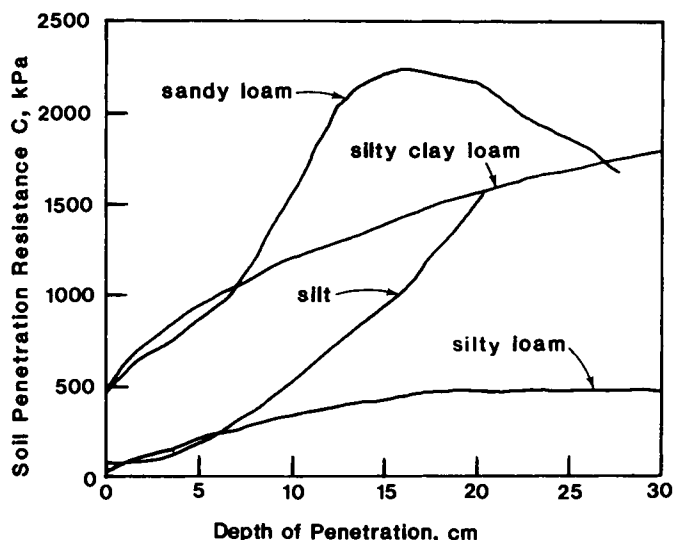
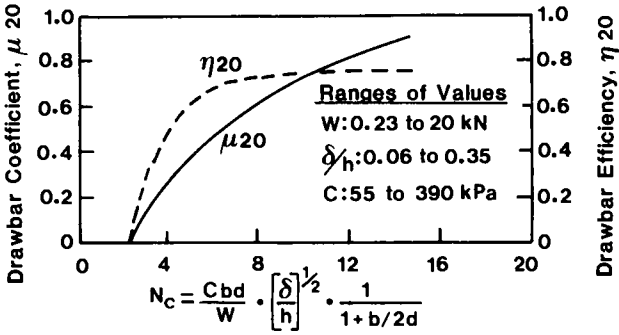


Fig. 4.7. Sample recordings of cone penetration resistance tests in some cohesive-frictional soils. (Turnage, 1978)

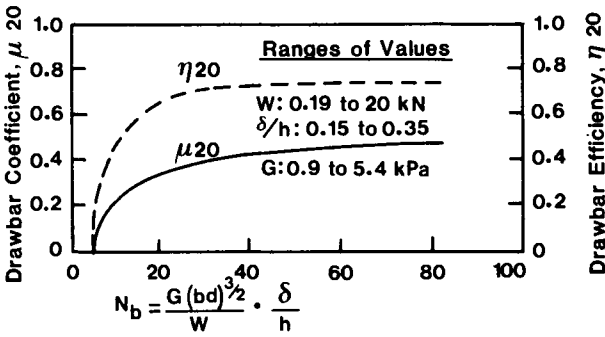
al. (1970) utilized the method to predict interfacial and subsoil stresses for a rigid wheel moving on soft soil, and Karafiath et al. (1971, 1978) have used it to predict the performance of a running gear.

According to the mathematical theory of limit equilibrium, the soil is assumed to be completely rigid up to the point of failure, whereupon it flows steadily under constant stress. This assumption results in the production of a definite failure load at zero displacement. The prediction of failure is governed by assumptions concerning (a) equilibrium or initial conditions, (b) failure criterion, (c) density, γ , and (d) boundary conditions (Terzaghi, 1943).

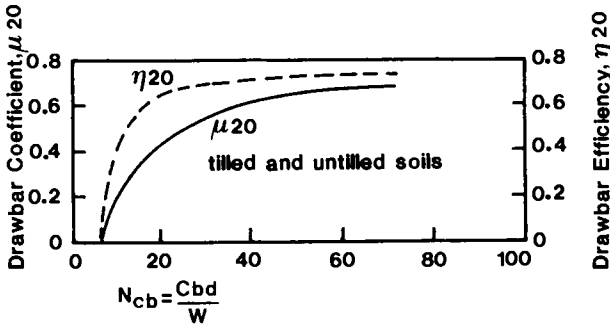
In the limit equilibrium analysis the stability of the soil mass is controlled or affected by the moving running gear. For a generalized case where the velocity and inertia terms are to be considered, it is possible to analyse the situation in terms of velocity fields associated with the dynamic conditions, and to prescribe the appropriate governing equations. The resultant formulations become most complex, and the mathematics arising therefrom do not allow for ready solutions. A simple alternative method for the generalized analysis can be used. This requires the superposition of inertia and velocity terms on a quasi-static basis. Since the dynamic forces are small in relation to the yield stress of the soil, it can be assumed that these forces do not affect the associated development of the stress and velocity fields in the quasi-static conditions.



(a) Cohesive clay



(b) Frictional sand



(c) Cohesive-frictional soils

Fig. 4.8. Relations of drawbar coefficient and drawbar efficiency at 20 percent slip to numerics N_c , N_s and N_{cs} for (a) cohesive clay, (b) frictional sand, and (c) cohesive-frictional soils (modified from Turnage, 1978).

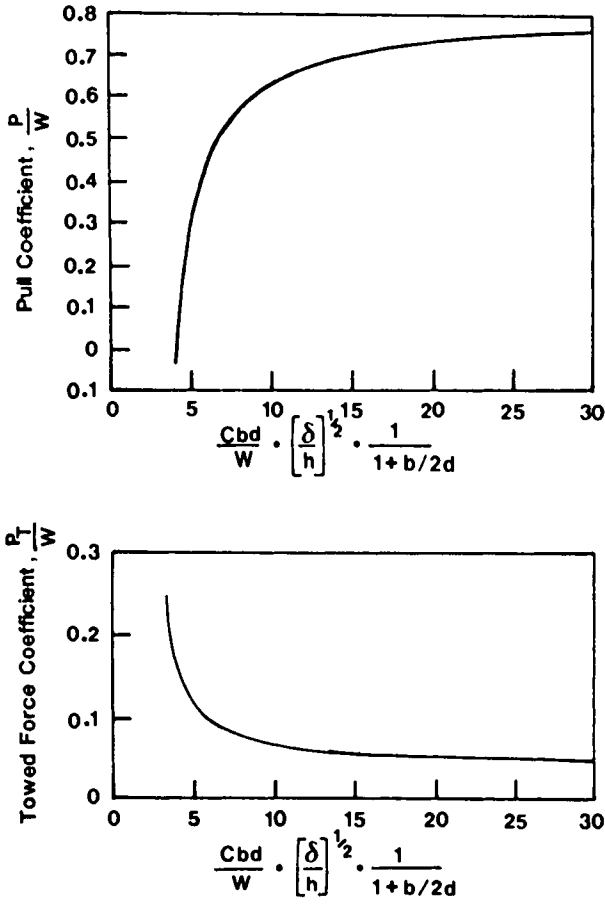


Fig. 4.9. Use of $\frac{Cbd}{W} \cdot \left(\frac{\delta}{h} \right)^{1/2} \cdot \frac{1}{1+b/2d}$ to consolidate field performance data of wheeled vehicles in wet, fine-grained soils.

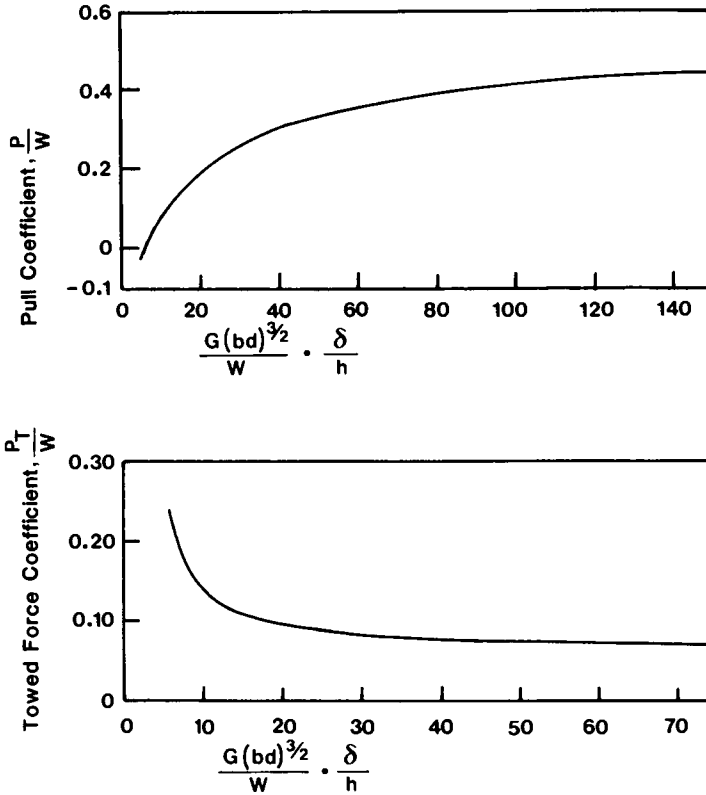


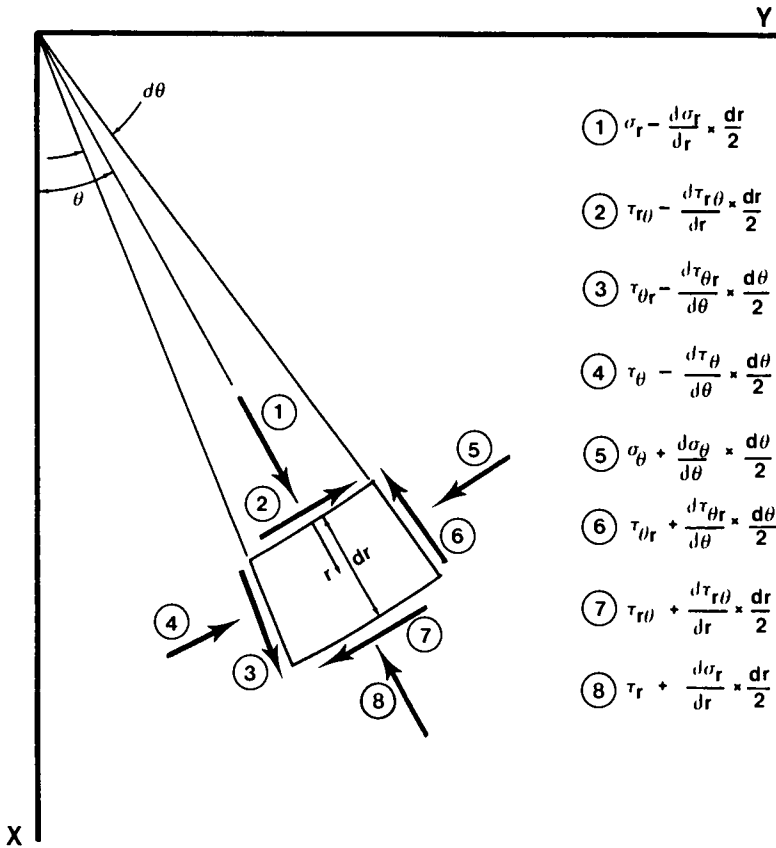
Fig. 4.10. Results of field tests of various wheeled vehicles in sand.

Thus, the associated stress field is a velocity field which describes the resultant flow. Yong and Japp (1968) have used this approach to show that constitutive relations for soil dynamical behaviour for accelerations developed in clay soils of less than 100 g's can indeed be adequately written.

In the following, the derivation of the limit equilibrium governing differential equations for a generalized cohesion-friction material is given. It should be noted that in a state of limit equilibrium any small element within the soil mass has to satisfy two conditions: (a) equilibrium, and (b) yield or failure.

4.6.1 Equations of equilibrium

The partial differential equations of equilibrium in polar coordinate form (Fig. 4.11) are given as follows:



$$\textcircled{1} \sigma_r - \frac{d\sigma_r}{dr} \times \frac{dr}{2}$$

$$\textcircled{2} \tau_{r\theta} - \frac{d\tau_{r\theta}}{dr} \times \frac{dr}{2}$$

$$\textcircled{3} \tau_{\theta r} - \frac{d\tau_{\theta r}}{d\theta} \times \frac{d\theta}{2}$$

$$\textcircled{4} \tau_\theta - \frac{d\tau_\theta}{d\theta} \times \frac{d\theta}{2}$$

$$\textcircled{5} \sigma_\theta + \frac{d\sigma_\theta}{d\theta} \times \frac{d\theta}{2}$$

$$\textcircled{6} \tau_{\theta r} + \frac{d\tau_{\theta r}}{d\theta} \times \frac{d\theta}{2}$$

$$\textcircled{7} \tau_{r\theta} + \frac{d\tau_{r\theta}}{dr} \times \frac{dr}{2}$$

$$\textcircled{8} \tau_r + \frac{d\sigma_r}{dr} \times \frac{dr}{2}$$

Fig. 4.11. Stresses on an element.

$$\frac{\partial \sigma_r}{\partial r} + \frac{1}{r} \frac{\partial \tau_{r\theta}}{\partial \theta} + \frac{\sigma_r - \sigma_\theta}{r} = \rho g \cos \theta$$

(4.25)

$$\frac{\partial \tau_{r\theta}}{\partial r} + \frac{1}{r} \frac{\partial \sigma_\theta}{\partial \theta} + 2 \frac{\tau_{r\theta}}{r} = -\rho g \sin \theta$$

4.6.2 Yield conditions

The diagram shown in Fig. 4.12 is a schematic representation of different types of vehicle interaction tools moving in soil. The soil mass is assumed to be isotropic, homogeneous and incompressible, and obeys the Mohr-Coulomb yield condition (Fig. 4.13).

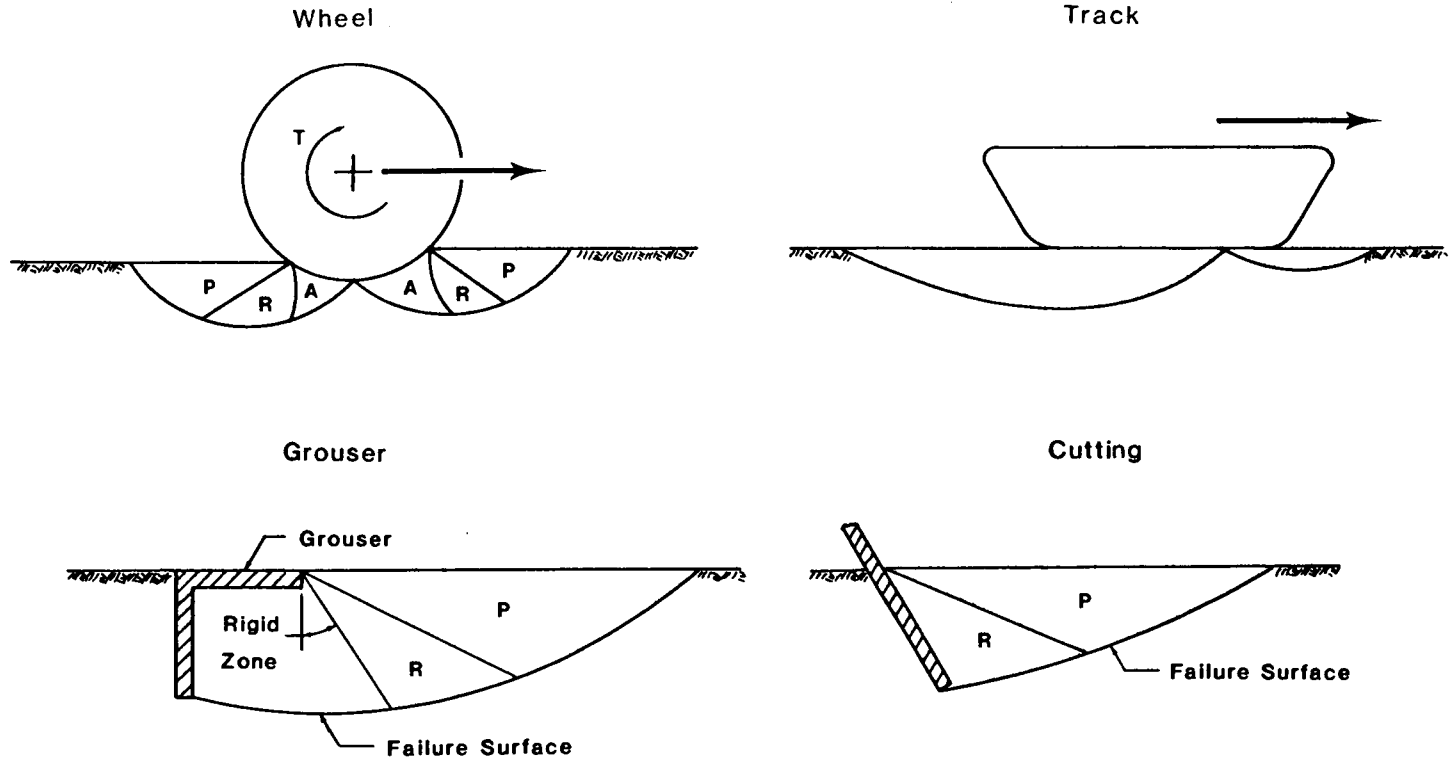


Fig. 4.12. Schematic diagram for failure mode beneath different types of traction tools.

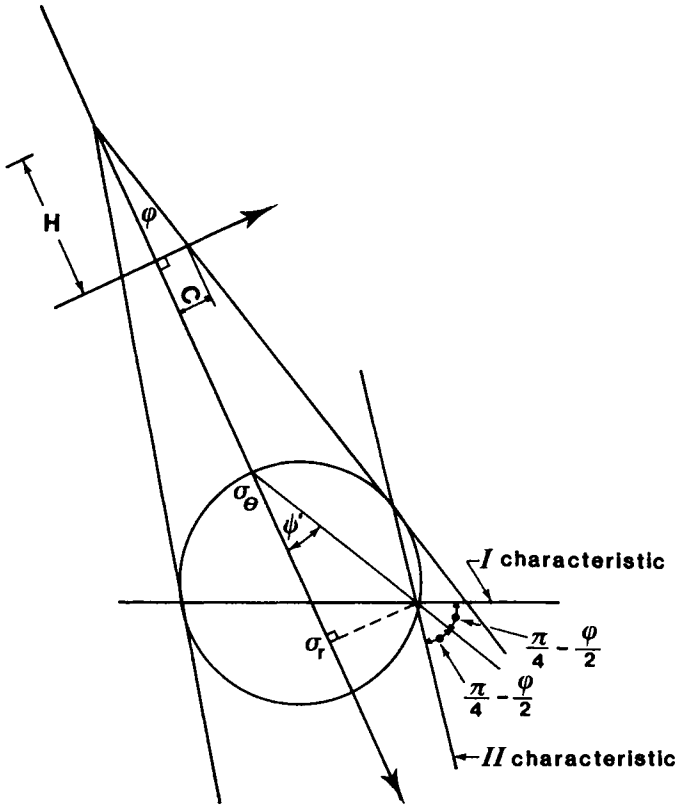


Fig. 4.13. Mohr circle and characteristics.

$$(\sigma_r - \sigma_\theta)^2 + 4\tau_{r\theta}^2 = (\sigma_r + \sigma_\theta + 2H)^2 \sin^2 \phi \quad (4.26)$$

where $H = c \cot \phi$;
 c = cohesion;
 ϕ = angle of internal friction;
 σ_r = radial stress;
 σ_θ = tangential stress and
 $\tau_{r\theta}$ = shear stress.

Figure 4.14 shows the polar coordinate system used for the above notation. The angle of friction δ between the interaction tool and soil is assumed to be constant.

In terms of polar coordinates, the Mohr-Coulomb yield condition for a mixed

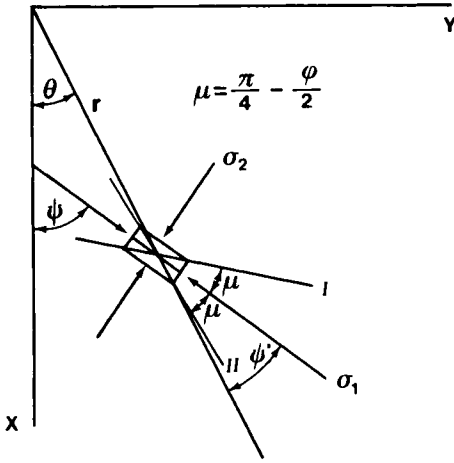


Fig. 4.14. Coordinate axes.

soil (c-phi) material can be expressed as follows:

$$\begin{aligned}
 \sigma_r &= \sigma(1 + \sin \phi \cos 2\psi') + c \cos \phi \cos 2\psi' \\
 \sigma_{\theta} &= \sigma(1 - \sin \phi \cos 2\psi') - c \cos \phi \sin 2\psi' \\
 \tau_{r\theta} &= \sigma \sin \phi \sin 2\psi' + c \cos \phi \sin 2\psi'
 \end{aligned}
 \tag{4.27}$$

where $\sigma = \frac{\sigma_x + \sigma_y}{2} = \frac{\sigma_r + \sigma_{\theta}}{2} = \frac{\sigma_1 + \sigma_2}{2}$ = mean stress

With the use of the similarity solution technique, the following are assumed:

$$\begin{aligned}
 \psi' &= \psi'(\theta) \\
 \sigma &= \rho g r S(\theta)
 \end{aligned}
 \tag{4.28}$$

where ρg = density;
 r = radial distance and
 S(theta) = stress function.

Substitution of eqs.(4.27) and (4.28) into eq.(4.29) will provide the following equations:

$$\frac{d\psi'}{d\theta} = \frac{\cos \theta - \sin \phi \cos (2\psi' + \theta) - S \cos^2 \phi}{2(S \sin \phi + \frac{c}{\rho g r} \cos \phi)(\cos 2\psi' - \sin \phi)} - 1 \quad (4.29)$$

$$\frac{dS}{d\theta} = \frac{S \sin 2\psi' - \sin (2\psi' + \theta)}{\cos 2\psi' - \sin \phi} \quad (4.30)$$

For cohesionless soil ($c = 0$), eqs.(4.29) and (4.30) can be written as:

$$\frac{d\psi'}{d\theta} = \frac{\cos \theta - \sin \phi \cos (2\psi' + \theta) - S \cos^2 \phi}{2S \sin \phi (\cos 2\psi' - \sin \phi)} - 1 \quad (4.31)$$

$$\frac{dS}{d\theta} = \frac{S \sin 2\psi' - \sin (2\psi' + \theta)}{\cos 2\psi' - \sin \phi} \quad (4.32)$$

For frictionless material ($\phi = 0$), for simplicity in solution we choose an x-y coordinate system as shown in Fig. 4.14. Using σ_2 and σ_1 as the major and minor principal stresses:

$$\left. \begin{array}{l} \sigma_x \\ \sigma_y \end{array} \right\} = 1/2(\sigma_1 + \sigma_2) \pm (\sigma_1 - \sigma_2) \cos 2\psi \quad (4.33)$$

$$\tau_{xy} = 1/2(\sigma_1 - \sigma_2) \sin 2\psi \quad (4.34)$$

Defining χ as a new variable where

$$2c\chi = 1/2(\sigma_1 + \sigma_2) - \rho g\chi \quad (4.35)$$

and substituting this into eqs.(4.33) and (4.34) the following equations are obtained:

$$\left. \begin{array}{l} \sigma_x \\ \sigma_y \end{array} \right\} = c(2\chi \pm \cos 2\psi) + \rho g\chi \quad (4.36)$$

$$\tau_{xy} = c \sin 2\psi \quad (4.37)$$

4.6.3 Soil cutting and grouser thrust (granular soil)

Application of limit equilibrium theories to analysis of soil cutting or single grouser thrust in soil requires the same solution technique described in the preceding, since the boundary conditions and soil failure mode are similar, (Fig. 4.12)

(i) Boundary conditions. Since Region 1 in Fig. 4.15 represents a Rankine passive zone, the boundary conditions along OC may be readily specified. The boundary conditions at point C are:

$$S = \frac{\cos \theta}{1 - \sin \phi} \quad (4.47)$$

$$\psi' = \frac{\pi}{2} - \theta$$

where $\theta = \pi/4 + \phi/2$

Substituting for θ , we obtain

$$S = \frac{\cos (\pi/4 + \phi/2)}{1 - \sin \phi}$$

and

(4.48)

$$\psi' = \pi/4 - \phi/2$$

The second of eq.(4.48) may be derived directly from the knowledge that the major principal stress acts in a horizontal direction in Region 1.

Since the boundary conditions at point B and along the boundary OB (in Figs. 4.15 and 4.16) are in no way defined, and assuming eq.(4.49), Fig. 4.17 describes the stress conditions at the rigid wall-soil interface, the assumption that the mass in zone O'ABO in Fig. 4.16 is rigid provides one with the knowledge that the direction of the major principal stress will be constant throughout this region. Thus the determination of ψ' at point A will be sufficient for the determination of ψ' at B.

In the case where the wall or surface is moving into the soil:

$$\tau_{r\theta} = \sigma_{\theta} \tan \delta \quad (4.49)$$

Substituting eq.(4.27) into eq.(4.49) we obtain:

$$\sin \phi \ 2\psi'_B = [(1 - \sin \phi \cos 2\psi'_B)] \tan \delta$$

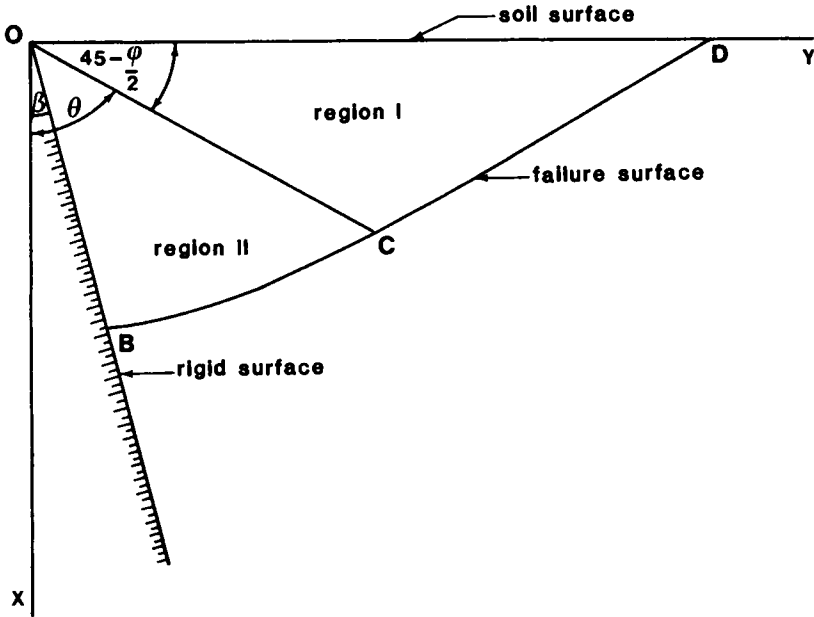


Fig. 4.15. Proposed analytical model of failure configuration for description of boundary conditions.

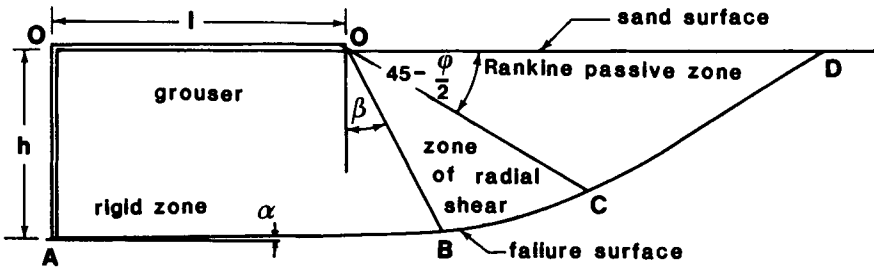


Fig. 4.16. Geometry of failure zone beneath grouser plate.

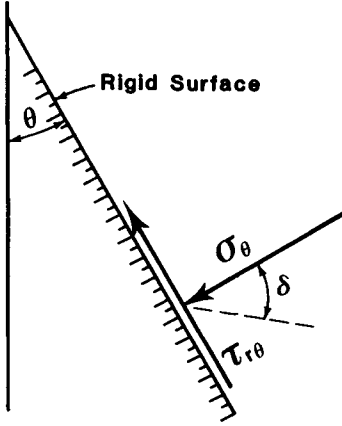


Fig. 4.17. Forces on a rigid surface moving through soil.

Hence

$$\sin \phi \sin 2\psi'_B \cos \delta = \sin \delta - \sin \phi \cos 2\psi'_B \sin \delta$$

$$\sin \phi \sin (180 - 2\psi'_B) \cos \delta = \sin \delta + \sin \phi \cos (180 - 2\psi'_B) \sin \delta$$

Therefore

$$\sin \phi \left[\sin (180 - 2\psi'_B) \cos \delta - \cos (180 - 2\psi'_B) \sin \delta \right] = \sin \delta$$

$$\sin (180 - 2\psi'_B - \delta) = \frac{\sin \delta}{\sin \phi}$$

We thus obtain:

$$\psi'_B = 0.5 \left[\pi - \delta - \arcsin \frac{\sin \delta}{\sin \phi} \right] \quad (4.50)$$

where ψ'_B is the angle of inclination of the principal stress direction to the θ -axis at point B.

To determine the stress function S_B , at point B, we employ an iterative solution (Runge-Kutta method), as follows:

- (1) estimate a value of S_B ,
- (2) by a process of numerical integration, work from point A to point C,
- (3) compare the value of S_C as determined above with the value calculated from eq.(4.48). If the difference is too large, estimate a new value of S_B and repeat the procedure.

By repeating the procedure until the two values of S_c obtained from eq.(4.48) and by calculation agree to within 0.01, the true value of S_B is obtained. Figures 4.18 and 4.19 show the variation of ψ' and S with θ respectively, for various values of the angle β .

(ii) Geometry of the failure surface. To obtain a complete solution of the rigid wall-soil interaction problem, we require the determination of the shape of the failure surface. From the experiments reported by Yong and Sylvestre-Williams (1969a) for granular soils, it was observed that lines AB and CD in Fig. 4.16 were straight. This is consistent with the assumption that zones O'ABO and OCD represent rigid and Rankine zones respectively. Since these are regions of constant state, it is thus only necessary to specify the equation of the spiral curve represented by BC in Figs. 4.15 and 4.16.

The solution to this part of the problem may be sought through the use of the method of characteristics. We recall that a characteristic is defined as a line along which discontinuities in derivatives propagate, or across which derivatives of the first or second order, or both, are discontinuous. On consideration of the the equations of variation of the present system, given as eqs.(4.31) and (4.32), it will be seen that the derivatives of ψ' and S become discontinuous when

$$\psi' = \pm (\pi/4 - \phi/2)$$

$$\text{or } \psi' = \pm \mu \tag{4.51}$$

$$2\mu = \pi/2 - \phi$$

We note that when $\psi' = \pm \mu$ in eqs.(4.31) and (4.32), the denominators of these equations vanish. The numerators may simultaneously vanish or may be different from zero. If the numerators vanish, then eqs.(4.51) define the characteristics of the system. If they are different from zero, eqs.(4.51) define a line of discontinuity which has been shown to coincide with the slip lines of the system. It has been shown that the slip lines form the envelope of the characteristics of any system (Prager, 1953; Harr, 1966) and as such, eqs.(4.51) define the slip lines of the present system.

The slip lines comprise two families of curves which intersect at an angle of $2\mu = \pi/2 - \phi$ and are inclined at angles of $\psi' \pm \mu$ to the radius vectors. The geometry of the slip lines in the Mohr plane is shown in Fig. 4.20 while the geometry in the physical plane is shown in Fig. 4.21.

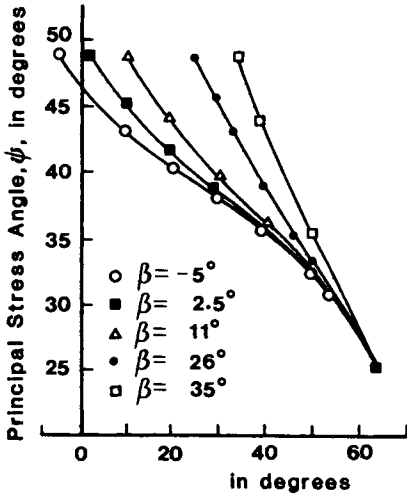


Fig. 4.18. Plot of principal stress angle $\Psi'(\theta)$ versus (θ) as a function of β .

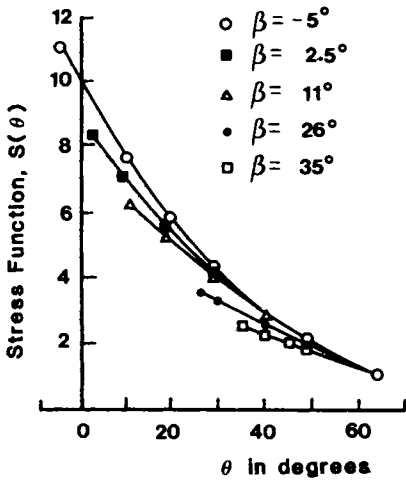


Fig. 4.19. Plot of stress function, $S(\theta)$, versus (θ) as a function of β .

The length of the slip line at any angle θ , can be obtained by (see Fig.4.22):

$$-\frac{rd\theta}{dr} = \tan [\pi - (\psi' \pm \mu)]$$

$$\frac{rd\theta}{dr} = \tan (\psi' \pm \mu)$$

$$\int_{r_0}^{r_\theta} \frac{dr}{r} = \int_0^\theta \cot (\psi' \pm \mu) d\theta$$

$$\begin{aligned} r_\theta &= r_0 \exp \left[\int_0^\theta \cot (\psi' \pm \mu) d\theta \right] \\ &= r_\beta \exp \left[\int_\beta^\theta \cot (\psi' \pm \mu) d\theta \right] \end{aligned} \quad (4.52)$$

where r_θ = length of radius vector at angle of θ to initial position;

r_β = length of radius vector at initial position and

β = angle of inclination of surface OB (Fig. 4.15) to vertical.

The equation of the C_+ characteristic, which defines the failure surface is given by:

$$\begin{aligned} r_\theta &= r_\beta \exp \left[\int_\beta^\theta \cot (\psi' + \mu) d\theta \right] \\ \mu &= \pi/4 - \phi/2 \end{aligned} \quad (4.53)$$

Equations (4.53) may be solved by a process of numerical integration, utilizing Simpson's rule, to yield the failure surface.

(iii) Prediction of horizontal forces. To compute the forces acting on the grouser and to provide a complete solution to the problem, the stresses acting within zone O'ABO (Fig. 4.23) must be estimated. Since no knowledge of the stress distribution within this zone is readily available, we resort to a simple static equilibrium approach as a first order approximation.

Assuming that the vertical force, P, acting on the top of the grouser produces a Coulombic friction force along the failure surface AB, we obtain:

$$T = P \tan \phi \quad (4.54)$$

acting along AB. The horizontal component T_H will be defined by:

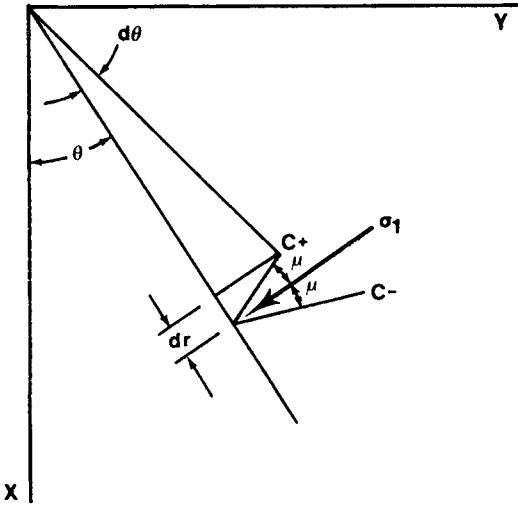


Fig. 4.22. Increment along radial slip line.

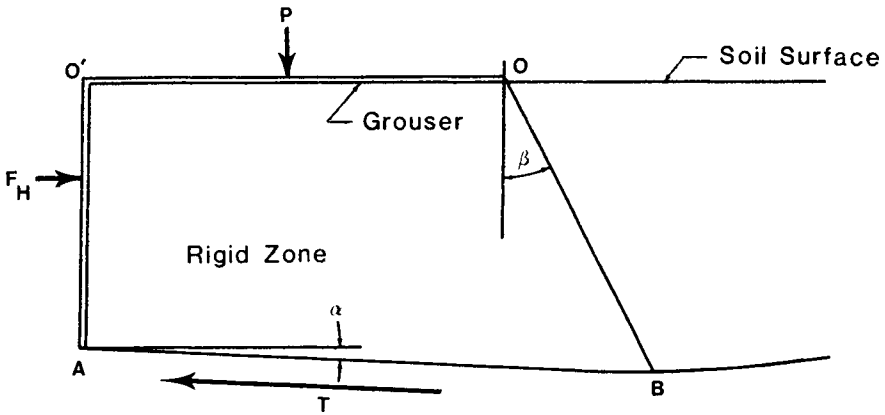


Fig. 4.23. Analytical model used for determination of forces acting in rigid zone.

$$T_H = (P \tan \phi) \cos \alpha \quad (4.55)$$

as shown in Fig. 4.23.

Figure 4.24 shows the predicted horizontal force for a grouser moving in sand using the analytical technique described in this Section - in comparison with measured values obtained by Yong and Sylvestre-Williams (1969).

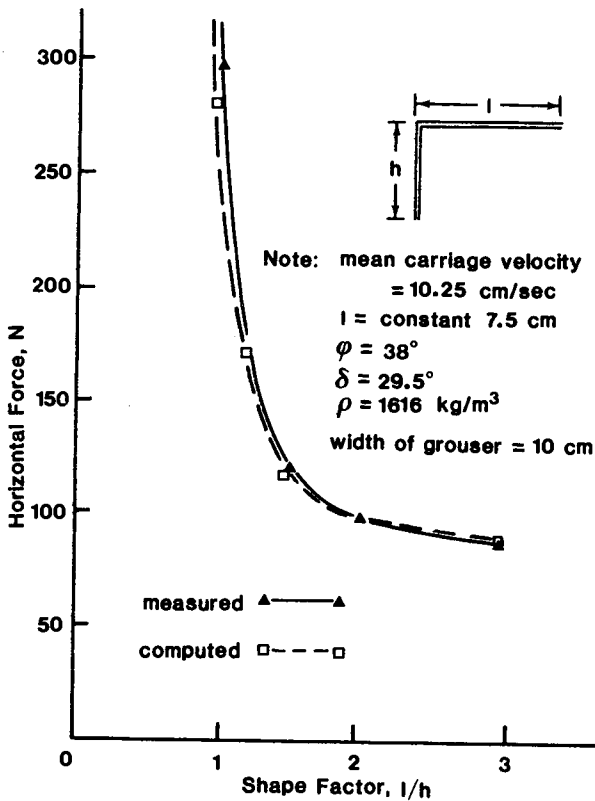


Fig. 4.24. Influence of grouser geometry on predicted and measured horizontal forces for constant elevation tests.

4.6.4 Wheel models

Yong and Windisch (1970) applied the limit equilibrium approach to predict the interfacial stress for a rigid wheel moving with constant speed on soft soil. Utilizing measured subsoil displacement data as a function of different wheel positions, we can calculate subsoil strain, strain rates and principal direct-

ions, hence direction of slip planes at any point in the subsoil can be determined, (Fig. 4.25). Adopting eqs.(4.45) and (4.46) along the slip planes and considering the loading-unloading dividing curves as a boundary condition (Fig. 4.26) we can determine the state of stress at any point in the soil continuum, and the wheel-soil interfacial stresses, Fig. 4.27, using the loading-unloading dividing curves as the locus of zero mean stress points.

The performance of a moving wheel (rigid or pneumatic) over a granular soil can be predicted using limit equilibrium techniques as follows, (Karafiath, 1971, 1978; Nowatzki et al., 1974). Casting the differential equations in Cartesian coordinates form:

$$dz = dx \tan (\theta \pm \mu)$$

$$d\sigma \pm 2\sigma \tan \phi \, d\theta - \frac{\gamma}{\cos \phi} [\sin (\varepsilon \pm \phi)dx + \cos (\varepsilon \pm \phi)dz] = 0 \quad (4.56)$$

where c = cohesion;

x, z = coordinates;

γ = unit weight of soil;

θ = angle between x axis and major principal stress and

ϕ = angle of internal friction.

The problem can be solved if the following wheel-soil interaction parameters are known, (a) wheel entry angle (α_e), (b) wheel rear angle (α_r), (c) wheel-soil angle of friction (δ), and (d) the angle of separation (α_m). Note that this requires an assumption of the existence of two failure zones (Karafiath et al., 1978) as shown in Fig. 4.28 - somewhat similar to the techniques used by Yong and Windisch (1970). To implement the analysis, α_m can be assumed and then corrected through a trial and error technique to satisfy the stresses at the separation point. Figure 4.29 (Karafiath et al., 1978) shows the relation between the measured and predicted results for a driven rigid wheel on granular soil. If the performance for specific wheel characteristics is required (load, input torque are specified), the solution becomes very complex since an iteration technique is required to satisfy the load and torque equilibrium.

4.7 SUMMARY

Analytical methods for prediction of traction mechanics can take several forms - from simple correlative techniques to application of sophisticated theories of interaction. The choice of technique depends not only on one's familiarity with the technique itself, but also with (a) types and amount of inputs available, (b) degree of detail required in the prediction or analysis, (c) level of confidence required or desired in analysis, (d) intent of the analysis or prediction.

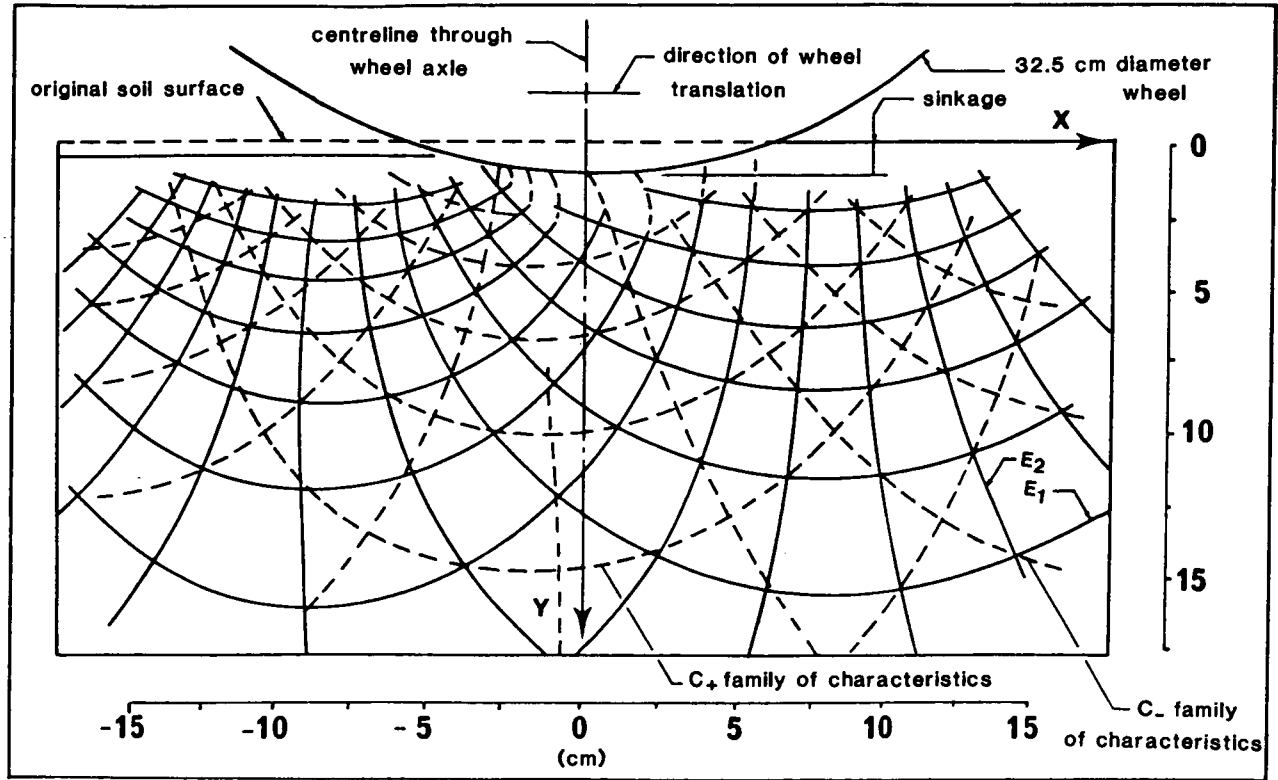


Fig. 4.25. Typical net of principal strain rate directions and corresponding characteristics.

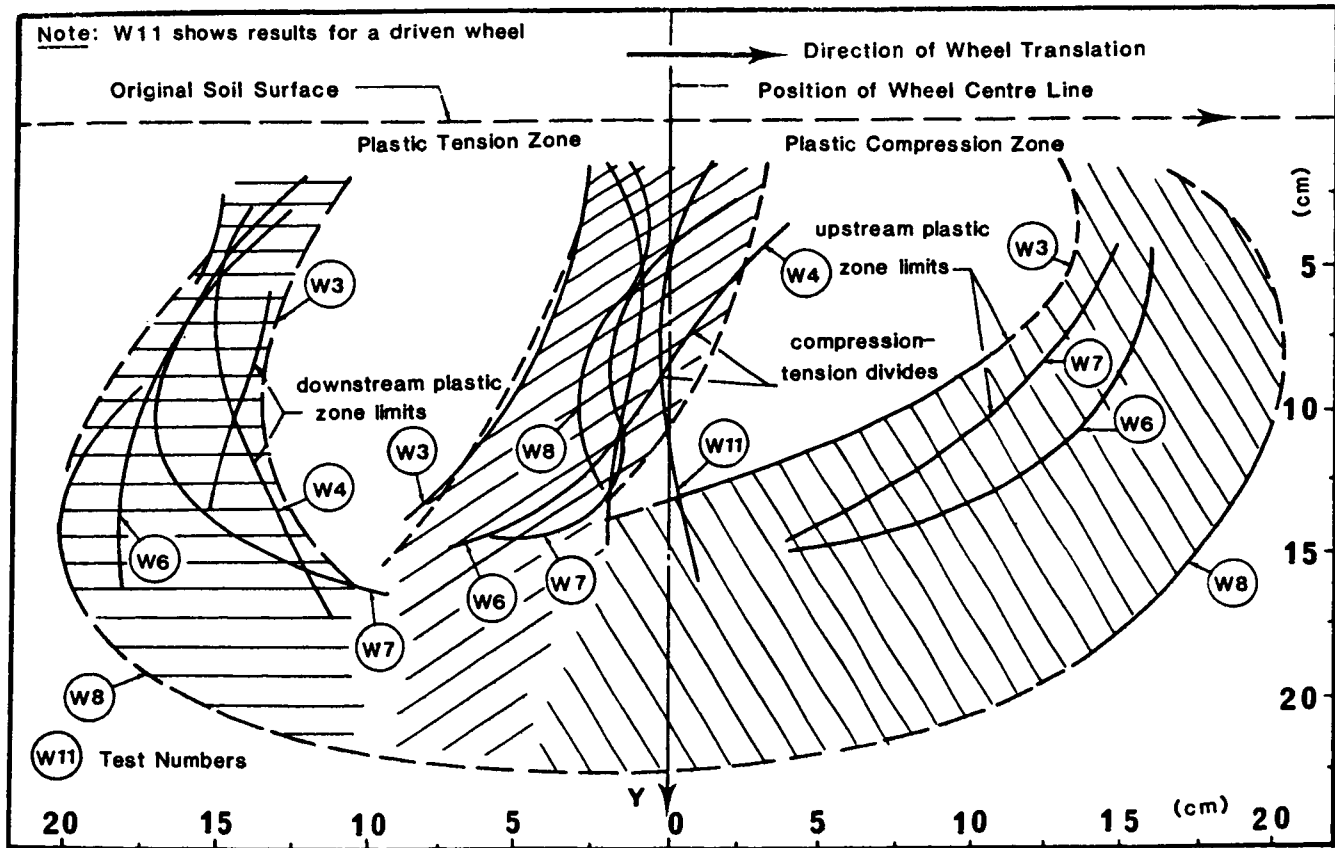


Fig. 4.26. Range of approximate plastic zone boundaries.

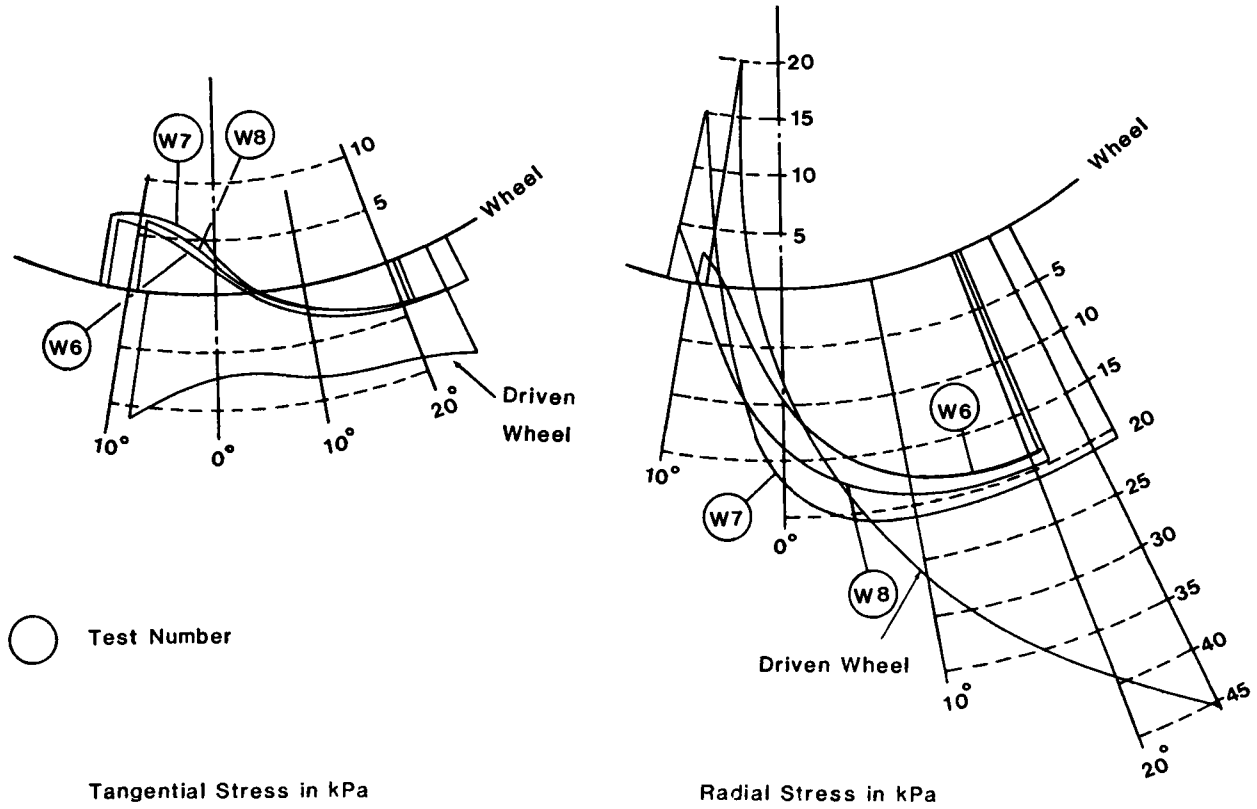


Fig. 4.27. Calculated soil-wheel contact stresses.

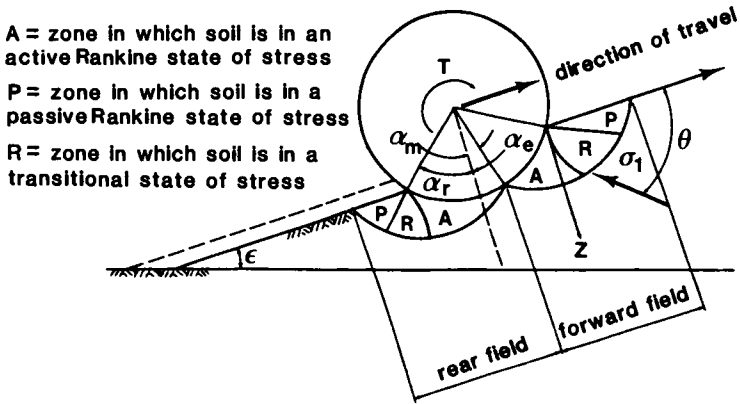


Fig. 4.28. Concept of rigid wheel-soil interaction (Karafiath et al., 1978).

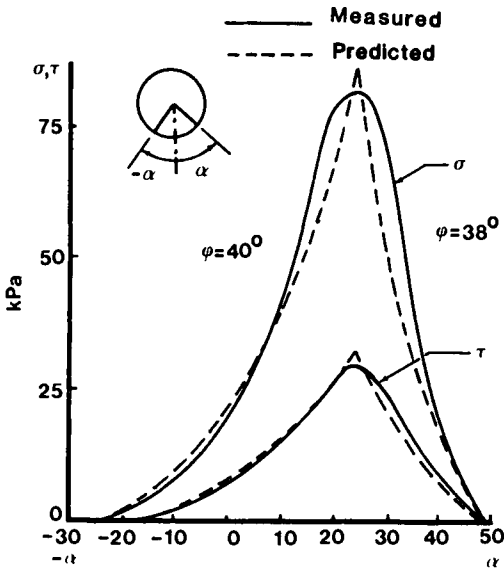


Fig. 4.29. Comparison of measured and computed stresses, driven wheel (Karafiath, 1971).

The simplest correlative procedure discussed in this Chapter has been one which takes the measurement of terrain bearing strength (or shear strength) and correlates it with tractive performance. In doing so, several indirect routes are followed - beginning with the basic terrain measurements through computations of motion resistance, flotation capability, etc. Obviously, the more data and correlations obtained, the better is the simple correlative model. The dangers inherent with this type of technique lie not in the nature of the technique but in the application of the procedure for predictive use to situations not covered in the correlations sought. The overeagerness by the uninitiated in applying such procedures to situations not covered by the measurement systems, and the inapplicability of the measurement system to certain field conditions all combine to remind the user to be properly aware of the particular correlative tool used for his purpose.

In the techniques for analysis using methods of dimensional analysis, it is observed that (a) extensive test information with proper parametric variation and control would be required, (b) whilst correlative information can be secured, insight into the fundamental operative mechanisms cannot be readily sought. Nevertheless, the technique is useful in that correlative functional relationships can be obtained - given the proper test information. However, as previously stated, the dangers in using this type of technique lie also in the extension of the "analysis" for prediction of situations not covered in the test program.

Progressing "upward" in analysis of the traction problem, we can seek solution of the problem in terms of (a) the constitutive relationships described by the supporting terrain material, and (b) the interaction mechanics described by the two participants - traction element and supporting terrain. In the former, we have two basic avenues of pursuit - (1) through limit equilibrium principles, and (2) through the use of stress-strain relationships where failure of the supporting terrain material need or need not occur under tractive loading. The use of constitutive relationships, with solutions sought through finite element methods (FEM), is discussed in Chapters 6 and 7. The use of interaction mechanics, leading to energy analyses, is discussed in Chapter 5.

In the limit equilibrium analyses discussed in this Chapter, the basic rigid plastic model inherent in the Mohr-Coulomb two-parameter failure theory is used. We note that the method of analysis presumes a failure condition in the terrain supporting material under the action of tractive forces. So long as the analytical conditions properly mirror the physics of the problem, the analytical technique is indeed rigorous and accurate. The drawbacks lie in the limitations of the use of the rigid-plastic model - which can be improved if sufficient attention is warranted.

REFERENCES

- Bekker, M.G., 1969. Introduction to Terrain-Vehicle Systems. The University of Michigan Press, Ann Arbor, Michigan. 846 p.
- Bekker, M.G., 1960. Off the Road Locomotion. The University of Michigan Press, Ann Arbor, Michigan. 220 p.
- Bekker, M.G., 1956. Theory of Land Locomotion. The University of Michigan Press, Ann Arbor, 520 p.
- Freitag, D.R., 1966. A dimensional analysis of the performance of pneumatic tires on clay. J. Terramechanics, 3-3:51-68.
- Freitag, D.R. and Smith, M., 1966. Center-line deflection of pneumatic tires moving in dry sand. J. Terramechanics, 3-1:31-46.
- Harr, M.E., 1966. Foundations of Theoretical Soil Mechanics. McGraw Hill, New York, N.Y. 381 p.
- Haythornthwaite, R.M., 1961. Methods of plasticity in load locomotion studies. Proc. 1st Int. Conf. on the Mechanics of Soil Vehicle Systems, Turin, pp.28-44.
- Kacigin, V.V. and Guskov, V.V., 1968. The basis of tractor performance theory. J. Terramechanics, 5-3:43-66.
- Karafiath, L.L., 1971. Plasticity theory and the stress distribution beneath wheels. J. Terramechanics, 8-2:49-60.
- Karafiath, L.L. and Nowatzki, E.A., 1978. Soil Mechanics for Off-Road Vehicle Engineering. Trans. Tech. Pub., Germany. 515 p.
- Mendelson, A., 1968. Plasticity Theory and Application. MacMillan, New York. 353 p.
- Nowatzki, E.A. and Karafiath, L.L., 1974. General yield conditions in a plasticity analysis of soil-wheel interaction. J. Terramechanics, 11-1:29-44.
- Ohde, J., 1938. Zur Theorie des Erddruckes unter besonderer Berücksichtigung der Erddruckverteilung. (The theory of earth pressure with special reference to earth pressure distribution). Die Bautechnik, Vol.16. pp. 150-159, 176-180, 241-245, 331-335, 480-487, 570-571, 753-761.
- Osman, M.S., 1964. The mechanics of soil cutting blades. J. Agricultural Eng. Res. 9-1:313-328.
- Prager, W., 1953. A geometrical discussion of the slip-line field in plane plastic flow. Trans. Royal Inst. Tech., Stockholm. pp.1-26.
- Reece, A.R., 1965. Principles of soil vehicle mechanics. Proc. Inst. of Mech. Engrs. (Automobile Division). 180-2A:2, pp.45-66.
- Siemens, J.C., Weber, J.A. and Thornburn, T.H., 1964. Mechanics of soils under the influence of model tillage tools. Amer. Soc. Agri. Engrs., Ann. Meeting. pp. 1-7.
- Terzaghi, K., 1943. Theoretical Soil Mechanics. John Wiley and Sons, Inc., New York, N.Y. 510 p.
- Turnage, G.W., 1978. A synopsis of tire design and operational consideration aimed at increasing tire drawbar performance. Proc. 6th Inter.Soc. Terr-Veh. Systems, Vienna. Vol.11:757-810.
- Wisner, R.D. and Luth, H.J., 1972. Off-road traction prediction for wheeled vehicles. Trans. Amer.Soc.Agri.Engrs. 17-1:255-262.
- Yong, R.N., Elmamlouk, H. and Della-Moretta, L., 1981. Evaluation and prediction of energy losses in track-terrain interaction. J. Terramechanics. 17-2:79-100.
- Yong, R.N. and Fattah, E.A., 1976. Prediction of wheel-soil interaction and performance using the finite element method. J. Terramechanics, 13-4:227-240.
- Yong, R.N., Fattah, E.A. and Boonsinsuk, P., 1978. Analysis and prediction of tyre-soil interaction and performance using finite elements. J. Terramechanics, 15-1:43-63.
- Yong, R.N. and Japp, R.D., 1968. Stress-strain behaviour of clays in dynamic compression. Vibration Effects of Earthquakes on Soils and Foundations, ASTM STP 450. Amer. Soc. for Test. and Mat'ls, pp. 233-262.
- Yong, R.N. and Sylvestre-Williams, R., 1969a. Analysis and Prediction of Grouser Thrust on Sand. Soil Mechs. Ser. No.26, McGill University, Montreal. 33 p.
- Yong, R.N. and Webb, G.L., 1969b. Energy dissipation and drawbar-pull prediction in soil-wheel interaction. Proc. 3rd Int. Conf. Int. Soc. Terr. Veh. Systems, Essen, 1:93-142.

- Yong, R.N. and Windisch, E., 1970. Determination of wheel contact stresses from measured instantaneous soil deformations. *J. Terramechanics*, 7-3 and 7-4:57-67.
- Yong, R.N., Youssef, A.F. and Fattah, E.A., 1975. Vane-cone measurements for assessment of tractive performance in wheel-soil interaction. *Proc. 5th Int. Conf. Int. Soc. Terr. Veh. Systems*, Detroit, 3:769-788.

NOMENCLATURE

A	contact area
C	penetration resistance
D	wheel diameter
DBP	drawbar-pull
H	tractive effort
L	track length
N_c, N_γ	bearing capacity factors
P	drawbar-pull, pressure or vertical force
P_c	carcass pressure
P_{cr}	inflation pressure above which the tyre will behave as a rigid wheel
P_g	ground pressure
P_i	tyre inflation pressure
R_b	bulldozing resistance
R_c	compaction resistance
R_t	flexing resistance
RT	motion resistance
S	slip
$S(\theta)$	stress function
T	torque or friction force
V	translational velocity
W	vertical load
Z	sinkage
a	empirical constant
b	track or wheel width
c	cohesion
d	tyre diameter
f_m	ratio of residual shear strength to contact stress
g	gravity acceleration
h	tyre or grouser height
k	function of soil and plate geometry
k_c	empirical constant

k_{τ}	displacement at peak shear stress or tangent modulus
k_{ϕ}	empirical constant
l	track contact length
n	empirical constant
r	radial distance
w	empirical constant
z	track or wheel sinkage, or plate penetration
Δ	shear deformation
α	angle of attack
γ	unit weight of soil
δ	friction angle, tyre or track deflection
μ	gear-soil interaction coefficient
ρ	density
$\sigma, \sigma_x, \sigma_y,$	normal stresses
$\sigma_{\theta}, \sigma_r$	tangential, radial stress
σ_1, σ_2	principal stresses
$\tau, \tau_{xy}, \tau_{r\theta}$	shear stresses
ϕ	soil friction angle

Chapter 5

MECHANICS OF ENERGY TRANSFER

5.1 INTRODUCTION

In Chapter 4 we discussed the use of analytical models in the evaluation and prediction of traction production - either in terms of tractive forces produced or in terms of mobility. Using semi-empirical and in some instances more rational analytical approaches to the evaluation of traction production, some success can be achieved in prediction of performance. However, until the actual physics of traction performance is understood, a proper means for more realistic predictions and evaluation cannot be attained.

In this Chapter we will develop the principles of interaction mechanics through the use of energy conservation as they apply to the phenomenon of traction mechanics. Whilst the body of detailed theory of energy transfer mechanics lies in the discipline of physics, we are nevertheless interested in how the basic principles apply to our general class of problems of machine-soil interaction.

5.2 PRINCIPLE OF ENERGY CONSERVATION APPLIED TO TRACTION MECHANICS

The principle of energy conservation is one of the basic laws of physics. It can be applied to the analysis of vehicle tractive element-soil interaction. The energy required to keep a tractive element in continuous motion on level ground must be equal to the energy generated by the element plus that dissipated in the tractive element supporting ground system.

Figure 5.1 shows a schematic representation of a tractive element interacting with a terrain surface and the resultant energy components which illustrate the problem. The kinematics of the situation represented in the figure can be expressed in terms of input energy and resultant work done as follows:

$$\begin{array}{rcl}
 \text{INPUT ENERGY} & - & \text{SLIP ENERGY} & - & \text{MOTION RESISTANCE} \\
 \text{(energy supplied to} & & \text{(wasted at the} & & \text{(energy expended in} \\
 \text{the tractive element)} & & \text{interface in forms} & & \text{overcoming resist-} \\
 & & \text{other than work done)} & & \text{ance to motion)} \\
 & & = \text{OUTPUT ENERGY} & & \\
 & & \text{(work available, drawbar-pull)} & &
 \end{array}$$

We note that this is the basic energy balance relationship as applied to a tractive element (wheel-track) in motion on a horizontal ground surface. From the relationship shown, it is clear that if a greater output energy is desired - i.e. drawbar-pull, the motion resistance and slip energies must be reduced (for

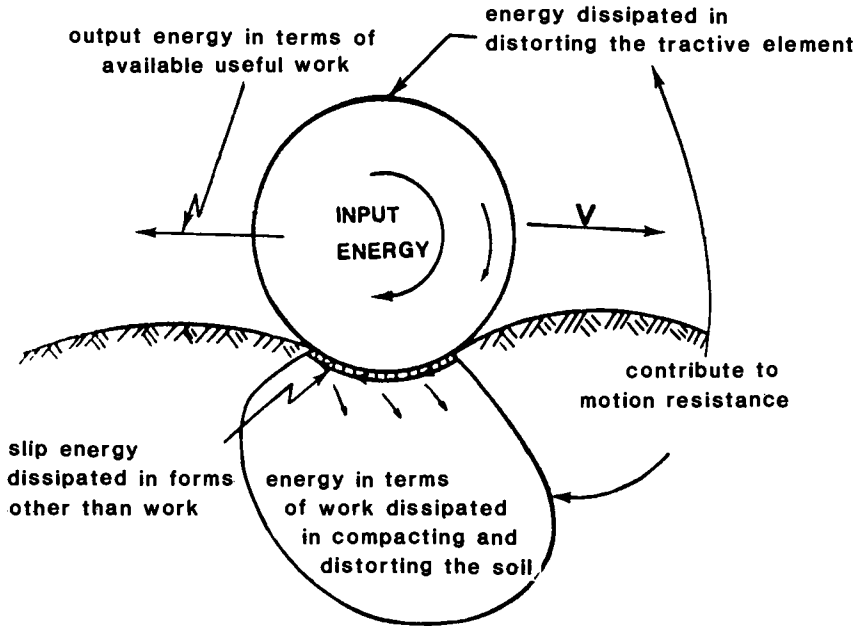


Fig. 5.1. Tractive element supporting ground energy system.

the same input energy). Since the input energy at the wheel hub is governed by the power plant and transmission system, it becomes obvious that if efficient traction capability is to be obtained, it is necessary to pay proper attention to provision of the optimum running gear system that minimizes the slip and motion resistance. A useful method for assessment of energy efficient traction for vehicle operation would be to define an "energy budget" as follows:

$$\begin{array}{rcl}
 \text{MAXIMUM AVAILABLE ENERGY} & - & \text{ENERGY EXPENDITURE} & = & \text{MAXIMUM WORK} \\
 \text{(maximum energy available} & & \text{(energy required to} & & \text{(output available)} \\
 \text{to driving hub - as} & & \text{overcome motion} & & \\
 \text{governed by power plant)} & & \text{and slip resistances)} & &
 \end{array}$$

5.3 ENERGY MODEL FOR TRACTION MECHANICS

In applying the principle of conservation of energy, i.e. energetics principle, to evaluate the tractive element-soil mobility performance, the different energy components participating in the interactions defined by the tractive element-soil system need to be properly identified and measured, or calculated. The energy concept for evaluation of traction was formally introduced by Yong and Webb (1969) to evaluate the motion performance of a rigid wheel on soft soil. Subsequently, the energy model was extended by Yong and Fattah (1976), Yong et al. (1978, 1980) to predict pneumatic tyre and also track performance on soft soils.

The basic principle used in the energy model evaluates the (moving) performance of a tractive element on ground surface in terms of the well-known energy balance equation:

$$\text{OUTPUT ENERGY} = \text{INPUT ENERGY} - \text{ENERGY LOSSES}$$

In the case of a moving tractive element, the units of this equation can be defined in terms of energy per unit time or per travel distance.

The energy balance equation is valid for any type of tractive element (wheel or track). However, its application may differ from one element to another depending on how one proportions or calculates the different energy components identified in the equations.

5.3.1 Input energy

The input energy supplied to a tractive element is controlled by (1) power plant and transmission system, and (2) maximum tractive forces which can be mobilized at the tractive element-soil interface. In most types of soil, the maximum mobilized traction forces and vehicle cruising speed will control the selection of the vehicle power-terrain system - since any input energy in excess of that required for mobilization is wasted in the form of slip energy, Fig. 5.2. The methods for calculating tractive forces are discussed in Chapter 3, and those for determining interfacial energy are discussed in Section 5.4.4.

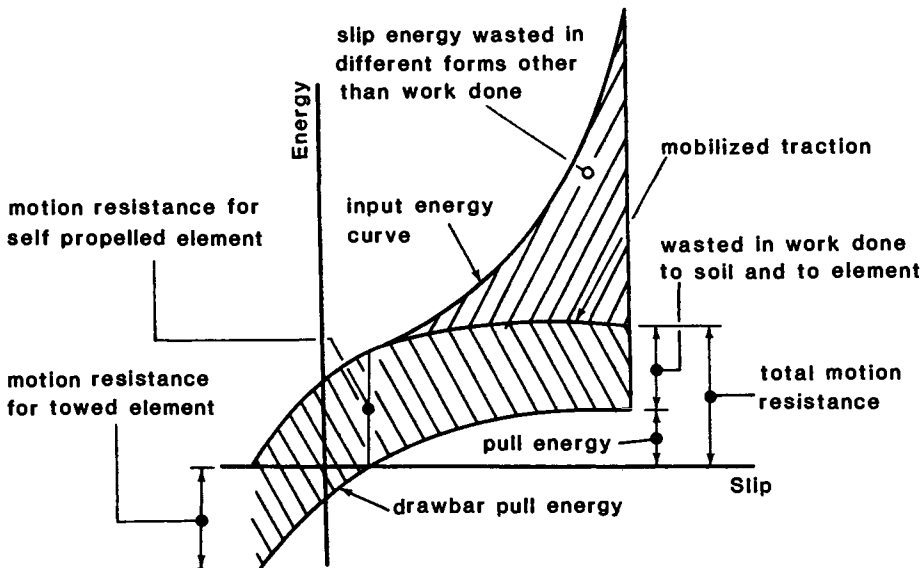


Fig. 5.2. Energy balance curves. Tractive element (wheel-track) moving with constant travel velocity.

5.3.2 Energy loss

The energy loss in an interacting tractive element-soil system consists of:

(i) Energy dissipated due to slip. That is, energy wasted in terms of relative motion between element and soil surface, and hence does not contribute to work done or actual motion resistance.

(ii) Substrate compaction and distortion energy. Both of these contribute directly to motion resistance of the tractive element. These two energy terms are spent in compacting the soil and distorting it vertically and horizontally, plus - in the case of flexible tyre - the energy spent in distorting the tyre. The relative magnitude of these types of energy is a function of compliances of the tyre and the soil.

The energy wasted due to hysteresis in the element is neglected since off-road vehicles generally travel at relatively low speeds.

5.3.3 Motion resistance and drawbar-pull

Assume a wheel moving with constant translational velocity V and angular velocity ω , (Fig. 5.3):

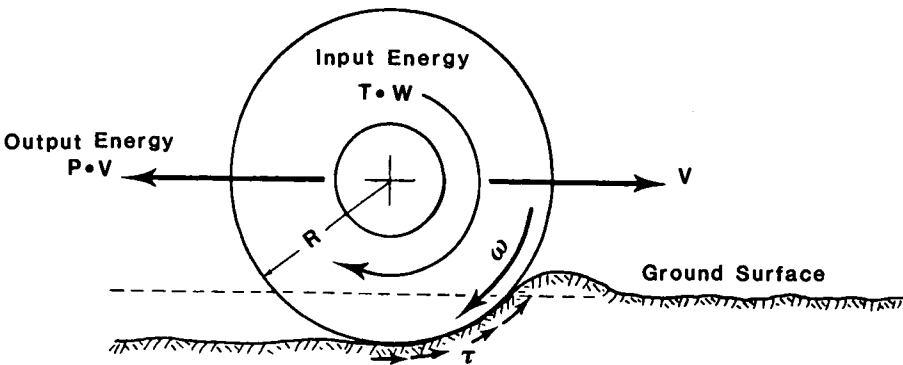


Fig. 5.3. Wheel-energy model.

For a unit wheel width, the energy balance equation per unit time can be written as:

$$T \cdot \omega = P \cdot V + D + E_f \quad (5.1)$$

$$\text{Input Energy} = \text{Output Energy} + \text{Work Energy} + \text{Interfacial Energy}$$

where T = torque moment at the hub, e.g. N.m;
 ω = rotational velocity, rads/sec;
 P = drawbar-pull, N;
 V = translational velocity, e.g. m/sec;
 D = work done in soil deformation, N.m and
 E_f = interfacial energy loss, N.m.

The energy per unit travel distance can be obtained by dividing eq.(5.1) with the translational speed of the wheel, V :

$$\text{Thus } \frac{T \cdot \omega}{V} = P + \frac{D}{V} + \frac{E_f}{V} \quad (5.2)$$

If the tangential stress at the wheel-soil interface is τ , and the slip velocity at the wheel-soil interface is $(\omega R - V)$

$$\text{Then } T = \Sigma \tau \cdot R \quad (5.3)$$

$$\text{and } E_f = \Sigma \tau \cdot (\omega R - V) \quad (5.4)$$

where R = wheel rolling radius.

Substituting into eq.(5.2):

$$\frac{R \cdot \omega \cdot f \tau}{V} = P + \frac{D}{V} + \frac{(\omega R - V) \cdot f \tau}{V} \quad (5.5)$$

$$\frac{f \tau}{L} = P + D/V \quad (5.6)$$

where L = wheel-soil contact length or, in physical terms:

Mobilized Traction Forces = Drawbar-pull + Work Energy/Unit Travel Distance

Thus the work energy per unit travel distance is the motion resistance of the wheel.

In the case of a track moving with constant speed V , and sprocket angular velocity ω (Fig. 5.4), the belt speed for an extensible track belt is $V_b = \omega \cdot R$, where R is the sprocket radius:

$$T \cdot \omega = P \cdot V + D + E_f \quad (5.7)$$

$$\begin{array}{l} \text{Input} \\ \text{Energy} \end{array} = \begin{array}{l} \text{Output} \\ \text{Energy} \end{array} + \begin{array}{l} \text{Work} \\ \text{Energy} \end{array} + \begin{array}{l} \text{Interfacial} \\ \text{Energy} \end{array}$$

where T = sprocket input torque-moment;

D = energy spent in compacting and distorting the soil and

E_f = energy dissipated at slip surface.

If the slip is very small, E_f can be assumed to be zero. With the assumption that the slip is constant along the track length, the interfacial energy can be calculated as:

$$E_f = (V_b - V) \int_L \tau \quad \text{and} \quad V_b = \omega R$$

where τ and L are the track soil tangential stress and contact length respectively.

Thus, $T = R \cdot \int_L \tau$; $\int_L \tau$ = mobilized traction force.

Equation (5.7) can now be written as:

$$\omega \cdot R \int_L \tau = P \cdot V + D + (V_b - V) \int_L \tau \quad (5.8)$$

Energy per unit travel distance can be obtained by dividing eq.(5.8) with the translation velocity of the track, V :

$$\omega \cdot R \int_L \tau = P + \frac{D}{V} + \frac{(V_b - V)}{V} \int_L \tau \quad (5.9)$$

$$\int_L \tau = P + D/V \quad (5.10)$$

which is the same as eq.(5.6).

Equations (5.6) and (5.10) show how the wheel or the track forces can be obtained from the energy balance equation - provided the work and input energies can be determined.

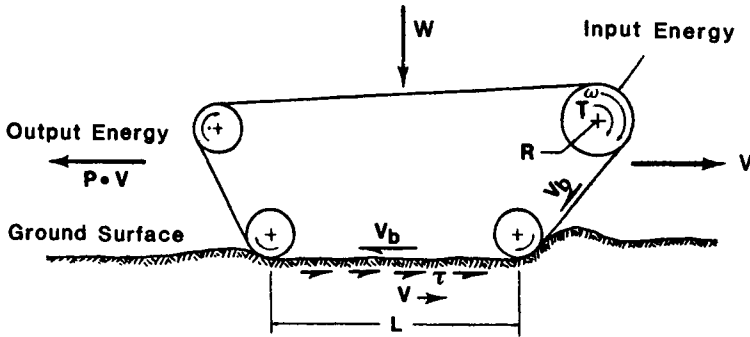


Fig. 5.4. Track-energy model.

5.4 VISIOPLASTICITY

The discovery that energy transfer mechanics could be realistically used to develop the energy model discussed in Section 5.3, was made through a series of studies by Yong and his co-workers through a period of several years. The method adopted was one that was successfully applied in the field of metal extrusion. They reasoned that since metal extrusion between two rollers could, in essence, resemble the wheel problem - if a half plane consideration of metal extrusion was considered - and since certain constitutive relationships in metal plasticity were adaptable to soils, the visioelasticity technique used in metal extrusion studies could be fruitfully used for the traction mechanics studies.

The visioelasticity method is a valuable laboratory technique for evaluating the effect of tractive element parameters on traction performance and subsoil response. It can be used to differentiate between the performance of different tractive element types. The method of analysis essentially states that if we can observe and measure the distortions occurring in the supporting terrain material (e.g. soil), such as the situation shown in Fig.5.1, the input loads or stresses (or forces) provoking the observed distortions can be deduced. The manner in which one determines the distortions in the substrate will be left to the investigator or analyst. The link between distortions (strains) and stresses provoking the strains of the substrate will be defined by the constitutive relationships of the supporting substrate material. Once we have obtained the information concerning stresses and strains in the substrate, it becomes a simple procedure to relate these to the surficial agent provoking these stresses and strains. In other words, the procedure utilized in invoking the visioelasticity technique is to (a) map out the resultant instantaneous strains in the supporting material, (b) determine the stresses causing the strains - through the appropriate constitutive relationships, and (c) relate these to the tractive element motion and interaction at the surface. The remaining sub-Sections will describe the method of analysis and evaluation.

5.4.1 Governing equations

We begin by examining the supporting substrate as a tractive element is made to move over the surface. If u , v , and w are velocities in the x , y and z directions respectively, the normal and shear strain rate components in the deforming soil can be written as:

$$\dot{\epsilon}_x = \frac{\partial u}{\partial x}, \dot{\epsilon}_y = \frac{\partial v}{\partial y}, \dot{\epsilon}_z = \frac{\partial w}{\partial z} \quad (5.11)$$

$$\dot{\gamma}_{xy} = \frac{\partial v}{\partial x} + \frac{\partial u}{\partial y}, \dot{\gamma}_{yz} = \frac{\partial w}{\partial y} + \frac{\partial v}{\partial z}, \dot{\gamma}_{zx} = \frac{\partial u}{\partial z} + \frac{\partial w}{\partial x} \quad (5.12)$$

The second invariant, I_2 , of the strain rate tensor is expressed as:

$$I_2 = 1/2(\dot{\epsilon}_x^2 + \dot{\epsilon}_y^2 + \dot{\epsilon}_z^2) + 1/4(\dot{\gamma}_{xy}^2 + \dot{\gamma}_{yz}^2 + \dot{\gamma}_{zx}^2) \quad (5.13)$$

Soft soil deformation beneath a tractive element such as that shown in Fig. 5.1 can be considered under the heading of unrestricted plastic flow. For a material in which the choice of reference state is arbitrary, (for example, rigid, perfectly plastic or viscoplastic materials in contra-distinction to an elastic or elastic-plastic solid in which there is no one stress-free state), the instantaneous reference state can be used and the rate of strain can be obtained with respect to the deformed medium (Prager and Hodge, 1951). The finite strain formulation given by Love (1959) is used, where the resulting strain rate equations although linear in velocity components referred to natural coordinates, contain the derivatives of the displacement with respect to these natural coordinates as coefficients. The rate of straining defined with respect to the deformed medium (spatial coordinates) is linear in the derivatives of the velocity components computed with respect to the spatial coordinates.

The continuity equation for the plane strain case can be written as:

$$\frac{\partial \rho}{\partial t} + \frac{\partial \rho}{\partial x} u + \frac{\partial \rho}{\partial y} v = 0 \quad (5.14)$$

The equations of motion of a plastic mass (momentum equations) can be written as:

$$\begin{aligned} \frac{\partial \sigma_x}{\partial x} + \frac{\partial \tau_{xy}}{\partial y} + \rho u \frac{\partial u}{\partial x} + \rho v \frac{\partial u}{\partial y} + \rho \frac{\partial u}{\partial t} &= X \\ \frac{\partial \sigma_y}{\partial y} + \frac{\partial \tau_{xy}}{\partial x} + \rho u \frac{\partial v}{\partial x} + \rho v \frac{\partial v}{\partial y} + \rho \frac{\partial v}{\partial t} &= Y \end{aligned} \quad (5.15)$$

where

- σ_x, σ_y = normal stresses in the x and y directions;
- τ_{xy} = shearing stresses;
- u, v = displacements in the x and y directions;
- ρ = density and
- X, Y = body forces.

The loading of soils due to the passage of a wheel is a transient phenomenon which falls between static and dynamic loading. In eq.(5.15) the acceleration or inertial terms must be examined. The third and fourth terms on the left hand side are the convective acceleration terms while the fifth term is the local acceleration. The body forces X and Y represent the matrix and gravitational potential.

For a plane strain plastic flow problem with the following conditions satisfied:

- (a) steady state process
- (b) negligible inertial and body forces
- (c) incompressible flow
- (d) elastic strains small compared to the plastic strains,

the continuity relation reduces to:

$$\dot{\epsilon}_x + \dot{\epsilon}_y = 0 \quad (5.16)$$

and the momentum equations reduce to:

$$\frac{\partial \sigma_x}{\partial x} + \frac{\partial \tau_{xy}}{\partial y} = 0 \quad (5.17a)$$

$$\frac{\partial \sigma_y}{\partial y} + \frac{\partial \tau_{xy}}{\partial x} = 0 \quad (5.17b)$$

Using the Levy-Mises relationship as a link between the strain-rate and stress:

$$\dot{\epsilon}_x = \frac{\sqrt{I_2}}{k} \sigma'_x \quad (5.18a)$$

$$\dot{\epsilon}_y = \frac{\sqrt{I_2}}{k} \sigma'_y \quad (5.18b)$$

$$\dot{\gamma}_{xy} = \frac{2\sqrt{I_2}}{k} \tau_{xy} \quad (5.18c)$$

where $k^2 = J_2 =$ second stress invariant (von Mises criterion);

$k =$ yield stress in shear of $1/\sqrt{3}$ yield stress in tension or compression;

$\sigma'_x, \sigma'_y =$ deviatoric stresses in x and y directions.

If $\dot{\epsilon}_y$ is subtracted from $\dot{\epsilon}_x$, the following equation results:

$$\dot{\epsilon}_x - \dot{\epsilon}_y + \frac{\sqrt{I_2}}{k} (\sigma'_x - \sigma'_y) \quad (5.19)$$

Solving for σ'_x gives:

$$\sigma'_x = \sigma'_y + \frac{k}{\sqrt{I_2}} (\dot{\epsilon}_x - \dot{\epsilon}_y) \quad (5.20)$$

Differentiating eq.(5.20) with respect to y gives:

$$\frac{\partial \sigma'_x}{\partial y} = \frac{\partial \sigma'_y}{\partial y} + \frac{k}{\sqrt{I_2}} \frac{\partial}{\partial y} (\dot{\epsilon}_x - \dot{\epsilon}_y) \quad (5.21)$$

The term $\partial \sigma'_x / \partial y$ in eq.(5.21) can be obtained by the use of eq.(5.17b) and by differentiating eq.(5.18c). The resulting equation in terms of deviatoric stresses is:

$$\frac{\partial \sigma'_y}{\partial y} = - \frac{\partial \tau_{xy}}{\partial x} = - 1/2 \frac{k}{\sqrt{I_2}} \frac{\partial}{\partial x} (\dot{\gamma}_{xy}) \quad (5.22)$$

Substituting eq.(5.22) into eq.(5.21) gives:

$$\frac{\partial \sigma'_x}{\partial y} = \frac{k}{\sqrt{I_2}} \frac{\partial}{\partial y} (\dot{\epsilon}_x - \dot{\epsilon}_y) - 1/2 \frac{k}{\sqrt{I_2}} \frac{\partial}{\partial x} (\dot{\gamma}_{xy}) \quad (5.23)$$

The right hand side of eq.(5.23) can then be evaluated for any point in the flow field where the strain-rates have been determined, and for which k is known.

5.4.2 Rate of doing plastic work, \dot{W}

Under the action of a moving tractive element, substrate soil straining occurs - as discussed in the previous sub-Section. The work performed which results in this straining can be computed. The procedure involved requires one to compute the rate at which stresses do work, \dot{W} , in connection with the change in shape. To do so, the stresses and rate of strain need to be known. The quantity can be expressed as:

$$\dot{W} = \sigma'_x \dot{\epsilon}_x + \sigma'_y \dot{\epsilon}_y + \tau_{xy} \dot{\gamma}_{xy} \quad (5.24)$$

If the total soil mass is compressible, the total rate of doing work on the soil must include the work done as volume changes are accommodated. The total work (deformation energy) can then be expressed as:

$$\text{Deformation Energy} = \int \text{Plastic Work Rate} + \int \text{Work done in producing Volume Change}$$

Since little volume change occurs in nearly-saturated or saturated cohesive soils under compression action, the second integral on the right hand side is zero.

$$\dot{W} = \sigma'_x{}^2 \frac{\sqrt{I_2}}{k} + \sigma'_y{}^2 \frac{\sqrt{I_2}}{k} + \tau_{xy}{}^2 \frac{\sqrt{I_2}}{k} \quad (5.25)$$

$$= \frac{\sqrt{I_2}}{k} 2 J_2 \quad (5.26)$$

where $J_2 =$ second invariant of the stress deviation.

$$= 1/2(\sigma'_x{}^2 + \sigma'_y{}^2 + \sigma'_z{}^2) + \tau_{xy}{}^2 + \tau_{yz}{}^2 + \tau_{zx}{}^2$$

$k =$ yield stress

Experience with cohesive soils shows that the material can be said to obey the von Mises criterion, $k^2 = J_2$.

$$\dot{W} = 2 k \sqrt{I_2} \quad (5.27)$$

Equation (5.27) shows that it is possible to calculate the rate of doing plastic work \dot{W} without first determining the stresses if a relationship between stresses and strains at a prescribed material stage, e.g. soil yield, can be found. In this case, we find that the von Mises criterion can be applied with some success in many organic soils. If the material is strain-rate dependent, the plastic work can also be obtained without calculating the stresses so long as the rate dependence of the yield stress is available. To demonstrate the kinds of results obtained with the application of this visioelasticity technique, we will show the deformation energy contours for some grousers moving in soil, and a typical set of energy contours developed under a moving wheel.

Figure 5.5 shows the deformation energy contours expressed as dissipative energy contours developed between and beneath moving grousers.

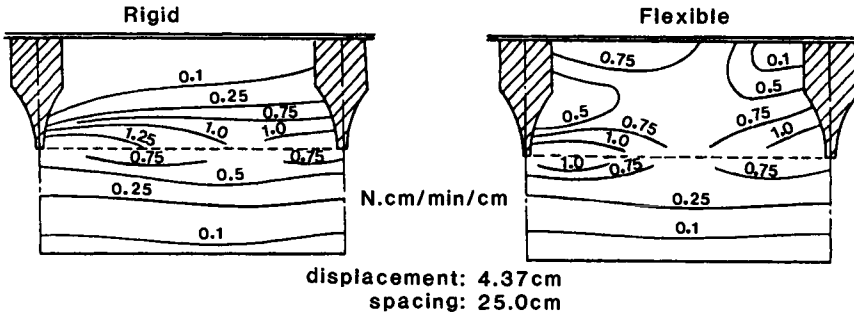


Fig. 5.5. Dissipated energy contours in the deformed soil mass. Aggressive element, displacement = 4.37 cm.

In Fig. 5.6 the deformation energy contours under a moving wheel are shown. As noted, these have been computed using the measured strains, and the application of the computational procedure detailed as the viscoplasticity technique.

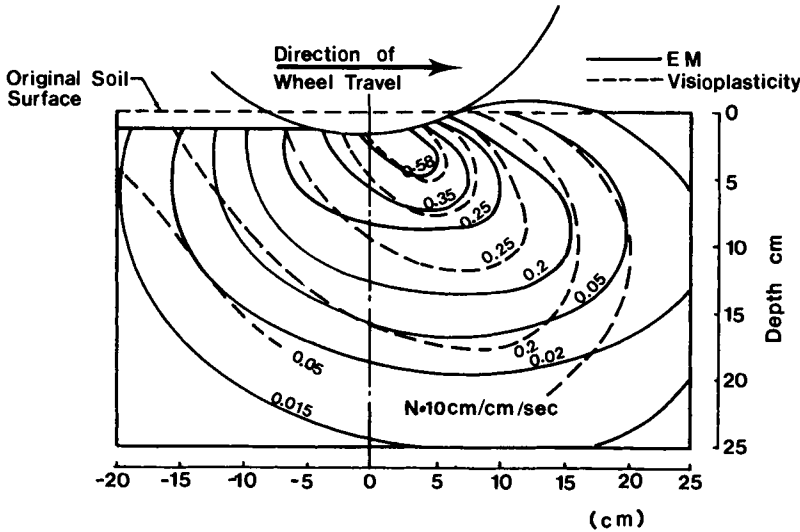


Fig. 5.6. Deformation energy contours (0 percent slip).

5.4.3 Parasitic energy components

Application of the principle of energy conservation to wheel-soil or track-soil interaction problems to predict the useful output energy (drawbar-pull), requires determination of the different parasitic energy components in the system.

In the case of a tyre moving on soft soil, the parasitic energy consists of (Fig. 5.1) (a) energy dissipated in distorting the tyre, (b) energy dissipated at tyre-soil interface due to slip, and (c) energy dissipated in distorting the soil. In the case of highly inflated tyres moving on soft soil, the tyre distortion is very small and can be neglected.

For a track, in addition to the mechanical energy lost in the track system, the soil parasitic energy consists of (Fig. 5.7), (a) distortion energy between grousers, Zone A, (b) energy dissipated at the slip surface between grousers and soil, and (c) energy dissipated at the soil beneath the slip surface.

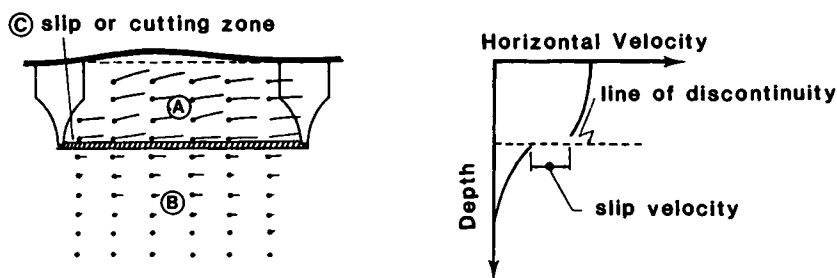


Fig. 5.7. Soil displacement pattern and horizontal velocity distribution due to grouser translation during development of thrust.

5.4.4 Interfacial (slip) energy

The interfacial energy, E_f , is the energy wasted by the frictional stresses at the wheel-soil interface, and it can be expressed as:

$$E_f = \sum_{\text{Total Area of Contact}} \left[\text{Frictional Stresses} \times \text{Elemental Area} \times \text{Elemental Slip Velocity} \right]$$

The methods of determining the frictional stresses at wheel-soil interface are explained in Chapter 2. In the case of tracked vehicles, the shear slip energy rate S.E. can be expressed as:

$$\text{S.E.} = \frac{\sum \left[\text{Shearing Stress} \times \text{Elemental Area} \times \text{Slip Velocity} \right]}{\text{Total Area of Slip Surface}}$$

The slip velocities used in the above equations are the difference in soil velocities above and below the discontinuity line (Fig. 5.7). Its value can be calculated on each segment along this line by using the experimentally recorded velocities on each side of the discontinuity region as provided by the visio-plasticity method. An approximation can be made by averaging the slip velocity along the slip line if the error involved is sufficiently small for the validation of such an approximation.

5.4.5 Soil deformation energy

The work required to deform the soil bearing material under a wheel or track can be evaluated with a knowledge of the strain-rate field, and the strain-rate invariants of representative soil elements in the bearing and interacting terrain material, as shown in Section 5.4.2. In that Section, we addressed the problem in terms of the rate of doing plastic work. In actual fact of course, this is the work required to deform the soil material - i.e. soil deformation energy. The determination of the rate of energy dissipated in deformation beneath a wheel or in zones (A) and (B) in a track system, as shown in Fig. 5.8, follows from eq.(5.27) as:

$$\text{For wheel } E_d = \int_{\text{Volume Deformed}} 2k \cdot I_2^{1/2} \quad (5.28)$$

In the case of a track

$$\text{D.E.} = 2b \sum_{1}^n \int_{X_1}^{X_2} \int_{Y_1}^{Y_2} k \cdot [I_2^{1/2}]_A \, dx dy \quad (5.29)$$

$$\text{D.E.} = 2b \sum_{1}^n \int_{X_1}^{X_2} \int_{Y_1}^{Y_2} k \cdot [I_2^{1/2}]_B \, dx dy \quad (5.30)$$

where $[I_2]_A$ = second invariant of strain rate tensor for the distortion zone (A)

$[I_2]_B$ = second invariant of strain rate tensor for the distortion zone (B)

Y_1, Y_2 = limits of integration from the soil surface to the grouser tip level

Y_2, Y_3 = limits of integration from the grouser tip level down to the end of the affected soil depth;

X_1, X_2 = limits of integration between the vertical axes of the grousers;

b = track width and

n = number of grousers at the track-soil interface.

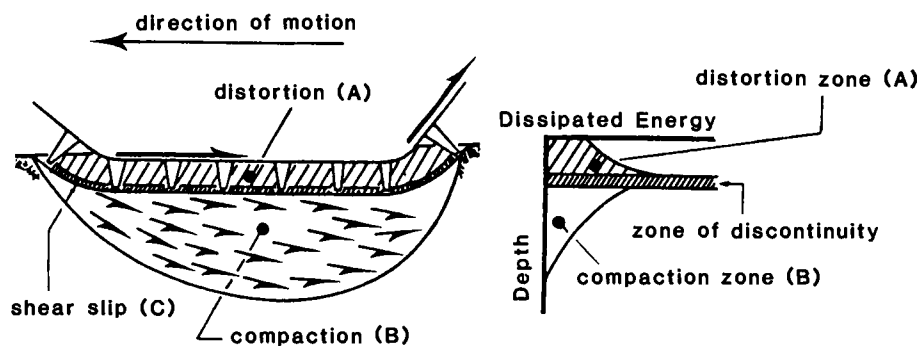


Fig. 5.8. Kinds of energy dissipation in soil beneath a track.

The limits of integration are illustrated in Fig. 5.9. The rate of energy dissipation in subsoil deformation can thus be determined for all the various system parameters studied with the available experimental data and eqs.(5.29 and 5.30).

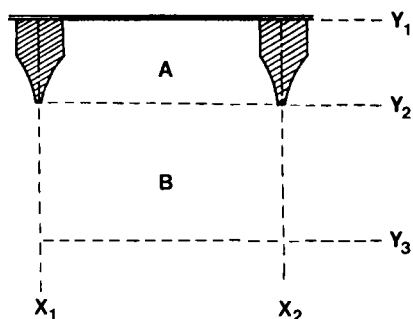


Fig. 5.9. Limits of integration.

The dissipation energy profile beneath a rigid wheel and a multi-grouser test moving on soft soil are shown in Figs. 5.10 and 5.11 respectively.

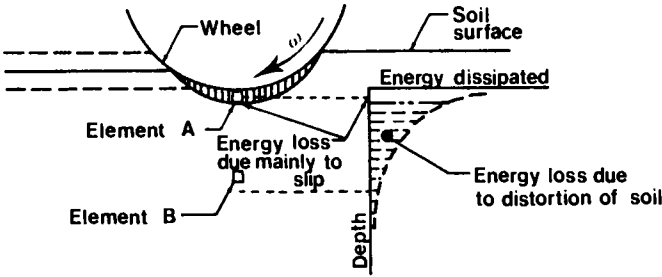


Fig. 5.10. Energy dissipation in substrate due to wheel soil interaction (Yong, 1973).

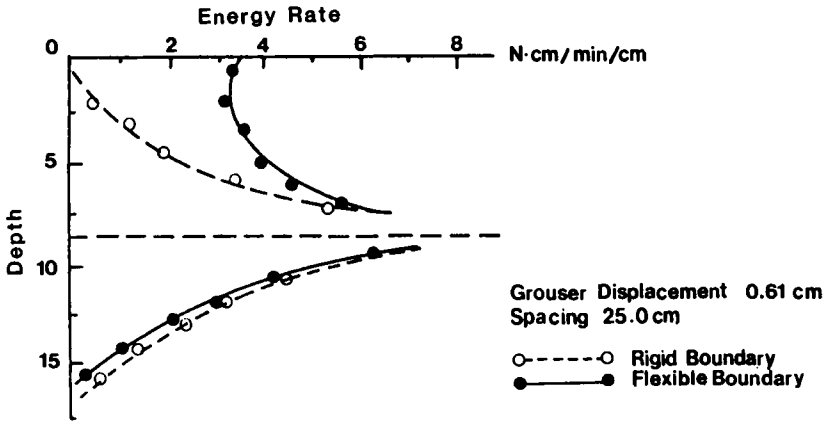


Fig. 5.11. Distribution of dissipated energy rate with depth (displacement = 0.62 cm).

5.5 TRACTION ENERGY BUDGET

We note in the development of the application of the viscoplasticity technique for the evaluation and analysis of traction problems in soils, that general energy dissipating mechanisms were identified in the reacting material, i.e. the material supporting the traction element. For the sake of simplicity, only soft soils have been used in the development of the associated plasticity relations needed to tie together the strains and strain-rate fields experimentally determined, with the stresses which obviously provoked the strains. The technique for evaluation and analysis can obviously be used for other kinds of supporting material - with the strict requirement that proper constitutive relations must be

available to analytically describe the observed performance of the support material.

5.5.1 Vehicle-terrain interaction

The elements and principles which interact and describe movement of a vehicle through vehicle-terrain interaction are essentially those which define the study of "Vehicle Traction Mechanics". Figure 5.12 generalizes the information shown in Fig. 5.1 for more effective presentation to indicate the overall problem. As developed in the previous Sections, the two principal participants and their various individual components which define the elements of the problem treated in vehicle traction mechanics are shown. Note that the running gear shown can either be a wheel (tyre) or track system - as the case may be. Whilst the general tendency is to consider the tyre or track as separate from the suspension system, it should be noted that the running gear system which provides the transfer of energy between the propulsion system and the contacting ground, consists of the entire unsprung mass - i.e. tyres, rims, axles, or tracks, bogies, sprockets and suspension. For the purpose of analyses, however, it is more convenient - and indeed simpler - to consider only that contacting element of interest, i.e. tyre or track/grouser as we have done in the previous Sections. In uncoupling the running gear system for ease in analysis, one makes the assumption that the system can be simply uncoupled and that the linear super-position theory applies.

The basic requirement for production of forward propulsion of any vehicle through a running gear system is that the ground contact elements should develop a thrust action, resulting thereby in vehicle motion opposite to the direction of the thrust. It is this thrust action that creates the many problems cited as surficial damage, immobilization, etc., whilst fulfilling at the same time the requirements for maximum tractive efficiency.

Energy expenditure at the interface arises because of excessive slip, i.e. high relative displacement between the running gear surface and the terrain surface - through surface shear or through the shear boundary layer, or both. Energy expenditure "through the interface" - as opposed to "at the interface" - is due to vehicle flotation requirements where substrate distortion and compaction occur. Figure 5.13 shows the parasitic energy components (discussed in the previous Sections) which participate at and through the interface in vehicle-terrain interaction. We note that as the slip rate increases, the amount of energy expenditure due to slip increases in an exponential fashion. The amount of energy expended in substrate distortion and compaction remains almost constant - i.e. almost independent of the slip rate, (Yong and Webb, 1969).

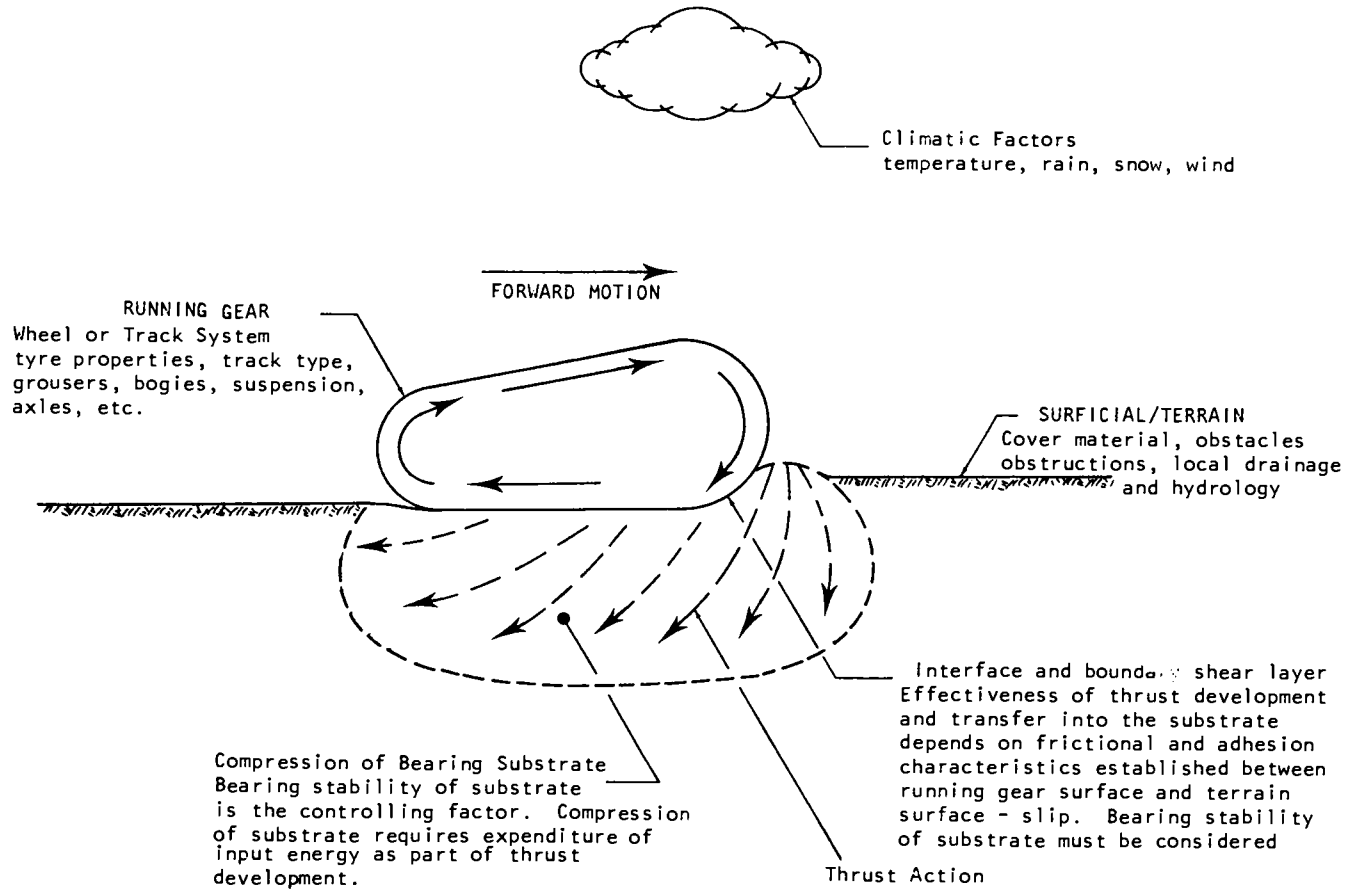


Fig. 5.12. Elements of vehicle-terrain interaction.

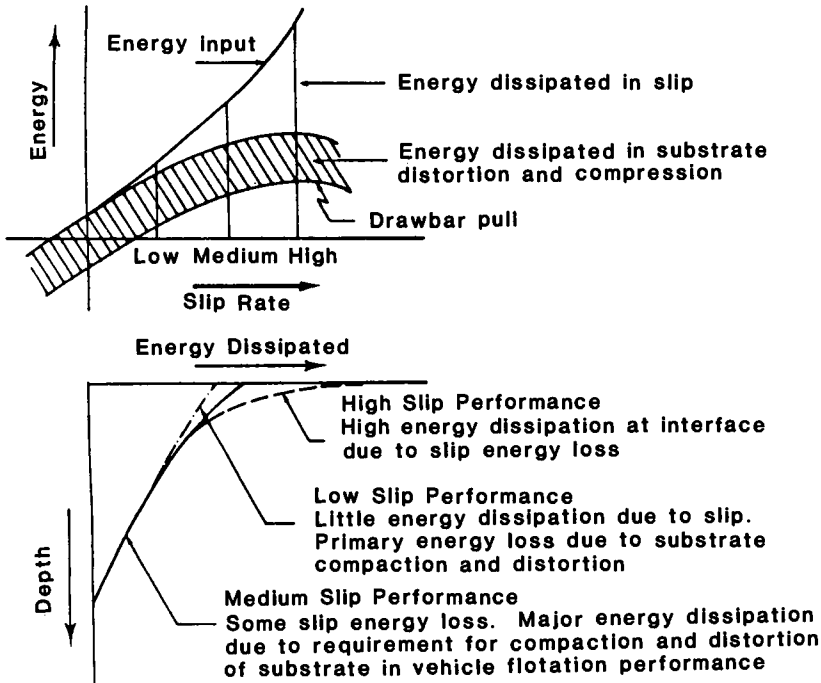


Fig. 5.13. Parasitic energy components and slip influence.

5.6 SUMMARY

Because of the importance of the actual contact mechanism established by an off-road vehicle in its interaction with the terrain, it is clear that attention should be directed to determining the best means for transfer of energy from the vehicle power train to run through its running gear. The elements of energy dissipation shown in Fig. 5.12, and the parasitic energy components shown in Fig. 5.13 which, in essence, particularize the problem to one of kinematics of the running gear system are, in fact, the items which define "motion resistance". In the simplest format and as noted in Section 5.3:

$$\begin{array}{rcl}
 \text{INPUT ENERGY} & & \text{OUTPUT ENERGY} \\
 \text{(Energy supplied} & - & \text{(Work available,} \\
 \text{to the} & & \text{drawbar-pull))} \\
 \text{driving hub)} & & \\
 & \text{MOTION RESISTANCE} & \\
 & \text{(Energy expended} & \\
 & \text{in overcoming} & \\
 & \text{resistances to motion)} &
 \end{array}$$

The "energy budget" can be defined as:

$$\begin{array}{rcl} \text{MAXIMUM AVAILABLE ENERGY} & & \text{ENERGY EXPENDITURE} & & \text{MAXIMUM WORK} \\ \text{(Maximum energy available} & - & \text{(Energy required} & = & \text{(Output} \\ \text{to driving hub} & & \text{to overcome} & & \text{available)} \\ \text{as governed by power plant)} & & \text{motion resistance)} & & \end{array}$$

Since the input energy is governed by the power plant and transmission system, if these are kept constant, it is clear that if a greater output capacity is desired - i.e. drawbar-pull - the motion resistance must be reduced. Thus, for efficient traction, it is necessary to pay the proper attention to provision of the optimum running gear system that minimizes motion resistance. In this manner energy efficient traction for vehicle operation can be obtained.

REFERENCES

- Love, A.E.H., 1959. The Mathematical Theory of Elasticity. Cambridge University Press, 624 p.
- Prager, W. and Hodge, P.G., 1951. The Theory of Perfectly Plastic Solids. Wiley, New York, 264 p.
- Yong, R.N., 1973. Analytical predictive performance for physical performance of mobility. J. Terramechanics, 10:47-60.
- Yong, R.N. and Webb, G.L., 1969. Energy dissipation and drawbar-pull prediction in soil-wheel interaction. Proc., 3rd Int. Conf. Int. Soc. Ter. Veh. Systems, Essen, 1:93-142.
- Yong, R.N. and Fattah, E.A., 1976. Prediction of wheel-soil interaction and performance using the finite element method. J. Terramechanics, 13:4, pp. 227-240.
- Yong, R.N., Fattah, E.A. and Boonsinsuk, P., 1978. Analysis and prediction of tyre-soil interaction and performance using finite elements. J. Terramechanics, 15:1, pp. 43-63.
- Yong, R.N., Elmamlouk, H. and Della-Moretta, L., 1980. Evaluation and prediction of energy losses in track-terrain interaction. J. Terramechanics, 17:2, pp.79-100.

NOMENCLATURE

D, D.E.	deformation energy
E_d	deformation energy
E_f	energy losses
I_2	second invariant of the strain rate tensor
J_2	second stress invariant
L	contact length
P	drawbar-pull
R	wheel rolling radius
T	torque moment
V	translational velocity
V_b	track-belt tangential velocity
W	wheel or track weight
\dot{W}	rate of doing plastic work
X	body force
X_1, X_2	integration limits
Y	body force
Y_1, Y_2	integration limits
b	track width
k	yield stress in shear
n	number of grousers at track-soil interface
u	x-velocity or displacement
v	y-velocity or displacement
w	z-velocity
$\dot{\gamma}_{xy}$	shear strain rate
$\dot{\epsilon}_x, \dot{\epsilon}_y, \dot{\epsilon}_z$	normal strain rates
ρ	density
σ_x, σ_y	normal stresses
σ_x^i, σ_y^i	deviatoric stresses
τ	tangential stress
$\tau_{xy}, \tau_{yz}, \tau_{zx}$	shear stresses
ω	rotational velocity

Chapter 6

FINITE ELEMENT MODELLING

6.1 INTRODUCTION

We discussed predictive modelling techniques in Chapter 4. At that time, we limited ourselves to an overall discussion of the kinds of techniques available - with some attention to the traditional tools for prediction of vehicle-soil or machine-soil interaction. In Chapter 5, we concentrated on the development of the models which utilized the energetics principle. The basic energy model was first presented - followed by the development of the method of analysis using the semi-empirical technique of viscoplasticity. In this Chapter, the finite element method of solution is presented. This procedure constitutes a powerful tool in the application of the energetics approach for prediction purposes.

We recall from Chapters 4 and 5 that in order to construct an analytical model for the purposes of evaluating or predicting future performance of a natural or man-made phenomenon, one should understand (a) how the phenomenon occurs, (b) what parameters affect its behaviour, (c) how it can be described physically, (d) how the response of the phenomenon can be measured or evaluated, and (e) how the phenomenon can be modelled physically.

We note from Chapter 4 that once we have established a physical model for the study of tractive element-soil interaction, a corresponding empirical or analytical model can be constructed and solutions sought to predict the physical model performance, i.e. tractive element performance and subsoil behaviour. The accuracy of the results predicted, using energy-based models, as with other types of models, is dependent on:

(a) the accuracy of the actual physical model used in experimentation and study to represent the problem,

(b) the accuracy of the energy and analytical models in representing the interactions occurring at the vehicle-terrain interface,

(c) the validity of problem idealization, and

(d) the accuracy of the mathematical solution chosen to implement the analysis.

The choice of a mathematical solution technique depends on:

(a) the assumptions required or utilized in constructing the governing equations of the analytical model,

(b) the type of available input data,

(c) the required output results,

(d) the required accuracy of the results to be predicted, and

(e) the efficiency and economy of the solution technique.

The capability of the predictive model, to accurately forecast actual performance of the real events, will obviously depend on the assumptions invoked and the idealizations introduced in the construction of the model. In this Chapter, we will focus on the use of energy principles in the analysis of vehicle-terrain interaction for the purpose of evaluation and prediction of vehicle performance. We will continue the study of a particular set of analytical tools - also subject to the strict requirements shown in the preceding. For the present, only the theoretical aspects of the energy and finite element models will be discussed. The application of these theories (discussed in this Chapter) will be given in Chapter 7.

6.2 FINITE ELEMENT METHOD

The use of the finite element method (FEM) as a numerical solution procedure for solving many kinds of linear and non-linear continuum mechanics problems may be found in several references. Its physically motivated base and its computability for various kinds of boundary conditions and constitutive relationships render it a useful technique for solution of initial boundary value problems. The FEM is capable of handling the following situations encountered by the vehicles' tractive element-soil problems:

- (a) complicated geometrical boundaries at the track or wheel-soil interface and the nearby soil surface,
- (b) effects of loading and unloading of the subsoil due to track or tyre motion,
- (c) the possibility of simulating the actual tractive element-soil movement, e.g. the rotational and translational movements of the tractive element, acceleration, etc.,
- (d) non-linear soil stress-strain relationships,
- (e) effect of confining pressure, volume change and strain rate on the sub-soil behaviour,
- (f) different soil layers with various physical properties and non-homogeneity,
- (g) simple specification of input data required, and
- (h) adjustable degree of accuracy.

Constructing a finite element computer model to predict the performance of a moving tractive element and soil response beneath it requires (a) establishment of the analytical relationships which represent the physical problem and the technique for solving them, (b) forming the loading boundary at the tractive element-soil interface, and (c) establishing soil or substrate material constitutive relationships.

6.2.1 Analytical relationships

The governing relationships of the finite element method are developed in this Section. When a body occupying a space S is subjected to force q , the equation of equilibrium in updated coordinate form may be obtained by using the principle of virtual work, and the external and internal work (Zienkiewicz, 1971; Zienkiewicz and Nayak, 1977; Bathe, 1982):

$$\int_V \rho \{q\}^T d\{u\} dV + \int_A \{P\}^T d\{u\} dA \quad (6.1)$$

and internal work done by:

$$\int_V \{\sigma\}^T d\{\epsilon\} dV \quad (6.2)$$

Strain and displacement are related as:

$$d\{\epsilon\} = [B] d\{\delta\}$$

Equating relationships (6.1) and (6.2), the equilibrium equation can be obtained as:

$$\{\psi\} = \{R\} - \int_V [B]^T \{\sigma\} dV = 0 \quad (6.3)$$

where

$$\{R\} = \int_V \rho [N]^T \{q\} dV + \int_A [N]^T \{P\} dA \quad (6.4)$$

and where

[] = matrix form;

{ } = column vector;

{R} = equivalent external nodal forces;

{ψ} = nodal forces - required to bring the assumed displacement pattern into nodal equilibrium;

{P} = surface forces per unit area of the deformed body;

{q} = body forces per unit mass;

[N] = shape function;

V and A = volume and area of the deformed body;

ρ = density of the deformed body;

$\{u\}$ = displacement of any point within a finite element;
 $\{\delta\}$ = displacement at nodal point;
 $[B]$ = displacement function and
 $\{\sigma\}$ and $\{\epsilon\}$ = vector forms of stress and strain.

In general, both $\{R\}$ and $\{\psi\}$ depend on displacement parameters $\{\delta\}$, and as stress may be a non-linear function of strain, special solution techniques will have to be used.

When the differential equations describing the behaviour of the substrate continuum beneath the tractive element are established, (Section 6.2.1), the basic steps for constructing finite element models will consist of:

- (a) problem idealization,
- (b) defining or constructing constitutive relations for the different materials in the system,
- (c) establishing the boundary conditions,
- (d) establishing the system linear or non-linear differential equations,
- (e) establishing a solution technique.

Finite element models, for different types of running gears operating on cohesive soils, have already been established by Yong et al. (1976, 1977, 1978). These include models concerned with:

- (a) soil cutting,
- (b) single grouser-soil interaction,
- (c) multiple grouser-soil interaction,
- (d) track-soil interaction,
- (e) rigid wheel and pneumatic wheel motion on soft ground.

6.2.2 Problem idealization

Advances in machine computational techniques and the huge storage capacity of existing computers permit any problem to be idealized in three-dimensional coordinates. Whilst the majority of engineering problems are generally three-dimensional in nature, considerable simplification in mathematical solution and consequent timesaving in preparation of data in computation can be realized if the problems are idealized as axisymmetric, two-dimensional or even one-dimensional problems. We appreciate that idealization into two- or one-dimensionality may reduce the accuracy of the model. However, the type of data available and the significance of the results obtained may, by and large, justify the simplification sought.

In the application of finite element modelling to continuum idealization, a specific or mixed type of finite element is used, where the behaviour of the material within each element represents the behaviour of the continuum within the area of the element. The elements are connected together through nodal

points which limit the boundary of each element. The behaviour of all the assembled elements should represent the behaviour of the continuum. The conditions of equilibrium should be satisfied within each element and for the whole continuum. The continuity and compatibility conditions should be satisfied between the elements' boundaries.

Constant plane strain triangular or quadrilateral elements are generally used to idealize the soil continuum. Higher order elements may be used for better accuracy. However, this accuracy may be lost or wasted because of the difficulty in obtaining an exact soil stress-strain relationship, or in specifying the boundary conditions. Higher order elements are more suitable for situations where the boundary conditions and properties of the materials can be exactly as specified. Special types of elements may be introduced at specific areas of the continuum as soil-surface interface or at places of dislocation or slip lines for better representation of the material behaviour in these areas.

The method of idealization of soil continuum will undoubtedly have an effect on the predicted results. Recognizing this, areas which have rapid changes or stress concentrations should be represented by smaller-sized elements in comparison to those which have constant or small changes of stresses. It should be noted that the method of numbering the nodal points of the finite elements in the continuum can also have a great effect on the storage capacity required for the computer model.

One of the drawbacks in the use of the finite element technique is the amount of input data required for idealization. Mesh generation or a computational technique to reduce the amount of input data is necessary to save time, effort, and to reduce the likelihood of mistakes.

In applying the FEM of analysis to vehicle traction mechanics, the running gear and soil cutting problems are considered as two-dimensional problems. Three types of elements are generally used in idealizing the soil continuum:

- (a) constant strain triangular element,
- (b) joint element to represent slip lines, and
- (c) joint element to represent the characteristics of the material at the tool-soil or vehicle-soil interface.

To develop the application of the FEM to traction mechanics problems, we will focus on a particular interaction involving thrust and development of both slip and shear failure in the soil substrate. As an example, the location of the elements discussed in the previous Chapters is shown in Fig. 6.1 for a blade-soil or grouser-soil interaction problem.

The derivation of the stiffness matrix which defines the load deformation characteristics of a triangular element in plane strain may be found in any text-book dealing with the development of the finite element technique, e.g. Zienkiewicz (1977) and Bathe (1982), and hence will not be described herein.

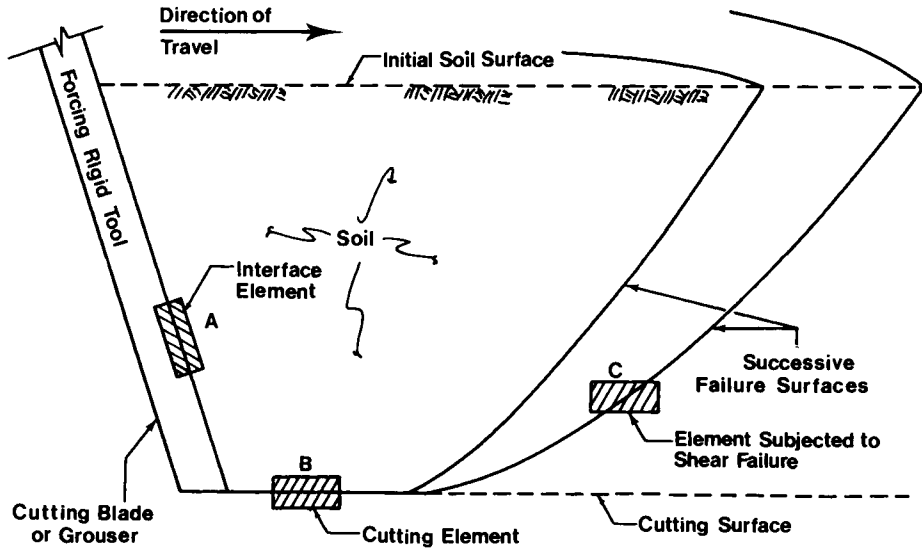


Fig. 6.1. Location of elements for development of idealized model.

6.2.3 Idealization of discontinuities

Several kinds of models are available for modelling discontinuities. A pin-ended one-dimensional element such as that shown in Fig. 6.2 can be used. This element can allow transfer of compressive stresses across a fault, but cannot sustain shear or tensile normal stresses. Duncan and Goodman (1968) have proposed three different procedures for utilization as follows: ubiquitous joint, orthotropic continuum and single joint analysis, as shown in Fig. 6.2. The ubiquitous joint analysis is based on the continuum approach in which the induced shear stresses are computed on a large number of plane orientations. The likelihood of slip or opening of joints that really exist is evaluated thereupon. The orthotropic continuum approach is based on linear elastic theory in which equivalent elastic parameters are computed for the parent mass influenced by three orthogonal joint sets. In single joint analysis, Figs. 6.2d and 6.2e, the stiffness formulation is obtained by considering the joint as either one- or two-dimensional. The stiffness of a joint is defined in terms of its normal and tangential stiffnesses. This approach is a modification of the concept proposed by Ngo and Scordelis (1967) for cracking in concrete elements.

In the one-dimensional single joint proposed by Goodman et al., (1968), and Heuze et al. (1971), the joint is defined by four nodal points as shown in Fig. 6.2d, with its thickness in the normal direction assumed as zero. This joint element, when inserted between two portions of the parent mass, can permit large relative displacements. One can also formulate the single joint analysis by using isoparametric elements as has been done by Zienkiewicz et al., (1970).

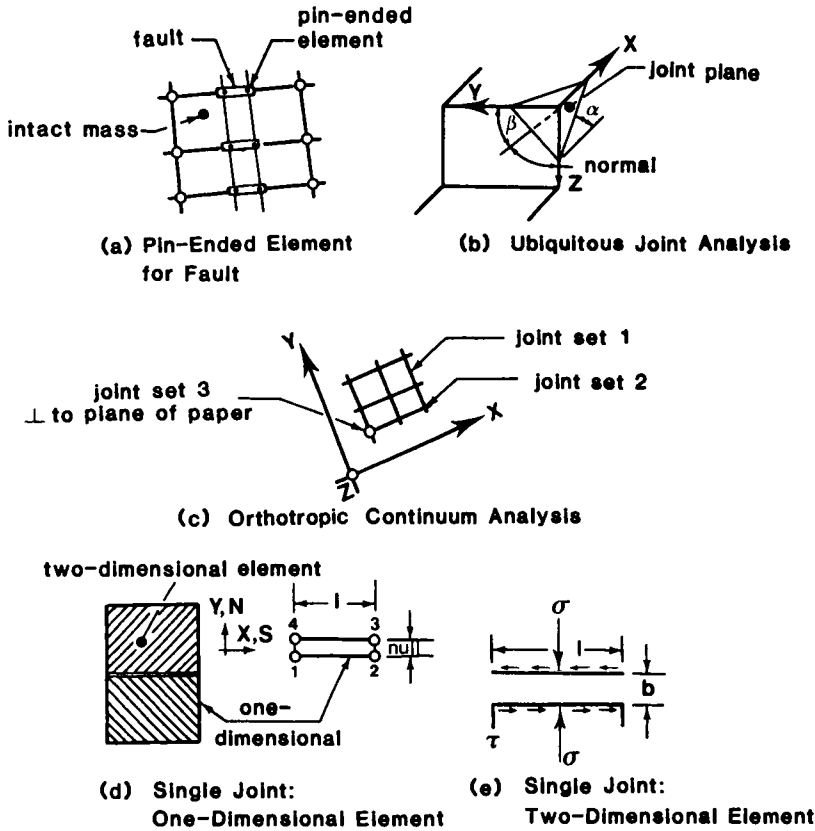


Fig. 6.2. Various models for discontinuities (joints). (Desai and Abel, 1972).

6.2.4 Joint element stiffness formulations

The stiffness properties of a joint element are discussed in this sub-Section along the lines developed by Goodman et al. (1968). The element, shown in Fig. 6.3 in a local coordinate system with the x -axis along the length, has a length L , but very small width. The origin is at the centre. The explicit formulation for the stiffness matrix $[k]$ is not shown here since this can be found in textbooks relating to the FEM of analysis. The stiffness matrix given in eq.(6.5) has 32 non-zero terms, but is seen to depend on only two quantities - i.e. the unit joint stiffness in the normal and tangential directions. It may be transferred to global coordinates (X, Y) by using transformation of axes without rotation.

$$(k) = \frac{1}{6} \begin{bmatrix} 2k_s & 0 & k_s & 0 & -k_s & 0 & -2k_s & 0 \\ 0 & 2k_n & 0 & k_n & 0 & -k_n & 0 & -2k_n \\ k_s & 0 & 2k_s & 0 & -2k_s & 0 & -k_s & 0 \\ 0 & k_n & 0 & 2k_n & 0 & -2k_n & 0 & -k_n \\ -k_s & 0 & -2k_s & 0 & 2k_s & 0 & k_s & 0 \\ 0 & -k_n & 0 & -2k_n & 0 & 2k_n & 0 & k_n \\ -2k_s & 0 & -k_s & 0 & k_s & 0 & 2k_s & 0 \\ 0 & -2k_n & 0 & -k_n & 0 & k_n & 0 & 2k_n \end{bmatrix} \quad (6.5)$$

6.3 PROBLEM IDEALIZATION

6.3.1 Soil-cutting idealization

In the finite element idealization of a soil-cutting problem, the model shown in Fig. 6.3 incorporates a predefined discontinuity at the level of the tool tip. The reason for including the cutting plane discontinuity in the finite element model is to represent the action of the cutting element, where severe relative displacements and separation of soil blocks take place. Such a discontinuity can be visualized as a thin soil layer on which the soil above slides on the soil mass below. This sliding behaviour is governed by the soil constitutive shear stress-relative displacement relationship.

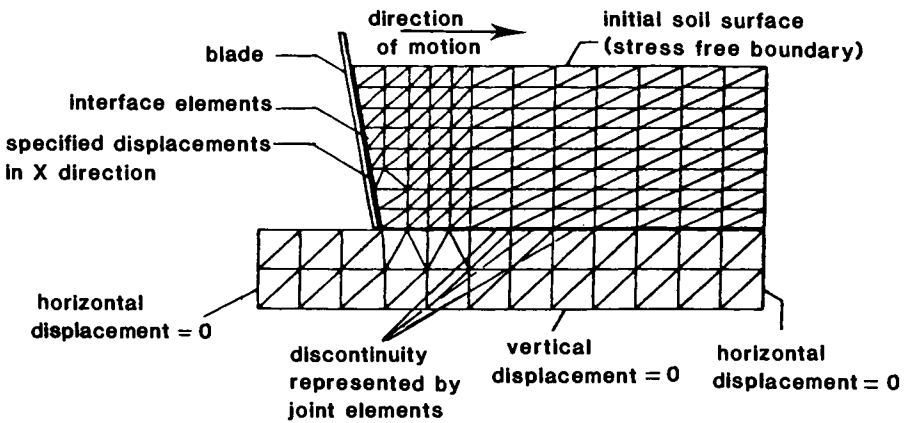


Fig. 6.3. Finite element idealization of a blade-soil system.

The discontinuity location is essentially predetermined since the tool is assumed to move at a constant elevation. This predefined discontinuity plane should not be confused with a failure plane which can initiate at the tool tip at any angle with respect to the horizontal depending on the direction of the maximum shear stress. The horizontal movement of a cutting or a traction tool often produces a series of failures in the soil which are usually induced from the level of the tool tip to the soil surface. While these failure surfaces can be modelled also as discontinuities, a prior specification of failure surfaces will limit the usefulness of the proposed model. Location of the failure zones or surfaces in the soil medium is determined by examining the maximum shear stress induced in each finite element after each increment of tool displacement. If the stress is found equal to or greater than the shear strength of the soil at that location, the stiffness values for this element are reduced to small magnitudes, and the element is considered to have failed in shear. This technique for determination of failure zones or surfaces does not allow cracking to take place, and hence, sliding along a series of failure surfaces is not possible. However, in the case where sliding along a failure surface is found to be of importance in describing the soil behaviour, an approach similar to that of Nilson (1968) can be adopted in which the topology of the discretization is altered by disconnecting cracked elements at their common nodes, and inserting a form of a joint element similar to those described in the previous Section along the cracked elements' common edge. By allowing these joint elements to transfer compressive stresses, but not shear or tensile normal stresses, we can represent the propagation of failure surfaces and subsequent sliding along these surfaces.

In conventional finite element theory, the displacements along the boundary between adjacent finite elements are required to be compatible, i.e. no gaps may open or relative displacements occur between adjacent elements. During the soil deformation process, relative displacements do indeed occur at the interface between the soil and the tool, representing thereby a discontinuity in the finite element displacement field. This type of discontinuity is shown in Fig. 6.1 as element A. Since the relative displacements occur in the tangential direction at the interface, the joint element, presented by Goodman et al. (1968) can be inserted between the tool surface and the soil mass, Fig. 6.2d, to allow for soil slipping along the metal interface.

A similar approach is employed to model the cutting plane discontinuity since the deformation mechanism of this plane, presented in Fig. 6.1 by element B, is similar to that of a rock joint - i.e. relative displacements occur across a thin discontinuity. The simulation of the assumed discontinuity can be the same as that employed for rock joints where the joint elements are placed to model the separation of the two blocks of continuum adjacent to the discontinuity surface which were initially in contact.

6.3.2 Soil-grouser interaction

A solution of the traction problem - that is, obtaining adequate traction at a suitable speed in a practical manner and at a reasonable cost - lies in an understanding of:

- (a) the manner in which stresses are applied to the soil, and
- (b) the reaction of the soil to the applied stresses.

Whilst soil cutting and grouser traction problems can be considered to be the same problem in principle, (both situations requiring analyses of soil stresses and deformations, as well as the evaluation of developed reactions on the cutting or traction devices), the purpose of a traction device is to cause deformation of soil in a certain manner so as to develop adequate traction capacity (optimum developed reactions) with minimum input work. The purpose of soil cutting is to achieve the maximum volume of soil cutting with the minimum input work. To achieve this it is necessary to change the geometry of the traction tools, or, in other words, the interacting boundary conditions, in order to reach the state of soil manipulation for the production of adequate traction.

Figure 6.4 shows typical soil idealizations for three types of single grousers. Plane strain conditions are assumed in cross-section, and constant strain triangles are employed to represent the soil mass. The cutting (joint) elements are placed on the plane where the cutting is anticipated and the cutting plane is assumed to start in all cases at the level of the grouser tip. It is understood that the cutting plane assumption can lead to a certain degree of error since the soil is forced to separate on a particular plane having a fixed position and direction. These errors however are, by and large, small and can be ignored.

Figure 6.5 shows a soil continuum idealization for three types of rigid multi-grousers. The location of the interfacial and cutting (joint) elements are shown in the Figure.

6.3.3 Tyre-soil idealization

The idealization of the soil bearing stratum in the finite element analysis is shown in Fig. 6.6. The element size is determined by the size of the tyre contact patch (footprint). Once the footprint length (FPL) of the tyre on the soil under consideration is known (predicted or measured), the depth of the soil stratum is automatically set as a function of n times FPL. In the idealization shown in Fig. 6.6, the depth is given as 5 FPL whilst the length of the soil stratum analyzed is 10 FPL. These dimensions are considered to be satisfactory since the effect of the end boundary condition is not significant. The advantage of this type of idealization is that the finite element formulation then becomes dimensionless. Hence this can be saved as block data in the main source of the computer model to generate actual values for any type of pneumatic tyre once the footprint length is known.

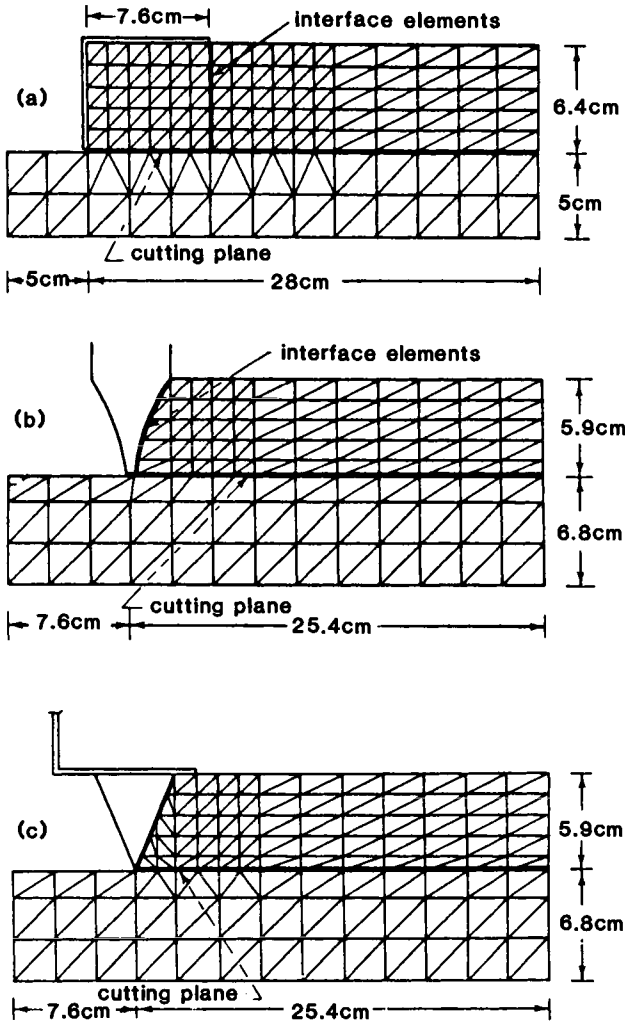


Fig. 6.4. Finite element mesh layouts for various single grousers.

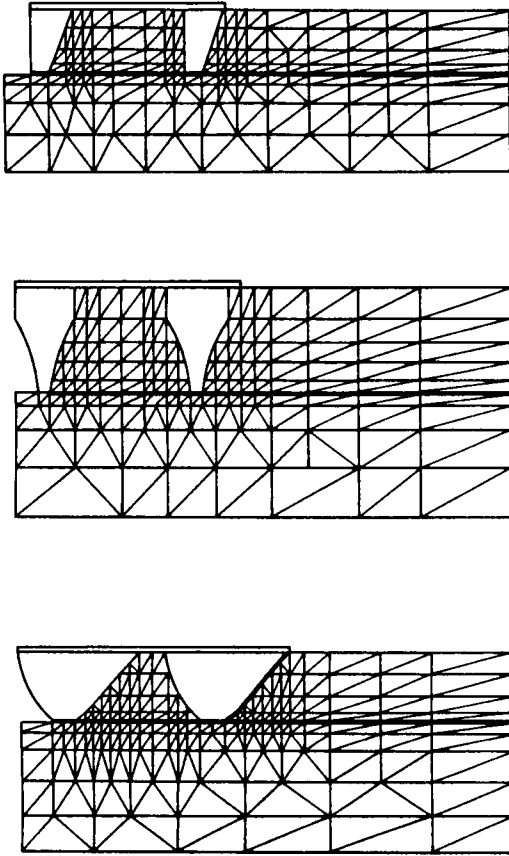


Fig. 6.5. Finite element mesh layouts for various rigid multi-grousers.

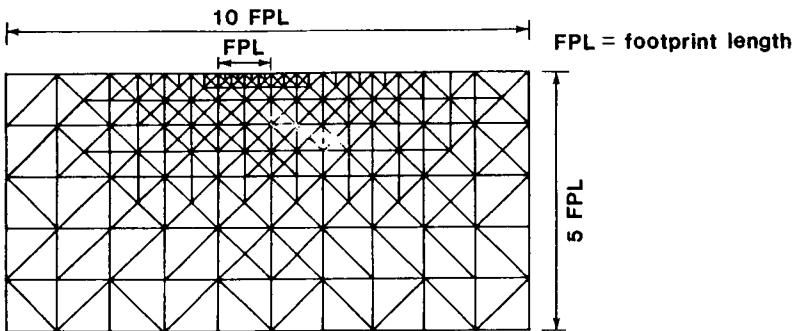


Fig. 6.6. Finite element discretization for the tyre-soil or track-soil system.

6.3.4 Rigid track-soil idealization

A rigid track may be considered as a pneumatic tyre with constant footprint length - Fig. 6.7. The idealization shown in Fig. 6.7 for the tyre-soil interaction problem can be used for track-soil system as well. The contact area of the track is well-defined.

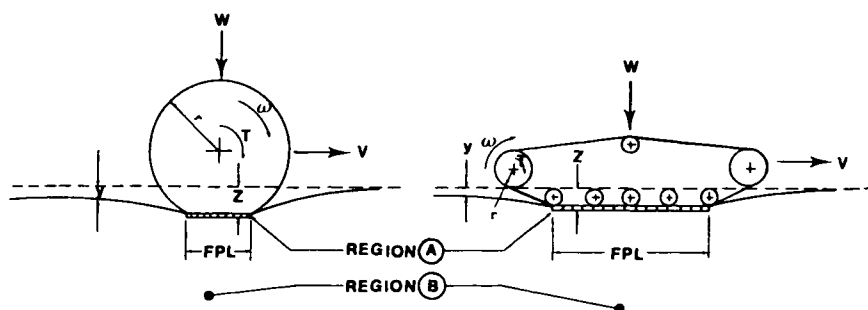


Fig. 6.7. Wheel and track operating mechanisms.

6.4 CONSTITUTIVE RELATIONSHIPS

In the previous Sections, the finite element formulations were derived assuming that the stress-strain behaviour of the material is known. A set of equations that defines the stress-strain behaviour of a material represents the constitutive law for the material. Constitutive relations for soils are derived, based on some simplified assumptions for the behaviour of the material. The number of variables used would depend upon the complexity of the model chosen to simulate soil behaviour. The use of non-linear analyses by the finite element method or other numerical techniques will be determined by the nature of the model chosen. In general, the more complex the model, the more the number of variables to be taken into account, and the more involved the non-linear analysis. For a realistic analysis, it must be possible to obtain values for the constants involved in the constitutive law from laboratory experiments.

The simplest constitutive law will be the one that assumes that soil behaviour can be represented by a linear elastic material. This linear elastic model has been used by many research workers in their investigations. Other workers have considered soil to be elasto-plastic or nonlinearly elastic.

The elasto-plastic approach idealizes the stress-strain curve for the soil, and uses the equations of elasticity in the elastic range and the equations of plasticity in the plastic range. The nonlinear elastic approach, on the other hand, does not idealize the stress-strain curve, but uses the equation of elasticity to solve for the stress state even after yielding in the soil has occurred. Any degree of nonlinearity can be accounted for in this approach. The

elastoplastic approach appears sound from a theoretical standpoint, but the practical problem involved in defining a yield limit and a flow law can pose a serious handicap. Inasmuch as the nonlinear elastic analysis represents the actual stress-strain relation obtained from tests on the bearing material, it seems reasonable to expect fairly good results from this type of analysis.

Whilst the finite element method described earlier can evaluate the numerical values of stress and strain in the continuum considered, it requires a knowledge of elastic parameters, i.e. the modulus of elasticity (E) and Poisson's ratio (ν). These parameters are normally established, through suitable test procedures on representative specimens, e.g. triaxial tests. In soils, the influences of the confining stresses on these elastic parameters are important.

In general, the stress-strain relationships for soils in three dimensions can be best described by using stresses and strains in the octahedral plane. In cohesive soils, the general constitutive law can be expressed in the following forms (Newmark, 1960):

$$\epsilon_{\text{oct}} = f_1(\sigma_{\text{oct}}, \tau_{\text{oct}}, \phi)$$

$$\frac{1}{2} \gamma_{\text{oct}} = f_2(\sigma_{\text{oct}}, \tau_{\text{oct}}, \phi) \quad (6.6)$$

$$\theta = f_3(\sigma_{\text{oct}}, \tau_{\text{oct}}, \phi)$$

where

f_1, f_2, f_3 = arbitrary functions;

ϵ_{oct} = octahedral normal strain;

γ_{oct} = octahedral shear strain;

σ_{oct} = octahedral normal stress;

τ_{oct} = octahedral shear stress;

$\phi = J_3''/\tau_{\text{oct}}^2$ = friction parameter;

J_3'' = third invariant of the deviator stress;

$= (\sigma_1 - \sigma_{\text{oct}})(\sigma_2 - \sigma_{\text{oct}})(\sigma_3 - \sigma_{\text{oct}})$;

$\sigma_1, \sigma_2, \sigma_3$ = principal normal stresses;

$\theta = \frac{\epsilon_1'' \epsilon_2'' \epsilon_3''}{(\frac{1}{2} \gamma_{\text{oct}})^2}$ and

$\epsilon_1'' \epsilon_2'' \epsilon_3''$ = first, second and third deviator strain components.

The effects of volume change, distortion and intermediate principal stress (σ_2) which are neglected in the two-parameter Mohr-Coulomb failure criterion

normally employed should be accounted for if they are felt to be significant issues. In the special situation of saturated clays, the extended Von Mises yield criterion may be adopted (Yong and McKyes, 1971) which consequently implies that the friction parameter (ϕ) is insignificant. In such instances, the formulation of eq.(6.6) can be reduced to:

$$\epsilon_{\text{oct}} = f_1(\sigma_{\text{oct}}, \tau_{\text{oct}}) \quad (6.7)$$

$$\frac{1}{2} \gamma_{\text{oct}} = f_2(\sigma_{\text{oct}}, \tau_{\text{oct}})$$

In the case of saturated or nearly-saturated clays, the volume change during shearing is negligible (Yong and McKyes, 1971), which leads to the consideration that changes in volume which occur due to immediate application of the hydrostatic stress component, are small in magnitude. Thus eq.(6.7) may be further reduced to:

$$\frac{1}{2} \gamma_{\text{oct}} = f_2(\sigma_{\text{oct}}, \tau_{\text{oct}}) \quad (6.8)$$

This relationship may be derived from triaxial tests conducted on representative soil specimens at different confining pressures. The octahedral normal stress (σ_{oct}), shear stress (τ_{oct}), and shear strain (γ_{oct}) can be determined as

$$\sigma_{\text{oct}} = \frac{1}{3} (\sigma_1 + \sigma_2 + \sigma_3)$$

$$\tau_{\text{oct}} = \frac{1}{3} \left[(\sigma_1 - \sigma_2)^2 + (\sigma_2 - \sigma_3)^2 + (\sigma_3 - \sigma_1)^2 \right]^{1/2} \quad (6.9)$$

$$\frac{1}{2} \gamma_{\text{oct}} = \frac{1}{3} \left[(\epsilon_1 - \epsilon_2)^2 + (\epsilon_2 - \epsilon_3)^2 + (\epsilon_3 - \epsilon_1)^2 \right]^{1/2}$$

where

$\sigma_1, \sigma_2, \sigma_3$, = major, intermediate and minor principal stresses and

$\epsilon_1, \epsilon_2, \epsilon_3$, = major, intermediate and minor principal strains.

E and ν can be evaluated from plane-strain triaxial test results using the following formulation:

(a) Hooke's law for an isotropic, linear, elastic material in a principal plane can be written as:

$$\epsilon_1 = \frac{\sigma_1}{E} - \frac{\nu}{E} (\sigma_2 + \sigma_3)$$

$$\epsilon_2 = \frac{\sigma_2}{E} - \frac{\nu}{E} (\sigma_1 + \sigma_3) \quad (6.10)$$

$$\epsilon_3 = \frac{\sigma_3}{E} - \frac{\nu}{E} (\sigma_1 + \sigma_2)$$

where

σ_i ($i = 1, 2, 3$) = major, intermediate and minor principal stresses and
 ϵ_i ($i = 1, 2, 3$) = major, intermediate and minor principal strains.

(b) For the case of plane strain, $\epsilon_2 = 0$, and the second equation in eq.(6.10) reduces to:

$$\sigma_2 = \nu(\sigma_1 + \sigma_3) \quad (6.11)$$

(c) For an incompressible material $\nu = 0.5$, and from the first equation of eq.(6.10) it can be shown that:

$$\epsilon_1 = \frac{3(\sigma_1 - \sigma_3)}{4E} \quad (6.12)$$

or

$$E = \frac{3(\sigma_1 - \sigma_3)}{4\epsilon_1} \quad (6.13)$$

The $(\sigma_1 - \sigma_3)/\epsilon_1$ term in eq.(6.13) represents the slope E_T of the deviator stress, $(\sigma_1 - \sigma_3)$, versus principal strain, ϵ_1 , curve. Thus in the plane strain case:

$$E = \frac{3}{4} E_T \quad (6.14)$$

6.5 JOINT ELEMENT CONSTITUTIVE RELATIONSHIP

As mentioned earlier, the cutting phenomenon caused by the movement of a traction element or a tool in a soil mass is idealized by inserting joint elements between the solid elements. In evaluating the stiffness of these elements, it is assumed that both normal and shear displacements vary linearly along the length of the element, which is compatible with the external boundary displacements of the continuum elements used herein.

The properties of these elements consist of a normal stiffness, k_n , and a shear stiffness, k_s , which are related to the normal and shear stresses acting on the element by:

$$k_n \Delta_n = \sigma_n \text{ and } k_s \Delta_s = \tau \quad (6.15)$$

where

Δ_n = average relative normal displacement across the element, and
 Δ_s = average relative shear displacement along the element.

The values assigned to k_s can be determined from the results of direct shear tests. The nonlinear tangential stress-displacement curves shown in Fig. 6.8 may be approximated by hyperbolae as follows:

$$\tau = \frac{\Delta_s}{a + b\Delta_s} \quad (6.16)$$

where

τ = cutting stress;
 Δ_s = shear displacement, and
 a, b = empirical coefficients.

The values of the coefficients (a) and (b) can be easily determined by transforming the stress-displacement data to another set of axes, on which the hyperbolae plot as straight lines. By transposing eq.(6.16), the following relationship may be obtained:

$$\frac{\Delta_s}{\tau} = a + b\Delta_s \quad (6.17)$$

If values of Δ_s/τ are plotted against values of Δ_s , as shown in Fig. 6.8, the resulting variation will be a straight line if the shear stress varies hyperbolically with displacement. It may be shown from the form of eq.(6.17) that coefficient (a) is the intercept, and coefficient (b) is the slope of the straight line on this transformed plot.

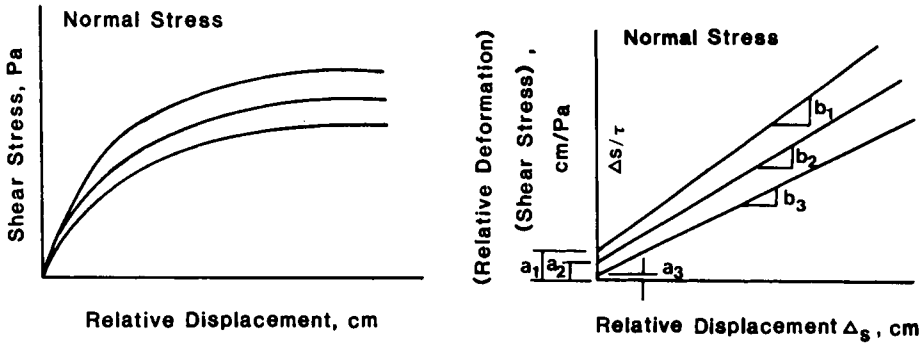


Fig. 6.8. Transformed linear hyperbolic plots for cutting and interface tests.

The reciprocal of coefficient (a) is the initial slope of the shear stress displacement curve, and is analogous to the initial tangent modulus of a stress-strain curve. The quantity called herein the initial shear stiffness, K_{sj} , has units of force per cubic length, or Newton per cubic cm for the curves shown in Fig. 6.8. The reciprocal of coefficient (b) is the asymptote approached by the shear stress displacement curve at the very large values of displacement.

The tangent stiffness value, representing the slope of a tangent to the shear stress displacement curve, may be readily found by differentiating eq.(6.17) with respect to Δ_s , and, eliminating Δ_s from the resulting equation, the tangent stiffness value may be expressed as:

$$K_{st} = \frac{1}{a}(1 - \tau b)^2 \tag{6.18}$$

Possible modes of behaviour for the joint element are shown in Fig. 6.9. It can be seen that in the compression and combined modes the adjacent continuum elements tend to overlap, a condition which occurs because compressive stresses require compressive relative displacements across the element which, for purposes of analysis, is assumed to be relatively thin.

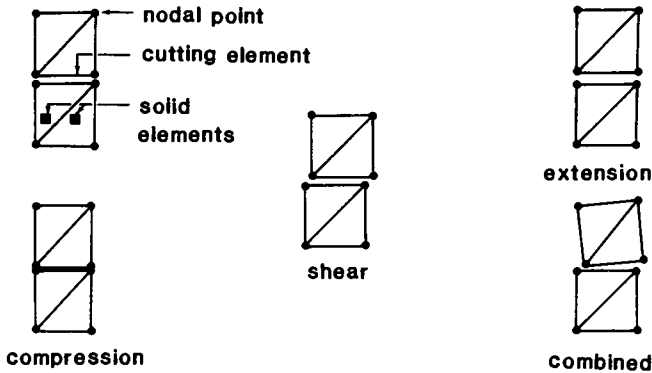


Fig. 6.9. Models of behaviour of cutting elements. (Modified after Duncan and Goodman, 1968).

The stiffness values assigned to these elements vary depending on the mode of behaviour and the element stresses. For compression, the value of k_n can be made equal to the initial elastic modulus of the continuum elements, and the value of k_s can be calculated using eq.(6.18). After an element fails in shear, with the element still in compression, k_s is reduced to a negligible value but the value of k_n is kept constant.

Both the shear stiffness, k_s , and the shear strength of the cutting zone depends on the value of the normal stress in this layer. The tangential stiffness values assigned to these elements will vary depending on the element normal stress. This can be achieved by considering the values of the coefficients (a) and (b) as functions of the normal stress existing in the element.

In a similar fashion, the properties assigned to the interface elements can be determined from the results of direct shear tests on specimens consisting partly of soil and partly of the traction tool material. Equation 6.13 is again used to predict the tangent stiffness modulus, provided that coefficients (a) and (b) are obtained from a soil-tool interaction test.

6.6 BOUNDARY CONDITIONS

The boundary conditions required for solving the finite element model for each of the major running gear-soil systems are discussed in this Section.

6.6.1 Soil cutting and grouser tractive elements

(i) Single grouser. In the two-dimensional soil-cutting or grouser tractive element-soil system, the boundary conditions can be (a) specified forces, (b) specified displacements, or (c) both. Assuming the direction of tool motion to be horizontal, the boundary conditions at the tool surface will be specified

horizontal displacements. The top soil (terrain) surface is considered a stress-free boundary unless there is a vertical load distributed uniformly on a grouser (tool (a) - Fig. 6.10, for example). At a reasonable distance from the tool the bottom boundary is assumed to move only in the horizontal x-direction. The boundary conditions are shown in Fig. 6.3.

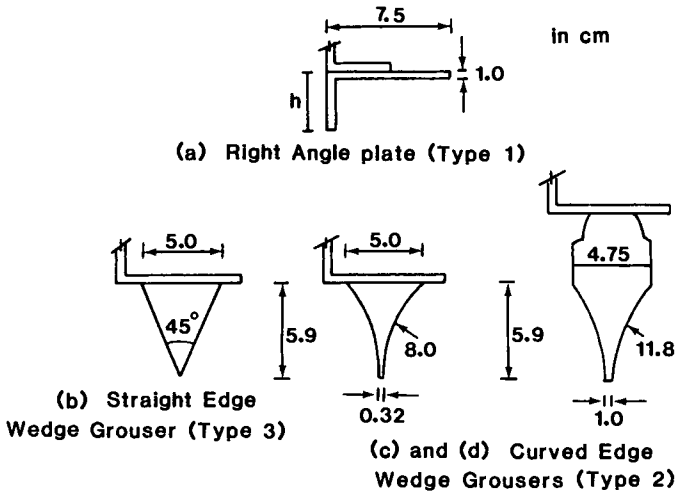


Fig. 6.10. Grouser geometrics.

(ii) Multi-grouser. There are two types of conditions at the loading boundary of the multi-grouser-soil interface. These are (a) constant elevation boundary, and (b) constant applied pressure boundary condition. In the constant elevation boundary condition the movement (translation) of the grouser system occurs at a constant height in relation to the initial soil surface. The depth of the grousers embedded in the soil is always constant.

In all idealizations for analysis of the problem, cutting joint elements are placed on the plane where the cutting is anticipated, and are assumed to start at the level of the grouser tip. No interface elements are placed between the soil and the face of the succeeding grousers, since experimental observations show that the confinement of the soil, due to the rigidity of the connecting top plate, creates a 'dead' zone between the adjacent grousers. Interface elements are inserted at the leading grouser-soil interface in the cases of the standard and passive elements shown in Fig. 6.5. Interface elements are not required for the leading grouser in the aggressive element because the horizontal plate on the top of the grouser creates a no-slip condition at the grouser face.

In the constant applied pressure boundary condition, the multiple grouser elements are free to move horizontally and vertically. They are, however, re-

strained from rotation along the longitudinal axis. The initial depth of the embedment of the grousers is considered equal to the height of the element. Cutting and interface elements are inserted at the same positions as the constant elevation boundary condition. In general the boundary conditions are similar to the constant elevation situation with one basic difference:

In the constant elevation boundary the interface behind the first grouser and the soil is considered as a free surface in order to avoid complete rigidity of the soil contained between the two grousers.

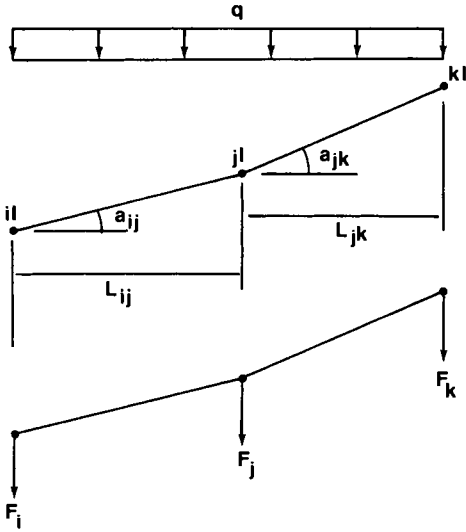
Although the adoption of such a boundary condition shows reasonable agreement between experimental and finite element results for the case of the constant elevation boundary condition, the same is not true for the constant pressure case. Under the application of a uniform pressure, the soil remains in constant contact with the grousers during grouser motion. Thus, the finite element analysis must assign both horizontal displacement and vertical pressure in boundary condition considerations.

The uniform vertical pressure is applied incrementally as equivalent nodal loads on the finite element mesh in the vertical direction. The inclination of the line representing the grouser surface between two successive nodes can be taken into account, as illustrated in Fig. 6.11.

6.6.2 Wheel-soil system displacement boundary condition

In formulating the analytical model for the wheel-soil mobility performance, it is necessary to simulate the action of the wheel moving on the supporting soil so that all important parameters which contribute to the wheel-soil interaction are considered. The wheel itself possesses both translational and rotational movements while the soil underneath the wheel is compressed (loaded) at the leading edge and unloaded at the trailing edge (Fig. 6.12). All the movements occur simultaneously and are essentially interdependent. The loading boundary conditions at the wheel-soil interface can be described in terms of the stress distributions (load boundary approach) or the resultant soil particle movement (displacement boundary approach) at the tyre-soil interface, both of which are dependent primarily on the slip rate, wheel load, tyre-soil relative stiffness, and tyre-soil surface characteristics. Once an appropriate loading boundary condition at the tyre-soil interface is properly imposed, the finite element method can be carried out to evaluate the response behaviour of the sub-soil stratum accordingly.

To adopt the displacement boundary condition in the finite element method for wheel-soil problems, the movement of any point on the wheel-soil interface has to be properly described so that the performance can be analysed with respect to



$$F_i = \frac{qL_{ij}\cos^3 a_{ij}}{2} + qL_{ij}\sin^2 a_{ij}\cos a_{ij}$$

$$F_j = \frac{q(L_{ij}\cos^3 a_{ij} + L_{jk}\cos^3 a_{jk})}{2} + q(L_{ij}\sin^2 a_{ij}\cos a_{ij} + L_{jk}\sin^2 a_{jk}\cos a_{jk})$$

$$F_k = \frac{qL_{jk}\cos^3 a_{jk}}{2} + qL_{jk}\sin^2 a_{jk}\cos a_{jk}$$

Fig. 6.11. Method of distributing the applied uniform pressure between successive nodes. Constant vertical pressure boundary condition.

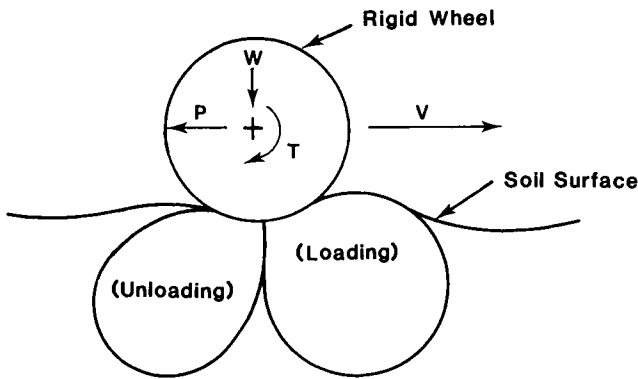


Fig. 6.12. Subsoil response beneath a moving rigid wheel.

the wheel position and slip rate. In general, the path of a moving point on a deforming pneumatic tyre can be expressed relative to a moving reference frame, i.e. the axle centre line. In the case of a rigid wheel, in which there is no deformation in the wheel itself moving through a soft soil (Fig. 6.13), the path of the moving point 'z' in the soil $\overline{B\bar{C}}$ or $\overline{A\bar{C}}$ follows a smooth trajectory.

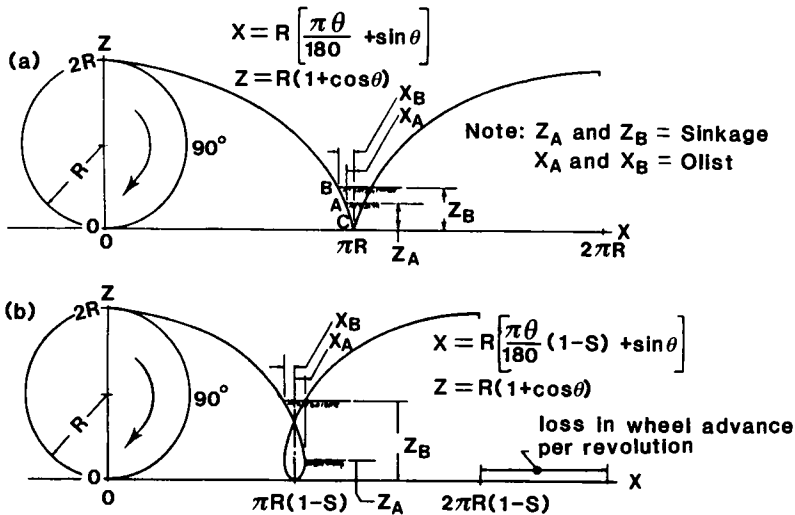


Fig. 6.13. Prolate cycloid of an undeformed tyre rolling with 25.5% slip

If there is no slip between the wheel and the soil, there will be no loss in the wheel advance (Fig. 6.13a), unlike the situation with some slip (Fig. 6.13b). If a deformable tyre moves on a rigid unyielding surface, the path of a point on the tyre will conform to the contour of the supporting surface so long as the point under consideration contacts the surface. In the most complicated situation in which both the tyre and the soil are deformable, the movement of a point in the tyre at the tyre-soil interface follows a rather irregular path affected by the relative stiffness of the tyre-soil system and slip rates.

The specification of displacement boundary conditions as input data has been successfully adopted in the finite element analysis of the performance of rigid wheels moving through a soft clay (Yong and Fattah, 1976). Typical soil particle paths (Fig. 6.14) were experimentally measured at different slips and used to assign the nodal positions of the wheel-soil interface corresponding to the wheel position and the degree of slip. In the analytical procedure, small vertical load increments are applied on the rigid wheel-soil interface nodal positions, until the sinkage (Z) reaches the predetermined dynamic sinkage (Step 1, Fig. 6.14b). The sub-soil stress distribution, strain field, displacement and reactions at the

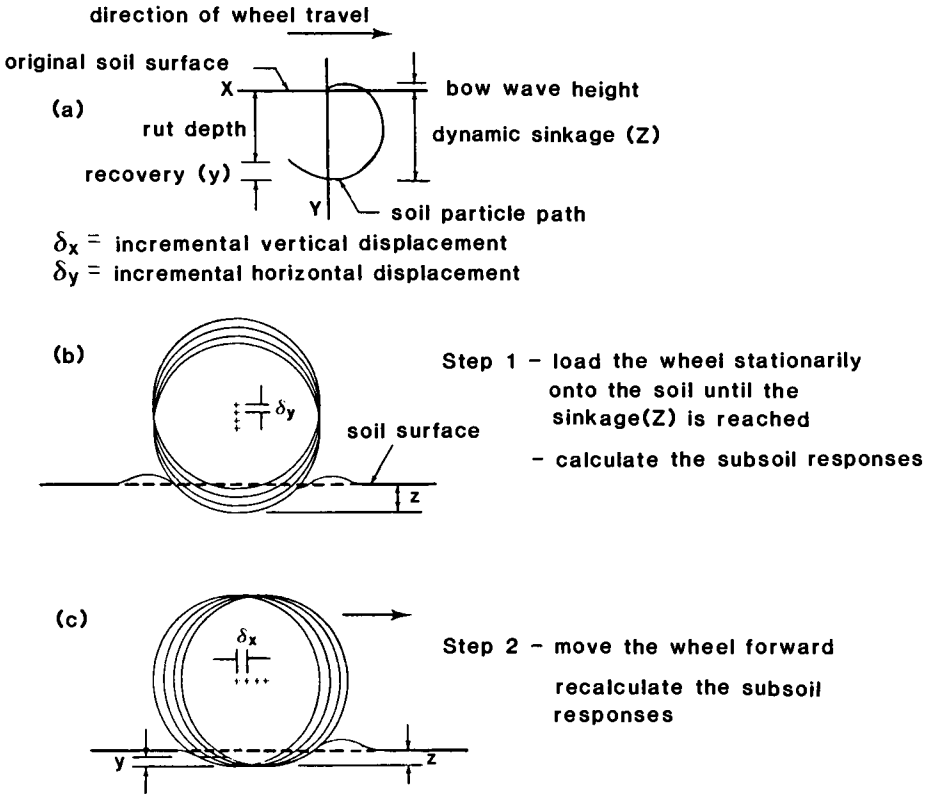


Fig. 6.14. Application of displacement boundary condition in the finite element method.

wheel-soil interface can be calculated at the end of each increment and added on to the previous values. The rigid wheel is then assumed to be moving at a constant translational velocity (Step 2, Fig. 6.14c). The displacements of the nodal points at the soil surface can be assigned with the knowledge of the soil particle path (Fig. 6.14a). At each small forward movement, the subsoil responses can be determined and augmented to the previous values. This process is repeated or, in other words, the wheel is kept moving forward at small distances and the subsoil stresses are calculated until the summation of the vertical reactions at the wheel-soil interface remains unchanged. The final solution is consequently carried out in terms of soil deformation energy and interfacial energy.

We should note that the displacement boundary condition approach outlined above represents an ideal situation since the boundary condition describes kinematic variation, soil-recovery and actual stress history under transient wheel loading. However, soil particle motion in the subsoil under wheel loading can only be measured in the laboratory under controlled situations. This type of

boundary condition specification is of limited use. In practice, it is easier to specify the loading boundary with measured or calculated normal and tangential stresses.

6.6.3 Wheel-soil system load boundary condition

In order to specify the pressure distributions at the tyre-soil contact area as input data in the finite element analysis, it is necessary to accurately determine the contact area, and the normal and tangential stress distribution as a function of tyre-soil relative properties and slip rates. Before any specific formulation can be attempted, it is instructive to investigate some similar situations in classical soil mechanics and actual measurements previously performed for wheel-soil problems.

As a first approximation, the tyre-soil interaction may be viewed as a footing of variable stiffness resting on a deformable soil surface without additional tangential stresses and tyre-soil movement. This situation is analogous to typical cases of flexible and rigid footings loaded vertically on clay and sand, as illustrated in Fig. 6.15. In flexible footings carrying central vertical loads, the contact pressure will be uniformly distributed and the resultant displacement pattern will be governed by the soil type. In the case of rigid footings, the displacement will be essentially uniform whilst the contact pressure distribution depends primarily on the soil type. In comparison to the actual tyre-soil situation, the tyre can act like a rigid or flexible footing depending on the stiffness of the tyre carcass, the inflation pressure of the tyre, and the soil stiffness. Moreover, the contact pressure distribution may be influenced by the size and shape of the contact (patch) area, the traction between the tyre and the soil, the normal slip rates, etc. It is necessary therefore to study the existing measurements of the wheel-soil contact pressures prior to establishing any rational expression regarding the contact pressures.

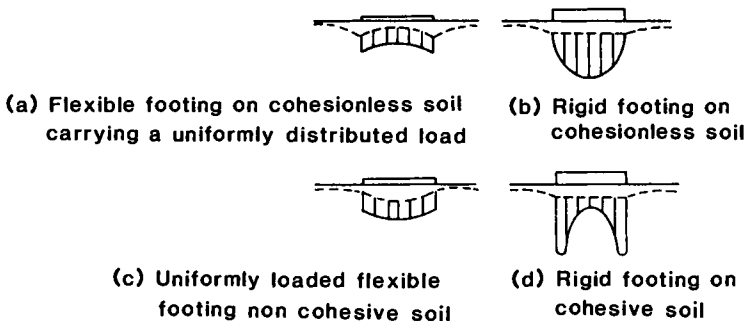


Fig. 6.15. Effects of footing flexibility on pressure distribution

In general, when a soft tyre passes over a stiff soil, the resultant normal stresses at the tyre-soil interface tend to be uniformly distributed in the central part. When the situation is reversed, i.e. a stiff pneumatic wheel moving over a soft soil, the normal stresses will be relatively constant at the central zone and will decrease towards both ends of the tyre-soil interface. The distribution pattern is not necessarily symmetrical and the maximum stress usually occurs ahead of the bottom dead centre of the wheel. The tangential stress shows the same trend and is mainly dependent on the changes in slip rate. Both normal and tangential stresses are always in one direction in the case of powered wheels. In a towed wheel, the direction of both stresses can be different between the leading and trailing edges.

6.6.4 Track-soil boundary conditions

A proper analytical solution of the track-soil system interaction requires the specification of the boundary conditions which satisfy the physical behaviour of the system. The load boundary approach can be adopted. However, it requires knowledge or information on the pressure distribution at the track-soil interface. The normal and tangential stress distributions need to be established as functions of track-soil relative properties and slip rate.

The pressure distribution below the track depends on its relative rigidity, which is a function of the number of wheels as well as the track pitch and wheel spacing ratio. Low speed vehicles such as construction tractors, provide a continuous track support with a relatively large number of small wheels closely spaced. Such an arrangement results in a more or less uniform pressure distribution along the ground contact area.

6.7 METHOD OF ANALYSIS

In tool-soil interaction studies nonlinearities occur in two different forms. The first is material or physical nonlinearity, which results from nonlinear constitutive laws (Section 6.4). The second is geometric nonlinearity, which derives from finite changes in the geometry of the deforming body (Desai and Abel, 1972).

Material nonlinearity alone encompasses problems in which the stresses are not linearly proportional to the strains, but in which small displacements and small strains are considered. Displacements refer to the changes in the overall geometry of the soil body, whereas strains are related to internal deformations. Because of the small displacements encountered in some cases, local distortions of an element can be ignored and the areas of the original, undeformed element can be used in computing stresses. In this case, the linear strain-displacement equations written for plane strain problems as:

$$\varepsilon_x = \frac{\partial u}{\partial x} \quad \varepsilon_y = \frac{\partial v}{\partial y} \quad (6.19)$$

$$\gamma_{xy} = \frac{\partial v}{\partial x} + \frac{\partial u}{\partial y}$$

where

$\varepsilon_x, \varepsilon_y$ = normal components of strain;
 γ_{xy} = component of strain and
 u, v = displacement components in the x- and y-directions,

are used.

Problems involving geometric nonlinearity arise both from nonlinear strain-displacement relations, written for a plane strain case as:

$$\varepsilon_x = \frac{\partial u}{\partial x} + 1/2 \left[\left(\frac{\partial u}{\partial x} \right)^2 + \left(\frac{\partial v}{\partial x} \right)^2 \right]$$

$$\varepsilon_y = \frac{\partial v}{\partial y} + 1/2 \left[\left(\frac{\partial u}{\partial y} \right)^2 + \left(\frac{\partial v}{\partial y} \right)^2 \right] \quad (6.20)$$

$$\gamma_{xy} = \frac{\partial v}{\partial x} + \frac{\partial u}{\partial y} + \frac{\partial u}{\partial x} \frac{\partial u}{\partial y} + \frac{\partial v}{\partial x} \frac{\partial v}{\partial y}$$

and from finite changes in geometry. In other words, this category encompasses large strain and large displacements.

The most general category of nonlinear problems is the combination of the material and geometric nonlinearities. It involves nonlinear constitutive behaviour as well as large strains and finite displacements. This Section begins with the explanation of the computational procedure adopted to treat material nonlinearity, followed by a brief discussion on geometric nonlinearity.

6.7.1 Material nonlinearity

Nonlinear stress-strain behaviour may be approximated in finite element analyses by assigning different modulus values to each of the elements into which the soil is subdivided for purposes of analysis, as shown in Figs. 6.4 to 6.6. The modulus value assigned to each element is selected on the basis of the stress or strain in each element. Because the modulus values depend on the stresses, and the strains in turn depend on the modulus values, it is necessary to make repeated analyses to insure that the modulus values correspond to the stress conditions for each element in the system.

Two techniques for approximate nonlinear analyses by the finite element method can be used. These are:

1. The direct iteration method, shown in Fig. 6.16. In this method, the same change in soil external loading is analyzed repeatedly. After each analysis, the values of stress and strain within each element are examined to determine if they satisfy the appropriate nonlinear stress-strain relationship. If the values of stress and strain do not correspond, a new value of modulus is selected for that element for the next analysis. The main advantage of this technique is the capability of the procedure to represent stress-strain relationship in which the stress decreases with increasing strain after reaching a peak value. The shortcoming of the iterative procedure is that it can only give the solution for the final level of applied load, and cannot consider the load and deformation history of the soil.

2. The incremental method, shown in Fig. 6.17. In this procedure, soil loading is considered to be applied in small increments. If the state of stress and strain at the start of an increment is known in each element, the state at the end of the increment can be found by an addition of incremental changes. The constitutive relationship to be used for each element may be determined at the beginning of each interval. Thus the nonlinear stress-strain relationship is approximated by a series of straight lines. The principal advantage of this procedure is that it provides a relatively complete description of the load-deformation behaviour, as results are obtained for each of the intermediate states corresponding to an increment of loading.

In the tool-soil interaction studies, it is essential that the soil deformation and stress fields are obtained and examined as the tool advances in the soil. For this purpose the incremental procedure is generally employed.

The incremental technique adopted in the analysis makes use of the plane-strain triaxial stress-strain curve to compute the value of the elastic modulus E , during each increment. The value of Poisson's ratio ν , is kept constant in the analysis.

The starting value of the modulus, E_0 , is taken as the initial slope of the plane-strain triaxial stress-strain curves at zero confining pressure. With the assumed value of Poisson's ratio, the stresses or strains in each element due to the first increment of displacement are computed using the elastic analysis. A new value of the modulus to be used in the second increment is computed by using the nonlinear curves. Either the stresses or strains computed in the elements can be used in the nonlinear curves to obtain the E values. The modified constitutive relation is used in the next increment of deformation. The process is continued until the desired total deformation is obtained.

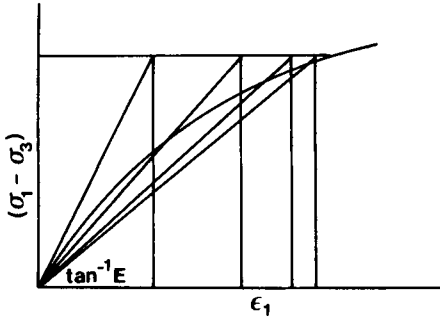


Fig. 6.16. Direct iteration procedure.

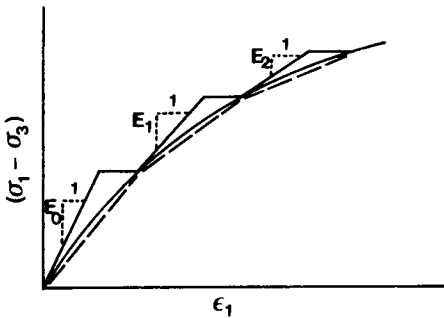


Fig. 6.17. Incremental procedure.

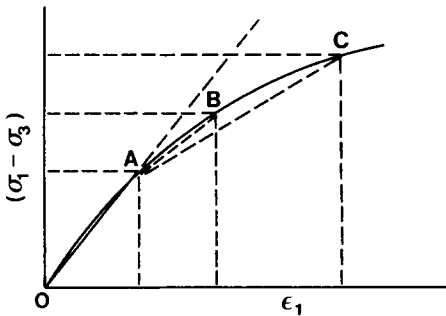
The modulus value E , is calculated in each increment as:

$$E = \frac{3/4(\sigma_1 - \sigma_3)_i - 3/4(\sigma_1 - \sigma_3)_{i-1}}{(\epsilon_1)_i - (\epsilon_1)_{i-1}} \quad (6.21)$$

where i represents the current increment state, and $i-1$ represents the previous increment stage. Figure 6.17 illustrates the incremental procedure.

There are several possible ways by which the solutions obtained by the incremental method can be improved. Since for every increment the elastic constants used are for the previous increment, it is necessary that the increments be quite small to obtain good results. Further, if there are abrupt slope changes in the stress-strain diagram, the method is likely to give unsatisfactory results. One of the ways to reduce some of these errors is to iterate a few times after each increment to bring the assumed E values close to the actual values. This procedure would also allow one to take larger load increments in the analysis.

In most problems, it is found sufficient to iterate two to three times at each increment to obtain compatible stresses and strains. The number of iterations at each increment may be reduced by predicting the value of E for a load increment based on the stresses or strains attained in the previous increment, and by using this value of E as a first trial in the computations. For soil stress-strain curves, parabolic prediction will work much better than linear predictions. Figure 6.18 diagrammatically illustrates the working of the linear prediction method.



Slope OA - first trial value for E without prediction for second increment.
 Slope AB - first trial value for E with linear prediction for second increment.
 Slope AC - actual E value for second increments after iterations.

Fig. 6.18. Incremental-iterative method with prediction.

6.7.2 Geometric nonlinearity

In the previous sub-Section the material or physical nonlinearity arising from material properties was considered. It is recalled that in the case of material nonlinearity, both strains and displacements are assumed to be small, but stresses are not proportional to strains. We should note again that, in addition to material nonlinearity, geometric nonlinearity occurs due to the finite changes in the geometry of the deforming soil in front of the cutting or traction tool. The combination of both nonlinearities is particularly simple if an incremental procedure is adopted.

If a full load-deformation analysis is required, it is common practice to proceed with small loading increments and to treat each such increment as a piece-wise linear one, with the tangential stiffness matrix evaluated at the start of the increment. If the nodal coordinates are continuously updated, the calculation procedure follows precisely the same pattern used in small displacements-infinitesimal strain analysis. Updating for a plane strain case takes the form:

$$\bar{x}_i = x_i + u_i \quad \bar{y}_i = y_i + v_i \quad (6.22)$$

where

\bar{x}_i, \bar{y}_i = the updated nodal coordinates at the end of the i^{th} increment;
 x_i, y_i = the nodal coordinates at the beginning of the i^{th} increment and
 u_i, v_i = the i^{th} displacements in the x- and y-directions, respectively,
 associated with the nodes.

Strains are now determined by the derivatives of displacements with respect to the updated coordinates.

It is possible to use the general definition of strains, known as the Green's strain tensor, which is valid whether displacements or strains are large or small. For the plane strain case, the Green strain tensor is defined by eq.(6.21). If displacements are small, the general first-order linear strain approximation is obtained by neglecting the quadratic terms (eq.(6.20)). Because the loading increments are small, it can be assumed that the strain increments are infinitesimal in the usual sense. In such a case, the linear strain approximation (eq.(6.20)) can be used. It is recognized, however, that the same may not be true of the accumulated values. In the limit of infinitesimal increments of loading, it may be shown that this procedure gives the so-called logarithmic strain, rather than simple displacement gradients (Fung, 1965). Whilst this is admittedly an approximation to the more formal definition of large strains, eq. (6.21), the degree of approximation appears to be consistent with that of the overall method.

6.8 SUMMARY

In this Chapter we discussed the requirements for establishing a finite element model for a continuum mechanics problem in general, and a tool-soil interaction problem in particular. In general, the analysis of a tool-soil interaction system requires the following steps:

- (1) System idealization. The actual soil continuum is idealized as an assemblage of elements that are interconnected at the nodal points.
- (2) Identify the loading and displacement boundaries for the system.
- (3) Establish the constitutive relationships for each element and material type.
- (4) Establish the force balance equations corresponding to the unknown joint displacements and solve these equations.
- (5) Calculate the internal elements stress and strain distributions.
- (6) Interpret the displacements and stresses predicted by the solution.

In practical analysis the most important steps of the complete analysis are (Bathe, 1982) the proper idealization of the actual problem as performed in step (1), and the correct interpretation of the results in step (5). In Chapter 7, application of the finite element method to the common vehicle-soil interaction systems is discussed. The following procedure documents the steps necessary for implementation of the FEM. (See Figs. 6.19 and 6.20.)

(1) Boundary conditions. Boundary conditions are assigned on the finite element mesh based on laboratory testing observations; i.e. insertion of the discontinuity finite elements, free surfaces, totally fixed or fixed in one direction boundaries.

(2) Constitutive behaviour. Stress-strain and stress-displacement relationships for the soil continuum and the discontinuities (clay-clay and clay-material) are obtained from laboratory tests and used in the model in a digitized form. Yield criteria are assumed, i.e. failure is determined by a strain or stress level determined by the user.

(3) Forces at the nodes due to selfweight are assigned as well as the initial displacement or load increment.

(4) Based on the nodal coordinates and the shape (area) of each element, individual stiffness matrices are formed, which are then assembled to a stiffness matrix for the whole continuum.

(5) The FEM governing equations are formed using the above global stiffness matrix.

(6) The equations are solved using Gaussian elimination and the modulus of elasticity previously determined from the actual curves using the incremental-iterative technique, and linear interpolation between the stress-strain curves to account for the correct confining pressure (and material nonlinearity)*.

(7) The solution of equations provides nodal displacements from which the nodal forces are calculated, after which the stresses, strains, strain rates, nodal velocities and deformation energy are calculated for the continuum.

(8) The nodal coordinates are updated, in the order to be used in the next increment: $x' = x + \Delta x$, $y' = y + \Delta y$ (accounting for geometric nonlinearity). The coordinates are updated so that small-strain theory assumptions remain valid and thus the problem solution is always sound.

* The starting value of the elastic modulus is taken as the initial slope at the stress-strain curve at zero confining pressure, and the stresses/strains are calculated using elastic analysis. The resulting modulus of elasticity is compared to the assumed one. If the difference is small, or the number of iterations exceeds a pre-specified value, then the obtained E value is used as the initial in the next increment, or, the stresses/strains are recalculated, and a new E is obtained. Not many iterations are required to converge the E value.

(9) Then (a) if a constant elevation (displacement) boundary problem is solved, only nodal displacements are assigned at step (2), (b) if a loading boundary problem is solved, only nodal loads are assigned at step (2), and (c) if a displacement/load boundary problem is solved, nodal displacements and boundary pressures are assigned at step (2).

(10) Return to step (4).

Note: The Poisson's ratio remains constant throughout the analysis.

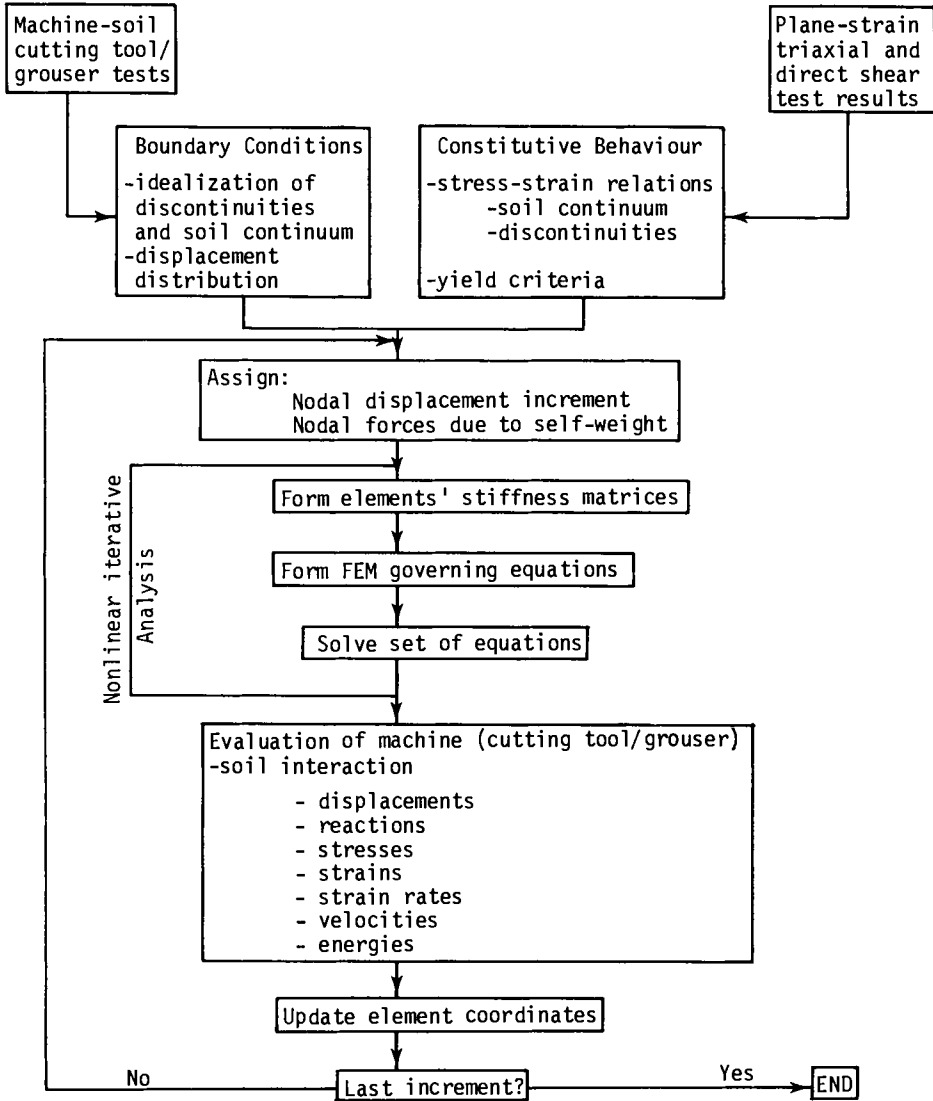


Fig. 6.19. Finite element implementation where the boundary condition of constant elevation prevails.

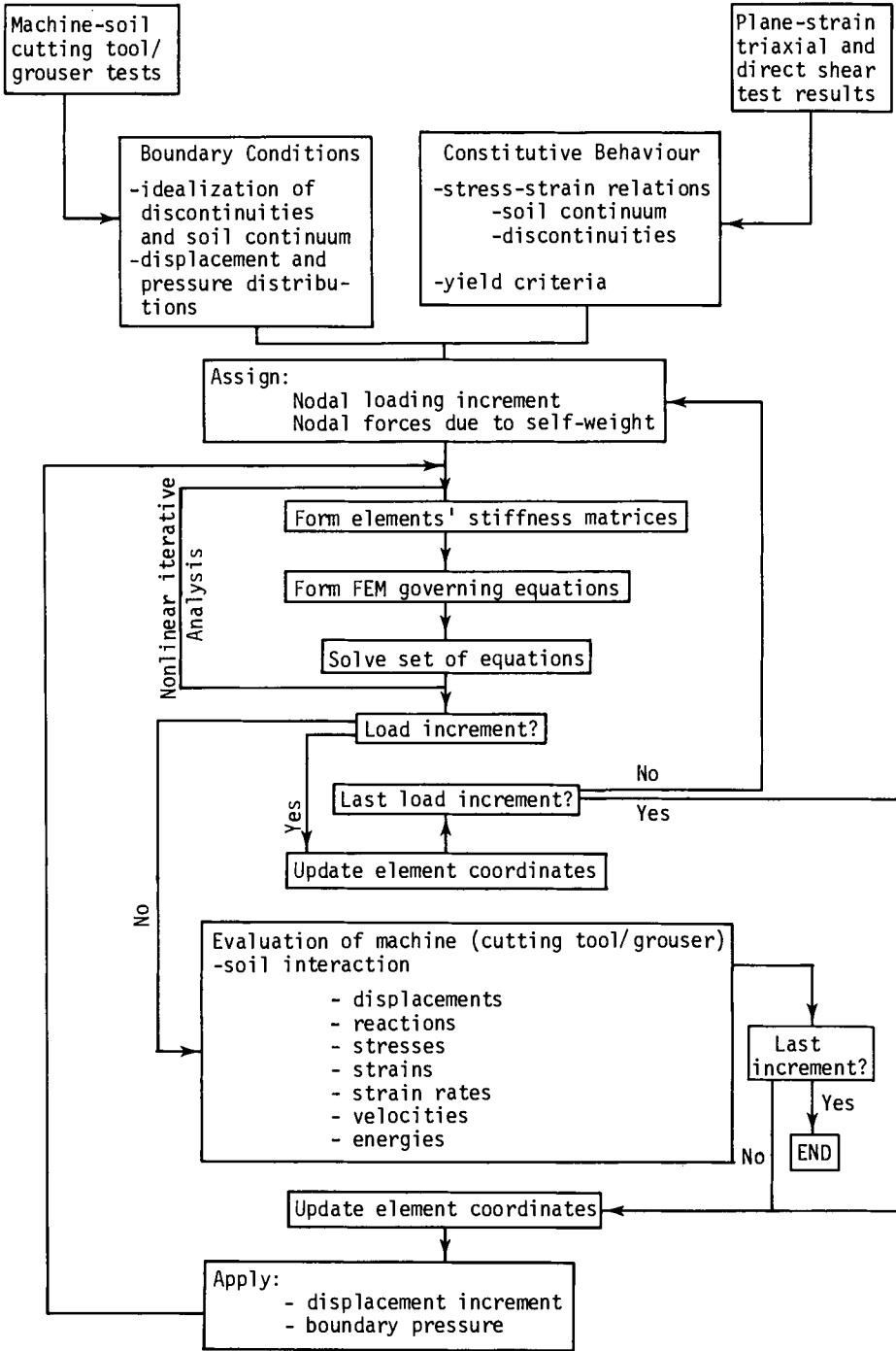


Fig. 6.20. Finite element implementation where the boundary condition of uniform vertical pressure prevails.

REFERENCES

- Bathe, K.J., 1982. *Finite Element Procedures in Engineering Analysis*. Prentice-Hall, Englewood Cliffs, New Jersey, 736 p.
- Desai, C.S. and Abel, J.F., 1972. *Introduction to the Finite Element Method*. Van Nostrand, New York, 477 p.
- Duncan, J.M. and Goodman, R.E., 1968. *Finite element analysis of slopes in jointed rocks*. Rpt. S-68-3, U.S. Army Engineer Waterways Experiment Station, Vicksburg, Miss.
- Fung, Y.C., 1965. *Foundations of Solid Mechanics*. Prentice-Hall, Englewood Cliffs, New Jersey, 525 p.
- Goodman, R.E., Taylor, R.L. and Brekke, T.L., 1968. A model for the mechanics of jointed rock. *J. Soil Mechs. Found. Eng., ASCE*, 94-3:637-659.
- Heuz, F.E., Goodman, R.E. and Bornstein, A., 1971. Numerical analyses of deformability tests in jointed rock. "Joint perturbation" and "No tension" finite element solutions. *Rock Mech., Felsmech. Mec Roches*, 3-1:13-24.
- Newmark, N.M., 1960. Failure hypotheses for soils. *Research Conf. on Shear Strength of Cohesive Soils*, University of Colorado, Boulder, pp. 17-32.
- Ngo, D. and Scordelis, A.C., 1967. Finite element analysis of reinforced concrete beams. *J. American Concrete Institute*, 64-3:152-163.
- Nilson, A.H., 1968. Nonlinear analysis of reinforced concrete by the finite element method. *J. American Concrete Institute*, 65-9:757-766.
- Taylor, D.W., 1948. *Fundamentals of Soil Mechanics*. Wiley and Sons, Inc., New York, 700 p.
- Yong, R.N. and McKyes, E., 1971. Yield and failure of a clay under triaxial stresses. *J. Soil Mechs. Found. Eng., ASCE*, 97-1:159-176.
- Yong, R.N. and Fattah, E.A., 1976. Prediction of wheel-soil interaction and performance using the finite element method. *J. Terramechs.*, 13-4:227-240.
- Yong, R.N. and Hanna, A.W., 1977. Finite element analysis of plane soil cutting. *J. Terramechs.*, 14-3:103-125.
- Yong, R.N., Fattah, E.A. and Boonsinsuk, P., 1978. Analysis and prediction of tyre-soil interaction and performance using finite elements. *J. Terramechs.*, 15-1:43-63.
- Zienkiewicz, O.C., Best, B., Dullage, C. and Stagg, K.G., 1970. Analysis of nonlinear problems in rock mechanics with particular reference to jointed rock systems. *Proc. 2nd Int. Congr. on Rock Mechs.*, Belgrade, 3:501-509.
- Zienkiewicz, O.C. and Nayak, G.C., 1971. A general approach to problems of plasticity and large deformation using isoparametric elements, *Proc. 3rd Conf. on Matrix Methods in Struct. Mechs.*, Wright-Patterson Air Force Base, Ohio, pp. 881-928.
- Zienkiewicz, O.C., 1977. *The Finite Element Method*. 3rd Ed., McGraw-Hill, New York, 787. p.

NOMENCLATURE

A	area of a deformed body
B	displacement function
E	modulus of elasticity
E_0	initial modulus of elasticity
J_3	third invariant of the deviator stress
N	shape function
P	surface forces per unit area of the deformed body
R	equivalent external nodal forces
S	space
V	volume of a deformed body
a	empirical coefficient
b	" "
f_1, f_2, f_3	arbitrary functions
k_n	normal stiffness
k_s	shear stiffness
k_{si}	initial shear stiffness
k_{st}	tangent stiffness
q	body forces per unit mass
u	x-displacement
v	y-displacement
x_i	nodal coordinate at the beginning of the i^{th} increment
\bar{x}_i	updated nodal coordinate at the end of the i^{th} increment
y_i	nodal coordinate at the beginning of the i^{th} increment
\bar{y}_i	updated nodal coordinate at the end of the i^{th} increment
Δ_n	average relative normal displacement across the element
Δ_s	average relative shear displacement along the element
γ_{oct}	octahedral shear strain
γ_{xy}	shear strain
δ	nodal point displacement
ϵ_{oct}	octahedral normal strain
ϵ_x, ϵ_y	normal strain components

$\epsilon_1, \epsilon_2, \epsilon_3$	principal strains
$\epsilon_1'', \epsilon_2'', \epsilon_3''$	first, second and third deviator strain components
ν	Poisson's ratio
ρ	density of a deformed body
σ_{oct}	octahedral normal stress
$\sigma_1, \sigma_2, \sigma_3$	principal stresses
τ	cutting shear stress
τ_{oct}	octahedral shear stress
ϕ	angle of friction
ψ	nodal forces

Chapter 7

APPLICATION OF FINITE ELEMENT MODELLING

7.1 INTRODUCTION

This Chapter discusses the application of finite element method (FEM) for prediction of (a) soil cutting, (b) traction element-terrain interaction, and (c) soil response to tractive force application. The requirement for prediction together with the type of parameters which represent the performance of each tool are also discussed and predicted performances are compared with the available measured experimental results.

7.2 SOIL CUTTING

In the study of soil cutting problems, the principal objectives are to predict (a) the force required to move the cutting blade through the soil, and (b) the soil response (failure mode). The effect of the geometric parameters of the blade on its performance, and the scheme for optimizing blade performance can also be investigated. In this Section, we will look at two examples for two flat blades cutting through soft cohesive soil. Analyses and actual soil cutting experiments are evaluated to show the applicability of the method of analysis.

7.2.1 Meshes and boundaries (idealization)

To begin the analysis, the problem to be studied must be idealized and the finite element mesh system generated to conform to the geometric and analytic constraints of the problem. The meshes adopted for 10° and 50° inclined soil cutting blades are shown in Figs. 7.1 and 7.2. The mesh patterns are so arranged that smaller elements are employed near the actual blades and larger elements in regions away from them. Joint (interface) elements are inserted between the soil and the blades to simulate the interface characteristics. In addition, joint (cutting) elements are placed on the plane on which cutting progresses. In the finite element idealization, the boundaries are placed on rollers so that (a) the horizontal movement is restrained on the sides, and (b) vertical movement is restrained on the bottom boundary. In the analysis, the blades are considered rigid. Uniform horizontal rigid displacements are applied at all nodal points at the blade-soil interface. The displacements are increased in increments of 0.25 cm, and self weight of the soil is considered in the analysis.

The generalized simple flow scheme shown in Fig. 7.3 illustrates the implementation of the computational procedure required to develop the outputs discussed in the following sub-Sections.

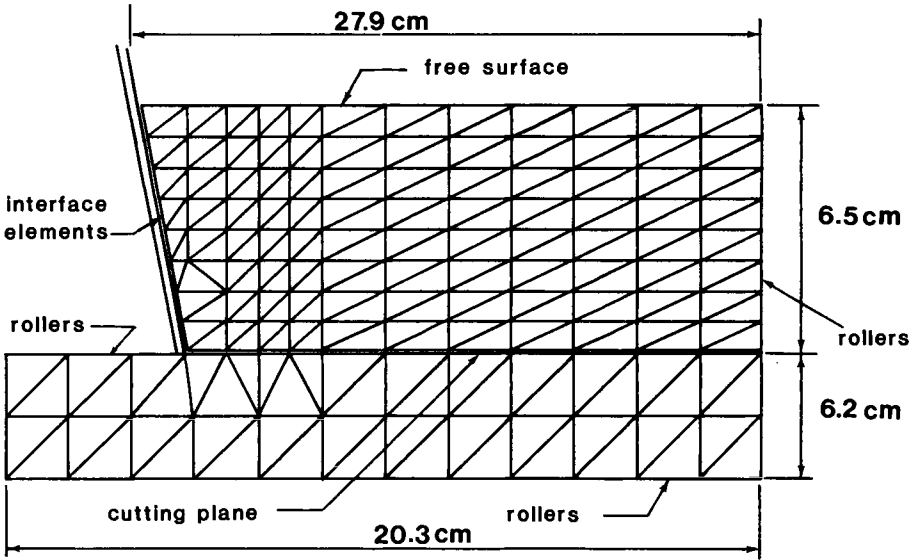


Fig. 7.1. Mesh layout for the 10° inclined blade-soil system.

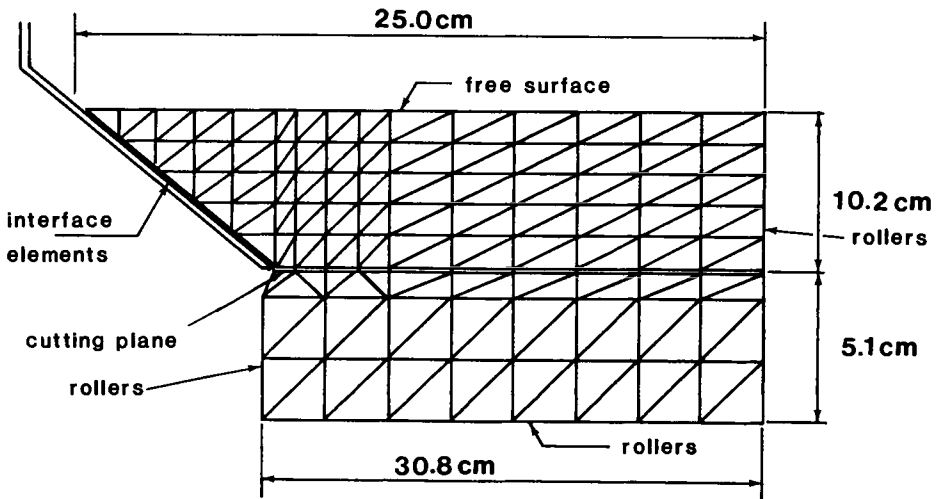


Fig. 7.2. Mesh layout for the 50° inclined blade-soil system.

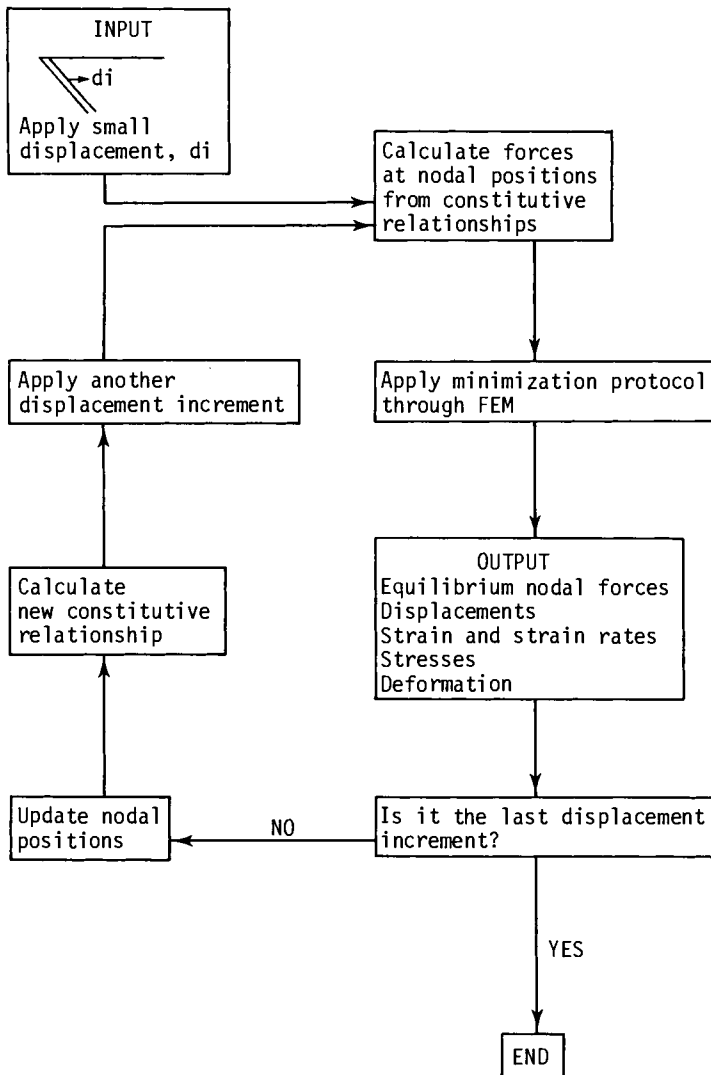


Fig. 7.3. Simplified flow scheme for computation using the FEM of analysis

7.2.2 Measured and calculated forces

As a means of testing the applicability of the finite element method (FEM) of analysis in a soil cutting problem, the simplest and quickest method is to compare predicted forces acting on the blade with measured values. The load-displacement results (curves) obtained from application of the finite element analysis are shown in Fig. 7.4 for horizontal force, and in Fig. 7.5 for vertical load for both the 10° and 50° inclined blades, respectively. The experimental results obtained from laboratory tests are also plotted on the same Figures for comparison.

The agreement between the experimentally obtained and the calculated finite element results is very satisfactory in the case of the horizontal forces for the two blade inclinations analyzed. In the case of the 50° blade, the difference is about three Newtons over the whole displacement range analyzed, with the analytical results lying always below the experimental curve. For the 10° blade, the errors are found to be almost negligible up to blade displacement of 1.0 cm, beyond which the analytical and test results diverge, with the predicted results again lying below the experimental values.

7.2.3 Deformation fields

Experimentally measured horizontal and vertical displacement fields deduced with the aid of distorting experimental test grids are shown in Fig. 7.6 together with the computed displacement fields obtained from the displacement of the finite element nodes, for a total cutting tool displacement of 2.5 cm in the horizontal direction. Whilst the deformation fields portray the horizontal and vertical displacements for the 10° inclined blade, similar diagrams can be generated for other blade inclinations. For simplicity and facility in comparison, the deformation fields illustrated in contour forms are plotted in the undeformed position.

The discontinuity in experimentally measured displacements at the level of the blade tip is clearly demonstrated in the diagram. The displacement contours are only discontinuous in the vicinity of the blades, but are continuous above and below the cutting plane. This implies that the discontinuity propagates with the blade movement. One should be careful to note that this is not the case in the finite element solution where the discontinuity is assumed to extend all the way to the end boundary. The deviation between the experimental and the analytical horizontal displacement fields indicates that the finite element solution underestimates the horizontal displacements in the zone near the soil surface, while it overestimates in the soil mass situated directly above the cutting plane.

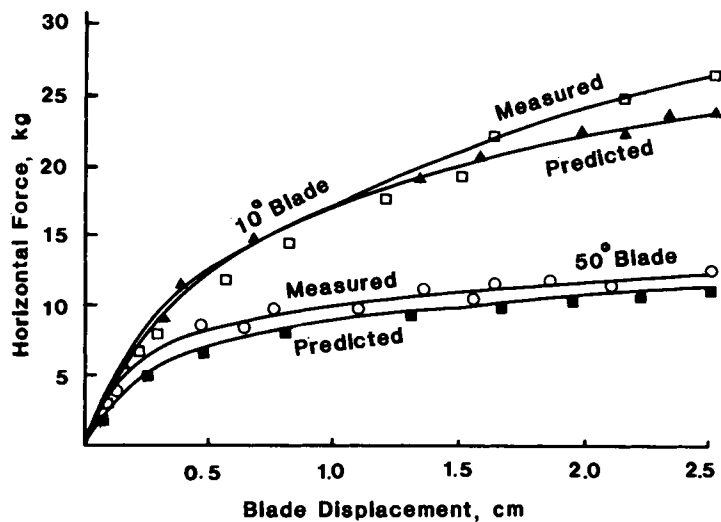


Fig. 7.4. Comparison of measured and predicted values of developed horizontal force on the 10° and 50° inclined blades. (Kaolinite clay).

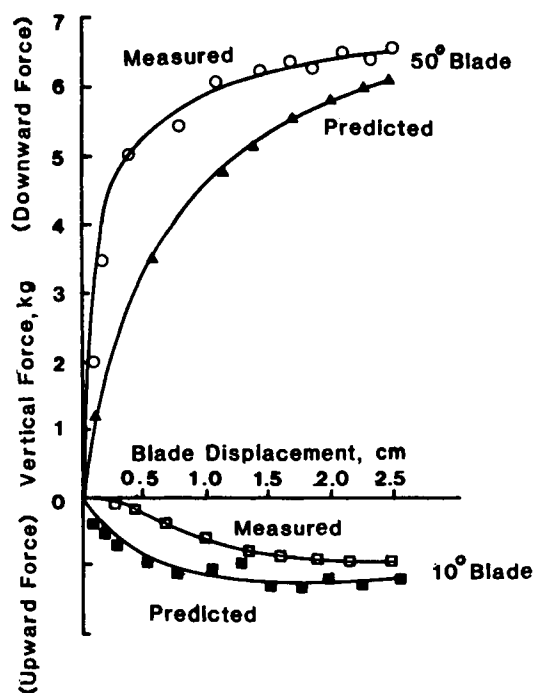


Fig. 7.5. Comparison of measured and predicted values of developed vertical force on the 10° and 50° inclined blades. (Kaolinite clay).

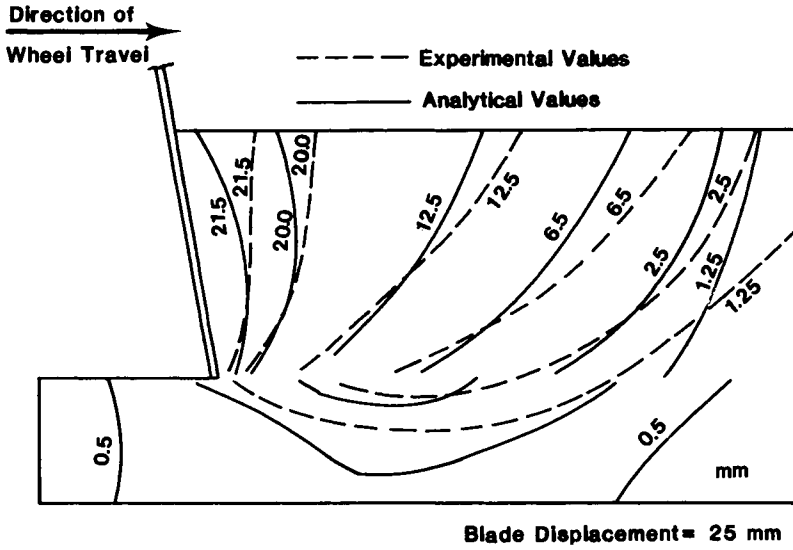


Fig. 7.6a. Experimental analytical horizontal displacement fields for the 10° inclined blade-soil system.

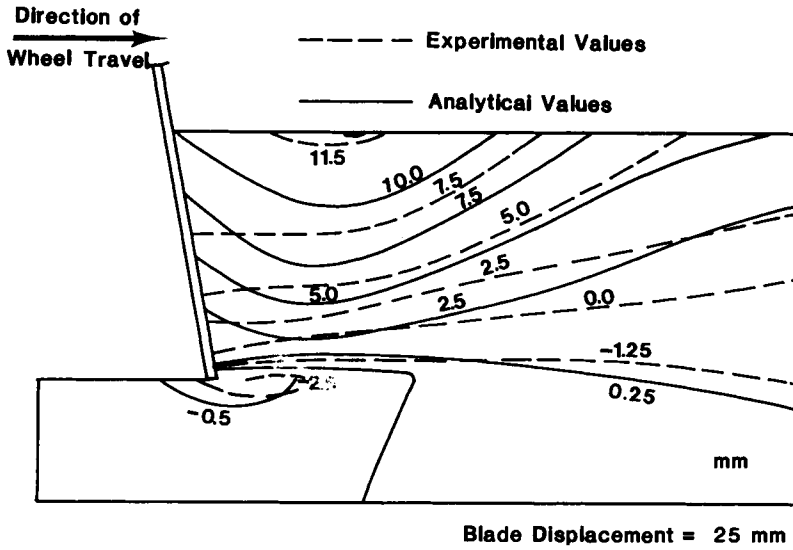


Fig. 7.6b. Experimental analytical vertical displacement fields for the 10° inclined blade-soil system.

7.2.4 Deformation energy

The deformation energy can be calculated from experimental information using one of two methods:

(1) Through application of the visioelasticity method (described in Chapter 5) to the experimentally recorded deformation fields. The application of the visioelasticity model demands the following requirements:

- (a) application of an admissible yield criterion,
- (b) measurement of a deformation field from experiments and calculations of the resultant strain rate fields within the loaded soil, and
- (c) selection of plasticity flow rules consistent with the choice of the yield criterion.

(2) The integration of the areas under the experimentally measured force-displacement curves.

The energy budget for a tool-soil system can be written as:

$$\text{WORK INPUT} = \text{DEFORMATION ENERGY LOSS} + \text{INTERFACIAL ENERGY LOSS}$$

$$\int_s F ds = D + I \quad (7.1)$$

As the system is in a state of dynamic equilibrium, the input energy is expended completely in producing plastic deformation of the soil as work output with negligible interfacial energy losses. Under such circumstances, eq.(7.1) can be reduced to:

$$\int_s F ds = D \quad (7.2)$$

Energy models for the analysis and prediction of tool-soil interaction performance require measurement or determination of response function performance. The results obtained from integration of the experimentally measured force-displacement curves can be considered as a measure of the work input, whilst the work output or the energy dissipated in the system characterizes the response function. The work output is determined by two methods: one by using the visioelasticity method described in Chapter 5, and the other by using the stress and strain fields determined through application of the finite element method of analysis.

(i) First method. For a material which follows the von Mises yield criterion, the total work done, and hence, the total energy dissipated in plastic deformation under plane-strain conditions, can be written as:

$$D = 2b \int_{t_1}^{t_2} \int_{x_1}^{x_2} \int_{y_1}^{y_2} K \sqrt{I_2} dx dy dt \quad (7.3)$$

(ii) Second method. The deformation energy during a time interval can be evaluated from the finite element solution by the following relationship (Desai and Abel, 1972):

$$D = \int_v \int_t [\sigma]^T d[\epsilon] dt dv \quad (7.4)$$

where $[\sigma]$ = element stress matrix;
 $d[\epsilon]$ = element incremental strain matrix;
 t = increment duration and
 v = element volume.

Either of these two methods can be used to calculate the developed soil deformation energy of the tool-soil system. As an example, the results obtained from their application are shown in Fig. 7.7 for the 10° and 50° inclined blades. Comparison of these results with those obtained from the integration of the areas under the experimentally measured force-displacement curves are also shown.

We should note that in the finite element analysis, the soil is treated as a non-linear-elastic-strain hardening material subject to boundary conditions of an incremental form, thus permitting calculations to be made for the description of the growth of stresses within the loaded soil from initial to final states. A solution of this form should provide better estimates of the energy dissipated within the soil, subject to the approximations made in the theoretical development. By and large, if the system is properly idealized, comparison of the finite element calculated values with experimentally obtained energy values, will show reasonable agreement. In Fig. 7.7, for example, the average deviation in estimate is of the order of 10%, while the maximum deviation is 18%.

7.2.5 Stress analysis

The output from the FEM of analysis can be used to detail the distributions of the horizontal, vertical and shear soil stresses in front of a moving cutting blade. Again, taking the 10° inclined blade, stress contours can be plotted at various displacements, e.g. 0.25 and 1.25 cm, as shown in Figs. 7.8 and 7.9. Similar diagrams can be obtained for other blade inclinations and blade movements. The stress fields developed in the soil in the 0.25 cm blade displacement situation are typical of stress distributions in the elastic range, whilst the corresponding stress fields obtained in the 1.25 cm displacement situation are considered to be indicative of the distributions in the plastic range.

It is important to note that the discontinuity in the calculated stress distributions shown in Figs. 7.8 and 7.9 in the soil mass is actually due to the

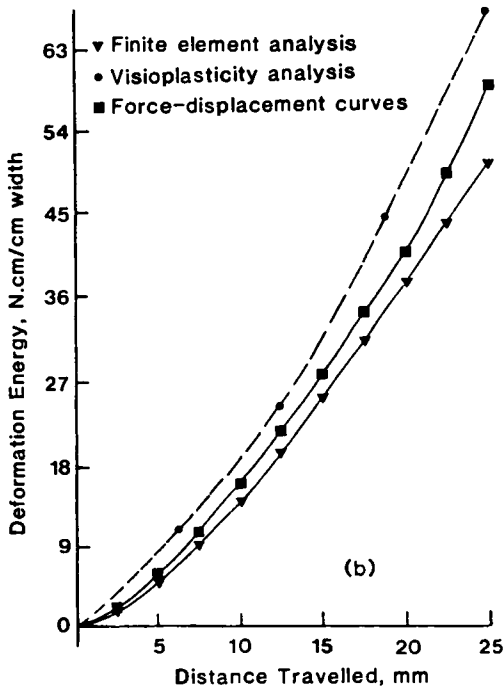
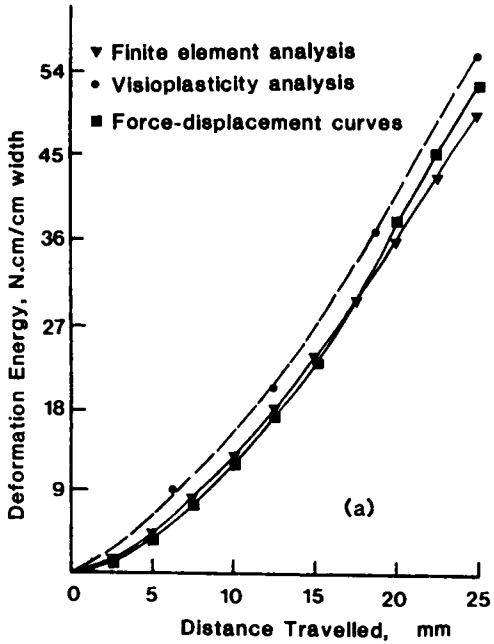
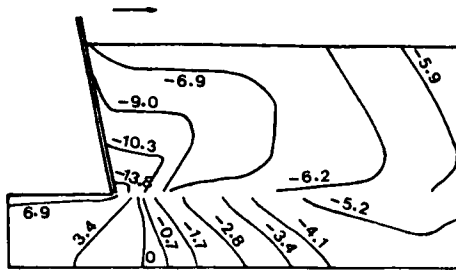
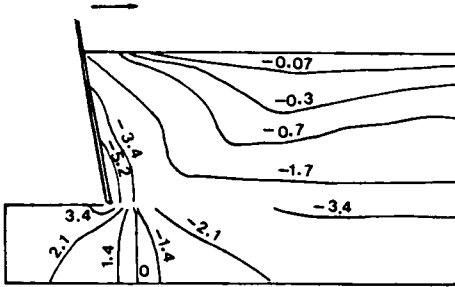
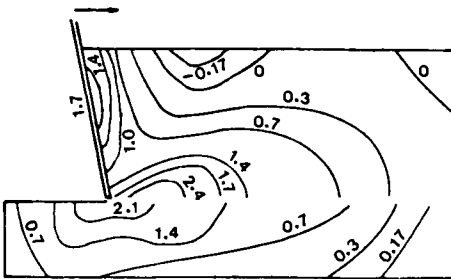


Fig. 7.7. Comparison of measured and calculated values of deformation energy for the (a) 10° inclined blade, and (b) 50° inclined blade - kaolin clay system.

(a) Horizontal Stress, σ_x (b) Vertical Stress, σ_y (c) Shear Stress, τ_{xy}

compression (-) in kPa

Fig. 7.8. Stress fields for the 10° inclined blade-soil system at 0.25 cm displacement.

effect of the cutting (joint) elements inserted at the level of the blade's tip. We need to recall that these elements were inserted, in the first place, to model the discontinuities in the stress and deformation fields to correspond to those occurring in the physical situation. The justification that the assumed analytical model with its assumed discontinuities can properly predict the physical response will be found through examination of the correlations between analytical and experimental results.

For an examination of Figs. 7.8 and 7.9 and other results for blades with

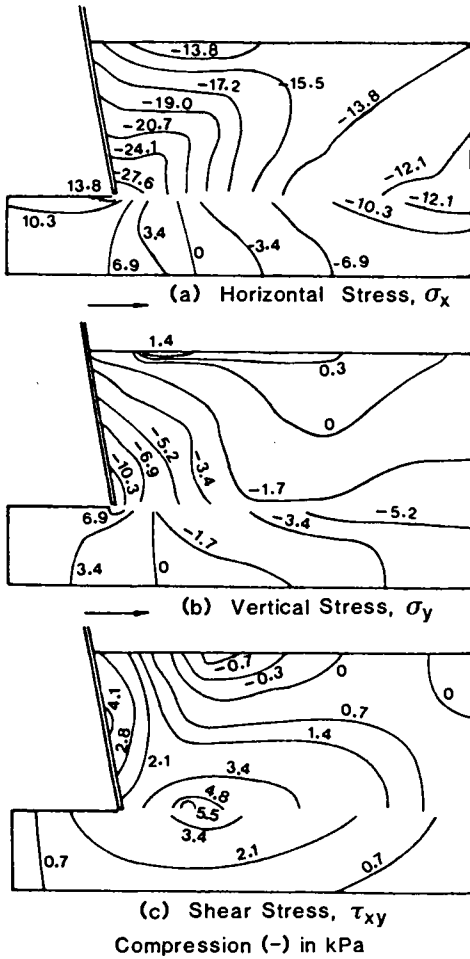


Fig. 7.9. Stress fields for the 10° inclined blade-soil system at 1.25 cm displacement.

different inclinations, several observations can be made in regard to the interaction between cutting tool and soil:

1. Stress concentrations are developed at the tip of the blades - as might be expected. Horizontal, σ_x , vertical, σ_y , and shear, τ_{xy} , stress values are highest in the vicinity of the blade tip. These concentrations are also characterized by a singular behaviour where changes occur in the magnitudes and, in some instances, in the directions of the stresses above and below the blade tip-point.

2. The effect of the plane of cutting (joint) elements on the horizontal

stress distribution is to divide the stress field into two differently stressed regions:

(a) the upper field, where the compressive stresses are high near the blade surface and which decrease with distance from that surface, and

(b) the lower field, where lower stresses, partly tensile and partly compressive, are developed. The compressive stresses increase with distance from the blades, while a zone of tensile horizontal stresses develops in the soil below the blade tip.

3. A zero vertical stress (σ_y) contour appears to develop in the upper part of the soil mass. This contour shifts downward with further blade progression in the soil, resulting in larger zones of vertical tensile stresses. This behaviour is likely due to the restraining influence of the fixed vertical end boundary which induces actions that result in larger zones of tensile stresses. As in the case of the horizontal stress field, the lower part of the soil mass (below the cutting plane) experiences a change from tensile stress below the blade tip to compressive stress away from the blade.

4. A zone of high shear stresses develops in front of the blade tip. The shear stresses in this zone are positive, indicating the shearing is a clockwise shearing action. These zones could be termed the "active" shear zones since the shear stresses continue to increase with increasing blade movement. Above the "active" shear zones, there exist zero shear stress contours with zones of negative shear stresses, i.e., shearing is anticlockwise above the zero contour. These zones are found to expand with larger negative values, indicating thereby an upward action resulting in the formation of the surcharge in front of the cutting blade.

Failure zones developed in the soil because of blade aggression can be located by determining the maximum shear stress induced in each element after each increment of blade movement. The extent of the failed zone is established on the basis of elements in the finite element grid, where the induced stresses in the elements equal the limiting stress of the soil (Yong and Hanna, 1977). Figure 7.10 shows an example of the development of the failure zones in relation to blade movement for the 10° inclined blade. From the Figure, we note that initial failure in two elements occurred in blade displacement increment number seven (1.75 cm of blade displacement). The failure patterns show that the elements fail initially at the leading edge of the blade and progress inwards toward the soil surface. The effect of the blade inclination on the shape and progress of the failure zones can be analyzed with this procedure. By and large, the more inclined the blade is, the more clearly defined is the shape of the failure plane - i.e. failure along single elements which define a plane as opposed to clusters of elements which indicate a broad zone of compression shear failure. The correlation of analytically predicted failure zones and actual experimental observations will substantiate the validity of the techniques for analytical predictions.

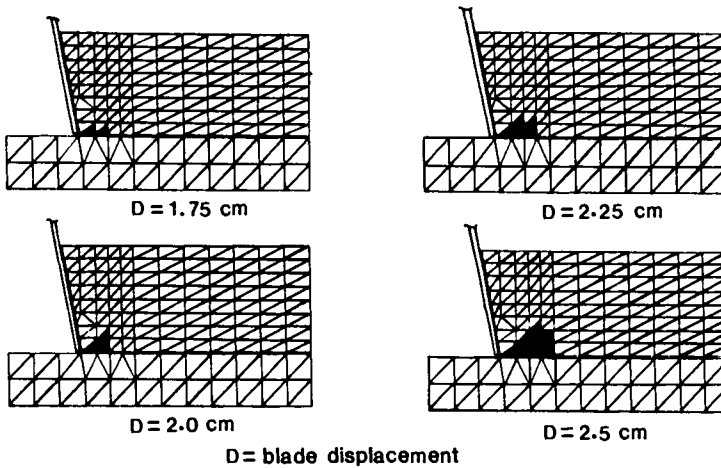


Fig. 7.10. Development of failure zones for the 10° inclined blade - kaolin clay system.

7.2.6 Normal pressure distribution

Using the calculation procedures shown in Section 6.8 and in Fig. 7.3, normal pressures developed on the surface of the intruding blades, as displacements are increased, can be calculated and represented as shown in Fig. 7.11, for both the 10° and 50° inclined blades. Whilst the normal pressure distributions throughout the cutting stage may be seen to be relatively uniform over about three-quarters of the blade surface, we note that, as expected, the normal pressure at the blade tip increases to about 150 percent of the average pressure over the whole surface for the 10° inclined blade. The effect of blade inclination is to change the distribution of the normal pressure somewhat - as shown in Fig. 7.11. In contrast to the 10° inclined blade, we can see that the normal pressures increase near the tip of the blade to about 200 to 300 percent of the average pressure over the whole blade surface.

7.3 GROUSER-SOIL INTERACTIONS

A solution of the traction problem - that is, obtaining adequate traction at a suitable speed in a practical manner and at a reasonable cost - lies in an understanding of:

- (1) the manner in which stresses are applied to the soil, and
- (2) the reaction of the soil to the applied stresses.

Bearing in mind this understanding, which is necessary to deal with an interaction process, a direction of approach may be established.

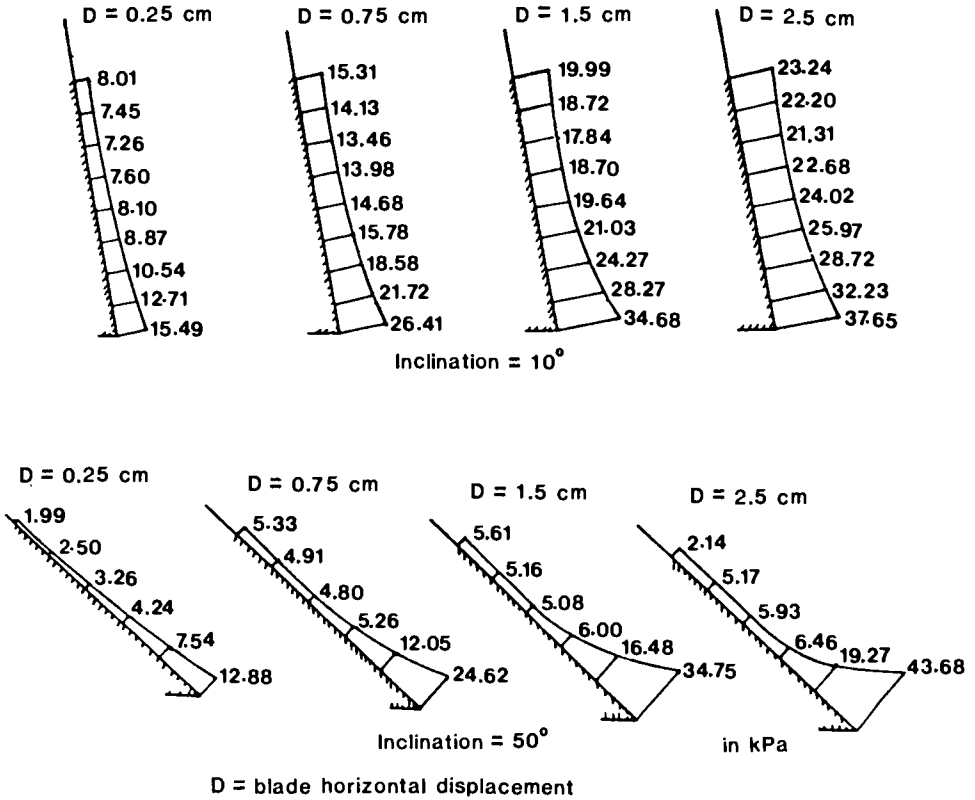


Fig. 7.11. Normal pressure distribution on the (a) 10° inclined blade, and (b) 50° inclined blade.

While soil cutting and traction problems can be considered to be one problem in principle, (both situations requiring analyses of soil stresses and deformations, as well as the evaluation of developed reactions on the cutting or traction devices), the purpose of a traction device is to cause deformation of soil in a certain manner in order to develop adequate traction capacity (optimum developed reactions). To achieve this, it is necessary to change the geometry of the traction tools or, in other words, the interacting boundary conditions, in order to reach the manner of soil manipulation for the production of adequate traction. The importance of accurate specifications of boundary conditions cannot be overemphasized.

We present an illustrative example in this Section to demonstrate the validity of the FEM for analysis of the problem.

7.3.1 Meshes and boundaries (idealization)

As in the soil cutting problem, the first step in the analysis is to produce a finite element mesh consistent with the geometry and physics of the problem. The mesh that might be adopted for the grouser chosen for the finite element analysis is shown in Fig. 7.12. Note the location of the cutting (joint) elements on the plane where soil cutting is anticipated. Interface elements are not required since the horizontal plate placed on top of the grouser creates a non-slip condition.

The sides and bottom boundary conditions are similar to those adopted in the soil cutting analysis. The horizontal movement is restrained on the sides and the vertical movement is prevented on the bottom. Uniform horizontal displacement is applied to all the nodes on the grousers' surfaces. To implement the analysis in the sequence shown in Fig. 7.3, displacements are increased in equal increments.

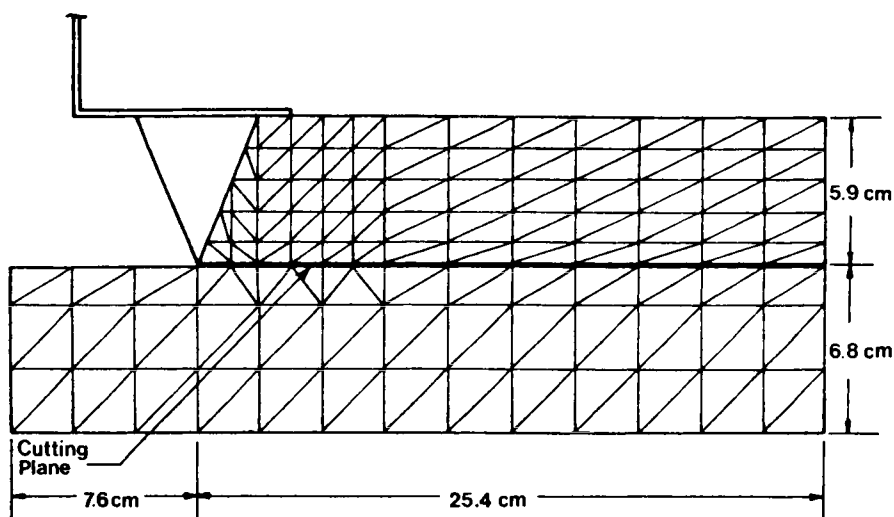


Fig. 7.12. Mesh layout for the triangular grouser-soil system.

7.3.2 Measured and calculated forces

The output from implementation of the computational procedure shown in Section 6.8 and in Fig. 7.3 will produce the force-displacement relations (predicted) for the various grouser-soil system as shown in Fig. 7.13, for comparison with an experimental test series on a soft kaolin clay. Plotted on the same Figure are typical load-displacement records, horizontal and vertical, obtained from the experimental study.

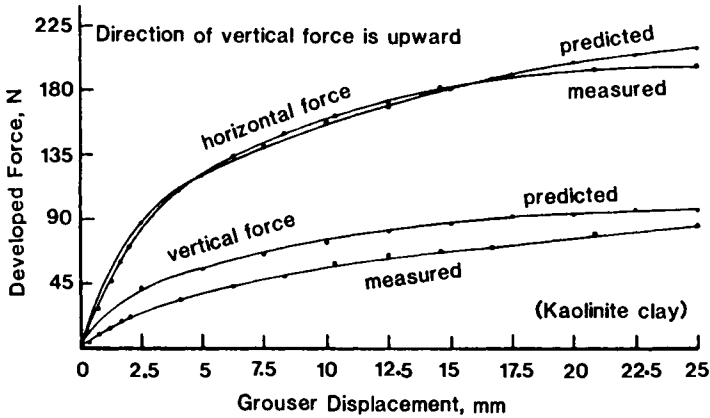


Fig. 7.13. Comparison of measures and predicted values of developed horizontal and vertical forces on the triangular grouser-kaolinite clay.

By and large, for the example shown, and from many other comparisons with other types of grousers, the agreement between the experimental and the finite element results, is generally very good - especially for comparisons involving developed horizontal forces. Some deviations between analytically computed (predicted) and experimental values for vertical forces can be expected for almost all cases because of the idealizations required in the development of the analytical model. The top boundary condition always presents a problem in idealization.

7.3.3 Deformation fields

The lateral advance of the single grouser (used as the example for discussion) into the soil will generate displacements in the soil in front of the advancing grouser. From the computational scheme previously discussed with the FEM, the output from the calculations can be used to map the soil displacement (i.e. deformation) field. Figure 7.14 shows both the horizontal and vertical soil deformation contours predicted with the FEM - for a specific grouser lateral penetration (2.5 cm). For comparison, actual experimental values obtained from laboratory tests, using a side grid technique for recording of motion, are also shown, in the Figure. In the experiments, no restraint on vertical soil motion beyond the top plate shown, was provided.

If one compares the computed deformation fields for the example grouser shown and for other types of grousers, with measured values, the following observation can be made:

(1) Computed horizontal deformation fields by and large correspond very closely with the experimentally measured fields. In general, the finite element computed values tend to indicate higher model rigidity than the actual physical system.

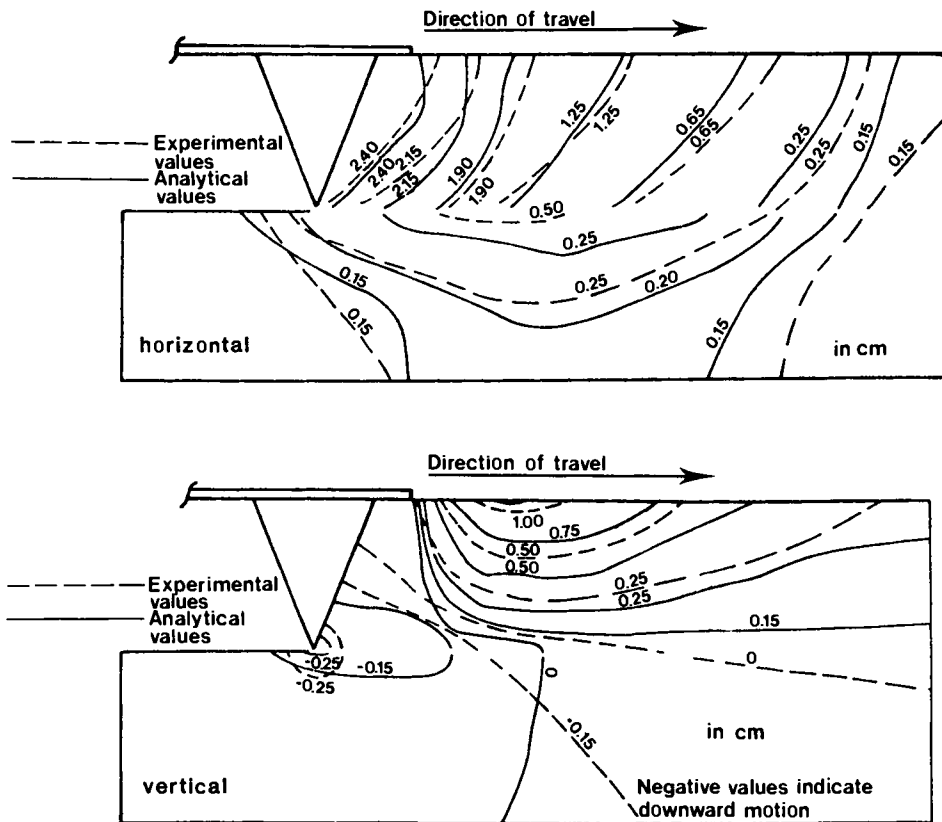


Fig. 7.14. Experimental and analytical deformation fields for the triangular grouser.

(2) The vertical displacement contours (i.e. vertical deformation fields) are very sensitive to the top boundary constraint. The confining or free boundary effect of the top horizontal plane must be properly modelled if correspondence between predicted and measured values is to be attained. The less accurately one models (analytically) the real top boundary condition, the greater is the deviation between predicted and "real" measured values. Note that the horizontal deformation field is less sensitive to the top boundary constraint modelling problem - because one is only concerned with horizontal displacements in the output scrutiny in this case.

(3) Deviations between predicted and measured values identifying the zero vertical displacement contour-line can be traced to the problem of location of the cutting plane discontinuities in the finite element model.

7.3.4 Deformation energy

We recall that in Section 7.2.4, the deformation energy of the tool-soil system was obtained by various methods. These methods were classified as follows:

Experimental - by integration of the experimentally measured force-displacement relationships.

Semi-analytical - by application of the viscoplasticity method described in Chapter 5, to the experimentally recorded deformation fields.

Theoretical - by calculating the deformation energy using the finite element method.

Using these same techniques for analysis of the triangular grouser problem (Fig. 7.15) we note that the predicted results using the finite element method show a good agreement with the experimentally calculated values. This same technique can be successfully used to produce acceptable predictions of deformation energy for other shapes or types of grousers - provided proper geometrical modelling is achieved.

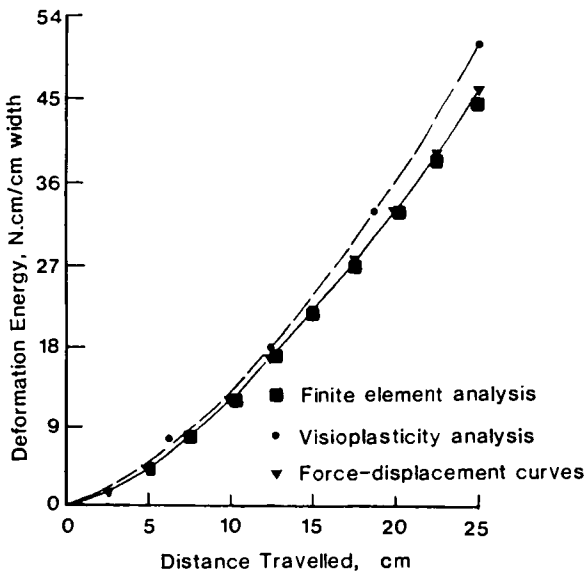


Fig. 7.15. Comparison of measured and calculated values of deformation energy for the triangular grouser - kaolin clay system.

7.3.5 Stress analysis

From a study of experimental displacement fields, Yong et al. (1979, 1980a) have established that there is no real need to place interface elements along

the soil-metal interface for most types of grouser-soil systems. Interface boundary conditions can be assumed as fixed in the x- and y-directions for the nodes connected to the "vertical" side of the grouser. The nodes attached to the horizontal interface need only be fixed in the vertical direction, but should remain free in the horizontal direction. With these assumptions for the interface conditions, reasonable computed stress distributions and consequently developed reactions will be obtained. In the case of the triangular grouser problem, for example, the distributions of the horizontal, vertical and shear stresses in the soil can be obtained from the FEM calculations.

Examples of the distributions of σ_x , σ_y , and τ_{xy} stresses for the triangular type grouser in its advance into the soil are presented in Figs. 7.16 and 7.17. The stress contours developed in the soil are the result of specific grouser displacements of 0.25 and 1.25 cm.

The stress fields developed in the soil in front of a moving grouser are obviously influenced by both the geometry of the grouser and the constitutive relationship of the soil. For a particular soil type, the difference in stress magnitudes can be attributed to the difference in the grouser toe geometry attack angle (angle between bottom portion of the interface and the cutting plane), and the top boundary condition. The importance of the top boundary condition can be seen by examining the plots of the shear stresses, τ_{xy} . These show a zero shear stress divide which indicates the existence of a small "dead" zone approximately defined by the area located between the grouser interface, and the line connecting the grouser toe with the leading edge of the top horizontal plate. Inside this area the material is shown to have negative shear (i.e. clockwise) values - near the grouser interface. Eliminating this physical top constraint will cause a corresponding elimination of the dead zone.

The development of the failure zones, as noted before from an examination of the stresses in the elements in the finite element grid for the triangular grouser example, is shown in Fig. 7.18. Three specific grouser displacements are shown in the Figure. These displacements which occur as a result of uniform increments in lateral advance of the grouser are identified as occurring at increments eight, nine and ten. Note that, by and large, the failed zones as shown in Fig. 7.18 do not start at the grouser's toes, but at approximately the same distances where regions of maximum shear stresses occur. Prior to displacement increment number eight, no failed regions can be identified. The localized failed areas near the point of intersection of the grouser interface with the free soil surface can be considered as localized areas of maximum shear due to stress concentrations. When the displacement increment reaches the tenth increment, these localized failed areas merge with the main failure zone.

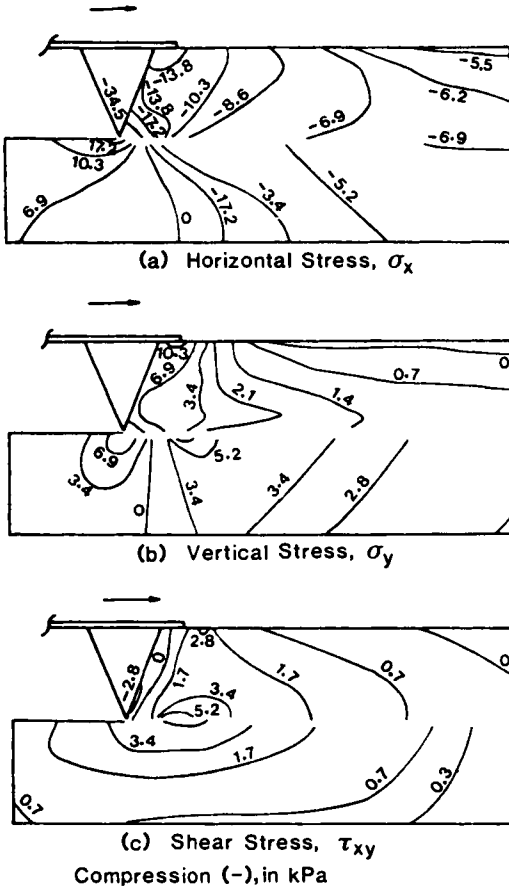


Fig. 7.16. Stress fields for the triangular grouser-soil system at 0.25 cm displacement.

7.3.6 Contact pressure distribution

Normal pressure distributions developed at the grouser-soil interface as a result of specific grouser displacements can be obtained by dividing the reactions developed at the interface nodal points by the areas of influence of each nodal reaction. Figure 7.19 shows the normal pressure distributions developed at the interface as a result of various grouser displacements. Larger peak values develop on the leading edge, accounting for the appearance of failed elements near this edge before the toe failure commences. Note that the influence of the top horizontal plate is also accounted for in the development of the normal stress.

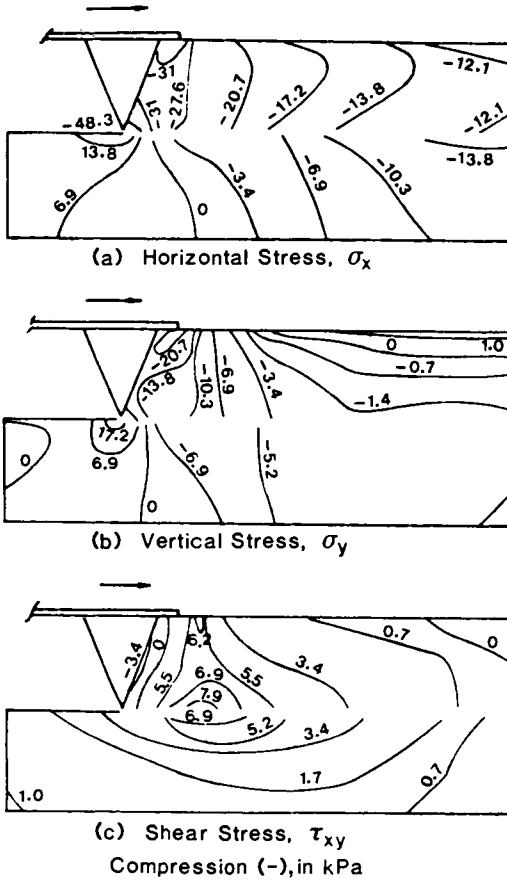


Fig. 7.17. Stress fields for the triangular grouser-soil system at 1.25 cm displacement.

Corresponding tangential stress distributions can also be calculated by resolving the horizontal and vertical reactions at the interface. These are shown in Fig. 7.20. The direction of the tangential reaction depends upon the relative magnitudes of the x- and y-reaction components. The presence of the top horizontal plate in the case of the triangular grouser shown, influences the direction of the reaction on the interface nodal points, resulting in a negative (downward) shear along approximately the top two-thirds of the inclined interface.

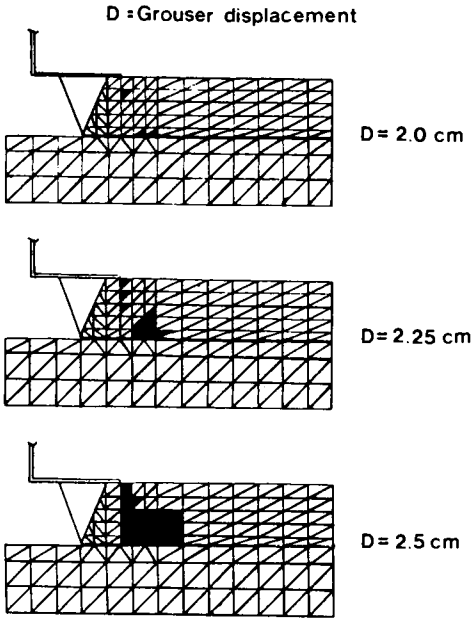


Fig. 7.18. Development at failure zones for the triangular grouser-soil system.

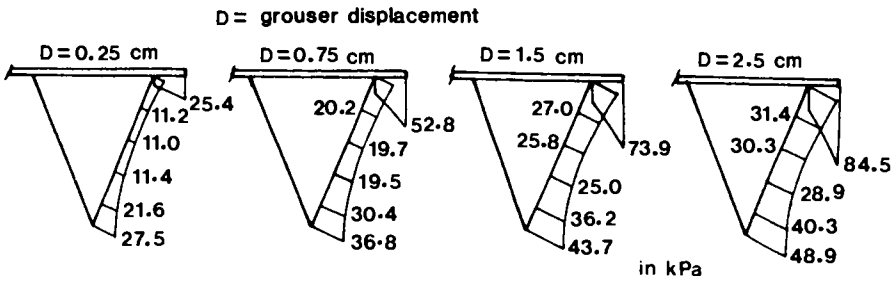


Fig. 7.19. Normal pressure distribution on the triangular grouser.

7.4 MULTIPLE GROUSER

The objective of modelling a multiple grouser-soil system is to study the effect of (a) grouser spacing, and (b) boundary conditions on the performance of the systems in terms of (i) required drag force, (ii) required work done to move the grouser, (iii) pressure distribution at grouser-soil interface, and (iv) soil response. To demonstrate the application of the FEM, a case of multiple grousers with one type of grouser geometrical configuration moving in soft soil is presented.

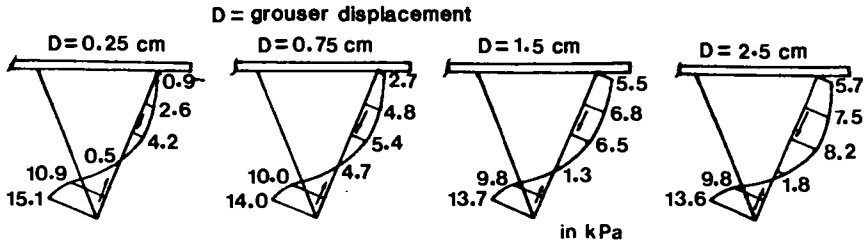


Fig. 7.20. Tangential pressure distribution on the triangular grouser.

7.4.1 Meshes and boundaries (idealization)

The mesh adopted for the multiple grouser soil system is shown in Fig. 7.21. The "passive" type of grouser chosen for this example has been deliberately done to demonstrate the FEM application for grousers other than the triangular grouser heretofore considered. This allows for a broader appreciation of the method of implementation and analysis. In the idealization of this "system", cutting joint elements are placed on the plane where the cutting is anticipated. This is assumed to start at the level of the grouser tip. No interface elements are placed between the soil and the face of the second grouser, since experience gained from previous experimental observations, Yong et al. (1979) shows that for small grouser spacings, the soil between the grousers moves in concert with the multiple grouser system as a rigid body. Interface elements are inserted on the leading grouser-soil interface.

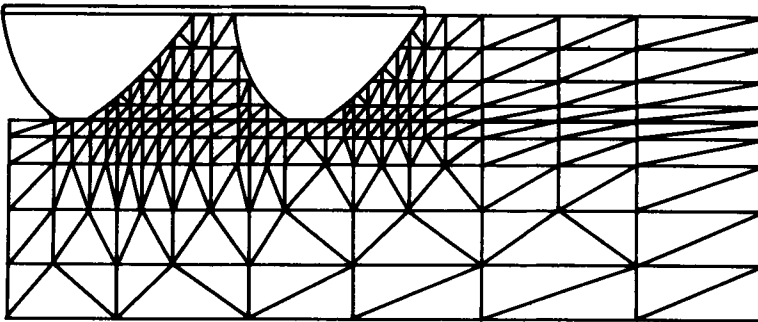


Fig. 7.21. Finite element discretization. Passive grouser. Spacing = 1.25 cm

Two types of boundary conditions can be adopted at the grouser-soil loading boundary, (a) grouser elements moving under constant elevation, or (b) grouser elements moving under a constant vertical load. The bottom and vertical bound-

aries of the mesh are restrained from the vertical and horizontal movements respectively. To implement the analysis, uniform horizontal movement is applied to all the nodes on both grouser surfaces, in successive increments of 0.5 cm each.

7.4.2 Measured and predicted forces

Whilst the leading grouser in a multiple grouser system can be considered to behave in a manner similar to that of single grousers described in Section 7.3, the second grouser of the multiple grouser system may thus be considered as a typical grouser in a vehicle track. In the general laboratory test system using multiple grousers moving in a soil bin, we need to subtract the effects of the leading grouser from the multiple grouser total force. By doing so, the force displacement relationships for the second or succeeding grousers may be obtained from the experimental results. These can then be compared to the finite element predicted values. From procedures previously described (Section 6.8 and Fig. 7.3) and implemented in the first part of this Chapter, predictions using the finite element method of analysis can be made - so long as the stress-strain relationship of the soil is identified. Using test results reported by Yong et al. (1979) for comparison, Figs. 7.22 and 7.23 illustrate the effects of assumed boundary condition, grouser spacing and boundary conditions on the required drag force. We note from the results shown that the agreement between the experimental and finite element results is generally satisfactory - indicating thereby the applicability and validity of the method of analysis or prediction.

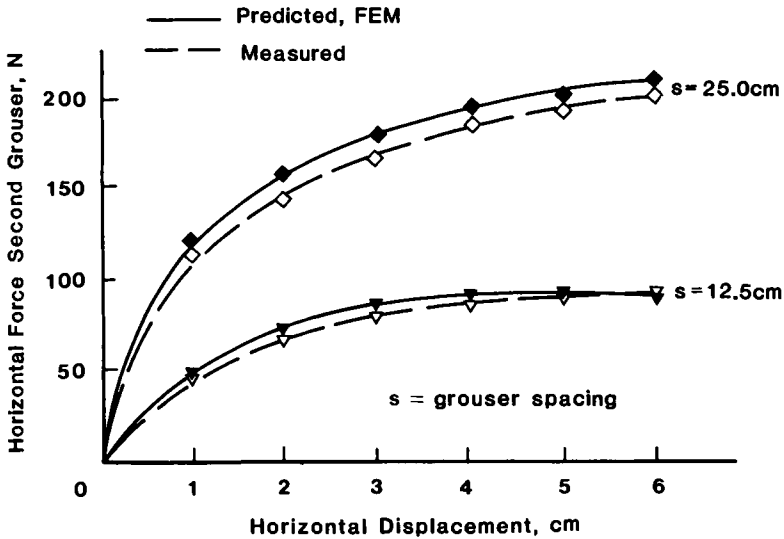


Fig. 7.22. Comparison of experimental and predicted horizontal forces on the second grouser at two grouser spacings. Passive grouser system, constant elevation.

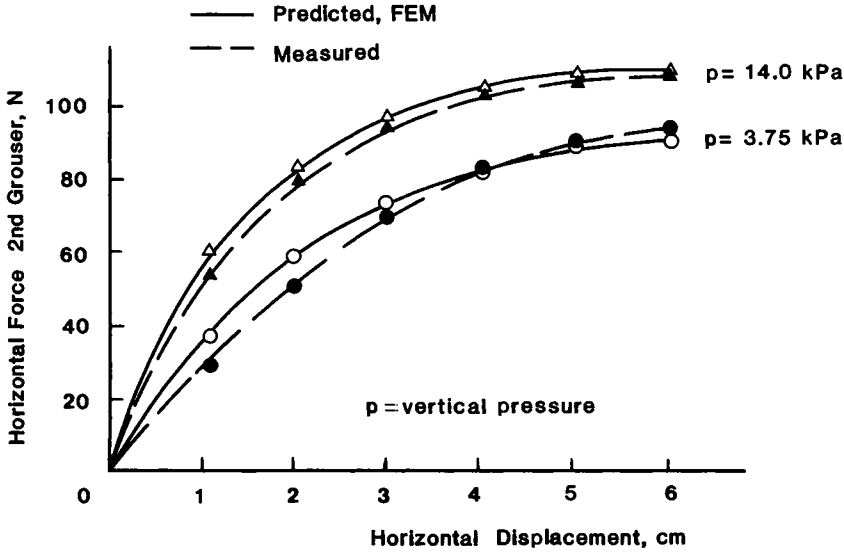


Fig. 7.23. Comparison of experimental and predicted horizontal forces on the second grouser. Passive grouser system. Grouser spacing = 12.5 cm at constant vertical pressure.

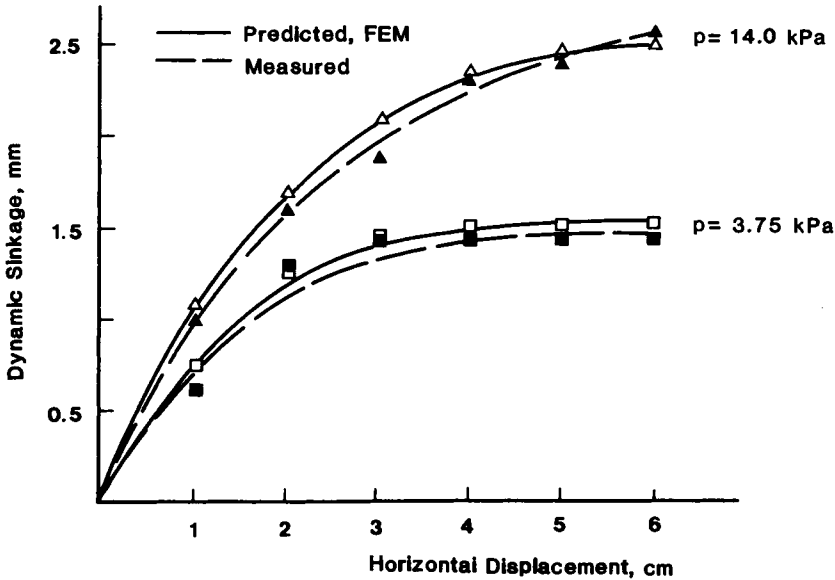


Fig. 7.24. Comparison of experimental and predicted dynamic sinkage. Passive grouser system. Spacing = 12.5 cm at constant vertical pressure.

7.4.3 Deformation fields

Since surface and subsurface soil deformations can be easily measured in transparent-sided soil bin experiments, correlations of the soil deformation beneath the multiple grousers with experimentally measured values provide a good technique for validating the finite element modelling. The experimental deformation fields can be obtained from photographic records of a deforming grid, inscribed on the soil at different intervals of time. Figure 7.24 shows a typical comparison concerning the dynamic sinkage of the passive multiple grouser system moving with constant lateral speed in the soil for two constant vertical pressure boundary conditions. The agreement between analytical and experimental results is rated satisfactory with a typical average deviation of the order of five percent and a maximum deviation never exceeding ten percent.

Typical soil deformation fields are shown in Figs. 7.25 and 7.26 plotted at 1.5 cm grouser displacement. These fields illustrate correlations in the horizontal direction for a passive grouser system accounting for the effect of increasing the bulldozing resistance and vertical displacement fields for constant pressure. Both the experimental and analytical fields reveal discontinuous horizontal displacements in the region between the grousers and in the vicinity of the leading grouser. At a distance from the leading grouser, the experimental field shows continuity while the predicted fields impinge on the right boundary as a result of the inserted cutting elements.

7.4.4 Deformation energy

The deformation energy is equal to that of the input work required to move the grousers. The methods for calculation have been described previously in Section 7.3.4. Figure 7.27 shows the relationships between the deformation energy and travel distance for multiple passive grousers with two different spacings and vertical pressures. Comparisons between experimentally obtained values reported by Yong et al. (1979), and theoretically predicted values, show that the analytical procedure (using FEM) describes the system well.

7.5 PREDICTION OF TRACK PERFORMANCE

As noted previously in Chapter 5, experimental observations of multiple grouser elements, moving in soft soil (Yong et al., 1979, 1980a) have led to the division of the deformed soil mass, beneath the track, into three separate zones of soil deformation (response) under multiple grouser traction loading. The energy dissipated in total soil deformation (response) can be divided into three separate components accordingly (Fig. 7.28).

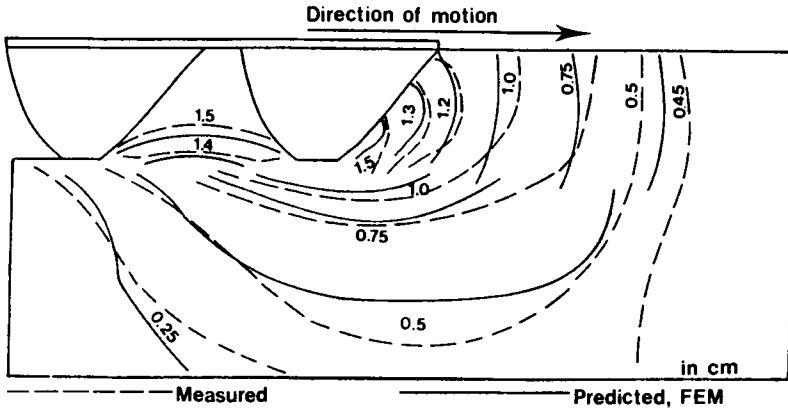


Fig. 7.25. Measured and predicted horizontal displacement fields. Passive grouser system. Spacing = 12.5 cm. 3.75 kPa constant vertical pressure.

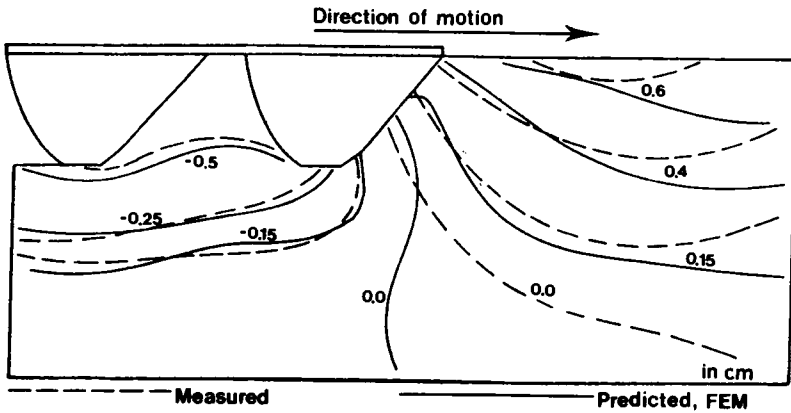


Fig. 7.26. Measured and predicted vertical displacement fields. Passive grouser system. Spacing = 12.5 cm at 3.75 kPa constant pressure.

The energy balance equation for the track/grouser soil system which is written as:

$$(\text{INPUT}) \text{ TORQUE ENERGY} = \text{PULL ENERGY} + \text{DISSIPATED ENERGY} \quad (7.5)$$

can be further decomposed to account for dissipated energy as follows:

$$\text{DISSIPATED ENERGY} = \text{DISTORTION ENERGY, D} + \text{COMPACTION ENERGY, C} + \text{SHEAR SLIP ENERGY, S} \quad (7.6)$$

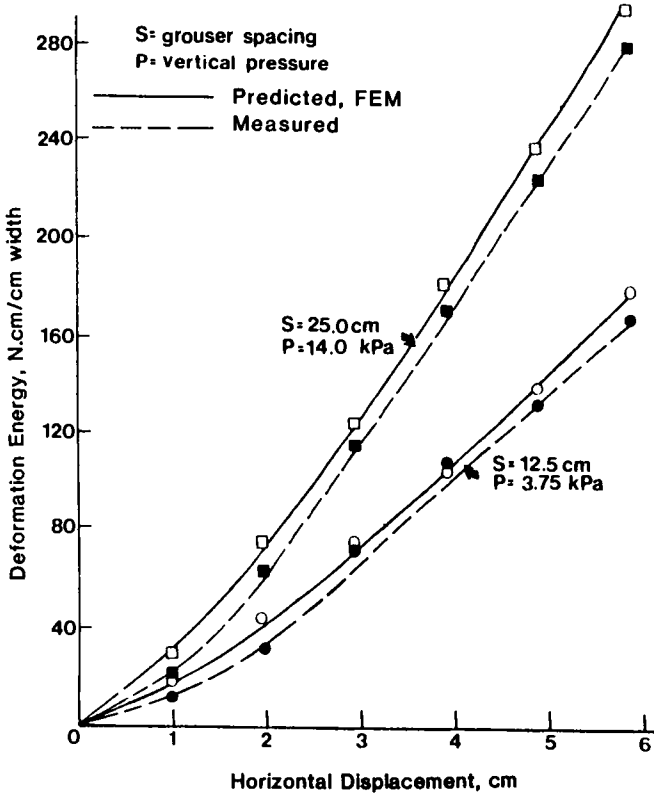


Fig. 7.27. Comparison of measured and predicted deformation energies. Passive grouser system, constant vertical pressure.

Thus, from eqs.(7.5) and (7.6), we will obtain:

$$M \cdot \omega = P \cdot v_c + DE + CE + SE \quad (7.7)$$

where M = input torque applied at the sprocket;

ω = angular velocity of the sprocket;

P = useful drawbar pull;

v_c = carriage (vehicle) velocity;

DE = distortion energy rate;

CE = compaction energy rate and

SE = shear slip energy rate.

Equation (7.7) may be normalized by dividing both sides by v_c to obtain:

$$E_i = P + D' + C' + S' \quad (7.8)$$

where E_i = specific input energy = $M/r(1 - i) = T/(1 - i)$;

r = sprocket wheel radius;

i = slip degree;

T = total horizontal mobilized traction;

D' = specific distortion energy = DE/v_c ;

C' = Specific compaction energy = CE/v_c and

S' = specific shear slip energy = SE/v_c .

The specific components of the energy dissipated in the soil between two successive grousers can be evaluated from the finite element solution by the following equation:

$$D', C', S' = (\int \{\sigma\}^T d\{\epsilon\} dV) / b \cdot v_c \quad (7.9)$$

where $\{\sigma\}$ = element stress matrix;

$d\{\epsilon\}$ = element incremental strain matrix;

V = element volume;

b = track width and

v_c = carriage (vehicle) velocity.

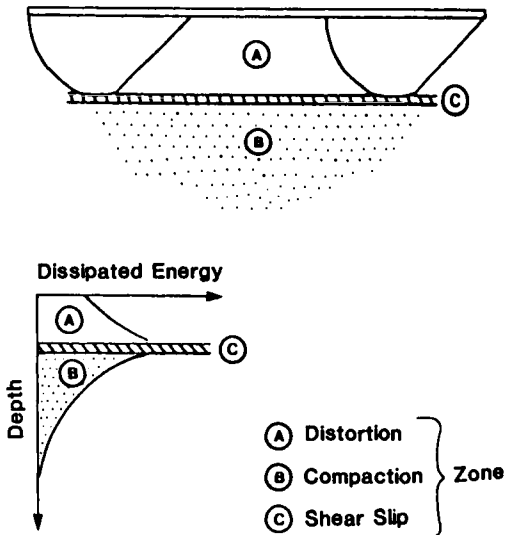


Fig. 7.28. Dissipated energy components.

This procedure for evaluation of the dissipated energy components allows us to predict the drawbar-pull, for a specified input energy, from the energy equations (eq. 7.7 or 7.8). The finite element method can provide the computation of the various components of the dissipated energy by integrating the strain rate field over the volume of each finite element.

The finite element track modelling input requirements and predicted performance information are illustrated in Fig. 7.29, using the load boundary approach as an example for the solution of the problem. The normal and tangential pressure distributions are approximated by suitable functions according to the track and soil characteristics. The predicted track performance can be evaluated in terms of (a) required input torque, (b) motion resistance, (c) drawbar-pull, and (d) sinkage, or, in energy terms and their coefficients, as (a) input, (b) output, and (c) losses. Track slip could be specified as input or output information.

7.5.1 Meshes and boundaries (idealization)

Idealization of the soil continuum beneath the track, with respect to undeformed and unloaded soil surface is illustrated in Fig. 7.30. By making the dimensions of the continuum idealization as fixed functions of the track footprint length, the amount of input data can be considerably reduced.

It is not unreasonable to assume that at a depth equal to five times the track contact length, no soil vertical movement occurs, and at a distance equal to four times the contact length from both ends of the track, no horizontal movement occurs. The load boundary at the track-soil interface requires a knowledge of the interfacial-stress distribution resulting from track loading and subsequent motion.

The pressure distribution at the track-soil interface depends on its relative rigidity. This is a function of the various parameters discussed previously in Chapter 3. According to the relative rigidity of the track, and the drawbar-pull height, and the drawbar-pull height slip rate, various assumptions can be made for idealizing the contact pressure distribution as discussed in Chapter 3.

Whilst the normal stresses imposed on the soil by the track weight depend solely on the track-soil relative stiffness, the tangential stresses are controlled by two additional factors - the track-soil surface characteristics and the slip velocity - (Chapter 3). As previously discussed in Chapter 3, the calculation of the applied torque, T , is based on the type of tangential shear stress distribution at the track-soil interface, i.e.

$$T = \int_0^L \tau \cdot \Delta L \cdot b \cdot r \quad (7.10)$$

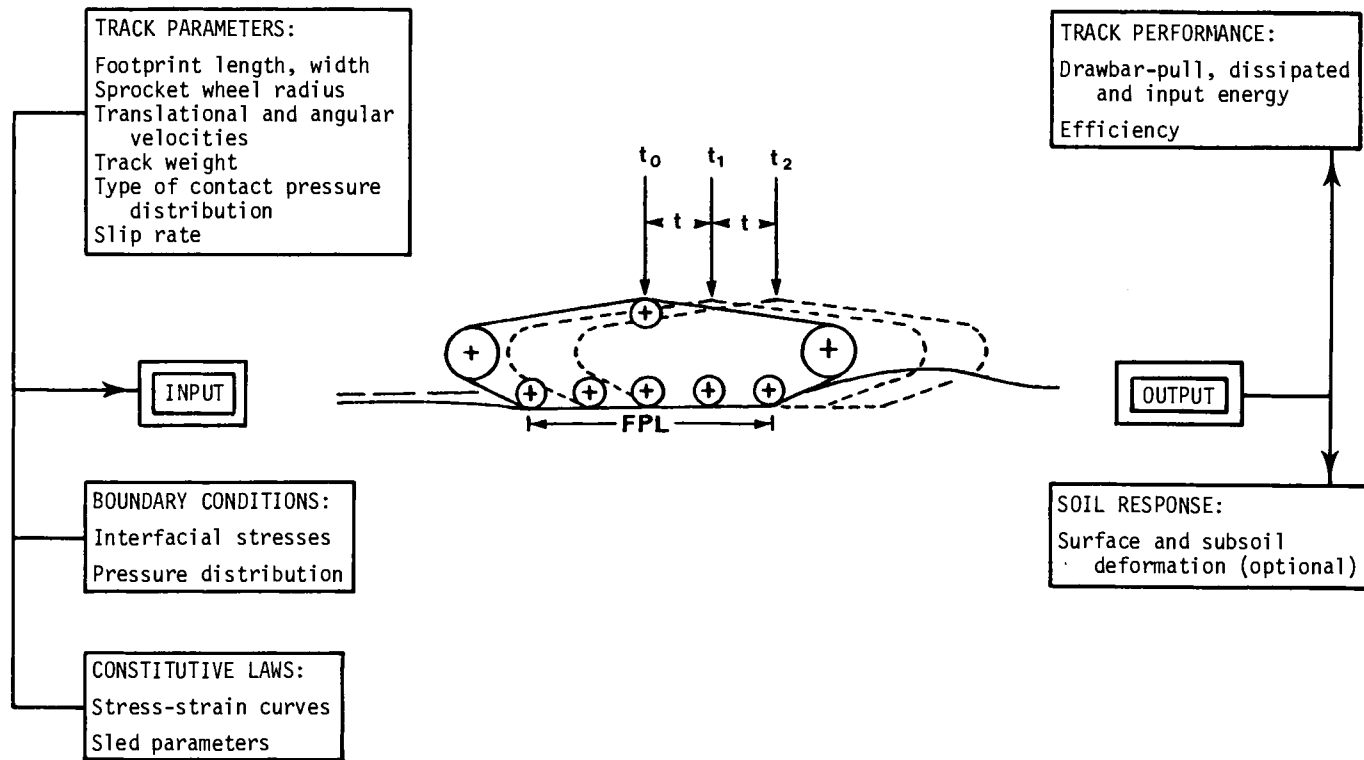


Fig. 7.29. Schematic diagram for the track computer model.

where τ = tangential stress value at track element ΔL ;
 L = contact track length;
 b = track width and
 r = sprocket wheel radius.

The magnitude of the tangential stresses is a function of slip (or relative displacement) and relative stiffness between the materials involved at the interface region. The different methods for predicting the tangential stresses have been previously discussed in Chapter 3. Figure 7.31 shows a typical shear stress-displacement relationship.

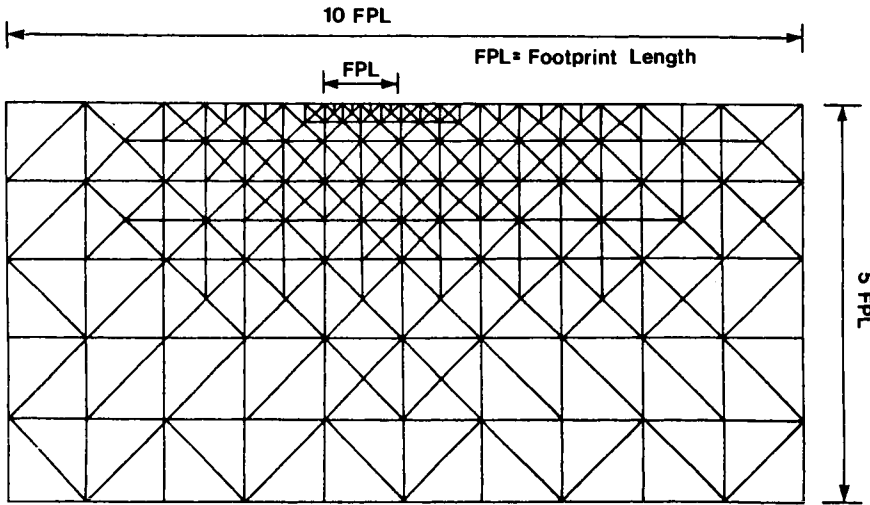


Fig. 7.30. Finite element discretization for the track-soil system.

7.5.2 Prediction of track performance

Figures 7.33 and 7.34 illustrate the predicted track performance in terms of input and output energy coefficients as a function of slip. The experimental results used in the analysis were determined from two-dimensional tests in the laboratory for a section track (Fig. 7.32) moving on soft soil with a constant translational velocity of 15 cm/sec. The track was equipped with full-sized passive grousers such as those used in the multiple grouser system (Fig. 7.21). The grouser spacing was 12.5 cm. The track input torque, drawbar-pull, translational velocity, track belt velocity and sinkage were measured and recorded. The energy coefficients shown in the Figures are, in effect, a normalizing procedure which takes the "vehicle" weight into account. This is a very useful procedure for comparison of efficiencies of various tractive systems. The coefficients can be calculated as follows:

$$\begin{aligned} \text{INPUT ENERGY} &= \text{PULL ENERGY} + \text{DISSIPATED ENERGY} \\ E_i &= P \cdot v_c + DE \end{aligned} \quad (7.11)$$

Dividing both sides by the product of the total weight and carriage velocity, i.e. $W v_c$, as follows:

$$\frac{E_i}{W v_c} = \frac{P}{W} + \frac{DE}{W v_c} \quad (7.12)$$

$$\text{we obtain } CE = CP + CDE \quad (7.13)$$

where CE = coefficient of input energy N.m/N.m;
 CP = coefficient of output energy N.m/N.m and
 CDE = coefficient of energy dissipated N.m/N.m.

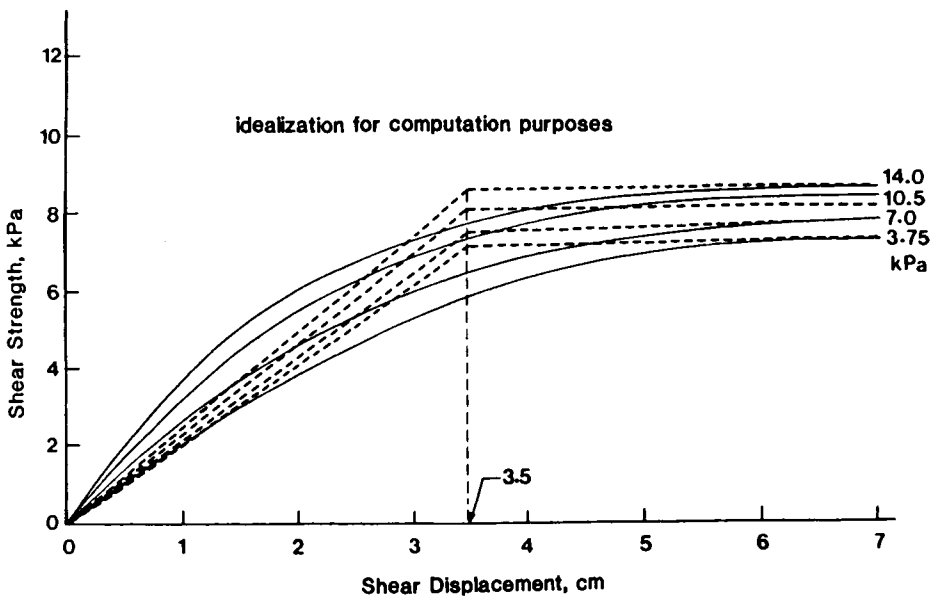


Fig. 7.31. Tangential stress-displacement relationship for the passive grouser system. Spacing = 12.5 cm.

In the finite element prediction, a rectangular normal pressure distribution is assumed at the track-soil interface. The tangential stress distribution at

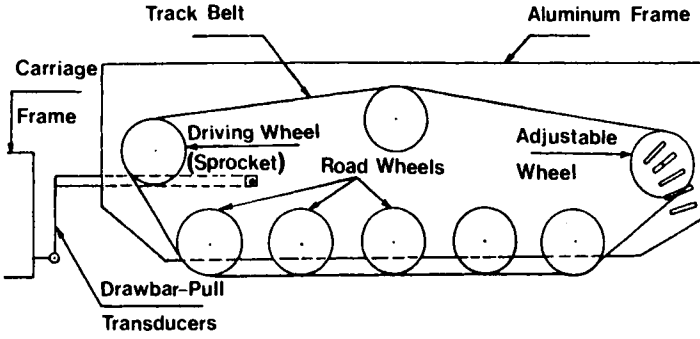


Fig. 7.32. Model track section.

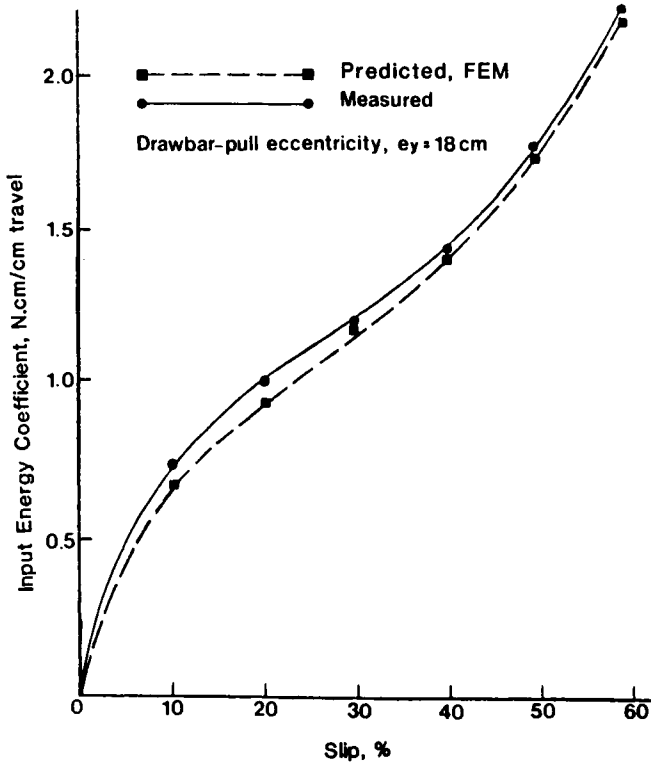


Fig. 7.33. Input energy coefficient prediction. Passive track.

the interface can be determined from translation tests in the laboratory, using a form of skid pads simulating the characteristics of the track material. As noted, the comparison between predicted and calculated performances shown in Figs. 7.33 and 7.34 indicates good agreement. The analytical model can obviously be improved by incorporating other track parameters as, angle of attack, wheel spacing, track tension ... etc. However, it is not clear at this time how much improvement will be obtained with higher levels of model sophistication - especially if we bear in mind that the real field terrain condition will impose terrain variabilities throughout the track traverse.

7.6 WHEEL-SOIL INTERACTION

In developing a wheel computational model which can analyse and/or predict the tyre-soil interaction with complete consideration of all parameters involved, the following requirements must be fulfilled:

1. The tyre-soil contact area which defines the loading boundary has to be predicted as a function of wheel load, inflation pressure, slip, tyre flexibility and soil stiffness.
2. The motion resistance or the energy dissipated due only to tyre deformation has to be predicted independently and separated from the energy spent in deforming the soil.

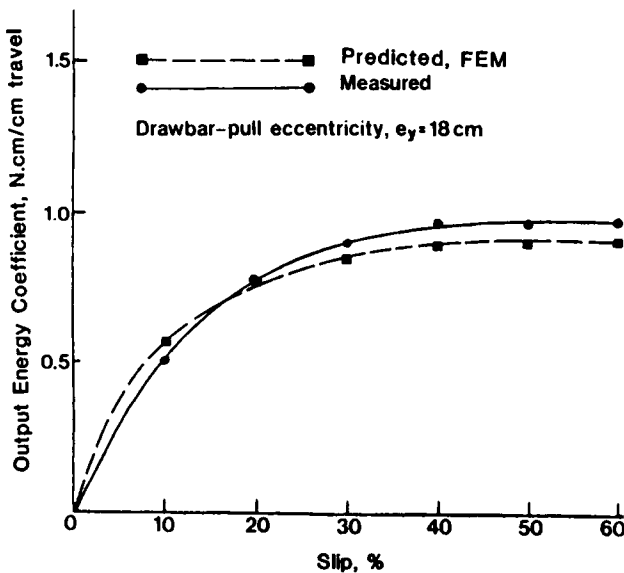


Fig. 7.34. Output energy coefficient prediction. Passive track.

3. The rolling resistance or the soil deformation energy due to tyre motion over the subsoil has to be evaluated carefully to achieve a high accuracy in predicting overall vehicle-mobility performance.

4. The tangential stresses along the tyre-soil interface have to be evaluated as a function of wheel load, tyre-soil surface characteristics and slip rate in order to predict the amount of torque required to keep the vehicle in continuous motion.

5. The energy dissipated at the wheel-soil interface due to wheel slippage has to be evaluated.

Note that the term "wheel" is used in the general context to mean both tyres and actual non-tyre wheels. For modelling purposes, the general wheel is used since this can be specialized (when needed) to address individual items describing the properties and characteristics of the wheel - e.g. flexibility and distortion of a tyre or elastic/rigid deformation properties of a "rigid" solid wheel. Adapting the finite element method to the wheel-soil interaction problem, the following items need to be satisfied:

1. The prediction will be complete if both tyre and soil behaviours under the moving tyre or wheel load are obtained.

2. The solution must satisfy the equilibrium and compatibility requirements.

3. The nonlinear stress-strain relationships of the subsoil obtained from a suitable test procedure should be directly employed without any unnecessary idealization.

4. The solution should provide all pertinent information, such as the amount of tyre deflection, dynamic sinkage, stress-strain fields in the subsoil and the required mobility performances such as drawbar-pull, tyre motion resistance and soil resistance.

5. The predicted wheel performance should be expressed in terms of forces, (input torque, drawbar-pull, motion resistance) and in absolute energy terms (input, output, losses) and/or in terms of energy coefficients.

7.6.1 Boundary conditions

Specification of the boundary conditions at the wheel-soil or tyre-soil interface requires determination of (a) contact area dimensions, and (b) load or displacement distributions. Because of (a) the nonlinear geometrical dimensions of the tyre, and (b) stiffness characteristics of the soil and the tyre, it is not always simple to specify the loading boundary exactly. In the following Sections the methods which can be adopted or which may lead to the determination of the boundary conditions at the tyre-soil interface are discussed.

(i) Load-carrying mechanism of tyre structure. One of the main requirements for operating the wheel-soil interaction model is the determination of wheel-

soil contact area and its interfacial stress distribution. In the case of tyres, accurate modelling of the load transfer mechanism from the wheel axle to the ground surface requires some appreciation of the load-carrying mechanism of the tyre structure. Whilst the actual tyre-load deformation mechanics problem is indeed complex if the various elements forming a tyre are to be considered, the modelling procedures described heretofore generally require only those aspects dealing with the gross mechanical response characteristics of the tyre.

In an inflated-undeformed tyre, the cords forming the tyre casing are tensioned by the inflation or internal pressure which is in excess of the external or atmospheric pressure. As the tyre is pressed against a horizontal undeformable surface, the casing will be deformed and flattened in the contacting region (Fig. 7.35). For the simplest case of a smooth-surfaced tyre without

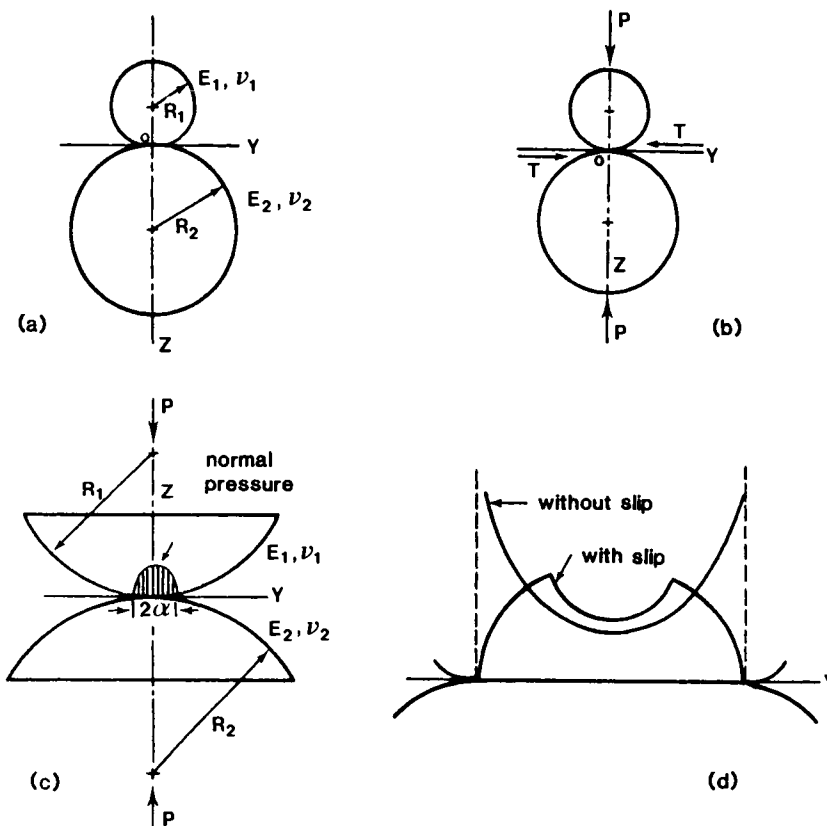


Fig. 7.35. (a) Undeformed spheres at cylinders in contact. (b) Formation of a small contact surface under normal force 'P'. (c) Force system in contacting bodies. (d) Distribution of tangential traction across the contact area. (Adapted from Mindlin, 1949)

tread, the cords in the part of the carcass which is in actual contact with the supporting ground will also lie in a flat plane parallel to the ground, or in other words, the cords in that area are in straight lines. The tensile forces in the contacting carcass are a function of the inflation pressure, rubber friction, and complex bending characteristics of the tyre casing. This latter aspect is especially critical in the transition zone between the tyre side walls and the contacting portion. Whilst the normal contact pressure between the tyre casing and the ground will be equal to the inflation pressure, considerable modification and variations will be developed around the edges of the contact area because of the pressure exerted by the bending effect of the tyre carcass in the transition zone.

In the case of tyres with treads, the actual contact pressure will be locally greater than the applied inflation pressure because of the thickness of tread rubber, tread pattern and number of plies used. We should note that these same items influence tyre carcass stiffness and contribute to the fact that the actual load carried by the tyre is higher than the product of the overall contact area and the applied inflation pressure. The normal pressure distribution at the contact interface may be expressed as:

$$p = p_i + f \text{ (tyre characteristics)} \quad (7.14)$$

where p = vertical pressure component at any point;

p_i = applied inflation pressure and

$f(--)$ = some functional relationship depending on the tyre structure, tyre driving or braking torque, tyre side forces, tyre velocity, etc.

The function f cannot be described in simple mathematical terms since the actual normal pressures acting on the contact area are generally irregularly distributed - even for a smooth-surfaced tyre.

Because of the complexity of all the factors involved, it is difficult to establish an accurate theoretical model which is capable of predicting the contact area and the pressure distributions are difficult to be established. Although the tyre can be treated as a structural shell approximated as an elastic running band supported elastically by the tyre side walls, the application of this model to consider the tyre-deformable ground system is limited. A good theoretical model should incorporate the degree of tyre flexibility as a function of carcass stiffness, inflation pressure and soil stiffness since these factors are responsible for the development of the contact area and the pressure distribution.

In the following Sections, the analytical procedures will be presented together with the supporting theories and related test results where appropriate.

It should be noted that because the tyre-soil interaction problem is indeed an extremely complicated problem, a certain degree of approximation is unavoidable in the course of theoretical model formulation.

(ii) Elastic bodies in contact. In the prediction of tyre performance on soil or other types of bearing strata, one of the necessary input parameters is the contact area which defines the loading boundary of the tyre-terrain interface. This influences the extent of the affected zone in the substrate. It is important, therefore, to develop an appropriate approach to predict the tyre-terrain contact area which is a function of tyre carcass stiffness, inflation pressure in the tyre casing, axial load and terrain bearing stiffness. In this respect, the Hertz theory of elastic contact (Hertz, 1881) is worth investigating. At the outset, it is important to make note that only the tyre may be safely considered as an elastic system. The bearing terrain will generally behave nonlinearly upon loading. Nevertheless, the direct use of elastic theory can be justified as a first approximation of suitable equivalent "elastic" parameters such as Poisson's ratio (ν) and modulus of elasticity (E) can be established. In the case of soil as a bearing (terrain) material, it has been shown from numerous soil mechanics studies that equivalent elastic properties can indeed be established - for application to stability analyses. These "elastic" properties are seen to depend on the soil physical properties, the confining pressure, and the level of strain encountered. We should also note that the proper use of an analytical/numerical technique is critical to the acceptability of equivalent elastic properties. The use of the Hertz contact theory in predicting the tyre-soil contact area will consequently call for a suitable selection of the required elastic parameters and a reasonable method to verify the predicted result.

When two elastic solids are brought in an unstressed state into contact at a single point O as in the case of spheres or cylinders (Fig. 7.35) both have a common tangent plane OY and a common normal OZ . If co-linear forces P are now applied to force the two spheres or cylinders together (Fig. 7.35b), deformation will occur, resulting in the development of a small contact area, in place of the previous contact point O . Hertz theory assumes that the contacting bodies are isotropic and linearly elastic, and also that the representative dimensions of the contact area are very small compared to the radii of curvature of the undeformed contacting bodies. In general, it is thus considered sufficiently accurate to represent the actual shape of the contact area by a flat elliptical surface. The theory leads to the determination of the magnitudes and orientations of the principal axes of the ellipse, the relative approach of the two bodies and the distribution of the normal stresses across the contact area. The effects of tangential stresses have been taken into account by Mindlin (1949) who superimposed additional force systems (e.g. tangential force) upon the Hertz normal forces (Fig. 7.35). These can arise in the contact problems of wheels and rails,

gear teeth, etc., and contacting bodies with unequal elastic moduli. With the addition of the tangential force (T), the normal pressure distribution is not significantly affected. The tangential traction becomes infinite along the boundary of the contact area as long as there is no relative slip between the two bodies (Fig. 7.35b).

In the case of two long cylinders in contact along their parallel lines, a "rectangle" of infinite length with the width $2a$ (Fig. 7.35) will be obtained, (Poritsky, 1950; Lubkin, 1962):

$$\frac{1}{R_1} + \frac{1}{R_2} = \frac{4P}{\pi a^2} \left(\frac{1-\nu_1^2}{E_1} + \frac{1-\nu_2^2}{E_2} \right) \quad (7.15)$$

where R_1, R_2 = undeformed radii of the cylinders;
 P = applied vertical load per unit length;
 a = half width of the contact area;
 ν_1, ν_2 = Poisson's ratios and
 E_1, E_2 = moduli of elasticity of the cylinders.

The normal pressure distribution (p) across the contact area is:

$$p = \frac{2P}{\pi a} \left(1 - \frac{y^2}{a^2} \right)^{1/2} \quad (7.16)$$

where y = distance from the centre of the contact area.

Assuming the tangential force (T) to be proportional to the normal force (P), then:

$$T = \mu P \quad (7.17)$$

where μ = the coefficient of friction.

If slip occurs over the contact area, eq.(7.15) can be modified to take into account the tangential stress (Poritsky, 1950), as:

$$\frac{1}{R_1} + \frac{1}{R_2} = \frac{4P}{\pi a^2} \left(\frac{1-\nu_1^2}{E_1} + \frac{1-\nu_2^2}{E_2} \right) / \left(1 + \frac{K_1^2}{K_2^2} \right) \quad (7.18)$$

$$\text{where } K_1 = \frac{2}{\pi} \left[\frac{1-\nu_1}{G_1} + \frac{1-\nu_2}{G_2} \right]$$

$$K_2 = \left[\frac{1-2\nu_1}{G_1} - \frac{1-2\nu_2}{G_2} \right]$$

$$G_1 = \frac{E_1}{2(1+\nu_1)}, \quad G_2 = \frac{E_2}{2(1+\nu_2)}$$

This solution leads to a slight decrease in the value 'a'.

The above formulation calls for the evaluation of the elastic parameters (E and ν) for both tyre and soil. Whilst these parameters can be readily established for soils, they need to be established for tyres for introduction in eqs.(7.15) and/or (7.18). The use of the Hertz elastic contact theory for derivation of the tyre elastic parameters and for prediction of the tyre-soil contact area will be described in the following Section.

(iii) Prediction of tyre-soil contact area. Although there have been some studies performed to investigate the tyre contact area with respect to the wheel load and the inflation pressure applied, these have been developed primarily for the benefit of tyres operating on rigid unyielding surfaces (Bekker, 1969; Sohne, 1969; Komandi, 1976; Abeels, 1976). In general, these studies are directed towards the prediction of tyre-rigid surface contact area and tyre deflection as a function of wheel load and inflation pressure in order to determine the load-carrying capacity of the candidate tyre. To focus the discussion and problem development, we will consider the yielding terrain material to be soil. When a pneumatic tyre is loaded on top of a deformable surface (soil), the contact area will depend mainly on the tyre-soil relative stiffnesses. The soil stress-strain characteristics which are ignored in the tyre-rigid surface investigations will indeed control the development of the contact patch. Apart from the fact that the contact area will indicate the capacity of the tyre in transferring the wheel load into the soil, it is noted that it also influences the development of the interfacial stresses and the zone of influence in the subsoil.

To adopt the contact theory for tyre-soil problems, the tyre can be idealized as a cylindrical body with infinite width, and the supporting soil modelled as another cylindrical body with infinite radius and width (Fig. 7.36). This idealization is consistent with the two-dimensional formulation of the finite element analysis employed herein. The contact area of the tyre-soil interface is thus approximated to be rectangular, of which the dimensions are to be predicted by the contact theory. The success of the prediction depends primarily on the selection of the appropriate elastic parameters (i.e. the elastic modulus E and the Poisson's ratio ν) involved for both tyre and soil. It is realized that whilst the tyre may be safely regarded as elastic, the supporting soil is essentially non-elastic. However, it is common to idealize the soil as an

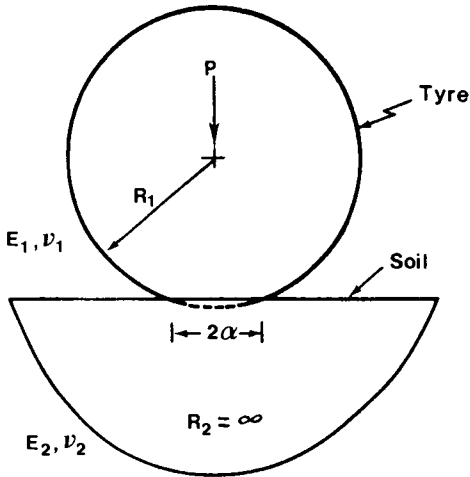
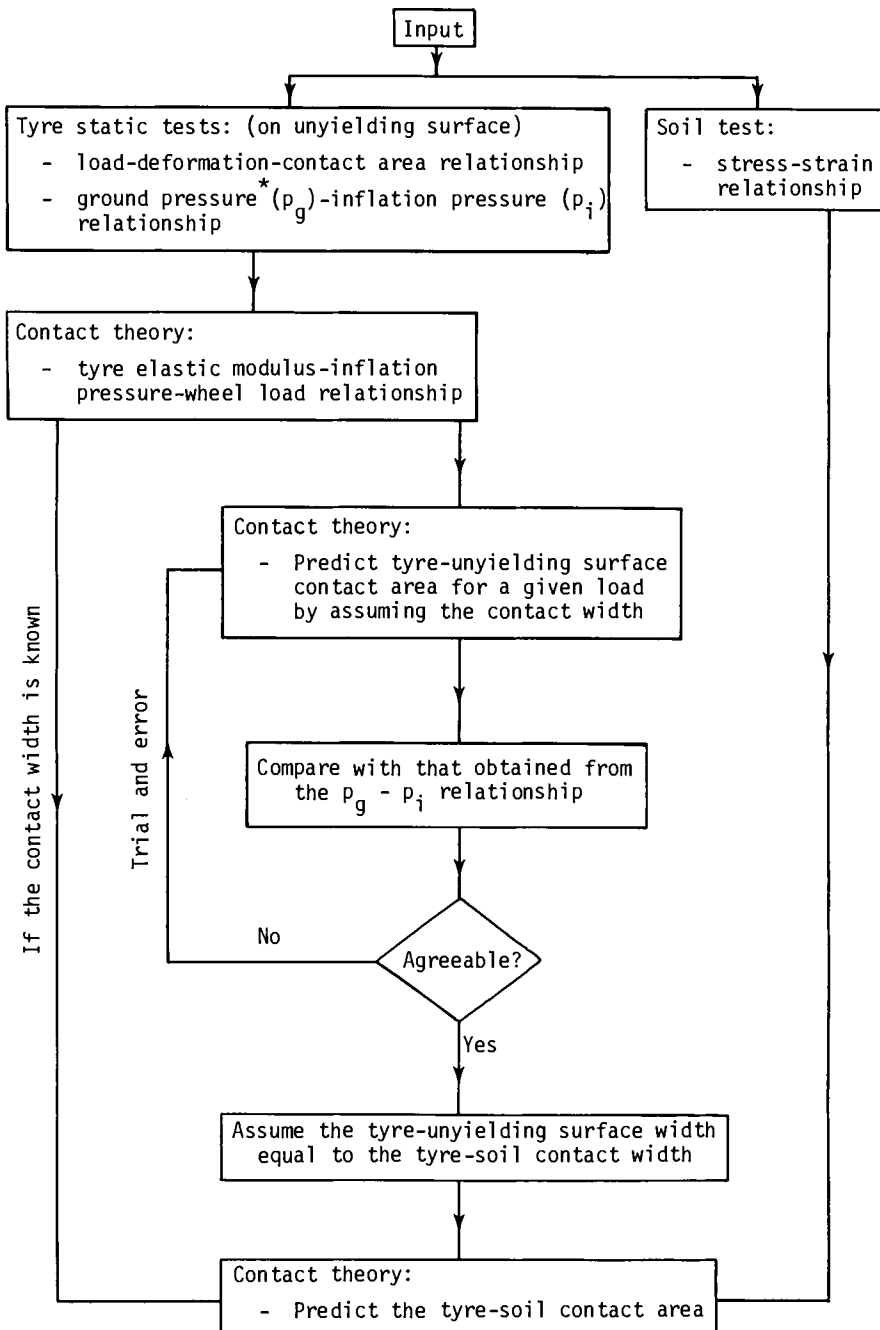


Fig. 7.36. Idealization of tyre and soil in contact.

elastic-linear strain hardening or elastic-plastic material so that the representative modulus of elasticity can be established to simplify the analytical procedure. For example, the use of the elastic theory in predicting the immediate settlement beneath a footing in classical soil mechanics (e.g. Lambe and Whitman, 1969) calls for the knowledge of soil elastic modulus which can be obtained by idealizing the soil as piecewise-linear. Although the tyre-soil situation is actually a three-dimensional problem, it is instructive to use the two-dimensional formulation as a first attempt to avoid mathematical complexity. Moreover, the tyre-soil contact area predicted by this approach will serve as an initial approximation in the actual analysis, after which further modification can be provided if necessary. The criteria which can be used to justify the validity of the predicted contact area are the facts that the tyre deformation and the energy spent in deforming the tyre when moving on a deformable soil, cannot be greater than those experienced in a rigid unyielding ground under the same wheel load and inflation pressure. The tyre deflection and the tyre deformation energy occurring in the yielding surface can be evaluated by the finite element method, while those in rigid unyielding surface can be measured and/or predicted.

The procedure for predicting the tyre-soil contact area shown schematically in Fig. 7.37 starts by performing laboratory tests to determine the properties of tyre and soil individually. For soil, the purpose is to obtain the stress-strain relationship which can be determined in the soil triaxial test under similar loading condition. As for tyre, it is necessary to determine the load-deformation behaviour and the corresponding contact area by loading the tyre



*The ground pressure (p_g) is obtained by averaging the wheel load over the contact area.

Fig. 7.37. Procedure of predicting tyre-soil contact area.

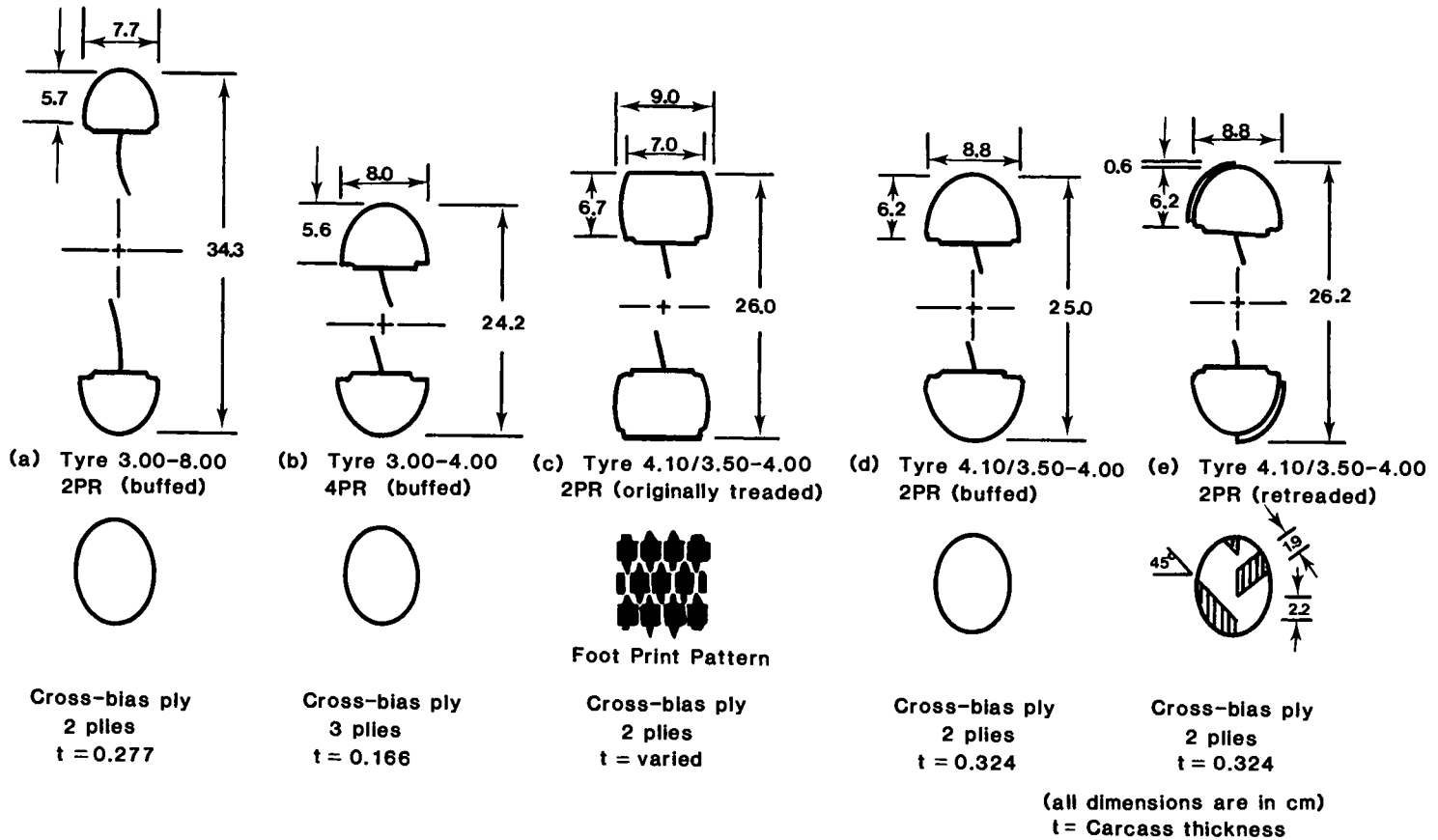


Fig. 7.38. Undeformed tyre sections.

vertically on a rigid unyielding surface. The Hertz contact theory is employed to evaluate the tyre composite modulus of elasticity through the use of eq. (7.15).

Figure 7.39 shows experimentally determined relationships between average ground pressure and inflation pressure for the different model tyres shown in Fig. 7.38 (Yong et al., 1980b). The predicted stationary tyre-soil contact areas utilizing the procedures shown in Fig. 7.37, and tyre-rigid surface test results (Fig. 7.39), are presented in Figs. 7.40 and 7.41. The effect of degree of slip on model tyre contact areas shown in Fig. 7.42 indicates that at low speeds there is no appreciable difference between the contact area for the stationary and moving tyre at any degree of slip. However, it is expected that for more

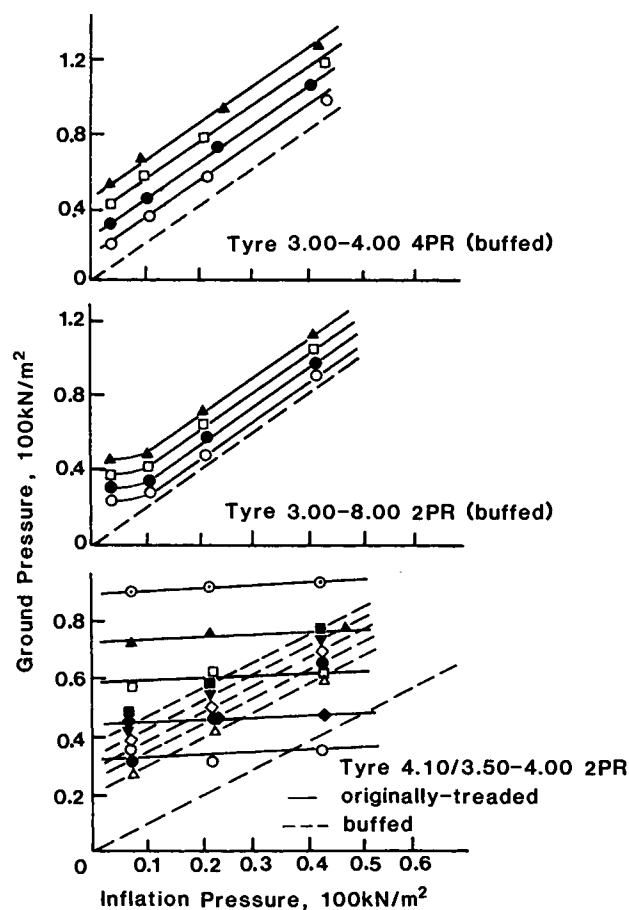


Fig. 7.39 Relationships of ground contact pressure and inflation pressure.

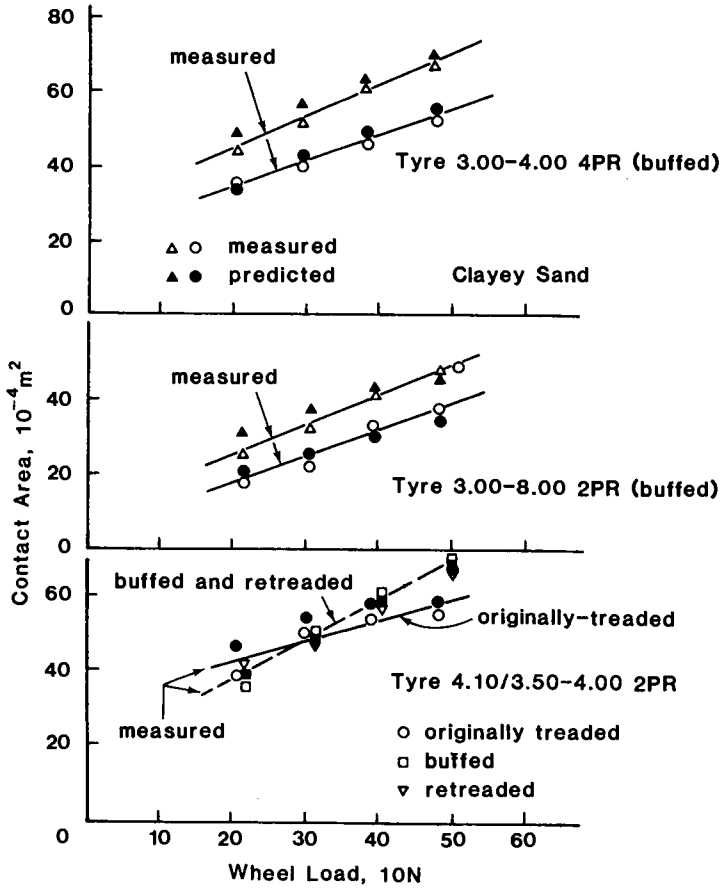


Fig. 7.40. Prediction at tyre-soil contact area on clayey sand.

flexible tyres there will be a measurable difference in contact patch (area) characteristics because of slip. This problem has yet to be fully evaluated. Utilizing the tyre-soil contact area as the load transfer patch in the boundary conditions formulation in the finite element model will greatly reduce the amount of calculation time and effort in the preparation of the experimental parameters required.

7.6.2 Prediction of tyre performance

The finite element modelling technique for prediction of soil response beneath moving tyres with respect to deformations, stresses and strains, can be used to calculate the different components identified in the tyre-soil system energy balance equation (Chapter 5). Figure 7.43 shows the finite element model necessary input and output information for evaluating tyre-soil interaction.

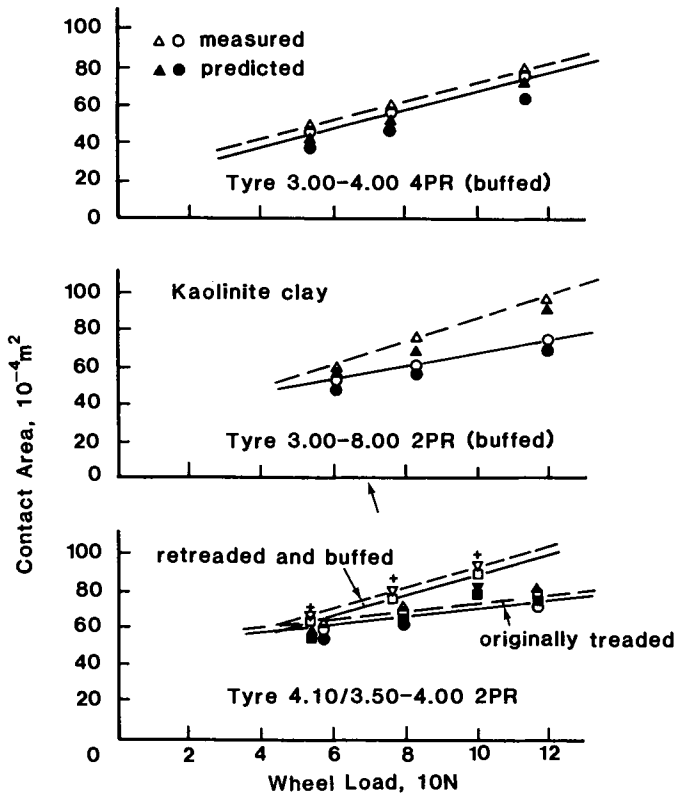


Fig. 7.41. Prediction of tyre-soil contact area on kaolinite clay.

As previously stated in Chapter 5, the energy components for a tyre moving on deformable ground surface consists of:

(i) Dissipation energy. This type of energy consists of (a) energy dissipated in distorting the tyre, (b) energy dissipated in deforming the soil, and (c) energy dissipated at the tyre-soil interface.

(ii) Input energy. Provided by vehicle engine, but controlled by transmission differential and tyre-soil interfacial characteristics.

(iii) Output energy. Energy produced in terms of available work for pulling another vehicle or other wheels in the same vehicle.

The procedures for calculating the different tyre-soil system energy components are presented as follows:

A. Tyre deformation energy. Calculation of the energy dissipated in deforming the tyre using its basic geometrical, structural, material and operating parameters can be difficult. The following pieces of information are generally required:

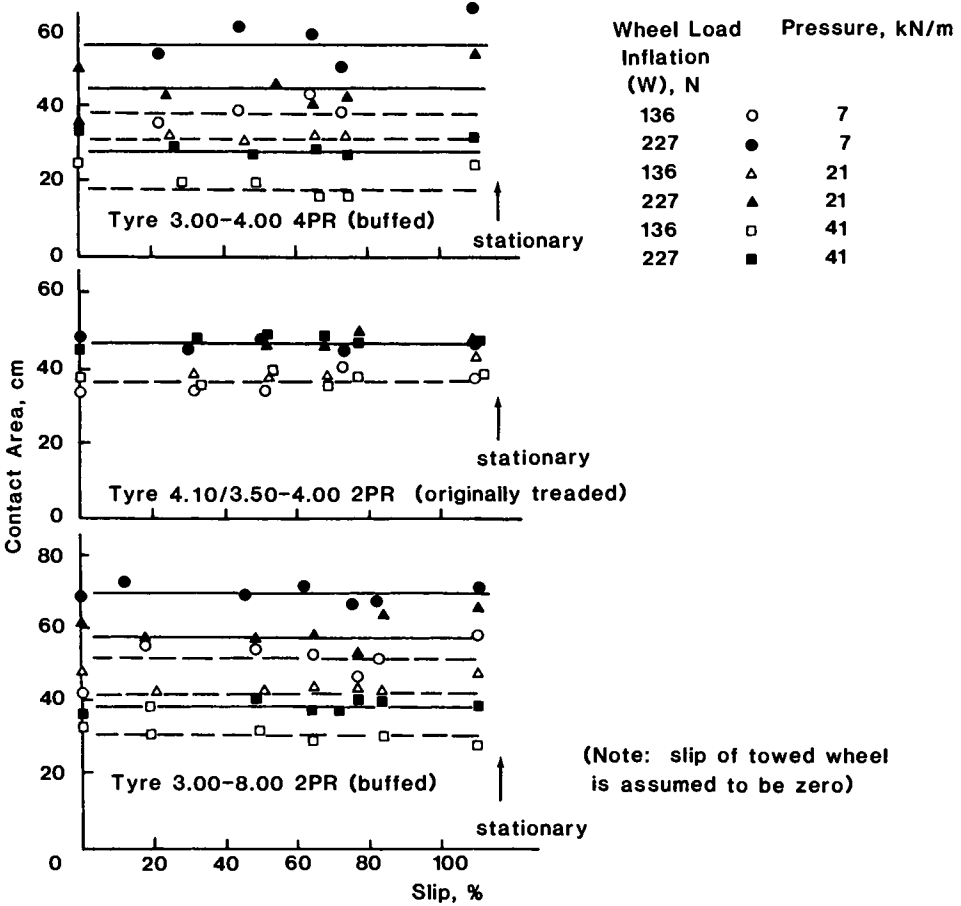


Fig. 7.42. Relationship of contact area and slip rate.

- (a) tyre deflection profile at the soil interface,
- (b) pressure distribution at the tyre-soil interface,
- (c) thermodynamic properties of the tyre composite materials, and
- (d) hysteresis and mechanical properties of the tyre material.

Available off-road models are generally concerned with low-speed vehicles. Hence the effect of heat generated in the tyre material may be neglected (item 'c') without any serious loss of accuracy in the development of the analysis. However, at higher speeds, it is not proper to ignore item 'c'.

Assuming that tyre distortion is due mainly to the normal pressure distribution at the tyre-rigid surface interface, and that the pressure is uniformly distributed throughout the contact area, the tyre motion resistance (R_t) or energy dissipated per unit travel distance can be expressed as (Bekker and Semonin, (1975):

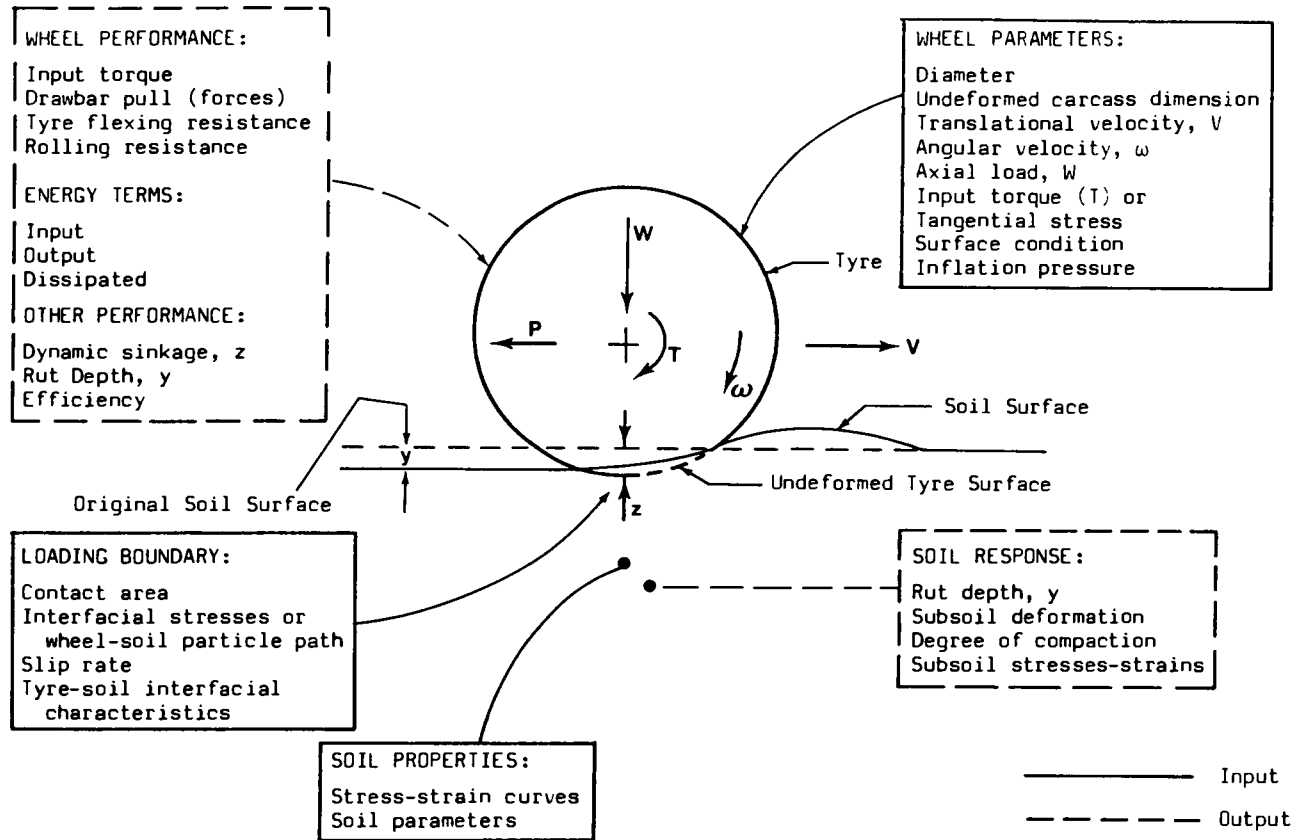


Fig. 7.43. Necessary input and output information for evaluating tyre-soil interaction.

$$R_t = \frac{3.581 B.P_g D^2 \epsilon (0.0349 \alpha' - \sin 2\alpha')}{\alpha' (D-2)} \tag{7.19}$$

where P_g = uniform ground contact pressure;

α' = $\alpha/2$, degrees;

D = tyre diameter = $2R$;

ϵ = 'energy recovery' factor (<1.0) = $1 - e^{-27.5\delta h}$ and

h = tyre carcass height above the ground.

The symbols used in eq.(7.19) are identified in Fig. 7.44. Utilizing eq.(7.19) requires a known relationship between ground pressure (P_g) and tyre deformation (δ) for a certain tyre load, e.g. Fig. 7.45.

When a pneumatic tyre is loaded on a yielding soil support, both the tyre and the supporting soil will deform an amount (Fig. 7.46), which is seen to depend mainly on the applied wheel load and the tyre-soil relative stiffnesses. The amount of tyre deformation can be calculated as the difference between the undeformed tyre configuration and the soil surface, obtained by using the appropriate pressure distribution in the finite element method. Neglecting the rebound effect of the tyre, its deformation energy can be calculated by:

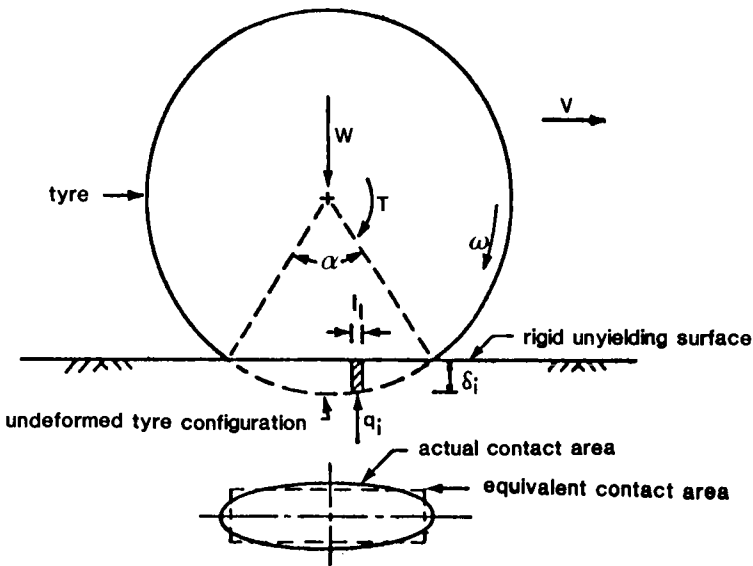


Fig. 7.44. Tyre moving on rigid unyielding surface.

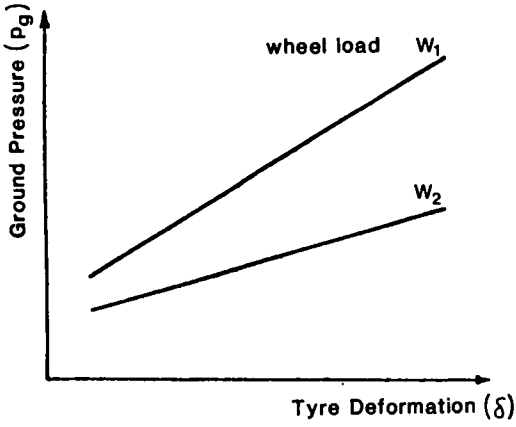


Fig. 7.45. Typical relationship of ground pressure and tyre deformation.

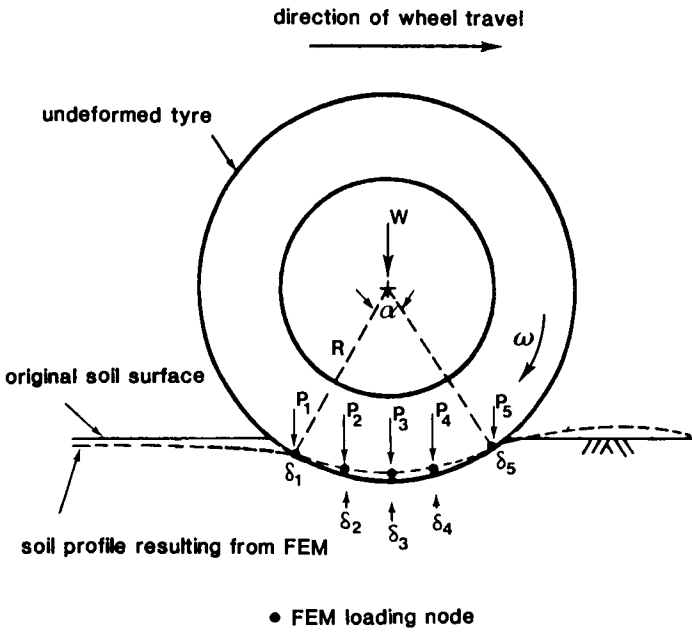


Fig. 7.46. Determination of tyre deformation.

$$E_t = \frac{B \cdot \sum_{i=1}^n P_i \cdot \delta_i}{(X_n - X_1)} \quad (7.20)$$

where E_t = tyre deformation energy per unit travel distance;

B = tyre width;

P_i = normal concentrated load at node i ;

δ_i = tyre deformation at node i ;

n = number of nodes along the tyre-soil contact area;

X_n = horizontal coordinate of the last node at tyre-soil interface and

X_1 = horizontal coordinate of the first node at tyre-soil interface.

Tyre deformation energy in terms of energy per unit time can be calculated as follows:

$$E_t' = E_t \cdot v \quad (7.21)$$

where v is the tyre translational velocity.

We note from eqs.(7.20) or (7.21) that the tyre deformation energy (E_t or E_t') can be evaluated with a knowledge of the contact area. This can be predicted in accordance with the procedure shown in Fig. 7.37, and the soil stiffness encountered (Yong et al., 1978b). Assuming as a first approximation that the contact area is not affected by the slip rate, as indicated in Fig. 7.42, the tyre deformation energy can then be predicted as if the tyre is stationary.

To begin the analysis, the tyre-soil contact area is first predicted with the knowledge of the soil elastic modulus determined by standard-soil testing techniques, such as that used in soil mechanics and geotechnical engineering (e.g. triaxial test). The tyre elastic modulus shown in Fig. 7.47 can be obtained by using the Hertz contact theory, eqs.(7.15) or (7.18). From Fig. 7.47, it can be seen that within a certain range of wheel load, the tyre elastic modulus varies slightly with the applied wheel load, and is not sensitive to the changes in the slip rate as shown by contact areas. Once the tyre-soil contact area is defined, the normal pressure intensity controlled by the wheel load can be determined by idealizing the distribution pattern in a parabolic form or any other chosen configuration, as might be indicated from tests or experience (Yong et al., 1978b). The finite element analysis can then be implemented to solve for the resultant subsoil displacement and tyre deformation energy can be calculated according to eqs.(7.20) or (7.21).

B. Soil deformation energy. This is the energy dissipated in deforming the soil beneath the moving wheel; the technique for its calculation has been presented in Chapter 6.

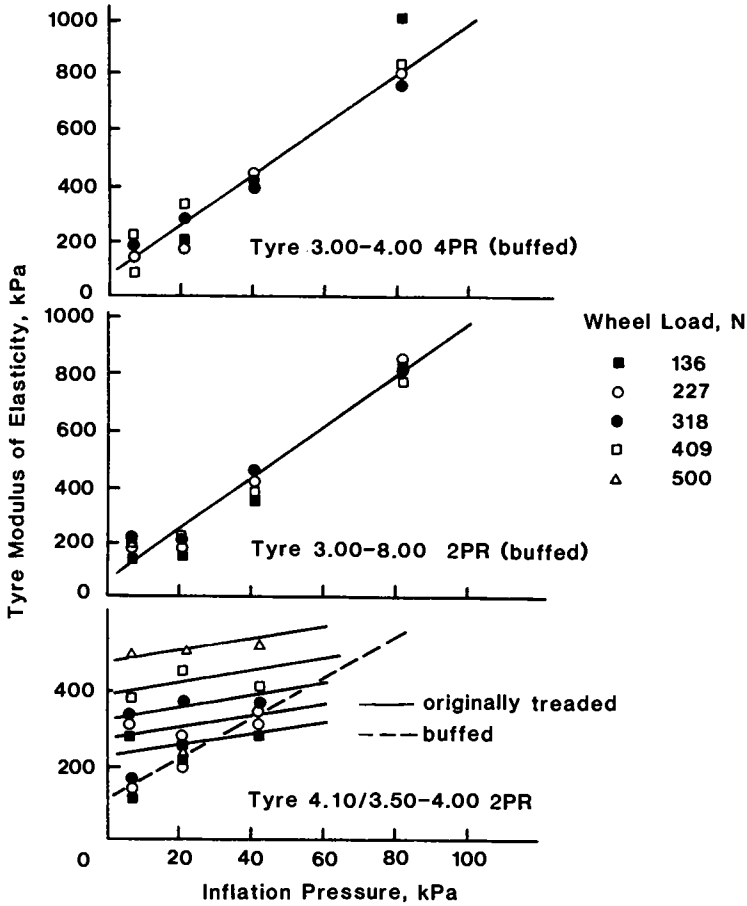


Fig. 7.47. Tyre modulus and inflation pressure relationship.

C. Tyre-soil interfacial slip energy. The energy dissipated at the tyre-soil interface is a function of (a) magnitude and distribution of tangential stresses at the tyre-soil interface, (b) degree of slip, and (c) tyre-soil contact area dimensions. Methods of calculating this energy were presented previously in Chapters 2 and 5. In finite element modelling, the following equation can be adopted for determining the tyre-soil interfacial energy, (Fig. 7.46):

$$E_f = B \cdot \sum_{i=1}^n \tau_i \cdot V_{si} \tag{7.22}$$

where E_f = interfacial energy per unit travel time;
 B = tyre width;

- τ_i = interfacial tangential force at node i ;
 V_{si} = tyre-soil slip velocity at node i and
 n = number of nodal points at tyre-soil interface.

The total dissipation energy is the sum of the following component energies, (1) tyre deformation, (2) soil deformation, and (3) tyre-soil interfacial energy.

D. Input energy. The input energy is the energy required to keep the tyre in constant travel. It is equal to the sum of the different types of dissipated energy and the required useful output energy. It is generated by mobilizing a certain amount of tractive effort at the tyre-soil interface which is sufficient to overcome all types of tyre motion resistance. If the maximum mobilized tractive force is less than the tyre motion resistance, the tyre will stall if the tyre-hub cannot generate the torque required to overcome the resistance. The tyre will demonstrate 100 percent slip if the provided torque is higher than the maximum mobilized tractive forces. Methods of evaluating tractive forces have been presented in Chapter 3. The tyre input energy can be calculated as follows, using the aid of Fig. 7.48:

$$E' = B \int_0^L \tau_s V_s dL \quad (7.23)$$

$$= B \int_0^L \tau_s R_s \omega dL \quad (7.24)$$

$$= B \cdot T \cdot \omega \quad (7.25)$$

where E' = input energy, N.m/sec;

B = tyre width, m;

ω = rotational velocity, rad/sec;

R_s = tyre rolling radius, m;

L = tyre contact length, m;

T = tyre input torque, N.m and

V_s = tyre interfacial velocity.

In finite element modelling, eq.(7.23) can be modified as (Fig. 7.46):

$$E' = B \sum_{i=1}^n \tau_i V_{si} \quad (7.26)$$

where n = number of nodal points at tyre-soil interface;

τ_i = tangential force at node i' and

V_{si} = tyre velocity at node i' .

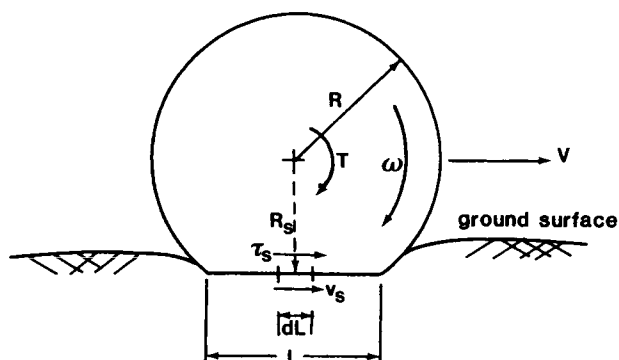


Fig. 7.48. Tyre-soil geometrical characteristics.

E. Energy balance and tyre-soil performance. With a knowledge of the tyre contact area and the normal and tangential stresses established at the loading surface, we can predict the useful output energy since the boundary conditions in the tyre-soil system can be established. For the finite element method, the loaded areas of the contacting tyres at the soil surface are defined by the predicted tyre-soil contact areas such as those shown in Figs. 40 and 41. The normal pressure controlled by the wheel load and the tangential pressure evaluated according to tyre-soil interfacial characteristics, (Chapter 3), are then applied on the contact area - with the soil constitutive relationships established by previously determined or identified stress-strain curves. All the related energy components in the following energy balance eq.(7.27) can then be determined - leading thereby to the determination of the useful output energy required:

$$E = D + E_f + E_t + P_v \quad (7.27)$$

where D = rate of soil deformation energy N.m/sec;

P_v = rate of useful energy = PV , N.m/sec;

V = translational velocity, m/sec, and

P = drawbar-pull, N.

The typical energy balances predicted in this manner using no upper limit on available input energy are shown for the mobility performances of a typical model tyre 4.10/3.50 - 4.002 PR (originally-treaded) for a constant width (Fig. 7.38), for the clayey sand; Figs. 7.49 and 7.50 for inflation pressure 40.2 and 80.4 kPa, respectively. The energy components are presented for unit tyre width and unit time. From the Figures, it is instructive to note that for the clayey sand, an increase in the inflation pressure from 40.2 kPa to 80.4 kPa leads to an increase in the useful output energy, (Yong et al., 1980b). Thus whilst the

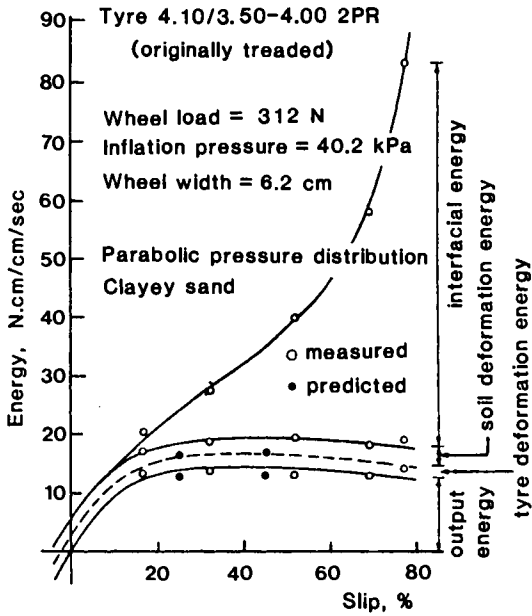


Fig. 7.49. Energy balance (rate) for tyre 4.10/3.50-4.00 2PR (originally-treaded) as a function of slip. Inflation pressure = 40.2 kPa. Load = 312 N.

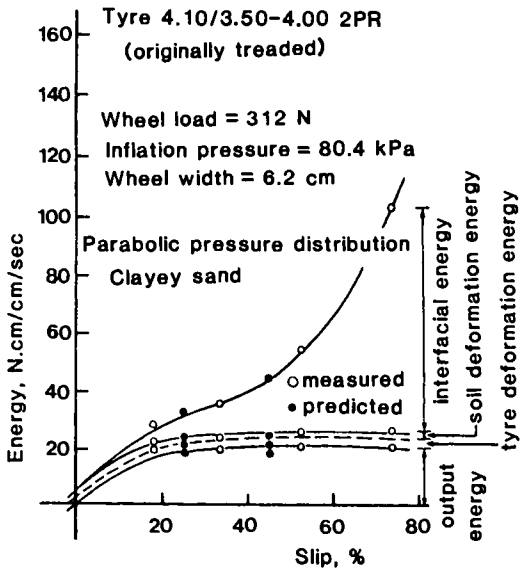


Fig. 7.50. Energy balance (rate) for tyre 4.10/3.50-4.00 2PR (originally-treaded) as a function of slip. Inflation pressure = 80.4 kPa. Load = 312 N.

input energy can be increased by the use of higher inflation pressures, the combined tyre and soil deformation energy measured, (and predicted), may not change significantly. We should be careful to note that whilst tyre deformation energy can be decreased by increasing tyre inflation pressure, soil deformation energy, in turn, may be changed because of the development of higher resistances. The net results of higher effective confining pressures, (Yong et al., 1980b), developed because of increasing normal pressures at the tyre-soil interface, will contribute to the changes in the development of motion resistance. The resultant effects will generally demonstrate themselves in terms of a net increase in the drawbar-pull for a higher inflation pressure - at the price of a higher required input energy.

In the case of the non-friction (kaolinite) clay, Figs. 7.51 and 7.52 indicate that by increasing the inflation pressure from 6.9 kPa to 40.2 kPa, a reduction in useful output energy is obtained. The higher torque at the lower inflation pressure, together with the lower combined tyre and soil deformation energies, all contribute to this reduction to output energy. Increasing the tyre inflation pressure decreases the tyre deformation energy, and increases the soil deformation energy, because of the higher than average normal pressure imposed on the tyre-soil interface.

The studies by Yong et al. (1978, 1980) indicate that tyre flexibility contributes significantly to the development of all the energy components (eq.7.27) in the tyre-soil system. Contrasting performances in the tyre can be obtained because of the properties and characteristics of the supporting soil. An increase in the tyre inflation pressure may allow for a favourable increase in the drawbar-pull in one soil (frictional), so long as the input energy available can be increased, whilst the reverse may be true in the case of a non-frictional soil (clay). The finite element model, if properly used, can account for tyre flexibility, as shown in Figs. 7.49 to 7.52.

7.7 SUMMARY

The application of the Finite Element Method (FEM) of analysis as a procedure for modelling and analysis/prediction of traction via tracks or wheels can lead to very successful results. The burden of responsibility in production of realistic (and obviously successful predictions) results lies in one's capability in properly modelling the situation at hand. In addition, it is imperative that the physical inputs and boundary conditions used in the implementation of the FEM be properly and accurately performed. The model and the answers derived will only be as good as the quality of information provided in implementing the analysis.

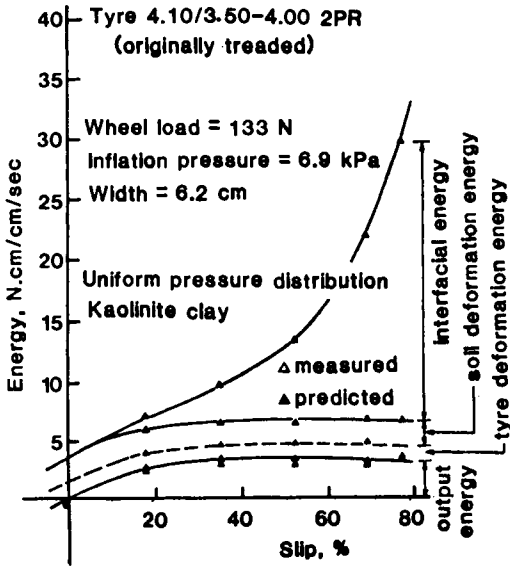


Fig. 7.51. Energy balance (rate) for tyre 4.10/3.50-4.00 2PR (originally-treaded) as a function of slip. Inflation pressure = 6.9 kPa. Load = 133 N.

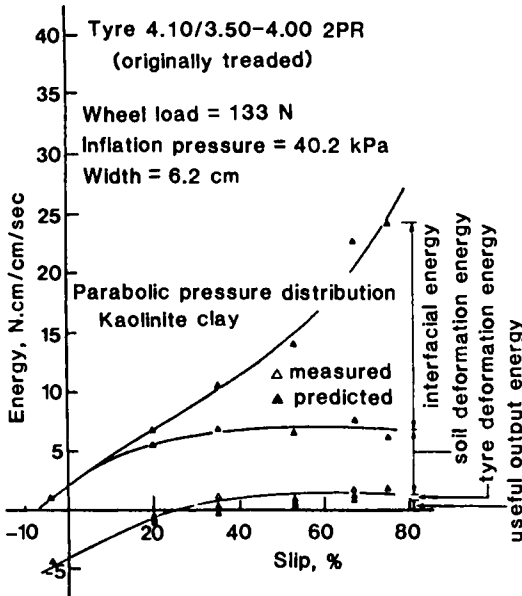


Fig. 7.52. Energy balance (rate) for tyre 4.10/3.50-4.00 2PR (originally-treaded) as a function of slip. Inflation pressure = 40.2 kPa. Load = 133 N.

REFERENCES

- Abeels, P.F.J., 1976. Tyre deflection and contact studies. *J. Terramechanics*, 13-3:183-196.
- Bekker, M.G., 1969. Introduction to Terrain-Vehicle Systems. The University of Michigan Press, Ann Arbor, Michigan, 846 p.
- Bekker, M.G. and Semonin, E.V., 1975. Motion resistance of pneumatic tyres. *J. Automotive Engineering*, April, pp. 6-10.
- Desai, C.S. and Abel, J.F., 1972. Introduction to the Finite Element Method. Van Nostrand Reinhold Company, New York, 477 p.
- Hertz, H., 1881. Ueber die Beruehrung fester elastischer Koeper, *Z. Reine Angew. Math.*, 92:156-171.
- Komandi, G., 1976. The determination of the deflection, contact area, dimensions, and load-carrying capacity for driven pneumatic tyres operating on concrete pavement. *J. Terramechanics*, 13-1:15-20.
- Lambe, T.W. and Whitman, R.V., 1969. Soil Mechanics. Wiley and Sons, Inc., New York, 553 p.
- Lubkin, J.L., 1962. Contact Problems. Handbook of Engineering Mechanics, Ed. by W. Flugge, McGraw-Hill, New York, Chapter 42.
- Mindlin, R.D. 1949. Compliance of elastic bodies in contact. *J. Applied Mechanics*, 16:259-268.
- Poritsky, H., 1950. Stresses and deflection of cylindrical bodies in contact with application to contact of gears and of locomotive wheels. *J. Applied Mechanics*, 17:191-201.
- Sohne, W., 1969. Agricultural engineering and terramechanics. *J. Terramechanics*, 6-4:9-30.
- Yong, R.N. and Hanna, A.W., 1977. Finite element analysis of plane soil cutting. *J. Terramechanics*, 14-3:103-125.
- Yong, R.N., Boonsinsuk, P. and Fattah, E.A., 1978a. Prediction of tyre performance on soft soils relative to carcass stiffness and contact areas. Proc. 6th Int. Conf. Int. Soc. Ter-Veh. Systems, ISTVS, Vienna, 11:643-675.
- Yong, R.N., Fattah, E.A. and Boonsinsuk, P., 1978b. Analysis and prediction of tyre-soil interaction and performance using finite elements. *J. Terramechanics*, 15-1:43-63.
- Yong, R.N., Youssef, A.F. and El-Mamlouk, H., 1979. Soil deformation and slip relative to grouser shape and spacing. *J. Terramechanics*, 14-3:103-125.
- Yong, R.N., El-Mamlouk, H. and Della-Moretta, L., 1980a. Evaluation and prediction of energy losses in track-terrain interaction. *J. Terramechanics*, 17-2: 79-100.
- Yong, R.N., Boonsinsuk, P. and Fattah, E.A., 1980b. Tyre flexibility and mobility on soft soils. *J. Terramechanics*, 17-1:43-58.
- Yong, R.N., Boonsinsuk, P. and Fattah, E.A., 1980c. Tyre load capacity and energy loss with respect to varying soil support stiffness. *J. Terramechanics*, 17-2: 131-147.

NOMENCLATURE

B	tyre width
C	compaction energy
C'	specific compaction energy
CDE	coefficient at dissipated energy
CE	compaction energy rate or coefficient of input energy
CP	coefficient of output energy
D	deformation energy loss, distortion energy or tyre diameter
D'	specific distortion energy
DE	distortion energy rate
E'	input energy
E_i	specific input energy
E_f	interfacial energy per unit travel time
E_t	deformation energy per unit travel distance
E_1, E_2	cylinders' moduli of elasticity
F	applied force
I	interfacial energy loss
L	contact length
M	torque
P	drawbar-pull or load per unit width
P_i	normal load
P_g	uniform ground contact pressure
R_s	rolling radius
R_t	motion resistance
R_1, R_2	undeformed cylinder radii
S	shear slip energy
S'	specific shear slip energy
SE	shear slip energy rate
T	tangential force, torque or mobilized traction
V	elemental volume
V_s	interfacial velocity
V_{si}	tyre-soil slip velocity
W	weight
b	track width
ds	incremental displacement

d [ϵ]	incremental strain matrix
h	carcass height
n	number of nodal points
p	vertical pressure
p_i	inflation pressure
r	radius
t	increment duration
v	translational velocity
v_c	vehicle velocity
δ	tyre deformation
ϵ	energy recovery factor
μ	coefficient of friction
ν_1, ν_2	Poisson's ratios
σ_x, σ_y	normal stresses
$[\sigma]$	stress matrix
τ	tangential stress
τ_i	interfacial tangential force
τ_{xy}	shear stress
ω	angular velocity

Chapter 8

COMPACTION

8.1 INTRODUCTION

Soil compaction constitutes one of the main applications of soil-vehicle traction mechanics. A proper selection of the type of roller compactor and specification for compaction - according to the soil type - can play an important part in the compactibility of the soil. We should note that whilst efficient and proper compaction are desirable features in construction engineering and soil engineering, these same aspects can be detrimental in such fields as agriculture or forestry, where a change in physical and mechanical characteristics of the soil would severely inhibit the capability of the soil to provide proper water-uptake to the plant root systems.

In the translating motion of off-road vehicles on initially unprepared ground, compaction of the soil occurs under the front set of wheels as well as the rear set. However, because the rear set of wheels will meet the soil partly compacted by the front set of wheels, the motion resistance to the rear set of wheels will be generally lesser. Thus, in computing the motion resistance for vehicles, there is considerable value in providing separate computations for motion resistances to the front sets and trailing sets of wheels, especially if the soil is highly compactible. A knowledge of soil compactibility and developed motion resistance would be highly desirable. In this Chapter, the elements of soil compactibility and prediction are addressed.

The objective of soil compaction in the field by moving rollers is to provide for production of a competent soil bearing stratum. The increased densification of the soil, together with the reduction in permeability of the compacted soil, combine to ensure that the developed, greater, compacted strength is maintained for a long time duration.

In field soil compaction, a layer of loose soil is compacted until its density and strength reach specific values established a priori from laboratory tests, and until the density and strength are approximately similar to the underlying layers of soil previously compacted. The objective of field soil compaction is to obtain specified characteristics with a minimum number of passes of the roller, or with a minimum amount of roller input energy (work) done.

In general, the compaction of layers of soil is accelerated by increasing the magnitude of roller-imposed normal stresses established at the roller-soil interface through the passage of the roller. However, if the roller-imposed normal stresses far exceed the local bearing capacity of the soil, i.e. if excessive local shear failure occurs, the soil will tend to extrude or flow under the

roller instead of compacting.

The value of imposed normal stress can be increased by increasing roller load in the case of rigid rollers, and/or changing surface configuration of the roller (sheepsfoot-kneading compaction), and increasing tyre load or increasing inflation pressure in the case of rubber-tyre rollers. Excessive sinkage and roller immobilization can occur if the general bearing strength of the soil is far exceeded. The required work done (input energy) by a roller to produce a specific degree of compaction is a function of:

- (i) Load. Static, sinusoidal, impact.
- (ii) Roller type. Solid (rigid) roller, pneumatic tyre roller, number of tyres in the roller, arrangement, roller load and speed.
- (iii) Tyre characteristics. Diameter, width, cross-sectional shape, inflation pressure, carcass stiffness and shape, tyre structure and tyre material mechanical properties.
- (iv) Soil. All the factors which control stress-strain behaviour of the soil during loading and unloading, such as; soil type, density, moisture content, soil structure, confining pressure, etc.

8.2 COMPACTION MECHANISMS

There are in general two types of compaction mechanisms, one for granular soil and the other for cohesive soil. The two mechanisms are different since the particle forces and the parameters which control soil properties are different for the two soil types.

8.2.1 Granular soil compaction

In granular soil, where the influence of surface forces is negligible, the arrangement of particles contributes mainly to the density of the soil and hence to its strength and manner of deformation.

The packing of grains of soil or other particular media is very strongly influenced by particle shape and size distribution. A knowledge of optimum packing conditions is desirable since soil-engineering problems concerned with stability, such as subgrade fill and embankments, require optimum density of the granular material for development of maximum resistance to shear displacement. The same requirement applies to the aggregates for concrete and bituminous mixtures. This requires a particular range of grain sizes to fill the voids created by packing particles which are either angular (e.g. crushed stone products) or rounded (e.g. river-washed gravels and sands). Figure 8.1 shows the required particle-size distribution for optimum packing based upon the condition of four large, rounded, particles as initial constraints. While this is an ideal situation, it demonstrates the need for an ideal distribution of grain sizes to achieve optimum density.

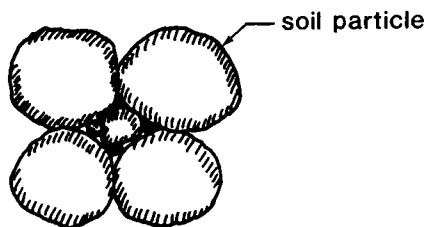


Fig. 8.1. Ideal particle-size distribution for optimum packing.

Ideal grain size distributions generally do not exist in natural soils. Figure 8.1 shows the required grain size distribution to fit the void spaces, and establishes one end of the scale. The other end of the packing spectrum is obtained by selecting particles of the same size. This means taking only the four large particles shown in Fig. 8.1 without having smaller particles filling the voids. It is possible to obtain various kinds of packing with uniform spheres. Maximum porosity for regular packing is obtained with a cubic packing (open packing), and minimum porosity exists in the tetrahedral rhombic packing (close packing). These are shown in Fig. 8.2.

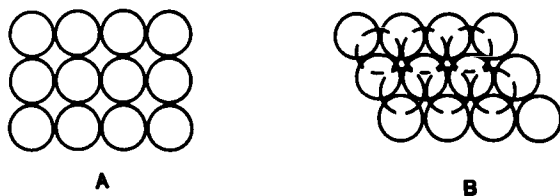


Fig. 8.2. Ideal packing of spheres. A. Simple cubic packing. B. Rhombic packing.

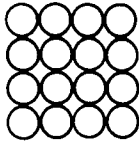
The five modes of regular packing that may be achieved by spheres of equal radius R , are (a) simple cubic, (b) cubic tetrahedral, (c) tetragonal spheroidal, (d) pyramidal, and (e) tetrahedral.

Defining the coordination number as the number of spheres in contact with any given sphere, and the density of packing D_p as the ratio of the volume of space occupied by solid matter to total volume, the porosity-density relationships for the five modes of packing may be arrived at (Table 8.1). The arrangement for the modes of packing is given in Fig. 8.3.

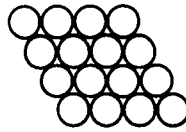
The number of adjacent particles in contact with any particle is related to porosity. The distribution of coordination number for several porosities, using stacked lead shot in a large cylindrical vessel to simulate well-packed aggregate, is shown in Fig. 8.4.

TABLE 8.1
Packing of spheres

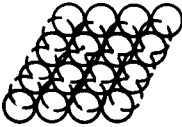
Type of packing	Coordination number	Spacing of layers	Volume of unit prism	Density	Porosity (%)
Simple cubic	66	2R	$8R^3$	$\pi/6$ (0.5236)	47.64
Cubic tetrahedral	88	2R	$4\sqrt{3}R^3$	$\pi/3\sqrt{3}$ (0.6046)	39.54
Tetragonal spheroidal	10	$R\sqrt{3}$	$6R^3$	$2\pi/9$ (0.6981)	30.19
Pyramidal	12	$R\sqrt{2}$	$4\sqrt{2}R^3$	$\pi/3\sqrt{2}$ (0.7405)	25.95
Tetrahedral	12	$2R\sqrt{2/3}$	$4/3 R^3$	$\pi/3\sqrt{2}$	25.95



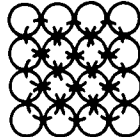
(a) Simple Cubic



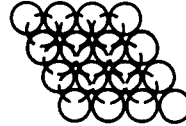
(b) Cubic Tetrahedral



(c) Tetragonal Spheroidal



(d) Pyramidal



(e) Tetrahedral

Fig. 8.3. Models of regular packing of equal spheres (Deresiewicz, 1958).

The relationship between the average number of contacts per sphere and porosity n may be obtained by assuming that statistically the grouping of the spheres as a whole may be regarded as groups of close-packed spheres in cubic array. Using m to represent the fraction of close-packed spheres, we have:

$$n = mn_{c.p.} + (1 - m)n_{cub} \quad (8.1)$$

where the subscripts c.p. and cub represent close-packed and cubic, respectively. On a unit volume basis, the average number of contacts N per square will be obtained as:

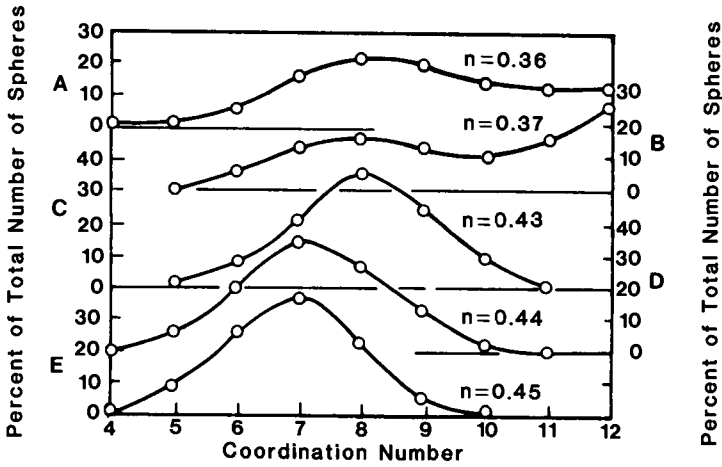


Fig. 8.4. Distribution of coordination number at several porosities (Smith et al., 1929).

$$N = \frac{\frac{N_{c.p.}}{V_{c.p.}} + (1 - m)\frac{N_{cub}}{V_{cub}}}{\frac{m}{V_{c.p.}} + \frac{(1 - m)}{V_{cub}}} \quad (8.2)$$

where $V_{c.p.}$ and V_{cub} represent the volume of close-packed and cubic array of spheres in terms of R , the radius of the spheres. The values of $N_{c.p.}$, N_{cub} , $V_{c.p.}$ and V_{cub} , may be obtained from Table 8.1. In this instance, $N_{c.p.}$ and $V_{c.p.}$ may be taken as either the pyramidal or tetrahedral type of packing.

Thus, from eqs.(8.1) and (8.2):

$$N = \frac{1}{\sqrt{2}-1} \left[6(2\sqrt{2}-1) - \frac{\pi\sqrt{2}}{1-n} \right]$$

which reduces to:

$$N = 26.4858 - \frac{10.77262}{1-n} \quad (8.3)$$

For particles of non-uniform size, porosity may be reduced if interstitial particles are available to fill the void spaces created by the larger particles, as in Fig. 8.1. The combination of packing that one can obtain is a function of gradation of particles, particle shape, texture and manner of placement.

The packing of unequal spheres, which represents real systems more closely, may be studied mathematically. In doing so, it is necessary to prescribe a set

of limiting conditions. The study by Wise (1952), for example, requires that one large sphere A be taken such that all other spheres of smaller sizes may be placed on its surface. The first two spheres must not only contact each other, but also touch A. Each new subsequent sphere to be added must touch, in addition to A, at least two others which are in contact with each other (Fig. 8.5). The network of triangles formed by joining the centres of spheres surrounding one sphere (shown in Fig. 8.5), should provide for triangles on different planes. A polyhedron is obtained if the vertices are joined to the centre of sphere A, since these triangles are, in effect, the faces of a polyhedron whose vertices are the centres of the spheres. Thus a set of tetrahedra associated with any given sphere may be obtained.

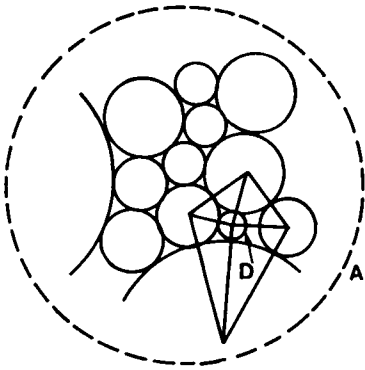


Fig. 8.5. Dense random packing of unequal spheres (Deresiewicz, 1958).

Wise (1952) expressed the properties of packing for the four radii in each tetrahedron in terms of a probability distribution function. In the case where the logarithms of the radii conform to a normal distribution of standard deviation $s = 0.4$, a mean radius of 1.08 and estimated mean density of packing of 0.8 is obtained. Figure 8.6 shows the distribution of spheres and the mean coordination number for a sphere with radius R .

Examination of the porosity of mixtures consisting of two sets of spheres with equal diameters, shows that the void volume in the experimentally loosest condition of the mixture is always smaller than that of the individual components under identical test conditions. The results given by Furnas (1931) for a mixture of two different grain sizes are shown in Fig. 8.7. In this case, the normal porosity value of the mixtures was $n = 50\%$, and the different curves shown in the Figure pertain to the different diameter ratios of the larger and smaller particles. The minimum porosity can be found for any d_1/d_2 diameter ratio, with an intermediate mixing proportion - as seen from Fig. 8.7. Note that the ratio $d_1/d_2 = 0$ refers to the case when the voids of a relatively coarse-grain skeleton (sand) are completely filled by very fine soil.

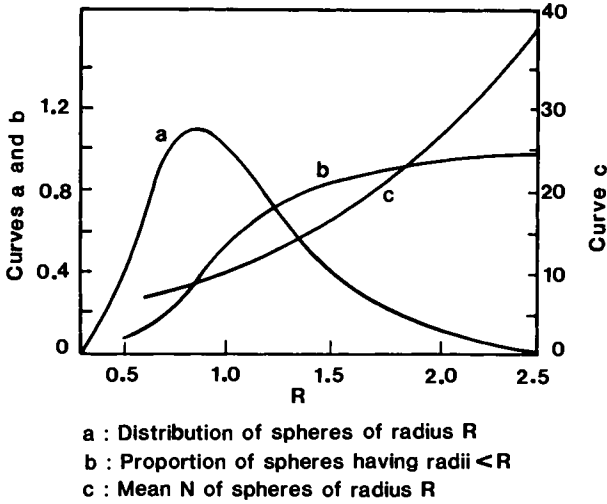


Fig. 8.6. Dense random packing of spheres having radii obeying a log-normal distribution of standard deviation = 0.4 (Deresiewicz, 1958).

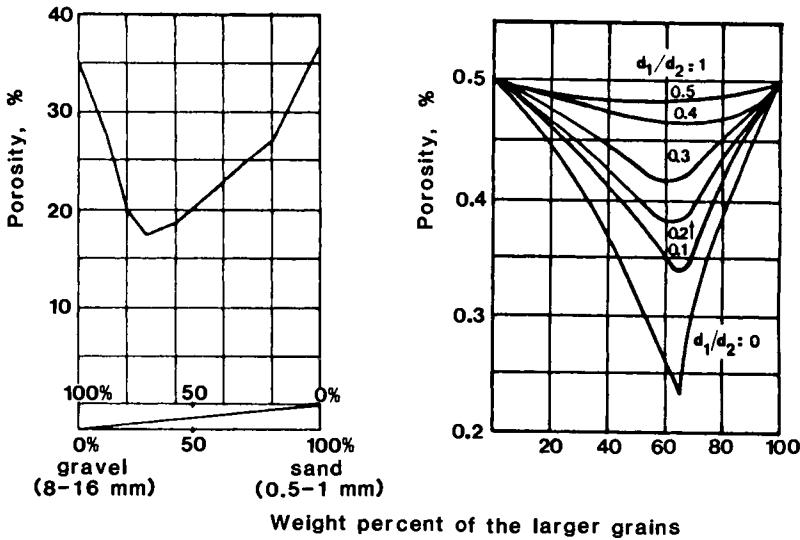


Fig. 8.7. Compactness of two-component mixtures.

Figure 8.8 shows the effect of a mixture of sand and clay on the dry density of the mix. In engineering practice and especially for stability considerations, optimum packing of granular particles is needed. Not only is shear strength increased through more particle contact and lateral support, but volume change

(subsidence and compression) through both particle rearrangement and compression is reduced because of optimum packing. With loose packing there is a tendency for particles to readjust to new positions of equilibrium under external stress, to attain a minimum potential energy level. This readjustment may be detrimental since it results in volume change. To avoid problems arising from loose packing of sub-surface granular material, it is necessary to compact the material prior to construction on the material. For shallow deposits of loose material, a vibratory compactor may be used successfully. For deep deposits of loose material it is necessary to resort to piling to achieve denser packing. Piledriving serves to vibrate the immediate vicinity of the pile, in addition to the use of the support itself.

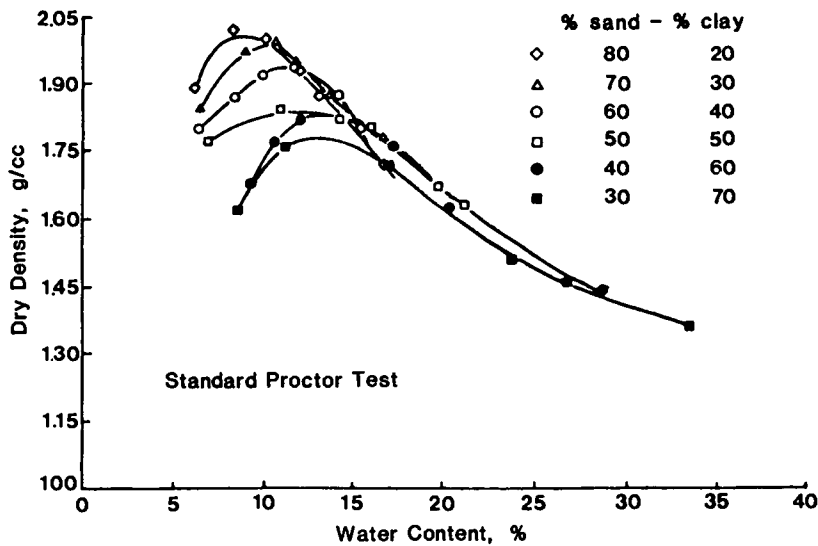


Fig. 8.8. Compaction curves for different proportions of clay-sand mixtures.

8.2.2 Cohesive soil

Figure 8.9 shows a characteristic soil moisture curve which relates the moisture water content to the compacted density of a cohesive soil. The lower curve is the relationship derived for a lower compactive effort. To explain the compaction process, Lambe (1958a) used the concept of "water deficiency" for the situation where any given soil particle under any given state of stress which requires a certain amount of water to fully develop its interaction potential with the neighbouring particles. The concept of particle interaction and theories relating to interparticle action are developed in detail in Yong and Warkentin (1975). For the present it is sufficient to note that the difference between this needed water, and the existing water in the compacted clay soil, is the

deficient water which the clay particle will try to absorb. The amount of water used in clay soil compaction is almost always less than that wanted by the soil; nearly all compacted plastic soils in the as-moulded state have a deficiency in water (Lambe, 1958a).

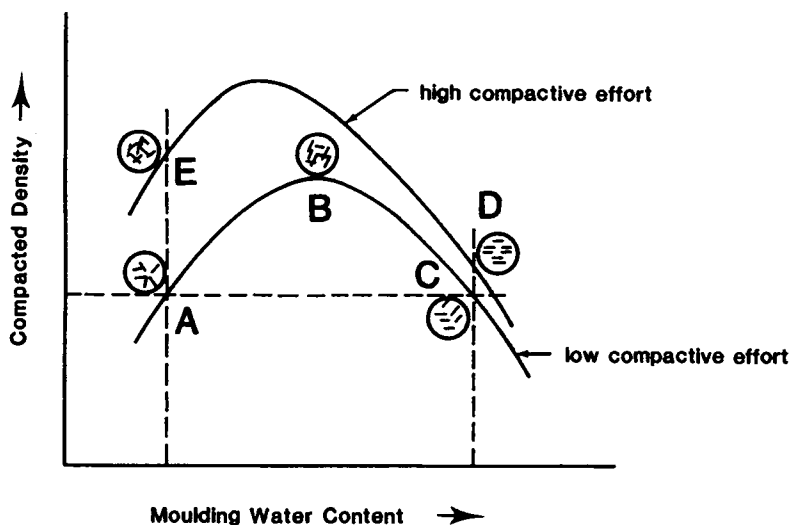


Fig. 8.9. Effects of compaction on structure (Lambe, 1958a).

At W_A in Fig. 8.9, there is insufficient water for the diffuse double layers of the soil colloids to develop fully. The resultant effect is a tendency toward flocculation of the soil particles (low degree of particle orientation and low density).

Beyond the optimum point, where the interaction potential is fully developed, a further increase of water from W_B to W_C results in dilution of the system. Thus, whilst the net effect is to provide a more orderly arrangement of particles at W_C than at W_B , the density of C is lower because the added water has diluted the concentration of soil particles per volume.

Figure 8.9 also shows what happens to soil structure when the compactive efforts, and thus compacted density, are increased. The greater the input work, the more oriented are the clay particles and, in general, the closer is the particle spacing. At high compaction water contents (and high degrees of saturation) increased compactive efforts may merely align particles (i.e. cause more particles to reach an oriented configuration) without significantly altering the particle spacing.

8.3 FACTORS INFLUENCING SOIL COMPACTIBILITY

The major factors which can influence the compactibility of soil are:

(i) Type of compaction. There are different types of compaction. These are: static, kneading, impact and transient (sinusoidal). These various types of compaction techniques produce different compactive products, mainly due to the manner in which the soil particles are arranged in the compaction procedure - and in the efficient development of the interaction potential. Figure 8.10 shows the effect of different roller compactions on a fine crushed rock and a medium clay.

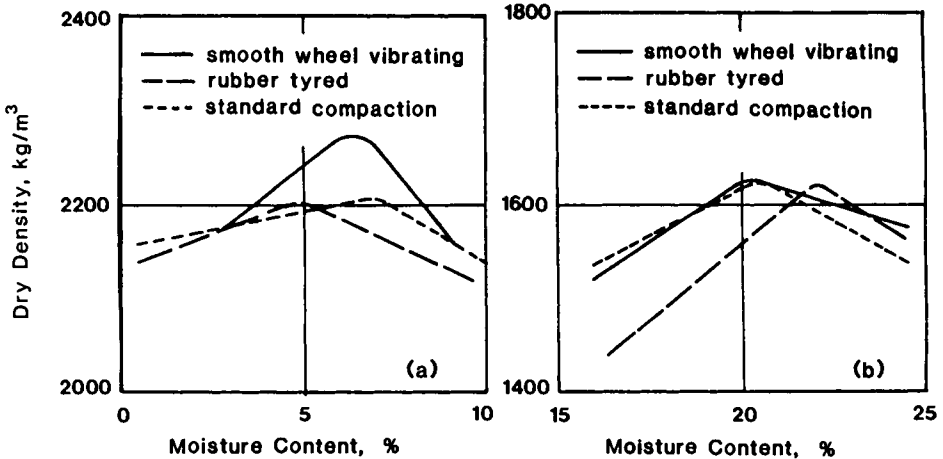


Fig. 8.10. Effect of different roller compactions. (a) Fine crushed rock. (b) A medium clay (adopted from Morris and Tynan, 1968).

The effect of types of compaction on stress deformation behaviour of cohesive soil is shown in Figs. 8.11 to 8.13. The effect of compaction conditions on the developed strength of clay soil has been previously investigated by Pacey (1956) and Lambe (1958b) from which it can be concluded that:

- increased compactive effort, dry of optimum, increases strength,
- increased compactive effort, wet of optimum, can result in a gain or loss of strength; the effect is small (Fig. 8.14),
- for the same compactive effort and same compacted density, dry-side compaction gives a higher strength than does wet-side compaction.

(ii) Amount of compaction. For any method of compaction, and for any clay at a given water content, the greater the compactive work, the greater is the resultant compacted density (particles closer together) - up to a certain value (critical density) beyond which any increase in compactive work will produce no appreciable difference in the compacted soil density (Fig. 8.15). The effect of roller load and surface configuration on soil compactibility has been investigated by Fattah et al. (1981). Figure 8.16 shows the compacted densities and den-

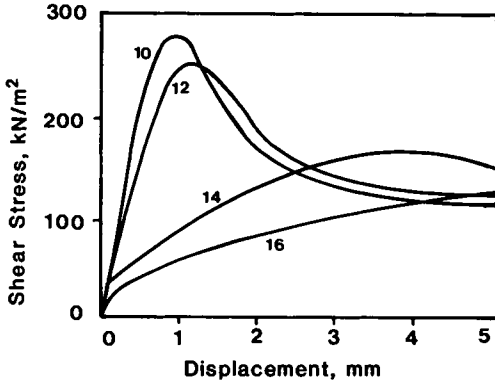


Fig. 8.11. Shear stress:displacement relations for AASHTO T 99 compaction at different moisture contents (Bell, 1977).

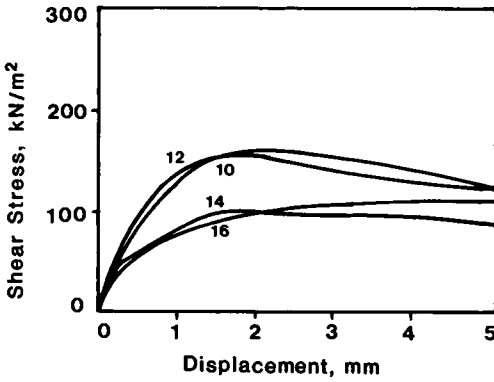


Fig. 8.12. Shear stress:displacement relations for static compaction equivalent to AASHTO T 99 compaction at different moisture contents (Bell, 1977).

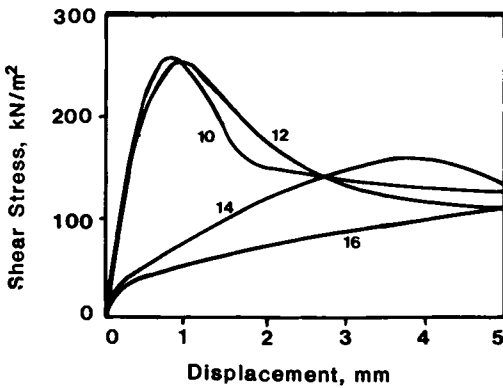


Fig. 8.13. Shear stress:displacement relations for kneading compaction equivalent to AASHTO T 99 compaction at different moisture contents (Bell, 1977).

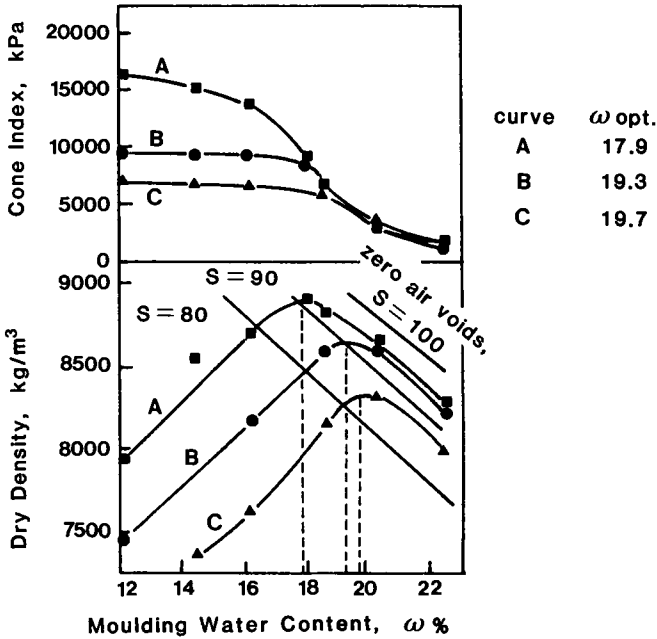


Fig. 8.14. Cone index and dry density vs moulding water content for Boston Blue Clay (adapted from Pacey, 1956).

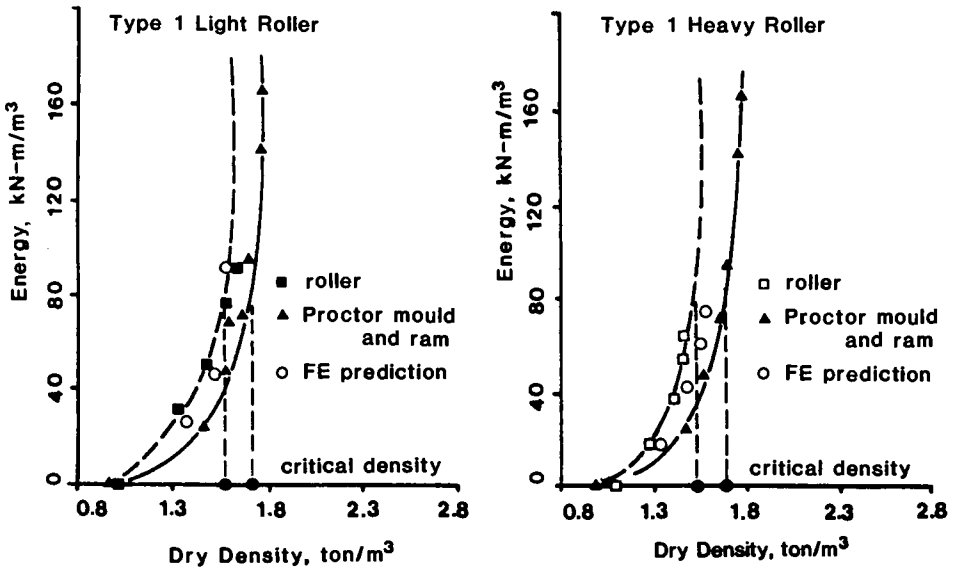


Fig. 8.15. Compaction energy - dry density relationships.

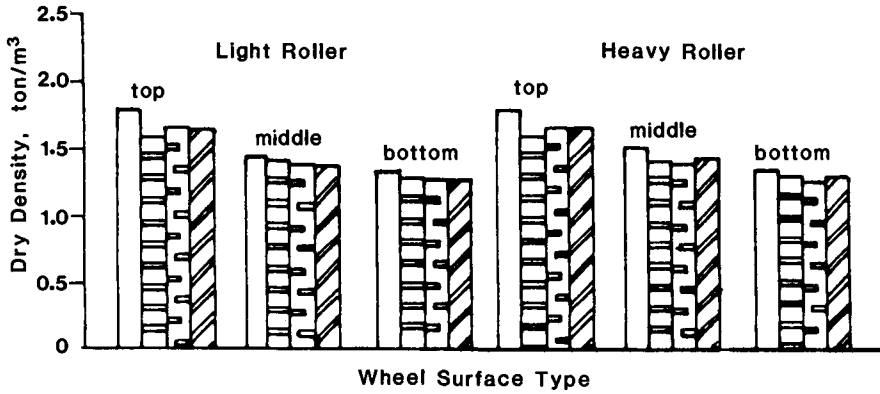


Fig. 8.16. Dry density profiles after sixteen passes.

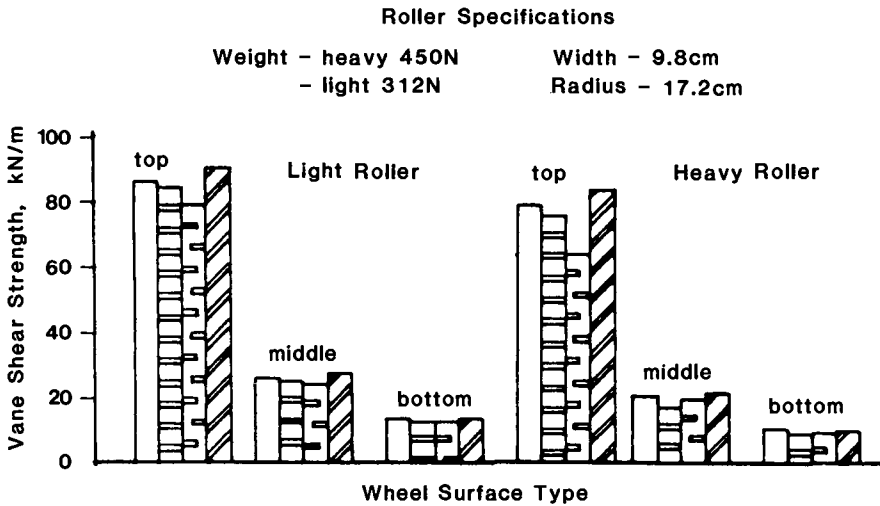


Fig. 8.17. Soil strength profiles after sixteen passes.

sity profiles obtained in compaction, using four different types of wheel surface configuration, whilst Fig. 8.17 shows the shear strength profiles developed for these same tests. The correlation between strength and density is obvious and can be noted in the Figures. The higher the dry density, the higher is the shear strength. As might be expected, the higher densities are found in the upper part of the compacted soil - indicative of the efficiency of the total compactive effort (Fig. 8.18).

Figures 8.19 and 8.20 show typical motion resistance and sinkage for a roller as a function of the number of passes. From the results shown in Figs. 8.15 to 8.20, it is noted that for certain roller characteristics, the soil properties remain fairly unchanged after a certain number of passes.

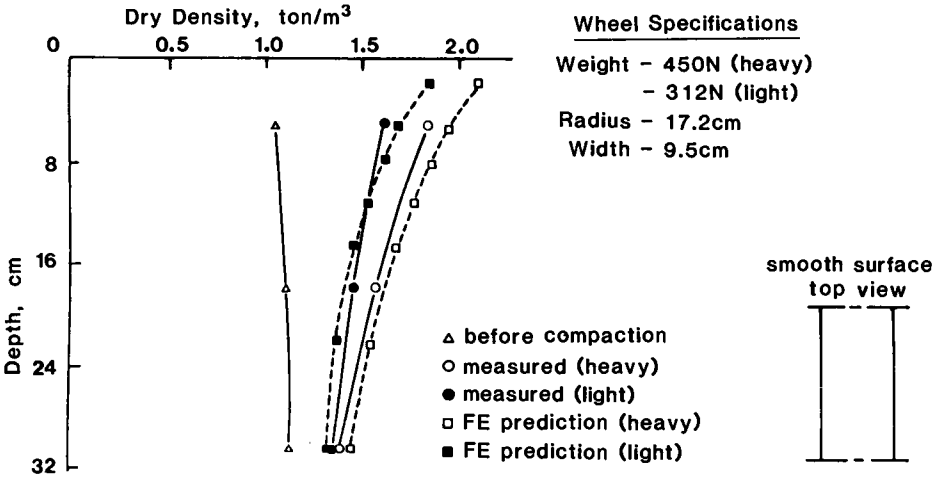


Fig. 8.18. Dry density vs depth after sixteen passes.

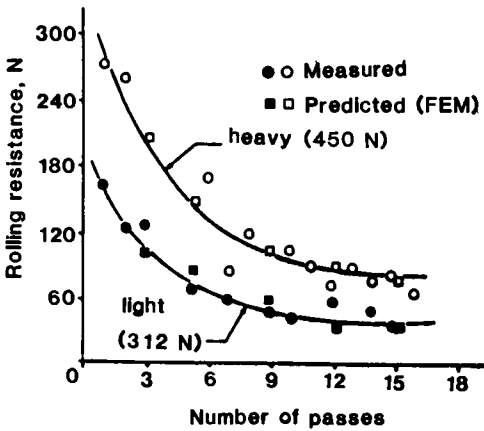


Fig. 8.19. Effect of number of passes on towed roller motion resistance.

8.4 PREDICTION OF COMPACTION USING FINITE ELEMENT METHOD

8.4.1 Introduction

The general procedure for specification of size and capability of roller equipment for compaction of soil fill material is one which depends to a very large extent on prior experience and assessment of results obtained from laboratory compaction tests on the soil fill material. The questions that need to be answered in a compaction program can be stated simply as follows:

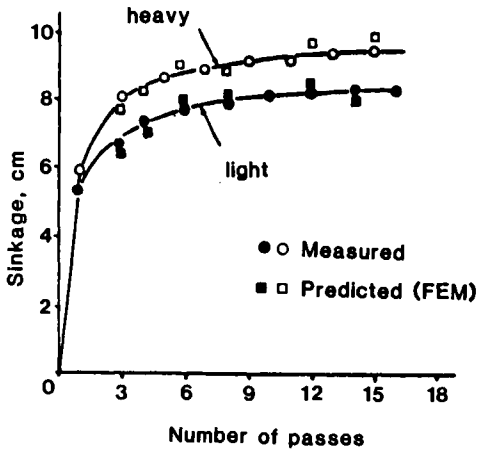


Fig. 8.20. Effect of number of passes on soil surface deformation.

1. What type and size of roller?
2. Lift thickness? Number of passes? Soil water content?

The answers to the above questions are not always sought through rigorous analytical means because of the lack of analytical models which deal specifically with the coupled surface interaction between roller and soil.

The problem of interest is one which is posed in terms of roller compaction efficiency, i.e. "How efficient is a particular roller in compacting a specified (known) soil?". The input energy (work done) required by a roller to produce a specific degree of compaction is a function of (a) roller type, (b) roller loading, (c) tyre properties and characteristics, and (d) soil. Efficient soil compaction matches the soil response (load/rebound) characteristics with lift thickness, number of passes and roller loading features to produce the maximum soil density for the desired fill thickness with the least amount of input work (roller passes and energy input).

In finite element modelling, soil compaction under a moving roller is predicted in terms of:

- (a) amount of work done in compaction per unit distance travelled by a moving roller for every pass, and
- (b) the total work required to produce a certain soil density or permanent deformation of the soil layer.

The format of the finite element analysis encompasses the transient loading nature of the roller (or tyre). By expressing the compaction effort delivered by a rigid roller in terms of the amount of compaction energy required to produce a specific resultant dry density of a particular soil lift thickness, the FEM analysis allows one to obtain an evaluation of soil type influence, lift thickness,

water content, number of passes, etc. on compaction efficiency. Roller compaction efficiency can be evaluated by comparing the work spent by the roller to produce certain density to that obtained in a standard Proctor test. Expressing compaction "efficiency" with reference to the standard Proctor test technique is arbitrary - i.e. the standard Proctor density is taken as "optimum" for a convenient reference state.

8.4.2 Method of analysis

The performance of a roller moving with constant speed on a soil surface is analysed similarly to that of a wheel (Chapters 6 and 7) by applying the principle of energy conservation. As in the wheel analysis (Chapter 5) the energy balance relationship equates the roller input energy (powered roller) or pull energy (towed roller), to the sum of the following energy components (Fig. 8.21).

(a) Energy spent in compacting the soil.

(b) Energy dissipated at roller-soil interface through slip between roller and soil surface (= 0 for towed roller).

(c) Energy dissipated because of distortion of the roller under load. This form of energy dissipation is negligibly small in the case of rigid rollers.

(d) Output energy (powered roller), i.e. drawbar-pull is equal to the towed force for the unpowered roller in the same vehicle.

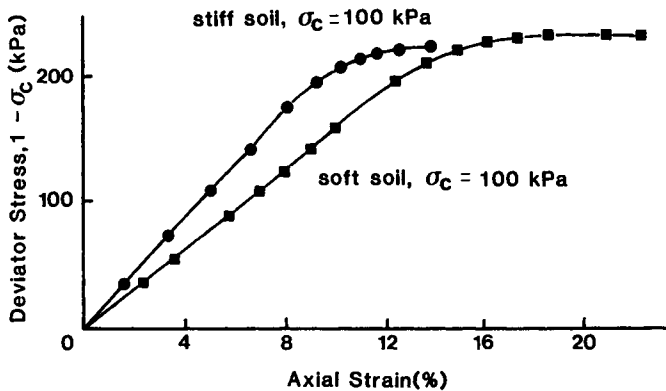


Fig. 8.21. Roller soil energy components.

For convenience in presentation of the analysis, it is assumed that at any stage of roller compaction, the soil continuum consists of two layers, as shown in Fig. 8.22, (Fattah et al., 1981). The underlying soil layer - i.e. the previously compacted layer has reached optimum or close to optimum density, and can be assumed to remain in the "as compacted" state. The soil in this layer behaves as an elastic or rigid material. The top layer is the current soil layer to be compacted, and is analyzed accordingly. If desired, a multi-layered compaction analysis can be performed where the underlying layers are also analyzed and considered as undergoing further densification. However, by and large, the increase in densities in the underlying layers is small - if efficient compaction is achieved - and can be ignored as a first approximation in the analysis given herein.

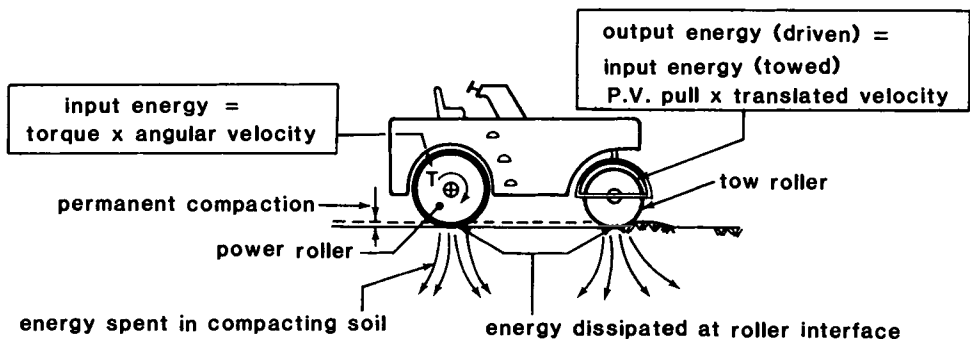


Fig. 8.22. Idealized soil continuum showing a developed two-layer system.

8.4.3. Analytical relationships

The governing equations used for the FEM method of analysis developed for rigid wheel motion and extended for pneumatic tyre motion on soil (Chapter 6), have been adapted for soil compaction analysis, (Fattah et al., 1981), and need not be repeated here.

8.4.4. Boundary conditions

To specify the load boundary at the roller soil interface, the two items required are (Chapter 7), (a) stress-distribution due to roller load and forward motion, and (b) contact area. The interfacial stress distribution can be specified in terms of known distributions based on previously available or reported measurements, as discussed in Chapter 7, (Yong et al., 1980). Methods for determining the roller-soil contact area have been presented in Chapter 7.

8.4.5 Constitutive relations

Since the roller load imposed in compaction is a transient type of loading, any point in the soil continuum is subjected to a state of loading or unloading according to its position with respect to the roller, i.e. for each roller pass the soil is subjected to a complete stress reversal cycle. The constitutive relationship should therefore encompass a complete stress reversal cycle. Because of the non-linear stress-strain behaviour of the soil, a non-linear elastic response can be used to represent the soil during loading, and an elastic response can be used for the unloading process. For loading and unloading of a soil element the following code can be used in the analysis:

$$\Delta w = \sigma_{ij} de_{ij} \quad (8.4)$$

where σ_{ij} = state of stress and
 de_{ij} = incremental state of strain,
 if $\Delta w < 0$ = the element is unloading and
 $\Delta w > 0$ = the element is loading.

After every wheel pass the soil density profile changes, hence the soil constitutive relationship should include a density term, or the soil continuum idealized into several layers, each with different constant densities.

8.4.6 Performance prediction

Since the finite element analytical model is basically a continuum mechanics model used for solving boundary value problems, the FEM solution predicts the subsoil stresses, strains, deformations and deformation energies resulting from the roller motion on the soil during the compaction process. The calculation procedures also allow for determination of surface deformations, roller motion resistance, changes in the roller-subsoil densities, and hence the work done.

Figure 8.20 shows the effects of the number of passes on soil surface permanent deformation for the case of a smooth rigid roller. As expected, the initial sinkage is high and decreases as the number of passes increases, to the point where the sinkage becomes relatively constant after a certain number of passes - according to the type and initial condition of the tested soil. The results show a good agreement between the finite element prediction and the measured sinkage value.

Figure 8.18 shows the finite element predicted and measured density profile after sixteen passes. The change in density is determined by calculating the change in the area of every finite element after every pass. The predicted values accord well with the measured values.

Figure 8.19 shows the predicted and measured roller rolling resistance (towed force) as a function of number of passes. The rapid decrease in the rolling resistance with increasing number of passes is expected because of the increase in density of the soil. The stiffness and strength of the soil layer will correspondingly increase whilst surface deformations will decrease with the increasing number of passes.

Figure 8.15 shows the relationships for the energy spent in compacting the soil versus dry density. In this Figure the finite element predicted results are compared with those calculated from the roller multi-pass tests, and the Proctor mould and ram tests.

To demonstrate the usefulness of the FEM, the example presented shows the effect of soil type and soil layering on pneumatic roller performance. In this example the roller load is 5250 N. Contact area of roller on rigid surface can be characterized as:

width = 15.8 cm; length = 20.8 cm.

The soil stress-strain curves are presented in Fig. 8.23. As noted in Chapter 3, the tangential stresses at the roller-soil interface can be determined from laboratory experiments. In the three test examples treated, it is assumed that the two separate cases for the single layer system have the same soil depth of 104 cm and that the two-layer system has layers of 20.8 and 83.2 cm thick, with the thinner layer on top. In the two separate considerations of the single-layer system, a soft soil and a stiff soil are considered separately.

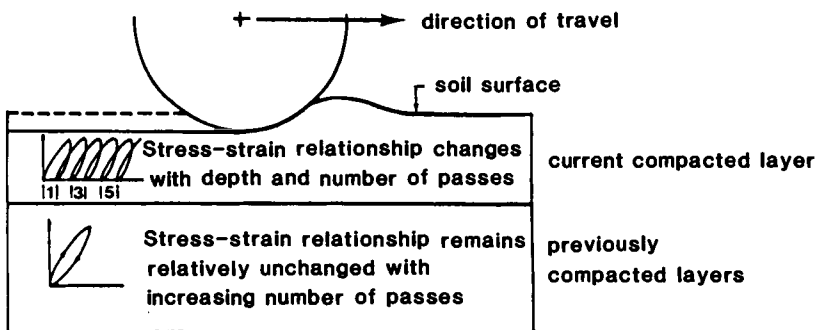


Fig. 8.23. Stress-strain curves of silty clay from triaxial tests.

Figure 8.24 shows the computed surface deformations for the three cases presented, whilst Fig. 8.25 shows the energy spent in compacting the soil as a function of slip. Dividing the results given in Fig. 8.25 by the deformations shown in Fig. 8.24, one obtains the specific compaction energy curves shown in Fig. 8.26, (Fattah et al., 1981). As expected, Fig. 8.26 shows that the stiff single soil layer requires more specific energy than that utilized for the soft single soil layer, because one requires more energy to compact a stiffer soil to the same permanent unit deformation, as compared to a softer soil. Thus, even though Fig. 8.26 shows that the soft single soil layer absorbs less specific compaction energy than the stiff layer, the total permanent deformation sustained is larger.

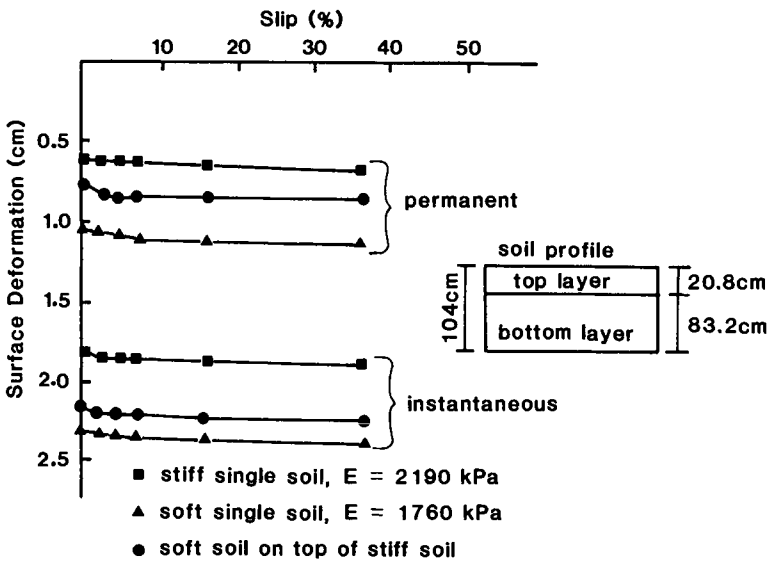


Fig. 8.24. Effect of type of soil on developed surface deformation due to passage of a pneumatic tyre - Load = 5250 N.

8.5 SUMMARY

The mechanism for granular soil compaction is mainly an arrangement of soil particles of different grain sizes to obtain maximum density. Effect of particle type of packing and mixture on compactibility of soil of cohesionless soil is discussed. For cohesive soil, water plays an important role in compactibility of soil. Factors affecting soil compactibility such as type of loading (static, kneading, impact, sinusoidal) and amount of compaction are discussed. The FEM model for predicting compactibility of soil due to moving smooth rollers can be used successfully to assess and evaluate soft soil compactibility.

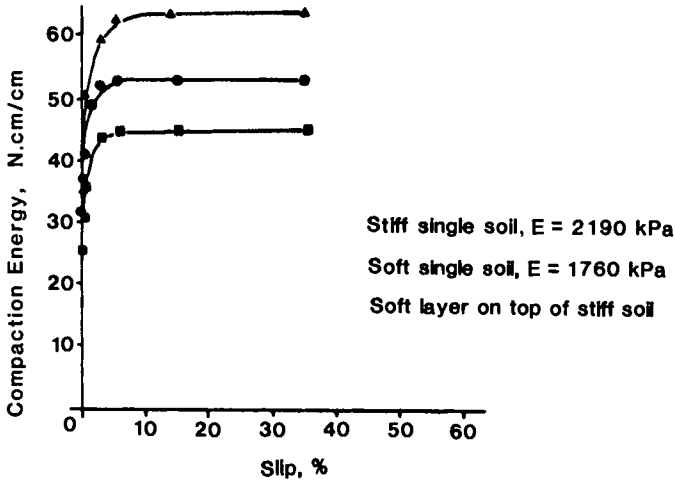


Fig. 8.25. Effect of type of soil on developed compaction energy due to passage of a pneumatic tyre - Load = 5250 N.

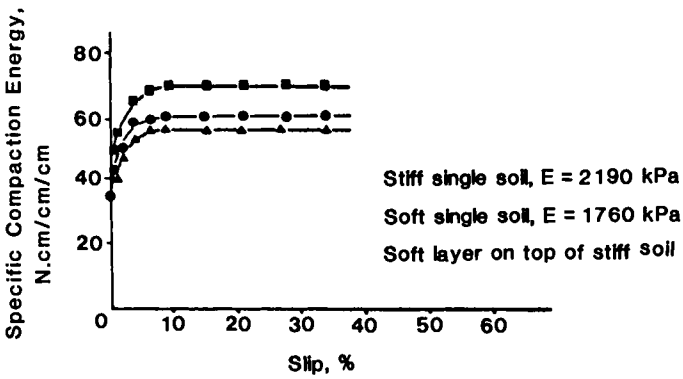


Fig. 8.26. Effect of type of soil on specific compaction energy requirements for a pneumatic tyre - Load = 5250 N.

REFERENCES

- Bell, J.R., 1977. Compaction energy relationships of cohesive soils. Transportation Research Record, 641, pp. 29-34.
- Deresiewicz, H., 1958. Mechanics of granular matter. Advanced Applied Mechanics, 5:233-306
- Fattah, E.A., Yong, R.N. and Ng, K.S., 1981. Compactability of soil under towed rollers. Proc. 7th Int. Conf. Int. Soc. Ter-Veh. Systems, Calgary, 11:585-608.
- Furnas, C.C., 1931. Grading aggregates 1. Mathematical relations for beds of broken solids of maximum density. Industrial and Engineering Chemistry, 23: 1052-1058.
- Lambe, T.W., 1958a. The structure of compacted clay. J. Soil Mech. Found. Eng. ASCE, 84:2, Pt.1, pp. 1654-1 to 34.
- Lambe, T.W., 1958b. The engineering behaviour of compacted clay. J. Soil Mech. Found. Eng. ASCE, 84-2, Pt.1, pp. 1655-1 to 35.
- Morris, P.O. and Tynan, A.E., 1968. The performance of compaction plant. Proc. ARRB Conf., 4-2:2049-2105.
- Pacey, J.G., 1956. The Structure of Compacted Soils. S.M. Thesis, Massachusetts Institute of Technology.
- Smith, W.O., Foote, P.D. and Busang, P.F., 1929. Packing of homogeneous spheres. Physics Review, 34:1271-1274.
- Wise, M.E., 1952. Dense random packing of unequal spheres. Philips Research Report, 7:321-343.
- Yong, R.N. and Warkentin, B.P., 1975. Soil Properties and Behaviour. Elsevier Scientific Publishing Company, Amsterdam, 449 p.
- Yong, R.N., Boonsinsuk, P. and Fattah, E.A. 1980. Tyre flexibility and mobility on soft soils. J. Terramech., 17:43-58.

NOMENCLATURE

E_i	soil stiffness
N	average number of contacts per square
$N_{c.p.}$	average number of contacts per square (close-packed)
N_{cub}	" " " " " " (cubic)
R	sphere radius
S	degree of saturation (%)
$V_{c.p.}$	volume of spheres in a close-packed arrangement
V_{cub}	" " " " " cubic "
W	moulding water content
d_1, d_2	particle size diameter
de_{ij}	incremental state of strain
m	fraction of close-packed spheres
n	porosity
$n_{c.p.}$	porosity of a close-packed arrangement
n_{cub}	" " " cubic "
s	standard deviation
π	constant
τ_c	confining pressure
τ_{ij}	state of stress
ω_{opt}	optimum water content (%)

Chapter 9

TRAFFICABILITY

9.1 DEFINITIONS AND REQUIREMENTS

Before embarking on a discussion of trafficability it is necessary to establish the difference between "mobility" and "trafficability". These two terms have often been used interchangeably although they do indeed represent two distinct phenomena. "Mobility" refers to the ability of a vehicle to establish motion between two designated points over a prescribed course. Thus, the "mobility" of a certain vehicle is generally discussed in terms of a certain degree of mobility over a prescribed terrain - referring to the relative ease or difficulty of the vehicle to establish traverse motion over the prescribed terrain. In the ultimate, if the vehicle cannot establish traverse motion, the mobility of the vehicle is said to be in a "no-go" situation. We can thus conceive of "mobility" as a term which refers to the vehicle under consideration.

On the other hand, "trafficability" refers to the capability of the terrain under consideration to provide the mobility of a particular set of vehicles. One refers, for example, to the trafficability of a particular piece of terrain as the ability of that piece of terrain to support vehicles and also to provide the capability of the particular vehicle to establish mobility. We should be careful to note that whilst a specific piece of terrain might be trafficable for a particular type of vehicle it might not, on the other hand, be trafficable for another type of vehicle - or even the same vehicle if, for example, the loading pattern of that vehicle is significantly increased.

Trafficability prediction is based on a knowledge of combinations of factors related to vehicles and those related to both terrain cover and substrate material. Factors related to vehicles are fixed and are easily determined, depending on the mechanical characteristics of those vehicles (Knight and Rula, 1961). The vehicle factors are mainly concerned with their tractive elements. These can be classified as:

- (a) wheels (tyres) - geometrical characteristics, cross-sectional shape, tread configuration (design), arrangements (dual or tandem), carcass stiffness, inflation pressure, type (towed or driven), load, ... etc.
- (b) tracks - type of track (i.e. rigid or flexible, continuous, linked, etc.) geometrical characteristics (length, width), angle of attack, angle of escape, number and characteristics of road wheels, grouser shape and geometrical arrangements, track flexibility, track tension, driving sprocket positions, ... etc.

The terrain cover and substrate factors are mainly those which are concerned with the strength and deformability of the cover and bearing material, and can

be classified as:

- (a) Fine-grained (cohesive). Moisture content, particle size, mineralogical composition, density, fabric and structure, ... etc.
- (b) Coarse-grained (sand). Particle size, density, moisture content, structure, ... etc.
- (c) Organic. Moisture content, density, type and strength of fibres, percent of minerals, ... etc.
- (d) Snow. Density, temperature, age, structure, ... etc.

An accurate determination of the cover and substrate factors in the field is difficult due to (a) nature of the tools used, (b) field conditions, and (c) material heterogeneity.

An exact definition and quantification of trafficability is quite difficult, since a specific terrain or ground surface can be trafficable for certain vehicles and not for others. In spite of the fact that the existing techniques for evaluating trafficability are implicitly based on the vehicle supporting ground strength, the terrain can be untrafficable due to natural or man-made obstacles, (mounds, ditches, trees) or due to extreme terrain roughness. Thus, the definition and quantification of trafficability should be restricted to special conditions such as flat ground surfaces bare of obstacles. In this case, trafficability of a particular tract can be defined as its ability to support a passage of certain off-road vehicles. It is important to note that the trafficability of a terrain can be assessed fully and comprehensively only by a consideration of the forces at the tractive element (track or wheel) - terrain interface for the vehicle concerned, and the substrate response under those forces. Theories and laws of mechanics of terrain-vehicle systems can be adopted, but this requires exact modelling of the vehicle and substrate material, and also requires an accurate determination of the relevant in situ material parameters. This approach requires time and computer facilities, and can only be economical for evaluation of performance of an off-road vehicle with respect to certain types of soil. In some situations, decision-makers cannot afford to wait. Their responsibilities demand that they be able to differentiate passable and impassable areas for the vehicles under consideration, bearing in mind that the traverse distances could be a few meters or a few kilometers - i.e. terrain variability can be quite severe. Decisions oftentimes need to be made rapidly and with simple terms of reference. Recognizing these requirements, and realizing the time penalty required for the proper application of analytical techniques for solution of the problem, a successful trafficability prediction procedure requires a simple portable tool and a technique where decision-makers can rapidly ascertain whether or not the vehicles under consideration can successfully negotiate the highly variable terrain they would encounter. To meet this need, several field measuring devices have been developed - with some relative meas-

ure of success for certain types of terrain. It must however be noted that none of these tools provide exact or even rational predictive techniques. Predictions of trafficability, by and large, are accomplished through painstaking field correlations. We will discuss this aspect of the problem at the conclusion of this Chapter. In the meantime, the existing common field tools and their corresponding data reduction techniques for trafficability predictions are presented in the bulk of this Chapter. Table 9.1 shows the classification of the field-sensing tools, the types of data obtained and the corresponding analytical techniques utilized for evaluation of the performance of the running gear.

9.2 THE CONE

The cone penetrometer used for soil trafficability studies and forecasting was developed by the U.S. Army Engineer Waterways Experiment Station. The instrument is composed of a 5/8 in. diameter, 3 ft long staff with a 1/2 sq.in. 30° circular cone on one end and a proving ring, dial, and handle on the other end, (Fig. 9.1). The force necessary to push the cone slowly through the soil is registered on a dial that ranges from 0 to 300. The measured value is the cone index (Knight and Meyer, 1961).

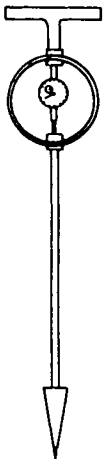
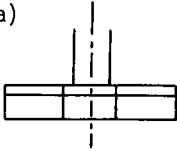
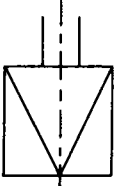
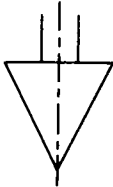


Fig. 9.1. Cone penetrometer (U.S. Waterways Experiment Station).

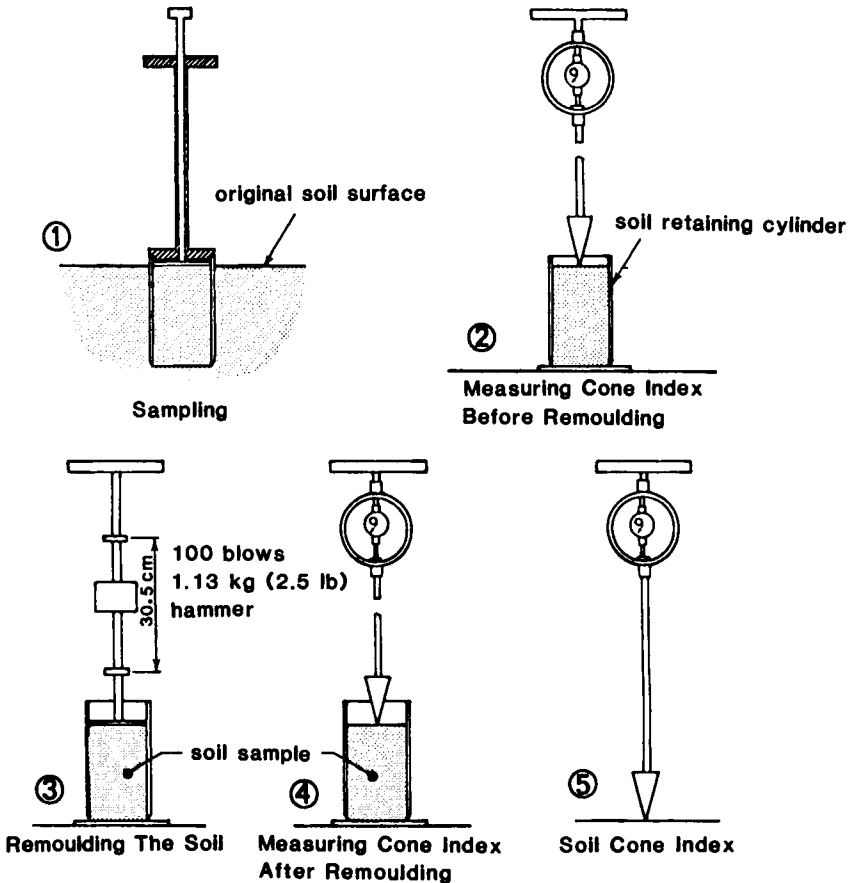
Many soils whose strengths are low in the in situ condition will become even weaker under the action (remoulding effect) of a vehicle. Thus, a remoulding cone index test is necessary. This test consists of measurement of the cone index of a sample of soil confined in a small cylinder before and after pounding it with 100 blows of a 2 1/2 lb hammer falling 12 in. A "remoulding index" is

TABLE 9.1

Some simple devices and methods of utilization

Device	Reduced information from field measurements	Approaches used
<p>(a)</p>  <p>Bevameter</p>	<p>(1) Bevameter values at the surface, C, ϕ, K_C, $K\phi$, n.</p> <p>(2) Tangential shear stress at the surface.</p>	<p>Drawbar-pull obtained by computations involving determination of rolling and bulldozing resistances.</p>
<p>(b)</p>  <p>Vane-cone</p>	<p>(1) Vane-cone values at different penetration depths, CI, C, ϕ.</p> <p>(2) Tangential stress at different depths.</p> <p>(3) Soil density at different depths (in case of sand).</p> <p>(4) Complete soil profile.</p>	<p>(1) Energy approach.</p> <p>(2) Clay number approach.</p> <p>(3) Power number approach.</p> <p>(4) Mobility index approach.</p> <p>(5) Simplified energy approach.</p>
<p>(d)</p>  <p>Cone</p>	<p>(1) Cone index at different depths, CI.</p> <p>(2) Soil density at different depths (in case of sand).</p> <p>(3) Some data about soil profile.</p>	<p>(1) Energy approach.</p> <p>(2) Clay number approach.</p> <p>(3) Power number approach.</p> <p>(4) Mobility index approach.</p>

obtained by dividing the cone index of the soil, after it has been pounded, by its cone index before the blows were applied. A "rating cone index", the final measure of a soil's trafficability, is obtained by multiplying the in situ cone index by the remoulding index. The rating cone index is meant to be a physical evaluation of the bearing and traction capacity of a remoulded soil, i.e., the trafficability of a soil. The procedure for determining the soil rating cone index (RCI) is presented in Fig. 9.2.



$$\text{RATING CONE INDEX (RCI)} = \frac{\text{soil cone index after remoulding (Step 4)}}{\text{soil cone index before remoulding (Step 2)}} \times \text{terrain soil index (Step 5)}$$

Fig. 9.2. Procedure for determining the soil rating cone index (RCI).

The rating cone index is particularly significant in that it can be compared to a vehicle index (termed "vehicle cone index") to determine whether a vehicle can or cannot traverse the soil. If the vehicle cone index is less than the

rating cone index, the terrain under consideration may be considered as passable and 50 vehicles of this type can pass in a careful straight-line traffic, or one vehicle can execute several manoeuvres without becoming immobilized. If the vehicle cone index is higher than the rating cone index, the area is considered impassable for the vehicle.

Knight and Meyer (1961) found that correlations between vehicle performance and soil strength are most consistent when the strength in the critical soil layer is considered. This layer lies between 6 and 12 in. below the surface. Using data collected in hundreds of tests with actual vehicles on different types of soils and at different seasons, the Waterways Experiment Station (WES) developed a system for evaluating the effects of a vehicle's characteristics (weight, contact, pressure, etc.) in terms of the cone index required for the vehicle. This cone index is determined from the mobility index through a correlative relationship which takes into account the type of tractive element and the soil. The mobility index is a dimensionless number obtained by applying certain characteristics of a vehicle to dimensionless formulae. Figure 9.3 gives a typical relationship between the mobility index and the vehicle cone index. Figure 9.4 shows a typical relationship used to predict pull coefficient and towed force coefficient for wheeled vehicles in wet, fine-grained soil.

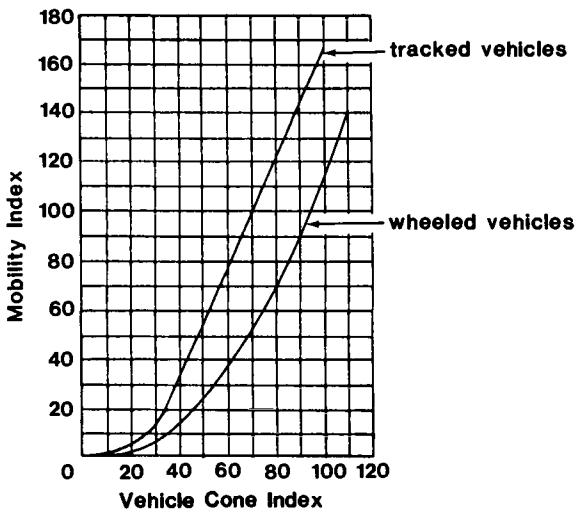
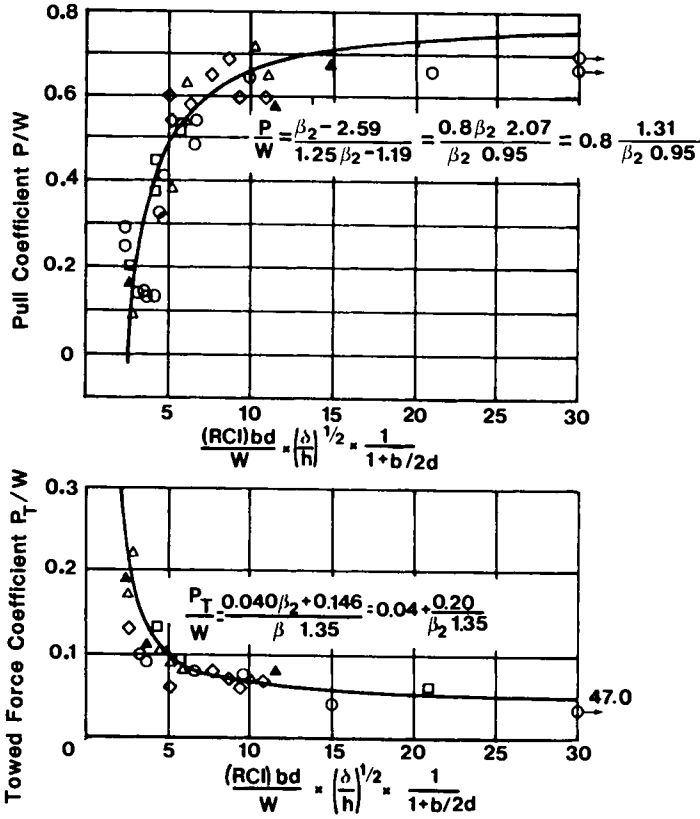


Fig. 9.3. Mobility index versus vehicle cone index.

Application of the cone index approach to predict performance of an off-road vehicle moving on snow or muskeg can lead to serious, erroneous results, since the use of the cone alone is not enough to identify strength characteristics of these two materials.



LEGEND

<u>Nom. Tyre Size</u>	<u>Vehicle</u>
42 x 40 - 16	Mexa 10x10
48 x 31 - 16	Mexa 8x8
14.00 - 18, 6 - PR	XM4 10E1
11.00 - 20, 12 - PR	M35A2 (MOD)
23.1 - 26, 10 - PR	Log Skidder

Note : $\beta_2 = \frac{(RCI) bd}{W} \times \left(\frac{\delta}{h}\right)^{1/2} \times \frac{1}{1+b/2d}$

Fig. 9.4. Use of $\frac{(RCI)bd}{W} \cdot \left(\frac{\delta}{h}\right)^{1/2} \cdot \frac{1}{1+b/2d}$ to consolidate field performance data of wheeled vehicles in wet, fine-grained soils (Turnage, 1972).

It should be noted that mobility index (XMI) is a dimensionless number obtained by applying certain characteristics of a vehicle to a certain formula. These formulae vary according to vehicle type (track or wheeled) (Knight and Rula, 1961). The vehicle cone index (VCI) is a dimensionless number obtained

through empirical curve-fitting relationships between the VCI and XMI. These relationships are dependent upon vehicle type, Fig. 9.3. The vehicle cone index (VCI) is purely a vehicle index and is not related to the soil cone index or any related results.

9.3 VANE-CONE DEVICE

The vane-cone device shown in Fig. 9.5 was developed by Yong et al. (1975) to be used as a portable tool in the field for evaluating the characteristics of the soil at or beneath the ground surface for engineering or trafficability purposes. The requirement for simplicity in use and portability dictated that the instrument be simple.

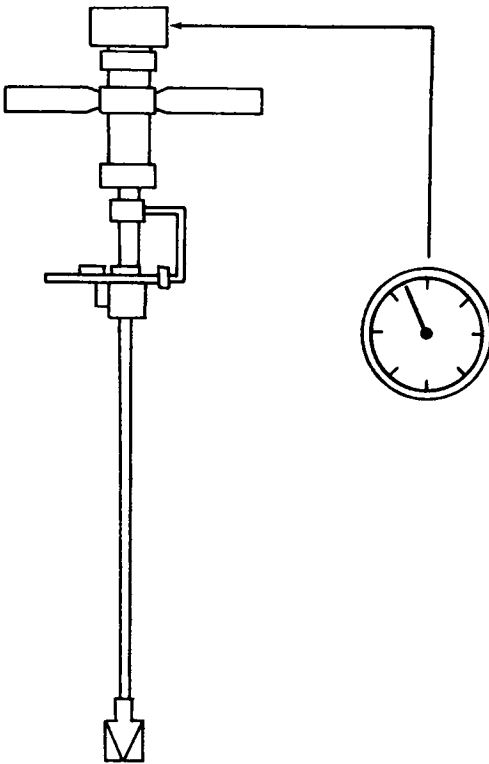


Fig. 9.5. Vane-cone device.

The device consists of a staff 15 mm in diameter and 1 m long with a vane-cone screw mounted at one end and two independent measuring devices for load and torque in addition to the loading handles at the other end. For measurements,

the device is then rotated to record the torque resistance of the vane-cone-soil system. Both the applied vertical load and the resultant shear are measured. This procedure can be repeated for more depths. The current capability for the device is to predict the trafficability with respect to soft soil.

The device was developed with the view of incorporating the two prime parasitic energies in the vehicle-soil system (compression and interfacial energy loss as explained in Chapter 5) in the procedure for forecasting trafficability. Figure 9.6 shows the kind of mechanisms developed with the application of the vane-cone device. The vane portion of the vane-cone device provides a shear strength evaluation of the soil, when the vane-cone is rotated. It should be noted that the soil shear mechanisms developed as the vane-cone is rotated are not unlike those for the annulus vane in the Bevameter-type device. The resistance values or shear strength measurements obtained thereby can be directly converted into slip energy loss relationships not unlike those obtained for the annulus device if, and only if, the proper energy transfer mechanics framework is provided with the annulus device. In actual fact, we observe that the Bevameter annulus device does not normally utilize this kind of a framework, and therefore the direct translation of annulus information to slip energy loss has not been obtained. Procedures, however, can be developed to translate the information in the energy format, if such is desired. It is clear from Fig. 9.6 that the shear and resistance mechanisms developed with the vane-cone device are not dissimilar to those produced with the Bevameter-type device. Whilst both deformation and interfacial energy losses can be sensed, the energy transfer analytical framework which utilizes the kinds of sensing device measurements made, has only been developed in conjunction with the vane-cone device.

9.4 VANE-CONE PREDICTION METHOD

In this predictive technique it is recognized that the actual traction mechanics evoked in wheel or track performance, in regard to subsoil deformation, is influenced by many factors such as wheel or track dimensions, loads, contact surface characteristics and angular and translational velocities. This performance may be discussed in terms of energy transfer mechanisms at the wheel or track interface, as noted in Chapter 5.

As discussed in Chapter 5, the energy transfer component associated with the subsoil deformation must obviously depend on the mechanics of transfer at, and beneath, the interface and is thus related directly to the interface input energy component. The procedure requires an analysis of the overall problem in terms of the rationale for partitioning the components of parasitic energy.

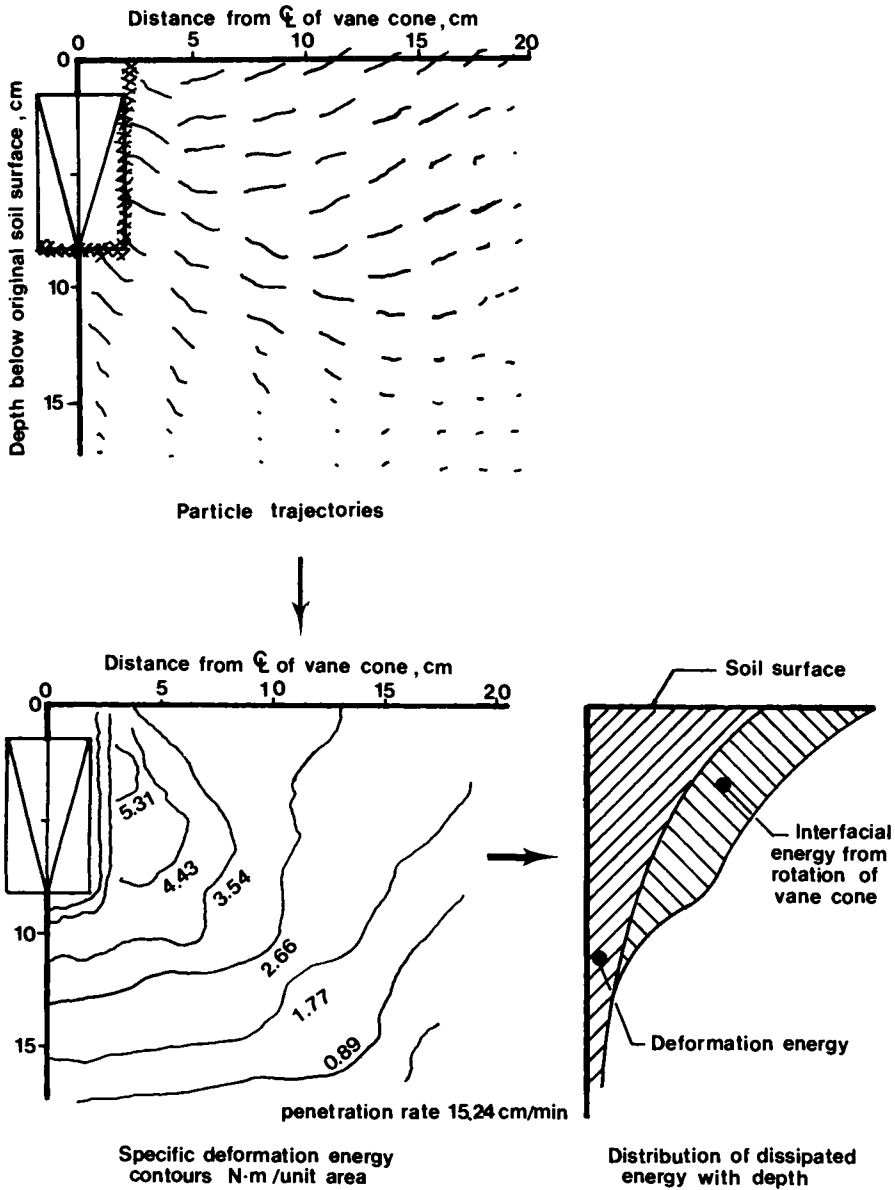


Fig. 9.6. Soil particle trajectories and corresponding dissipative energy field developed by penetration of a 30° vane-cone penetrometer.

9.4.1 Assumptions and limitations

Currently, the developed analytical approach for using the vane-cone data for trafficability prediction is limited to soft soils.

The assumptions adopted for deriving the analytical technique are:

(a) There are linear relationships between the wheel or track dynamic sinkage and vane-cone penetration depth for the same specific deformation energy of the wheel or track and the vane-cone (Fig. 9.7).

(b) There is a definite relationship between the angle of entry and the angle of escape.

(c) There is a relationship between the cone penetration pressure and the applied pressure from the specific tractive element.

(d) The tangential stress at the wheel-soil or track-soil (tractive element soil) interface is constant, and is the same as that of the vane-cone interface.

Adopting the following assumptions and using continuum mechanics theories, the following equations can be derived:

Input Energy Prediction, I.E.

$$I.E. = \frac{mbd}{2} \left[\frac{W^2(1+2S)^2}{N_c p^2 b^2} + \delta d \right]^{1/2} \cdot \tau \cdot \omega \quad (9.1)$$

Slippage (or Interfacial) Energy Prediction, S.E.

$$S.E. = \frac{mbd}{2} \left[\frac{W^2(1+2S)^2}{N_c p^2 b^2} + \delta d \right]^{1/2} \cdot \tau \left(\omega - \frac{2V_c}{0.935d} \right) \quad (9.2)$$

Deformation Energy Prediction, D.E.

$$D.E. = b \cdot V_c \cdot [A]_0^y \quad (\text{See Fig. 9.8}) \quad (9.3)$$

where

$$y = K \left[\frac{W^2}{N_c p^2 b^2 d} \right] + \alpha e^{\beta(h/2r)} \quad (9.4)$$

Pull Energy Prediction, P.E.

$$P.E. = I.E. - S.E. - D.E. \quad (9.5)$$

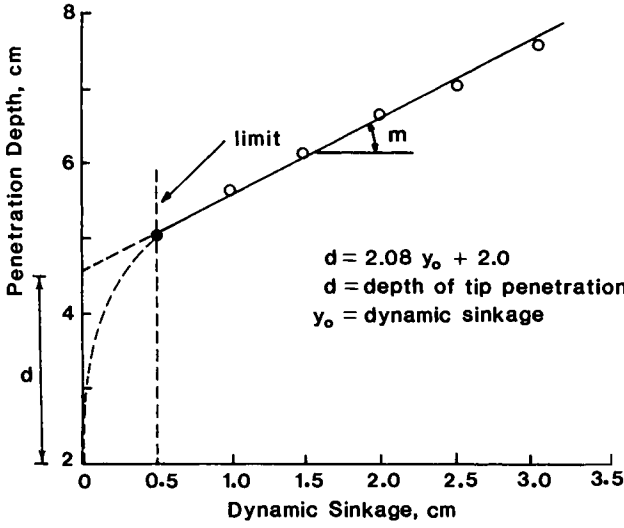


Fig. 9.7. Dynamic sinkage versus penetration depth at the self-propelled point.

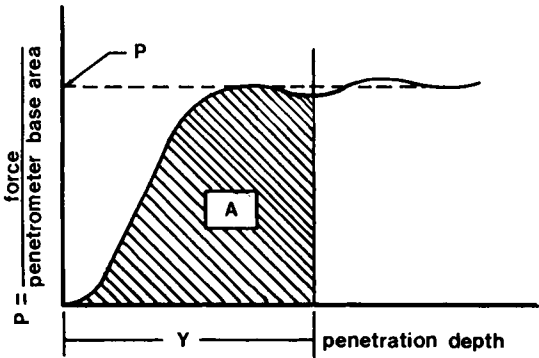


Fig. 9.8. Pressure-penetration diagram for vane-cone penetrometer.

where

- W = wheel or track load;
- p = pressure beneath the penetrometer;
- b, d = wheel width and diameter, or track-width and length;
- h, r = penetrometer height and radius;
- δ = tread height, or grouser depth;
- S = slip;
- V_c = translational velocity;
- ω = angular velocity;

τ = tangential shear stress obtained at the outer edge of the vane component;

m = factor taking the effect of backward contact area equal to 1.31;

N_c = bearing stability factor which is dimensionless and equal to 0.225 for $\phi = 0$;

K, α, β = dimensional factors obtained from visioelasticity analyses (semi-analytical analyses) for the purpose of deformation energy prediction. For cohesive material, $\phi = 0$ and in the case of lb in units, $K = 1.21$, $\alpha = 0.97$ and $\beta = 0.230$ and

y = cone penetration depth at which the specific deformation energies for the cone and wheel or track are the same.

9.5 PLATE PENETRATION

The plate penetration approach for prediction of trafficability developed by the land locomotion laboratory consists of a plate penetration device with a steel plate (circular or rectangular) and a loading system for the plate, together with a measuring system for the load and sinkage. Figures 9.9 to 9.11 show different types of plate penetration devices. Because of the relatively large weight of the device, it is not easily portable, in the sense that two men are needed to move the device from one location to another within the same site. In addition, the device needs to be anchored to the ground to resist the uplift from the jack system used to apply loading to the plate. Since the penetration load is normally greater than the weight of the device, most plate penetrometer devices are mounted on vehicles equipped with data acquisition systems for recording, and instant analysis of the results. Under such circumstances, it is not unusual to use the vehicle itself as a reaction frame for the penetration device.

To calculate tractive-element wheel(track)-soil motion resistance using the plate penetration method, empirical equations have been developed as noted in Chapter 4. Three specific values are needed; namely, k_c , k_ϕ and n (Bekker, 1969; Willis et al., 1965; Uffelmann, 1961). These values are dimensionless and should theoretically be independent of plate size. A minimum of three different plate sizes are required to provide correlative relationships whereby these empirical "constants" can be deduced. Ideally, the pressure-sinkage relationships obtained from tests with the various plates will describe a family of parabolae which plot as parallel straight lines on a logarithmic plot, as seen for example, in Fig. 9.12a. The slope of these lines is defined as the coefficient n , whilst the pressure intercepts at $z = 1$ are taken as constant terms to be used for the calculation of k_c and k_ϕ (Wisner and Smith, 1961). The intercept k is expressed as:

$$k = \frac{p}{z^n} \quad (9.6)$$

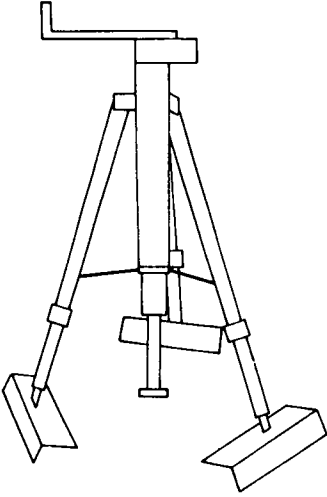


Fig. 9.9. Portable penetrometer.

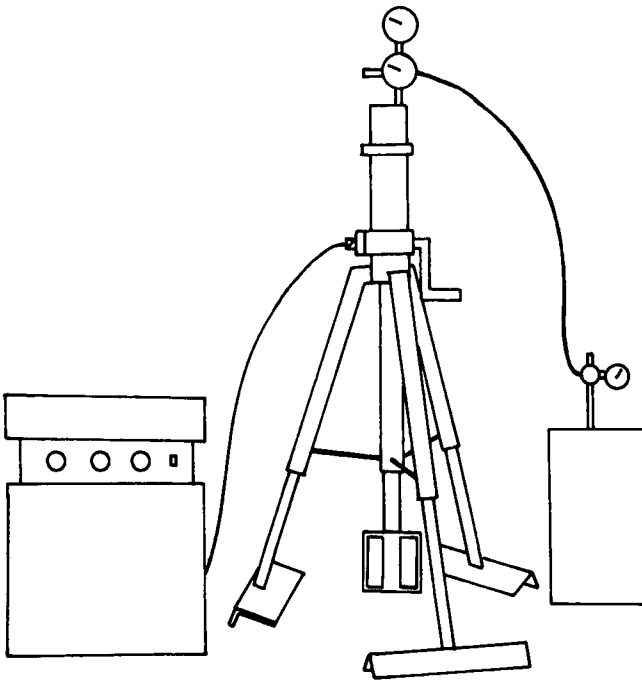


Fig. 9.10. Portable shear device.

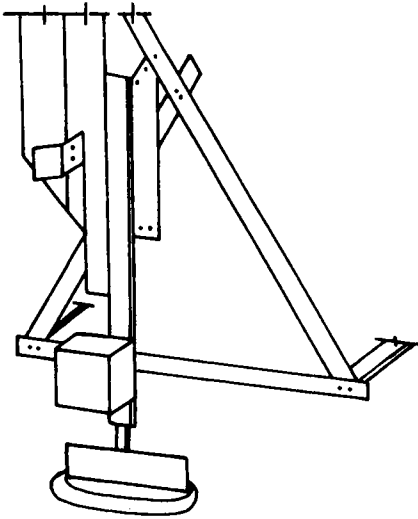


Fig. 9.11. Bevameter.

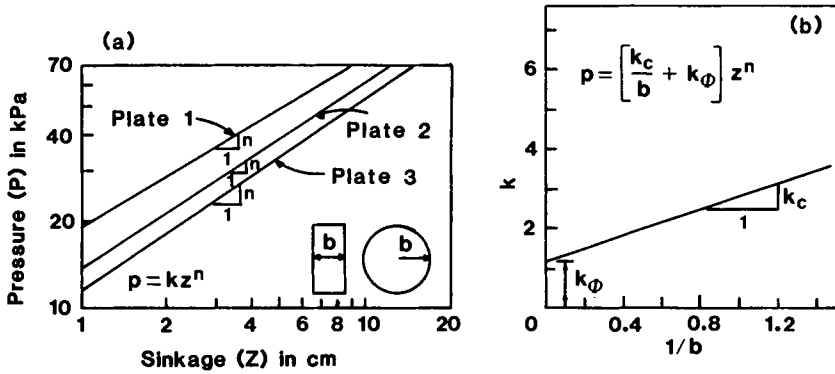


Fig. 9.12. Pressure-sinkage relation (Wisner and Smith, 1961).

By plotting the values of k , as obtained for example in Fig. 9.12a against the inverse of the penetration plate diameter (or width) b , the empirical coefficients k_ϕ can be obtained as the ordinate intercept, whilst the coefficient k_c is obtained as the slope. Taking note of eq.(9.6), we obtain:

$$k = \frac{p}{z^n} = \frac{k_c}{b} + k_\phi \quad (9.7)$$

The two empirical terms, k_c and k_ϕ , can be obtained analytically using eq.(9.7) with multiple tests, using various sizes of penetration plates, or graphically as shown in Fig. 9.12b. Note, however, that in practice, one should determine the sensitivity of the empirical constants to the size of b , plus other terrain properties and characteristics. Some investigators, for example, have reported considerable difficulty in obtaining valuable values of k_c , k_ϕ and n from plate penetration tests since, by and large, linear relationships such as those shown in Fig. 9.12 cannot be easily drawn or obtained. Figure 9.13 illustrates the problem by showing typical results of plate tests for sand, while Fig. 9.14 shows some actual test results for clay. Recent studies by Wong and his co-workers have sought to improve the data gathering and reduction systems - with considerable improvement in facility of use of the test system itself (Wong, 1980).

The drawbar-pull prediction of a certain tractive element requires a knowledge of the tractive force at the element-soil interface, and also the motion resistance developed - as noted in Chapters 4 and 5. In the plate penetration prediction approach, the tangential tractive stresses are measured by means of a shear box or a sled test (laboratory), or by a torsional instrument (vane or annular ring), (Fig. 9.15).

The tractive test results obtained from any of these are plotted in terms of the tangential stress against the tangential soil deformation under different applied normal pressures. Figure 9.16 shows tangential stress-deformation relationships either increasing to a maximum and dropping toward a horizontal asymptote, as in the two top graphs, or increasing in a regular fashion toward a horizontal asymptote. The former shape is characteristic of a cohesive soil whilst the latter is characteristic of cohesionless soils. The shapes of these curves can be described by different numerical curve fitting techniques, the details of which have been presented in previous Chapters.

9.6 SUMMARY

The choice of the type of field sensing tool for use in assessing terrain trafficability and for prediction of total vehicle mobility will depend on (a) circumstances prevailing, e.g. cost, timing, accuracy required, etc., (b) personal preference and bias, (c) degree of portability of instrument to be used, and (d) degree of educated awareness of the user.

In making a choice of field measuring (sensing) device, it is important to distinguish between the requirement for (a) prediction of terrain trafficabil-

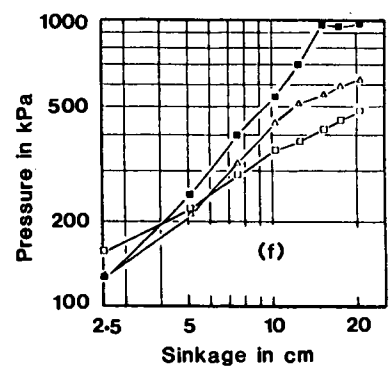
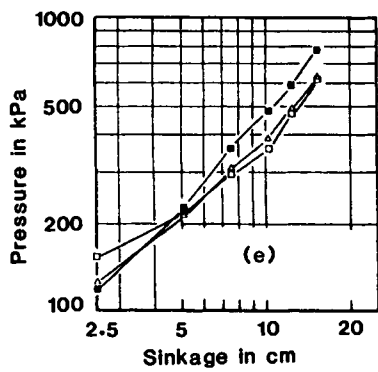
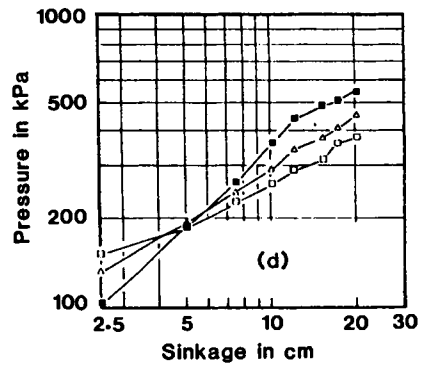
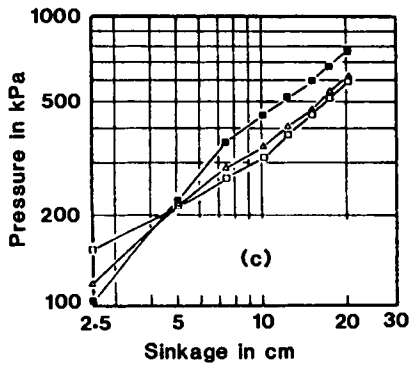
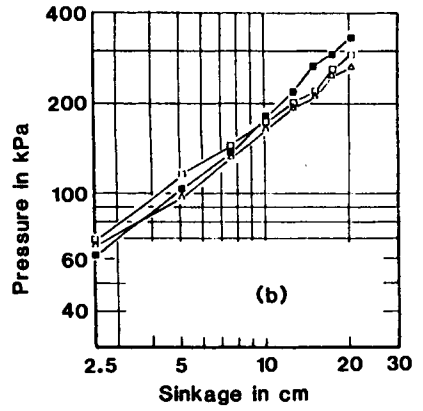
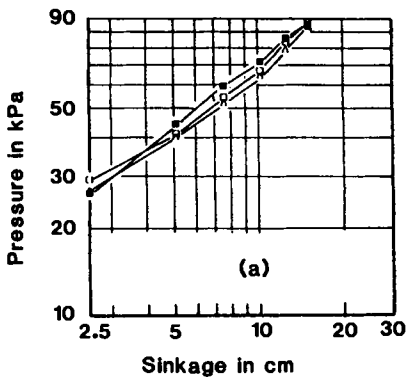


Fig. 9.13. Plate penetration curves (Wisner and Smith, 1961).

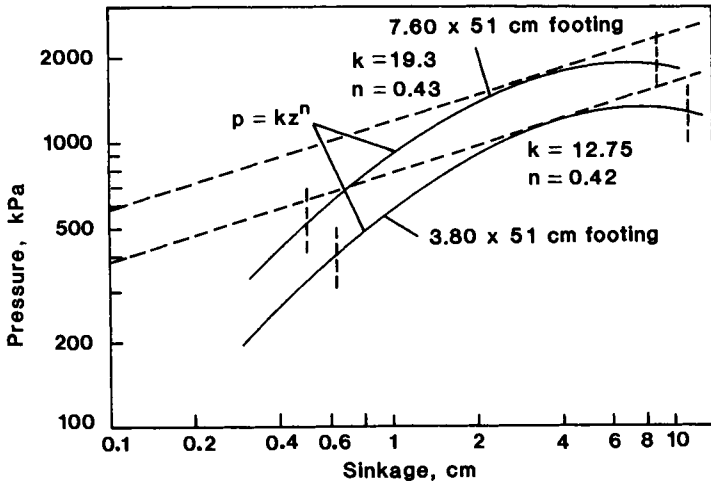


Fig. 9.14. Plate penetration curves for clay (Willis et al., 1965).

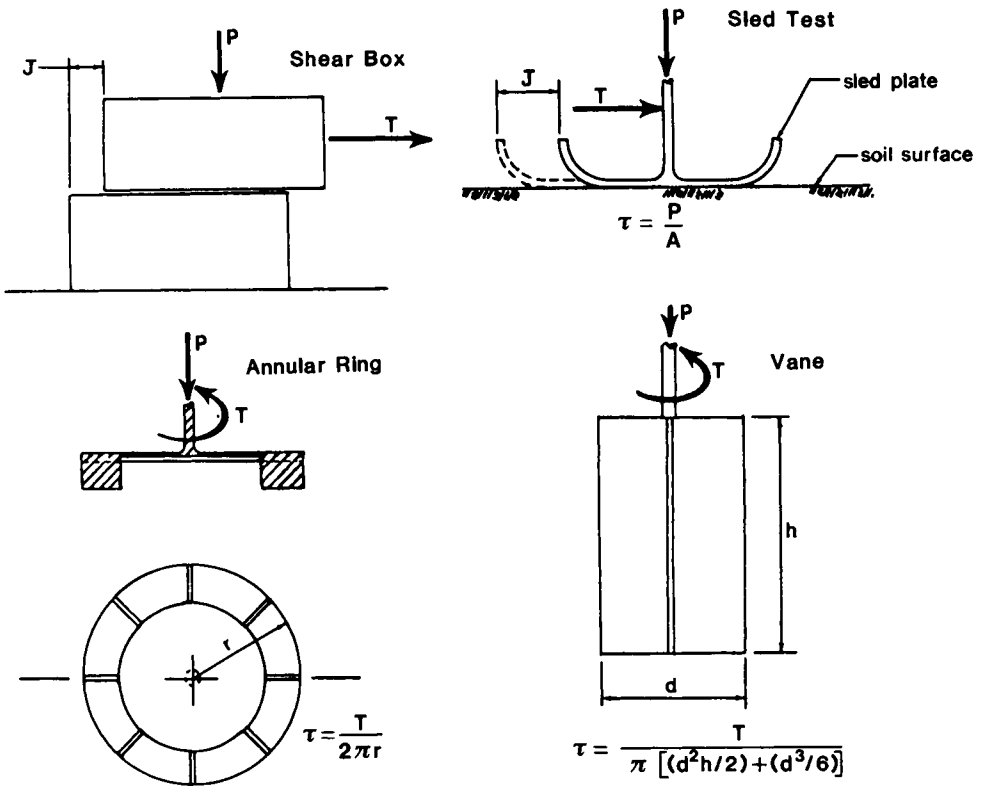


Fig. 9.15. Devices for measuring tractive element-soil tangential stresses.

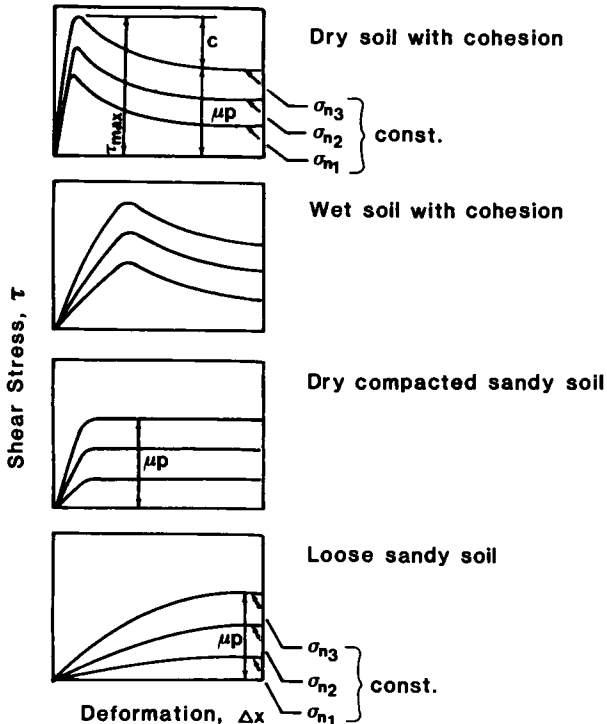


Fig. 9.16. Tangential stress-deformation relationship.

ity, and (b) prediction of vehicle mobility performance. It is also necessary to fully appreciate the differences between the need to assess terrain capability for purposes of vehicle mobility evaluation - as opposed to the requirement for decision-making in regard to type of vehicle to be used for the terrain being studied. The underlying reasons for the above concerns are mainly those dealing with (a) "what the tools really measure", and (b) "what the data reduction techniques specifically address".

By and large, all the tools used will measure - in one fashion or another - the strength of the supporting material. How one converts the measurements obtained is obviously the problem at hand. The temptation to directly equate for example, the penetration resistance obtained by the plates, the cones, and the vane-cones to vehicle flotation pressure or capability would indeed be most pressing. Can this be done? Should this be done? Quite obviously, because of the geometric differences between the plate and the cone, the penetration resistances measured - for the same terrain - will not likely be similar. The next question that one would need to ask is "which one should we use?"

As noted, the experience associated with the cone demonstrates that actual correlations between vehicle performance (mobility) can be obtained with the penetration value - not a direct flotation assessment using the actual pressure-resistance value, but a correlation between this number and a performance characteristic. In essence, the plate penetration approach reaches the same end point - albeit by a different route which relies on a semi-theoretical framework for development of the use of the empirical constants. The vane-cone technique on the other hand, depends on the principle of similarity and converts its information into equivalent energy format for correlation with specific vehicle performance.

In essence, the user is confronted with two distinct pieces of information:

1. The measurements made can constitute direct information on terrain response properties.
2. The method of data reduction, or the analytical model used for reduction of data, can be used as recommended by previous practice, or indeed modified, or even improved to suit the user's needs and ideas.

We need to emphasize that the user is not wedded to any 'associated' data reduction technique peculiar to the sensing tool used. He should indeed be free to improve on the method for analysis of test data to fit his particular frame of reference and the specific problem at hand.

REFERENCES

- Bekker, M.G., 1969. Introduction to Terrain-Vehicle Systems. University of Michigan Press, Ann Arbor, Michigan. 846 p.
- Knight, S.J. and Meyer, M.P., 1961. Soil trafficability classification scheme. Proc. 1st Int. Conf. Mech. Soil-Veh. Systems, Torino, pp. 567-574.
- Knight, S.J. and Rula, A.A., 1961. Measurement and estimation of the trafficability of fine-grained soils. Proc. 1st Int. Conf. Mech. Soil-Veh. Systems, Torino, pp. 371-386.
- Turnage, G.W., 1972. Tire selection and performance prediction for off-road wheeled-vehicle operations. Proc. 4th Int. Conf. Int. Soc. Ter.-Veh. Systems, ISTVS, Stockholm, Sweden, pp. 61-82.
- Uffelmann, F.L., 1961. The performance of rigid cylindrical wheels on clay soils. Proc. 1st Int. Conf. Mech. Soil-Veh. Systems, Torino, pp. 111-130.
- Willis, B.M.D., Barret, F.M. and Shaw, G.J., 1965. An investigation into rolling resistance theories for towed rigid wheels. J. Terramechanics, 2-1:24-53.
- Wisner, R.D. and Smith, M.E., 1961. Discussion - An analysis of pneumatic tire performance on deformable soils. Proc. 1st Int. Conf. Mech. Soil-Veh. Systems, Torino, pp. 762-769.
- Wong, J.Y., 1980. Data processing methodology in the characterization of mechanical properties of terrain. J. Terramechanics, 17-1:13-41.
- Yong, R.N., Youssef, A.F. and Fattah, E.A., 1975. Vane-cone measurements for assessment of tractive performance in wheel-soil interaction. Proc. 5th Int. Conf. Int. Soc. Ter.-Veh. Systems, Detroit, 3:769-788.

NOMENCLATURE

K	dimensionless factor obtained from viscoplasticity analysis
N_c	bearing stability factor
RCI	rating cone index
S	slip
V_c	translational velocity
W	wheel or track load
b	wheel, track or plate width
d	wheel diameter or track length
h	penetrometer height
k_c, k_ϕ	dimensionless empirical parameters
m	dimensionless factor
n	dimensionless empirical parameter
p	pressure beneath the plate or the penetrometer
r	radius
z	depth
α	dimensionless factor obtained from viscoplasticity analysis
β	" " " " " "
δ	tread height or grouser depth
τ	tangential shear stress
ω	angular velocity

AUTHOR INDEX

Numbers underlined refer to the pages on which the authors are listed in reference sections of the relevant chapters.

- Abeels, P.F.J. 235, 253
 Abel, J.F. 163, 182, 191, 202, 253
 Adams, J.I. 20, 41
 Ahlvin, R.B. 40, 41
- Barret, F.M. 293, 298, 300
 Bathe, K.J. 159, 161, 188, 191
 Bekker, M.G. 26, 41, 76, 86, 95, 96,
 98-100, 106, 132, 235, 242, 253,
 293, 300
 Bell, J.R. 267, 278
 Berthelot, M. 51, 86
 Bertin, J. 51, 86
 Best, B. 162, 191
 Boonsinsuk, P. 56, 58, 87, 92, 132,
 136, 154, 160, 191, 238, 246, 249,
 251, 253, 273, 278
 Brawner, C.O. 24, 41
 Brekke, T.L. 162, 163, 165, 191
 Brown, R.L. 37, 41
 Brusentsev, A.I. 68, 69, 86
 Busang, P.F. 261, 278
- Casagrande, A. 23, 24, 41
 Cho, S.W. 60, 61, 86
- D'Avello, F.S. 45, 47, 86
 Della-Moretta, L. 92, 132, 136, 154,
 212, 220, 253
 Deresiewicz, H. 260, 262, 263, 278
 Desai, C.S. 163, 182, 191, 202, 253
 Dowell, J.T. 28, 41
 Dullage, C. 162, 191
 Duncan, J.M. 162, 175, 191
- Elmamlouk, H. 92, 132, 136, 154, 212,
 217, 218, 220, 253
- Fattah, E.A. 26, 41, 56, 58, 60, 87, 92,
132, 133, 136, 154, 160, 179, 191,
 238, 246, 249, 251, 253, 266, 273,
 276, 278, 288, 300
 Finney, A. 44, 47, 49, 86
 Foote, P.D. 261, 278
 Freitag, D.R. 98, 99, 105, 132
 Fung, Y.C. 187, 191
 Furnas, C.C. 262, 278
- Gasslander, J.E. 49, 86
 Goodman, R.E. 162, 163, 165, 175, 191
 Graber, M. 28, 41
 Guskov, V.V. 68, 77, 78, 86, 100, 132
- Hanamoto, B. 78-80, 86
 Hanna, A.W. 160, 191, 206, 253
 Harr, M.E. 120, 132
 Harrison, W.L. 33, 36, 41
 Haythornthwaite, R.M. 106, 132
 Hertz, H. 233, 253
 Heuze, 162, 191
 Hodge, P.G. 142, 154
- Irwin, G.J. 26, 41
- Janosi, Z. 78, 79, 80, 86
 Japp, R.D. 110, 132
 Jarrett, P.M. 26, 27-29, 41
- Kacigin, V.V. 68, 77, 78, 86, 100, 132
 Karafiath, L.L. 107, 126, 130, 132
 Kliffoth, F. 58, 86
 Knight, S.J. 10, 26, 41, 281, 283, 286,
 287, 300
 Kolobov, G.G. 58, 86
 Komandi, G. 235, 253

- Lambe, T.W. 236, 253, 264, 265, 266, 278
- Lea, N.D. 24, 41
- Lee, R.A. 26-29, 41
- Liston, R.A. 51, 86
- Love, A.E.H. 142, 154
- Lubkin, J.L. 234, 253
- Luth, H.J. 74, 75, 86, 105, 132
- MacFarlane, I.C. 20, 21, 25, 41
- McKyes, E. 171, 191
- Mellor, M. 36, 41
- Mendelson, A. 116, 132
- Meyer, M.P. 26, 41, 46, 86, 283, 286, 300
- Mindlin, R.D. 231, 233, 253
- Morris, P.O. 266, 278
- Murphy, N.R. 40, 41
- Nayak, 159, 191
- Newmark, N.M. 170, 191
- Ng, K.S. 266, 273, 276, 278
- Ngo, D. 162, 191
- Nilson, A.H. 165, 191
- Nowatzki, E.A. 107, 126, 130, 132
- Ohde, J. 106, 132
- Osman, M.S. 106, 132
- Pacey, J.G. 266, 268, 278
- Poritsky, H. 234, 253
- Prager, W. 120, 132, 142, 154
- Prandtl, L. 53, 86
- Radforth, J.R. 28, 41
- Radforth, N.W. 20, 21, 22, 30, 41
- Reece, A.R. 106, 132
- Rula, A.A. 10, 41, 281, 287, 300
- Schwanghard, H. 60, 61, 86
- Scordelis, A.C. 162, 191
- Semonin, E.V. 242, 253
- Shaw, G.J. 293, 298, 300
- Siddall, J.N. 51, 86
- Siemens, J.C. 108, 132
- Smith, M. 98, 99, 132
- Smith, M.E. 293, 295, 297, 300
- Smith, W.O. 261, 278
- Sohne, W. 235, 253
- Stagg, K.G. 162, 191
- Sybel, V.H. 60, 61, 86
- Sylvestre-Williams, R. 106, 120, 125, 132
- Taylor, R.L. 162, 163, 165, 191
- Terzaghi, K. 107, 132
- Thornburn, T.H. 106, 132
- Traffic Research Team, 18, 41
- Turnage, G.W. 45, 74, 86, 105-108, 132, 287, 300
- Tynan, A.E. 266, 278
- Uffelmann, F.L. 293, 300
- Warkentin, B.P. 10, 11, 16, 17, 41, 75, 87, 264, 278
- Webb, G.L. 106, 132, 136, 151, 154
- Weber, J.A. 106, 132
- Whitman, R.V. 236, 253
- Willis, B.M.D. 293, 298, 300
- Windisch, E.J. 106, 125, 126, 132
- Wise, M.E. 262, 278
- Wisner, R.D. 74, 75, 86, 105, 132, 293, 295, 297, 300
- Wong, J.Y. 28, 41, 296, 300
- Yong, R.N. 10, 11, 16, 17, 26, 33, 41, 56, 58, 60, 69, 75, 86, 87, 92, 106, 110, 120, 125, 126, 132, 133, 136, 150, 151, 154, 160, 171, 179, 191, 206, 212, 217, 218, 220, 238, 246, 249, 251, 253, 264, 266, 273, 276, 278, 288, 300
- Youssef, A.F. 26, 41, 60, 87, 92, 133, 212, 217, 218, 220, 253, 288, 300
- Zienkiewicz, O.C. 159, 161, 162, 191

SUBJECT INDEX

- Air cushion vehicles, 50
- Analytical methods, 91
 - energy model, 136
 - finite element, 157
 - limit analysis, 106
 - visioplasticity, 141
- Angle of attack, 70, 213
- Annular ring, 26
- Beviameter, 2, 295
- Boundary conditions, 175
- Bulldozing resistance, 98
- Characteristics, 116
- Compaction, 257
 - amount of, 270
 - analysis, 272
 - cohesive soil, 264
 - efficiency, 271
 - factors, 266
 - granular soil, 258
 - mechanisms, 258
 - prediction FEM, 270, 275
 - resistance, 98
 - types of, 266
- Compactive effort, 266, 271
- Cone index
 - remoulding, 283
 - vehicle, 287
- Cone penetrometer, 283
- Constitutive relationships, 169
- Contact
 - area, 235, 236
 - of elastic bodies, 233
 - patch, 166, 240
 - pressure, 181, 232
 - pressure distribution, 181, 182, 214
 - stress, 101
 - theory, 235
- Coordination number, 260
- Deformation
 - energy, 148, 201, 212, 220, 241, 246
 - field, 198, 210, 220
- Dimensional analysis, 73, 102
- Displacement boundary condition, 179
- Dissipation energy, 241
- Drawbar-pull, 68, 102, 138, 226
- Dual tyres, 46
- Dynamic sinkage, 98, 179, 291
- Energy
 - budget, 136, 150
 - coefficients, 227
 - conservation, 135, 272
 - deformation, 148
 - interfacial, 147
 - losses, 138
 - model, 136
 - parasitic components, 147
- Failure zones, 206, 213
- Finite element
 - application, 195
 - boundaries, 195, 209
 - boundary conditions, 175
 - constitutive relationships, 169, 173
 - discontinuities, 162, 165
 - idealization, 160, 164, 166, 195
 - joint element, 163
 - mesh, 195, 209
 - method, 158
 - types, 161
- Flexing resistance, 98
- Flotation, 43, 45, 50
- Grouser
 - multiple, 216
 - shape, 61, 65

- sinkage, 65
 - soil interaction, 166, 207
 - spacing, 61
- Inorganic terrain, 9
- Input energy, 137, 241, 248
- Interfacial energy, 147, 247
- Iteration methods, 184
- Joint elements
 - constitutive relationships, 173
 - stiffness, 163, 174
 - types, 162
- Limit
 - analysis, 106
 - equilibrium, 90, 95, 107, 116
- Load boundary condition, 181
- Mobility
 - definition, 281
 - index, 286
- Modulus of
 - deformation, 79, 80, 83
 - elasticity, 170
- Motion resistance, 95, 98, 135, 138, 242, 257, 293
- Multiple grouser, 61, 63, 216
- Muskeg
 - classification, 21
 - properties, 21
 - strength, 25
 - terrain, 20
- Nonlinearity
 - geometric, 186
 - material, 183
- Normal pressure distribution, 207, 214, 227, 234
- Obstacles, 38
- Octahedral state, 170
- Output energy, 241, 249
- Particle
 - distribution, 259
 - size, 10
- Peat
 - properties, 21
 - terrain, 20
- Plastic
 - flow, 143
 - work, 145
- Plate
 - penetration, 96, 293
 - size, 293
- Pneumatic tyre, 74, 235, 244
- Predictions, 92
 - dimensionless analysis, 102
 - energy model, 136
 - energy transfer, 135
 - factors, 93
 - finite element, 157
 - parameters, 93
 - plate approach, 96
 - requirements, 92
 - semi-empirical, 102
- Pull energy, 291
- Rolling resistance, 279
- Roughness, 39
- Running gear, 1, 2, 95, 151
- Shear deformation, 76, 77, 79
- Similarity solution technique, 114
- Sinkage, 43, 52, 96, 226
- Sled parameters, 81
- Slip, 52, 65
- Snow
 - classification, 31
 - properties, 32
 - strength, 33

- terrain, 31
- Soil
 - behaviour, 16
 - classification, 10
 - compaction, 257
 - consistency limits, 14
 - packing, 259
 - properties, 12
 - types, trafficability purposes, 40
- Soil cutting, 117, 164, 174, 195
- Soil particle path, 179
- Sprocket wheel, 70
- Stress
 - concentration, 205
 - distribution, 202, 213
 - tangential, 53, 79, 215, 230, 233
- Tangential traction, 234
- Terrain
 - cover factors, 37
 - ground slope, 38
 - material, 9
 - patches, 5
 - roughness, 39
 - soil index, 285
 - support, 52
 - types, 9
- Threshold density, 35
- Track
 - belt flexibility, 61, 69
 - boundary pressure, 63
 - parameters, 60
 - performance, 65, 220, 226
 - prediction, 220
 - type, 48
 - wheel number, 69
- Traction
 - force, 60, 74, 102
 - mathematical modelling, 75
 - mechanics, 1, 5
 - mechanisms, 6, 52-55, 58
- Tractive effort, 72, 100
- Tractive element
 - soil parameters, 3
 - soil performance, 4
 - types, 52, 175
- Tractive force, 80, 81
- Trafficability, 2, 5, 281
- Tyre
 - carcass stiffness, 232
 - contact area, 235
 - deformation energy, 241
 - inflation pressure, 57, 232
 - interfacial slip, 247
 - performance, 240
 - size, 45
 - traction, 48, 73
 - tread configuration, 56, 74
 - type, 45
- Vane-cone
 - device, 288
 - prediction method, 289
- Vane-shear, 26, 30
- Vegetation, 39
- Vehicle mobility, 1, 5
- Visibility, 39
- Visioplasticity, 141
- Walking elements, 50
- Wheel, 44
 - boundary conditions, 230
 - soil interaction, 229